# DISSECTING THE FUNCTION AND INTERACTOME OF PLEKHS1 IN PROSTATE TUMORIGENESIS

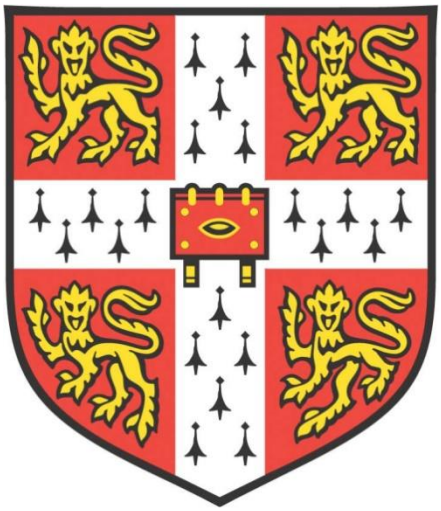

**Piotr Krzysztof Jung**

**Wolfson College**

**The Babraham Institute**

**Cambridge**

**UK**

**This dissertation is submitted for the degree of Doctor of Philosophy**

**June 2020**

# DECLARATION

The work presented in this dissertation was undertaken in the Inositide Laboratory, under the supervision of Dr Len Stephens FRS, at the Babraham Institute. This dissertation is the result of my own work and includes nothing which is the outcome of work done in collaboration except as declared in the Preface and specified in the text. It is not substantially the same as any that I have submitted, or, is being concurrently submitted for a degree or diploma or other qualification at the University of Cambridge or any other University or similar institution except as declared in the Preface and specified in the text. I further state that no substantial part of my dissertation has already been submitted, or, is being concurrently submitted for any such degree, diploma or other qualification at the University of Cambridge or any other University or similar institution except as declared in the Preface and specified in the text. It does not exceed the prescribed word limit set out by the Biology Degree Committee.

Signed: _____Piotr Jung_____

Date: _____16-6-2020_____

Piotr Krzysztof Jung

Cambridge

# SUMMARY

Phosphatidylinositol(3,4,5)trisphosphate ($PI(3,4,5)P_3$ or $PIP_3$) is the lipid product and key signalling output of Class I phosphoinositide 3-kinases (PI3Ks) and acts as a coordinator of a huge network that controls cellular processes such as metabolism, cell growth and movement. Mutations that augment the activity of this network are amongst the most common drivers of tumour progression.

Upon binding of many ligands to their receptors, Class I PI3Ks are activated and 3-phosphorylate the ubiquitous phospholipid $PI(4,5)P_2$ to yield $PIP_3$ in the plasma membrane. This leads to the local accumulation of a variety of $PIP_3$-sensor proteins, typically hosting $PIP_3$-binding pleckstrin homology (PH) domains. These $PIP_3$-sensors then propagate the PI3K signal *via* a multitude of mechanisms to regulate keystone effectors like Akt, mTOR and PRex proteins that shape cell behaviour on many levels. Loss of the tumour-suppressor and $PIP_3$-3-phosphatase PTEN, leads to constitutive activation of the $PIP_3$-network and is a very common event in many human tumours, including prostate cancer. Mouse models in which *Pten* and/or Class I PI3K signalling can be conditionally deleted in the prostate have been developed and used to show that unrestrained Class IA PI3K signalling can drive over growth of tissues and eventually cancer.

The PI3K signalling pathway has been studied intensively for many years, however, due to a variety of intractable problems, the endogenous proximal upstream regulators and downstream effectors of Class IA PI3Ks are still largely unknown in either health or disease.

To identify the potential interactors, that could include both activators and targets, of Class IA PI3Ks in healthy and *Pten*$^{-/-}$ mouse prostate tissue, we engineered mouse strains in which selected subunits of their Class IA PI3Ks could be specifically biotinylated *in vivo* (AviTag technology) and hence efficiently purified. Using this methodology, we have found that PLEKHS1 was specifically recovered with Class IA PI3Ks and that association was dramatically increased in *Pten* $^{-/-}$ prostate.

To further investigate the function and interactions of PLEKHS1 *in vivo,* we generated two mouse models: a *Plekhs1*-null line (*Plekhs1*$^{-/-}$) and a strain in which endogenous *Plekhs1* was AviTagged(Plekhs1$^{Avi/Avi}$). We also performed experiments with cells

transfected with *Plekhs1* constructs and with recombinant *Plekhs1 in vitro* to dissect its structure/functions.

The transfection studies confirmed that PLEKHS1-PI3K interaction is dependent on PLEKHS1 phosphorylation and suggest PLEKHS1 can activate Class IA PI3K signalling. *In vitro* studies performed by Dr Tamara Chessa showed the isolated PH domain of PLEKHS1 interacted selectively with $PI(3,4)P_2$ and $PIP_3$ and suggest that PLEKHS1 can also function downstream of Class I PI3Ks. Using *Plekhs1*$^{Avi/Avi}$ mice we were able to efficiently recover PLEKHS1 from healthy and *Pten* $^{-/-}$ prostates and have identified a set of proteins that can interact selectively with PLEKHS1 *in vivo*. We observed increased interaction with Class IA PI3Ks, confirming the above results, and phosphorylation of PLEKHS1, in *Pten* $^{-/-}$ tissue. Importantly, the absence of PLEKHS1 substantially reversed the impact of loss of PTEN on the prostate weight, phosphorylation of Akt and levels of $PIP_3$, with no or small effects on healthy prostate.

Collectively, these data suggest that PLEKHS1is an unexpectedly important activator, and effector, of Class IA PI3K signalling in *Pten* $^{-/-}$ mouse prostate.

# TABLE OF CONTENTS

# LIST OF TABLES

# LIST OF FIGURES

# LIST OF APPENDICES

## TABLE OF ACKNOWLEDGEMENT OF ASSISTANCE

**1. Initial training in techniques and laboratory practice and subsequent mentoring:**

Dr K. Anderson – PhD mentoring. Initial training in lipids extraction

Dr T. Chessa- mouse colony management, breeding strategy, prostate isolation, streptavidin- and GFP-mediated pulldowns

Dr D. Spensberger- Cripsr/Cas9 technology, T7 assay, genotyping

Mr Keith Davidson- isolation of mouse tissues

**2. Data obtained from a technical service provider (e.g. DNA sequencing, illustrations, simple bioinformatics information etc.)**

Genewitz- sanger sequencing

**3. Data produced jointly (e.g. where it was necessary or desirable to have two pairs of hands)**

Dr K. Anderson – co-performance of mass spectrometry experiments

Dr T. Chessa- isolation of mouse prostates, co-performing GFP-mediated pulldowns, data analysis

Mr Keith Davidson- isolation of mouse tissues

**4. Data/materials provided by someone else (e.g. one-off analysis, bioinformatics analysis, where parallel data or technical provision in a very different area is needed to provide a connected account in the thesis)**

Dr J. Clark and Dr I. Niewczas – synthesis and provision of mass spectrometry standards

Dr J. Clark – membrane lipids measurements

Dr D. Spensberger – zygote injection of Crispr reagents. Implantation of blastocysts to female mice

Dr T. Chessa- construction of plasmids, immunoprecipitation experiment, RNAseq data analysis

Dr D. Oxley and Dr J. Webster- mass Spectrometry analysis

Dr D. Oxley and Dr J. Webster- preliminary data analysis of proteomics project

Dr A. Segonds-Pichon – statistical analysis

Dr F. Krueger- analysis of published RNAseq dataset

# LIST OF ABBREVIATIONS

| | |
|---|---|
| ABD | Adaptor Binding Domain |
| ABL | Abelson Murine Leukaemia Viral Oncogene Homolog 1 |
| ADT | Androgen Deprivation Therapy |
| AKT | AKT Serine/Threonine Kinase 1 |
| ALK | Anaplastic lymphoma kinase |
| AMPK | 5' AMP-Activated Protein Kinase |
| AP | Anterior Prostate |
| AR | Androgen Receptor |
| ATF2 | Activating Transcription Factor 2 |
| ATM | Ataxia Telangiectasia Mutated |
| AVI | Avitag |
| BCR | Breakpoint Cluster Region Protein |
| BH | Breakpoint-Cluster Region Homology Domain |
| BLAST | Basic Local Alignment Search Tool |
| BPH | Benign Prostatic Hyperplasia |
| BRAF | B-Raf Proto-Oncogene |
| BRCA | Breast Cancer Gene |
| CA | Catalytic subunit α |
| CB | Catalytic subunit β |
| CD | Catalytic subunit δ |
| CDC | Cell Division Cycle |
| CDK | Cyclin Dependent Kinases |
| CHEK | Checkpoint Kinase |
| CIP | Calf Intestinal Alkaline Phosphatase |
| CMV | Cytomegalovirus (plasmid) |
| CRISPR | Clustered Regularly Interspaced Short Palindromic Repeats |
| CRPC | Castration-Resistant Prostate Cancer |
| DLP | Dorsal-Lateral Prostate |

| | |
|---|---|
| DP | Dorsal Prostate |
| DSB | Double Strand Breaks |
| EE | EE epitope tag |
| EGF | Epidermal Growth Factor |
| EGFP | Enhanced Green Fluorescent Protein |
| ERK | Extracellular Signal-Regulated Kinases |
| ES | Embryonic Stem Cells |
| FRT | Flippase Recognition Target |
| FYVE | Zinc Finger Domain Named After Four Cysteine-rich Proteins: Fab 1, YOTB, Vac 1 and EEA1 |
| GFP | Green Fluorescent Protein |
| GPCR | G-Protein Couple Receptor |
| GRB | Growth Factor Receptor Bound Protein |
| GSK-3 | Glycogen synthase kinase-3 |
| GTP | Guanosine-5'-triphosphate |
| HGSC | High-Grade Serous Carcinoma |
| HOXB | Home box Protein Hox-B |
| HSP | Heat Shock Protein |
| IGF | Insulin Growth Factor |
| INDELS | Insertion and/or Deletion |
| INPP | Indole-3-Propanol Phosphate |
| IP | Immuno-Precipitation |
| IPSC | Induced Pluripotent Stem Cells |
| IRS | Insulin Receptor Substrate |
| ITGB | Integrin Subunit Beta |
| KC | Keratinocyte Chemoattractant |
| KIP | CDK Interacting Protein |
| KO | Knock-Out |
| KRAS | KRAS Proto-Oncogene |
| LKB | Liver Kinase B1 |
| LP | Lateral Prostate |
| LPA | Lysophosphatidic Acid |

| | |
|---|---|
| MAPK | Mitogen-Activated Protein kinase |
| MEK | Mitogen-Activated Protein Kinase Kinase |
| MLH | MutL Homolog 1, Colon Cancer, Nonpolyposis Type 2 |
| MSH | Melanocyte Stimulating Hormone |
| NF | Nuclear Factor |
| PALB | Partner and Localizer of BRCA2 |
| PAM | Protospacer Adjacent Motif |
| PC | Prostate Cancer |
| PCR | Polymerase Chain Reaction |
| PDGF | Platelet-Derived Growth Factor |
| PDK | Pyruvate Dehydrogenase Kinase |
| PH | Pleckstrin Homology |
| PI | Phosphatidylinositol |
| PIK | Phosphatidylinositol 3-Kinase |
| PIN | Prostatic Intraepithelial Neoplasia |
| PIP | Phosphatidylinositol phosphate |
| PKB | Protein kinase B |
| PLEKHS1 | Pleckstrin Homology Domain Containing S1 |
| PMS | Phenylmethylsulfonyl Fluoride |
| PSA | Prostate Specific Antigen |
| PTEN | Phosphatase and Tensin Homolog |
| PTM | Post-Translational Modification |
| PX | Phox homology domains |
| RAF | Rapidly Accelerated Fibrosarcoma |
| RBD | Receptor Binding Domain |
| RTK | Receptor Tyrosine Kinase |
| SB | Sleeping Beauty |
| SCC | Squamous Cell Carcinomas |
| SCNA | Somatic Copy Number Alterations |
| SDS | Sodium Dodecyl Sulfate |
| SH | Src Homology domain |
| SHP | Small Heterodimer Partner |

| | |
|---|---|
| SMAD | Family of proteins similar to the gene products of the Drosophila gene 'mothers against decapentaplegic' (Mad) and the C. Elegans gene Sma |
| SOX | SRY-Box Transcription Factor |
| SPOP | Speckle-Type POZ Protein |
| STK | Serine/Threonine Protein Kinase |
| TMT | Tandem Mass Tag |
| TNF | Tumour Necrosis Factor |
| TOR | Target of Rapamycin |
| mTORC2 | Mammalian Target of Rapamycin Complex 2 |
| TRAIL | TNF-Related Apoptosis-Inducing Ligand |
| TRAMP | Transgenic Adenocarcinoma of the Mouse Prostate |
| TSC | Tuberous Sclerosis Complex |
| UGS | Urogenital Sinus |
| UVRAG | UV Radiation Resistance Associated Regulator |
| VEGF | Vascular Endothelial Growth Factor |
| VP | Ventral Prostate |
| VPS | Vacuolar Protein-Sorting Protein |
| WAF | Cyclin-Dependent Kinase Inhibitor |
| WT | Wild type |

# 1 INTRODUCTION

## 1.1 PI3K Signalling Pathway

Phosphoinositide 3-kinases (PI3Ks) are a family of enzymes that phosphorylate the 3-OH group of inositol phospholipids in the cytoplasmic faces of a variety of cell membranes to generate 3-phosphorylated phosphoinositides. Those lipids act as secondary messengers initiating further signalling by activating downstream proteins. The PI3K signalling networks regulate a wide range of cellular processes, including proliferation, apoptosis, chemotaxis, cell survival, trafficking and glucose homeostasis. There are a variety of factors which determine the outcome of PI3K signalling, including, the PI3K isoform involved, the precise second messenger lipid generated and the cellular location[1]. Mutated forms of PI3Ks and components of their signalling networks play a significant role in cancer, myopathies, neuropathies and ciliopathies. PI3Ks also play important roles in metabolism, immunity and cardiac processes[2]. The PI3K family consists of 3 different classes of enzymes, where the Class I, which is the most studied is divided into two subgroups: Class IA and Class IB [3] [4].

### 1.1.1 Class I PI3K

Characteristically, the Class I PI3K can be acutely activated by a wide variety of cell surface receptors and intracellular signalling molecules such as receptor tyrosine kinases (RTKs), G protein-coupled receptors (GPCRs) and small GTPases. Class I PI3K are heterodimers, containing a "p110" catalytic subunit and a regulatory subunit, in all Metazoan and Choannoflagellate species. In Amoebozoa, including Dictyostelium, there are p110-catalytic subunits but no known p85-like regulatory subunits. Mammals, in contrast to *Drosophila melanogaster* or *Caenorhabditis elegans*, have four isoforms of Class I PI3K catalytic subunits: p110α, p110β, p110γ and p110δ[5].

Upon cell activation, RTKs can phosphorylate tyrosine residues in either their cytoplasmic domains (e.g., PDGF β-receptors) or associated adaptor proteins (e.g., insulin receptor substrate (IRS) proteins); GPCRs drive activation and disassociation of

heterotrimeric G-proteins and release of G-βγ subunits or GTP-bound-G-α-subunits. Different Class I PI3Ks can be activated by binding either appropriately tyrosine phosphorylated proteins (see below) or G-βγ subunits. These binding reactions lead to activation of the PI3K catalytic subunits and enhanced phosphorylation of the membrane lipid phosphatidylinositol-4,5-bisphosphate ($PI(4,5)P_2$, $PIP_2$) and generation of phosphatidylinositol-3,4,5-trisphosphate ($PI(3,4,5)P_3$, $PIP_3$) which acts as a secondary messenger. Phosphatase and Tensin Homolog (PTEN) is a dual protein and lipid phosphatase, which directly antagonises the function of Class I PI3Ks, by dephosphorylating $PIP_3$ (and $PI(3,4)P_2$) to yield $PIP_2$ (and PI(4)P)[6].

A large family of proteins can bind $PIP_3$ selectively. Many of these proteins are cytosolic and bind $PIP_3$ *via* plekstrin homology (PH) domains. As a result, following receptor activation when $PIP_3$ accumulates, these binding proteins become concentrated into the cytoplasmic face of the membranes housing the $PIP_3$. There are two, canonical members of this family of $PIP_3$ binding proteins; the serine/threonine kinases, 3-phosphoinositide-dependent kinase 1 (PDK1) and Akt/protein kinase B (PKB) (Figure 1.1) [7] [8]. Akt can mediate a plethora of the cellular consequences of Class I PI3K activation, such as proliferation and cell survival. It can actively contribute to inhibition of apoptosis, by inactivating proapoptotic factors, such as Bad and Pro-caspase-9 and Forkhead family transcription factors, which stimulate expression of pro-apoptotic agents, such as Fas-ligand (FasL) [9] [10]. It was reported that Akt increases resistance to proapoptotic processes in prostate cancer cells by suppressing cell responses to tumour necrosis factor (TNF)-related apoptosis inducing ligand (TRAIL)[11]. Furthermore, there are important interactions between the PI3K/Akt pathway and the NFκB pathway, another central regulator of cell survival in lymphoma cells [12]. In addition to cell survival, targets of Akt include keystone regulators of glycogen metabolism, protein synthesis and cell cycle control[7]; such as the mammalian target of rapamycin (mTOR), glycogen synthase kinase-3 (GSK3), insulin receptor substrate-1 (IRS-1), the cyclin-dependent kinase inhibitors p21CIP1/WAF1 and p27KIP1. These connections are mediated by Akt's ability to phosphorylate and inactivate GSK3-β, which results in an increased level of cyclin D1, and inhibition of the Forkhead family transcription factors and the tumour suppressor tuberin (TSC2). These processes lead to stimulation of cell cycle progression and a

decreased level of one of the members the universal cyclin-dependent kinase inhibitor (CDKI) family: p27[Kip1] [13] [14]. Collectively, this complex web of interactions means that Akt and the Class I PI3Ks, that are the key determinants of its activity, are a key signalling node controlling and integrating many aspects of cell biology.

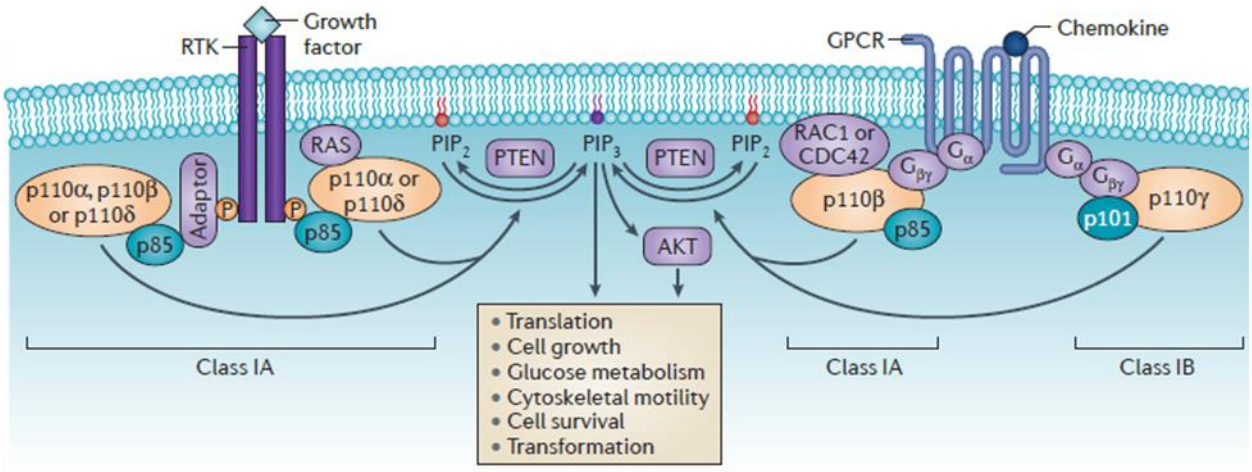


**Figure 1.1 Signalling by Class IA and IB PI3K**

*Upon stimulation of RTKs or GPCRs, Class I PI3Ks become active at the cell membrane. In these settings, the Class IA PI3Ks are activated primarily via interactions between the SH2 domains in their regulatory subunits and canonical phosphorylated tyrosines in YXXM motifs in either the RTKs or their adaptor proteins. Small GTPases such as Ras, Rac or CDC42 can activate all Class I PI3K catalytic subunits directly. Gβγs can bind and activate Class IA (p110β-containing) and B PI3Ks directly. The activated Class I PI3Ks then drive phosphorylation of $PIP_2$ to generate $PIP_3$. $PIP_3$ then acts as a secondary messenger and triggers Akt- dependent and Akt-independent cellular processes, such as cell growth, proliferation, apoptosis, survival and motility.*
*Adapted from Thorpe et. al. Nature Reviews Cancer, 2015*

#### 1.1.1.1 The Class IA PI3K

The Class IA PI3Ks contains three members, named after their catalytic subunits: PI3Kα, PI3Kβ and PI3Kδ, where the catalytic subunits, which gave them their name, are encoded by PIK3CA (p110α), PIK3CB (p110β) and PIK3CD (p110δ) genes respectively[15]. P110sα and β are very broadly expressed p110δ has a more restricted distribution and is highly expressed in a number of immune cells including B and T lymphocytes. These catalytic subunits form active complexes with 3 different regulatory components: p85α (with two additional splicing variants: p55α and p50α), p85β and p55γ encoded by PIK3R1, PIK3R2 and PIK3R3 respectively [16]. All three regulatory subunits are broadly expressed. In the p110 catalytic subunits it is possible to distinguish five distinct domains: an N-terminal adaptor binding domain (ABD) which can bind to p85 regulatory subunits, a Ras-binding domain (RBD), a C2 domain which binds to the cell membrane, a helical domain and a kinase catalytic domain. On the other hand, regulatory subunits also have five clear domains: an SH3 domain and a BH domain (Bar homology) near the N-terminus (except in p55γ and the two smaller splice variants of p85α) and two SH2 domains, which are separated by an iSH2 (inter-SH2 domain), which binds to the catalytic subunits.

A network of cooperative interactions both within the heterodimeric PI3K complexes and between the heterodimers and their regulators and/or interactors (e.g., Gβγs, Ras, PTEN etc.) underpin their ability to be dynamically and selectively activated by many receptors and generate a rapid-acting ubiquitous messenger, $PIP_3$.

Interactions between the N-SH2 domain of p85s and the C2, helical and kinase domains of p110s lead to powerful constitutive suppression of the lipid kinase activity of the complex. A similar interaction occurs between the C-SH2 domain and the kinase domains of p110β and p110δ. These inhibitory contacts are broken when the SH2 domains of the regulatory subunits bind to appropriate tyrosine-phosphorylated peptides and hence the complex is activated[17 18].

Heterotrimeric Gβγ subunits can bind to the C2 domain-helical domain linker in p110β (and p110γ, see below) and directly activate PI3Kβ. This property renders PI3Kβ potentially sensitive to GPCR activation.

The RBD domain of p110α can bind to, and be activated by, GTP-bound and active Ras-family small GTPases like H-Ras, K-Ras and N-Ras. It seems likely that p110δ can also be activated by Ras-family GTPases although this is not entirely clear. In contrast, p110β can bind and be activated by activated, GTP-bound members of the Rho-family GTPases, Rac and CDC42.

Recent work has indicated that in cells that p110-free p85α exists[19] and can homodimerize[20] via a BH:BH domain interaction and an interaction between the SH3 domain and a proline-rich SH3 ligand in p85α. Importantly, p85α homodimers, but not p85α heterodimers nor monomers, can bind to active forms of PTEN and protect them from ubiquitination-mediated degradation. These results indicate that accumulation of p85α homodimers can lead to stabilisation of active PTEN and inhibit class I PI3K signalling. It appears there are p85α mutations (e.g., I133N, in the region of p85α that binds PTEN) that accumulate in cancer that reduce this form of brake on class I PI3K signalling[20].

These different activation mechanisms combine to mean that class IA PI3K act as highly selective coincidence detectors under physiological conditions in vivo[21] .

Hence, in isolation tyrosine phosphorylated peptides only activate relatively weakly until combined with activated small GTPases or Gβγ subunits. This means that specific combinations of different stimuli can work synergistically. Hence, although p110β appears to be relatively weakly activated by receptor-stimulated production of Gβγs in isolation, in combination with appropriate activation of phosphotyrosine-based signalling it can be activated intensely and become the dominant Class I PI3K activity[22] [23] [24]. Hence Class IA PI3Ks can be activated by large variety of extracellular ligands, including, but not limited to, epidermal growth factor (EGF), lyso-phosphatidic acid (LPA), immune-complexes, platelet-derived growth factor (PDGF), vascular endothelial growth factor VEGF), insulin and insulin-like growth factor (IGF)[25].

#### 1.1.1.2 Class IB

Class IB PI3K is represented only by one isoform- PI3Kγ[26]. This subclass forms a heterodimeric complex containing catalytic subunit p110γ and one of two regulatory subunit s; p101 or p87 (known also as p84). According to the current knowledge, Class

IB PI3K is selectively regulated by GPCRs. There appears to be two sites in the complex that can bind to Gβγ directly; p101 and the C2-helical domain linker (like in p110β, described above) [27 28]

This strongly suggests, that p101 acts as an adaptor, which sensitizes PI3Kγ to stimulation by Gβγ[29]. PI3Kγ is also activated by GTP-bound Ras-family GTPases and this input appears to operate synergistically with Gβγs[30 31 32 33]

Interestingly, however, whilst it appears activation of Gβγs alone can lead to stimulation of PI3Kγ, activation of Ras alone, without coincident activation release of Gβγs, does not lead to significant activation of PI3Kγ[33].

Originally, it was thought that p110γ was exclusively expressed in immune cells. However, through further studies, it was shown that p110γ is distributed more widely but at much lower levels, including its expression in endothelial cells, microglia, neurons, tubular cells of the kidney and exocrine and endocrine pancreatic or prostate gland cells[34].

### 1.1.2 Class II PI3K

The Class II PI3K are the relatively least understood subfamily of PI3Ks. *Drosophila melanogaster* and *Caenorhabditis elegans* have only one Class II PI3K (piki-1 and PI3K68D, respectively), whereas vertebrates are characterised by possessing three different Class II PI3K isoforms. Two of them, PI3KC2α and PI3KC2β are ubiquitously expressed whereas PI3KC2γ is expressed mostly in the liver [5 35]. Interestingly, as opposed to Class I PI3K, Class II PI3K do not act as transducers of signal downstream from cell membrane receptors. Recent work indicates they have key roles in control of clatherin-dependent endocytosis where PI3K Class IIα has a key role by producing $PI(3,4)P_2$ to regulate assembly of endocytic pits prior to release from the plasma membrane [36] In other settings, Class II PI3Ks appear to function via their ability to generate PI(3)P as their primary lipid product, for example in control of the primary cilium[37]. In terms of structure, Class II PI3K contains a conserved catalytic domain with a non-structured N-terminal region, C-terminal phox-homology (PX) domain and C2 domain. In contrast to Class I, Class II PI3Ks function as a monomers and appear to capable of generating different, but physiologically important, lipid products in vivo.

### 1.1.3 Class III PI3K

Class III PI3K synthesize phosphatidylinositol 3-phosphate ($PI(3,4)P_2$), which plays a key role in membrane trafficking. There are three core subunits in this class: a catalytic subunit with kinase activity: VPS34 (or PIK3C3), the regulatory, protein kinase-like, subunit VPS15 and, the tumour suppressor, Beclin-1. Dependent on the presence of ATG14 or UVRAG as a 4$^{th}$ member of the class III PI3K complex, there can be two different complexes, one of which plays a major role in regulation of macroautophagy whilst the second has an important role in endocytosis. The lipid product of VPS34 in vivo is PI(3)P; which acts as a membrane identity signal to recruit proteins containing FYVE or PX domains to control membrane identity transitions in the endolysosomal membrane system and through that trafficking of a large variety of proteins[38 39].

## 1.2 PI3K in Cancer

A number of studies have indicated that the Class I PI3K network is the most frequently mutated pathway in human tumours. PIK3CA being the second most frequently mutated oncogene and PTEN being one of the most commonly mutated tumour suppressors[40 41]. Even if the *PTEN* and PIK3CA genes are unaltered, some cancers take advantage of mutations in other components of the Class I PI3K signalling network. These additional potential drivers of the Class I PI3K signalling network in cancer include activated kinases, such as Akt, mutations leading directly (mutations in Ras) or indirectly (e.g. mutations in Ras-inhibiting RasGAPs (GTPase activating proteins)) to activation of Ras-family GTPases, loss of activity of liver kinase B1 (LKB1, also known as STK11), type II inositol polyphosphate-4-phosphatase (INPP4B) or tuberous sclerosis (TSC)[42]. The strong case indicating a link between genetic alterations of various components of the Class I PI3K pathway and tumour progression as well as the potential druggability of some of them made the Class I PI3K-Akt-mTOR network a very attractive target for development of potential anti-cancer therapeutics. Development of potential drugs which could inhibit or control the activity of some members of this pathway is challenging due to the fundamental role this pathway plays in normal cells and tissues. The emergence of high resolution structures of the Class I PI3K enzymes [17 43 44] and advances based on biochemical studies have resulted in the generation of several

compounds affecting the pathway[45], some of them showing promising preclinical results[46] [47]. There are still many challenges regarding usage of agents targeting components of PI3K signalling pathway in patients. In comparison to agents targeting key oncogenes such as BCR-ABL, anaplastic lymphoma kinase (ALK) and B-RAF, Class I PI3K and mTOR inhibitors have only shown moderate successes[48] [49] [50]. A number of factors, such as dosage of the drug, time of exposure, toxicity and patient tolerance all play a big part in clinical potency of the agent. It has been suggested, that at advanced stages of tumorigenesis the PI3K pathway is not as crucial for cancer cell survival as it was previously reported. In that study, substantial blockade of PI3K$\alpha$ did not induce cancer cell apoptosis, indicating that Class I PI3K signalling network function had become redundant [51] [52]. Recent studies on genetically engineered mice, have suggested that mutations in PIK3CA do not drive tumorigenesis to the extent that other oncogenes can[53] [54]. Further studies on the PI3K-Akt-mTOR axis, targeting particular components, optimising dosing protocols and testing for potentially synergistic drug combinations will be essential to fully realise the potential of inhibitors of the Class I PI3K network[55].

## 1.3 Prostate Tumorigenesis

### 1.3.1 Function and anatomy of prostate

The prostate is a male accessory gland found in the large majority of mammals and only a very limited number of non-mammalian species. The main role of this organ is to produce components of the seminal fluid and contribute to the ejaculation process. Development of the prostate and regulation of its function during adult life depends on androgens, male hormones produced in testis. Androgens bind to androgen receptors (AR), which is a hormonal transcription factor which, in the prostate, is concentrated mainly in the stromal and epithelial cells. During prostate organogenesis, androgen signalling is activated alongside a variety of other cellular pathways to regulate formation of the fully functional organ. Many genes and cellular processes essential for organogenesis, once dysregulated, play a major role in carcinogenesis[56] [57].

The prostate starts developing at a late stage of embryogenesis and finishes during

puberty. Prostate develops from the urogenital sinus (UGS) and is characterised by a branched structure. It develops from the ventral part of the cloaca, located in between the bladder and the urethra. Human prostate is a uni-lobular acorn-shaped organ, with distinguishable zones: a peripheral zone, a transitional zone and a central zone - each of them surrounded by fibromuscular stroma (Figure 1.2A). The peripheral zone is the site where the majority of prostate cancers occur, whilst most cases of non-malignant, benign prostatic hyperplasia (BPH) are found in the transitional zone.

In contrast to the human prostate, rodent prostate has four distinct lobes: the anterior prostate (AP), the dorsal prostate (DP), the lateral prostate (LP) and the ventral prostate (VP), named after their orientation with respect to the urethra (Figure 1.2B). Interestingly, each of the lobes displays different patterns of branching, histology and secretory ability[58]. In both rodent and human prostate there are 3 types of cells. 1) Luminal cells, heavily involved in secretion of seminal fluids and lining the lumen. 2) Basal cells, which surround the layer of luminal cells. 3) A very small population of neuroendocrine cells, which are characterised by morphology that is similar to that of basal cells. In addition, the structure described above is surrounded by a mixture of smooth muscle cells, fibroblasts, myofibroblast that create the basal membrane and a stromal compartment, that contains a variety of immune cell types. Different populations of prostate cells are known to express diverse and unique protein markers. For example, luminal cells express the cytokeratins 8 and 18 and are AR-positive; basal cells express cytokeratines 5 and 14, and the p63 transcription factor; whereas neuroendocrine cells are characterised by presence of chromogranin A and synaptophysin [59] [60].

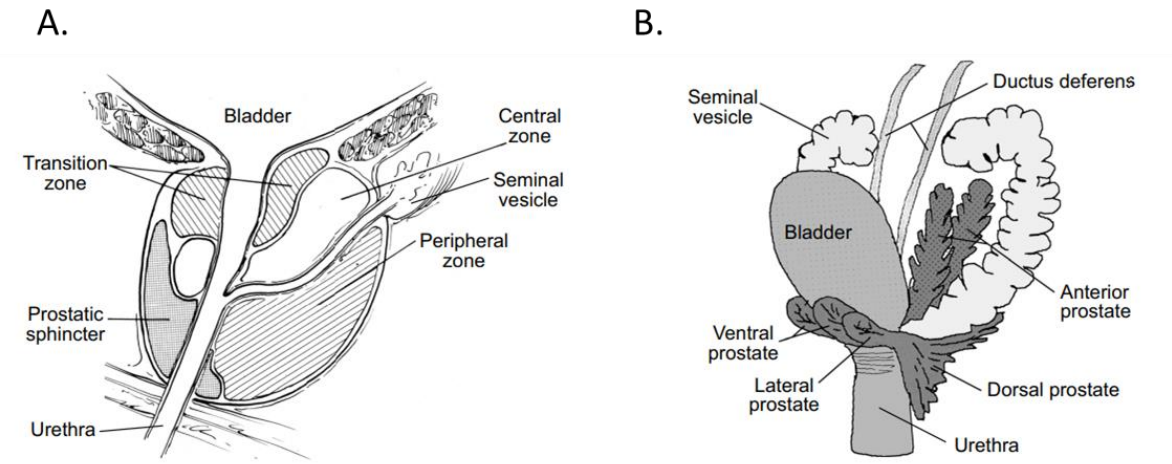


**Figure 1.2 Overview of prostate anatomy**

A. *Schematic of human prostate with a number of regions highlighted: peripheral zone, transition zone and central zone. Bladder, seminal vesicles and urethra are labelled to clarify the positioning of particular prostate zones.*
B. *Schematic of mouse prostate with a number of regions highlighted: anterior prostate (AP), ventral prostate (VP), lateral prostate (LP) and dorsal prostate (DP). Bladder, seminal vesicles and urethra are labelled to clarify the positioning of particular lobes.*

*Adapted from Francis et. al, Cold Spring Harb Perspect Med, 2017*

### 1.3.2 Overview on prostate tumorigenesis

Prostate cancer is the third most common cancer type worldwide and second most common cancer in men. It is estimated by the American Cancer Society, that approximately 191, 930 new cases are going to be diagnosed and 33,330 deaths will occur in the United States in 2020. These predictions will make prostate cancer the 5$^{th}$ biggest cause of cancer-related death in general [61].

Prostate cancer is a very heterogeneous disease, often remained asymptomatic for a very long time and therefore not diagnosed nor treated for many years. In the earliest stages prostate hyperplasia or a prostatic intra-epithelial-neoplasia (PIN) stage of cancer can be identified. These are considered benign stages in the disease progression process; however, high grade PIN is a strong predictor of a risk of progression to full-

blown prostate cancer. There are also difficulties in discriminating between treatable and untreatable types of cancer. At present, excepting some hereditary cases, prostate cancer is a disease of old age, with the biggest numbers of diagnosed patients being around 70 years old [62].

Currently there are two factors which reflect severity and stage of prostate cancer 1) Gleason grade (which measures tumour differentiation) and 2) PSA levels (serum prostate-antigen), however neither of them appear to be very accurate predictors of clinical outcome [63] [64] [65]. After the diagnosis of cancer, patients are treated with radiotherapy and/or radical prostatectomy, which give a very promising prognosis. In patients with locally advanced or metastatic cancer, androgen deprivation therapy (ADT) is applied. ADT works on two levels 1) by blocking androgen synthesis (e.g. abiraterone) or by blocking the function of androgen receptors (e.g. enzalutamide, bicalutamide). Initially, ADT treatment gives a very effective clear and beneficial response, however, relapses can occur within 2 years of initial treatment. After the relapse, the cancer usually comes back in a more aggressive form and shortens life expectancy to 16-18 months [66]. Unfortunately, a large proportion of patients develop castration-resistant prostate cancer (CRPC), which has poor survival rates and a limited spectrum of treatments available due to its heterogenic nature [67] [68].

As mentioned above, ADT treatment can fail to prevent prostate tumour progression in some patients. These failures can arise for multiple reasons. One such reason is the synthesis of androgens inside the tumour, which can be the result of an active mevalonate pathway, involved in the generation of cholesterol[69]. Some work has suggested that *PTEN* loss can lead to dysregulation of the mavalonate pathway and hence could be a trigger of development of androgen-independent and castration-resistant prostate cancer[70]. Several studies also suggested a correlation existed between moderately higher cholesterol levels and prostate cancer recurrence rate [71]. It was also shown that inactivation of *PTEN* is strongly correlated with primary tumours (37%) and even more with metastatic form of cancer (50%). Previous studies also indicate that *PTEN* loss is linked to hyperplasia and the prostatic intra-epithelial-neoplasia (PIN) stage of cancer, which could then be followed by more aggressive, metastatic forms of the disease. In these studies, the tissues that showed the earliest signs of metastatic tumour progression were lymph nodes and lung tissue [72] [73].

Furthermore, recent studies have shown that PTEN is inactivated in ~50% of prostate cancer cases, usually due to alterations in its copy number[74].

## 1.3.3 Gene mutations in prostate cancer

### 1.3.3.1 Germline alterations

There is strong evidence suggesting heritable traits are a crucial risk factor in development of prostate cancer (PC). Very interestingly, studies on twins suggest that the heritable component in the risk of developing PC is approximately 40% greater than in other common cancers, such as colon or breast [75].

There are many genes implicated in the heritable forms of PC. A number of these are involved in DNA repair mechanisms. Such genes include the very well known BRCA1 and BRCA2 as well as CHEK2, ATM and PALB2. There are also mutations in MLH1, MSH2, MSH6 and PMS2, that are responsible for Lynch syndrome. BRCA1 and BRCA2 have been intensively studied in context of breast and ovarian cancer. Proteins encoded by both of these genes are involved in homologous recombination of DNA[76]. Men, who are diagnosed with germline mutations in BRCA1 or BRCA2 typically develop PC at a much younger age and are ranked at diagnosis with a higher Gleason grade in comparison to the patients with sporadic PC [77]. Previous studies suggest that the risk for diagnosis of PC for men below 65 years old is almost 1.8-fold higher for carriers of BRCA1 loss-of-function mutations and almost 4.5-fold higher for carriers of BRCA2 loss-of-function mutations. When taking the full age range under consideration, the risk of developing PC is 8.6-fold higher for carriers of BRCA2 loss-of-function mutations [77] [78]. Lynch syndrome, which is the most common cause of an inherited form of stomach, colorectal and gynaecologic cancer, also increased the risk of developing PC [79] [80]. It was shown, that the chance of male carriers of MSH2 mutations being diagnosed with PC is approximately 10-fold higher compared to sporadic PC. CHEK2 and homeobox protein HOXB13 are engaged in the double-strand DNA (DSB) repair system. Evidence suggests that carriers of CHEK2 mutations and the HOXB13-G84E variant have much greater chances of developing PC. Men with a mutation with HOXB13 are 4.5-fold more likely to have PC than those without the mutations, although it wasn't proven that HOXB13

increased the aggressiveness of the cancers [81] [82] [83].

#### 1.3.3.2 Somatic alterations

In contrast to germline alterations, somatic alterations arise in prostate cells during the life course, such alterations include dysregulation of oncogene and tumour suppressor activity. A wide variety of factors contribute to acquisition of somatic mutations. An important factor is the acquisition of structural lesions that lead to genomic rearrangements, such as deletion, insertion or uncontrolled amplification of chromosome regions. Somatic copy number aberrations (SCNAs) very often result in deletion of tumour suppressors and amplification of oncogenes. Rearrangements of large chromosomal regions may lead to gene fusions resulting in the promotion of oncogenes. Point mutations, which include missenses and nonsense mutations as well as indels, can result in the loss of function in crucial genes, although these kinds of mutations are less frequent in PC. It is important to distinguish two groups of mutations: one group, known as passenger mutations, do not contribute to the pathogenesis, while the group, known as driver mutations, eliminate tumour suppressors and promote oncogenes. In addition to this knowledge, other cellular mechanisms can contribute to prostate tumorigenesis, including alterations at the level of DNA methylation, alterations in expression and regulation of miRNA and other gene functions and gene expression control mechanisms [84] [85] [86].

## 1.4 PI3K Signalling in prostate cancer

The PI3K pathway is one of the most commonly altered signalling pathways in human cancers, including PC. It is estimated that in 25 to 70% of metastatic prostate tumours the PI3K signalling pathway is upregulated. The *PTEN* gene on chromosome 10q23 is amongst the most mutated tumour suppressors in PC. Heterozygous and homozygous mutations leading to reduced or lost PTEN expression occur in ~40% of PC, whereas inactivating mutations occur in an additional 5-10% of cases[84].

The PI3K pathway is also linked to resistance to many common anti-cancer therapies, including targeted therapies or anti-angiogenic therapies and immunotherapies[87]. Alterations in Class I PI3K signalling network activity are also strongly associated with

more aggressive forms of prostate cancer, which are resistant to some of the conventional curative strategies like ADT.

Class I PI3Ks are heavily involved in prostate tumorigenesis, and are expressed in both cancer cells and non-cancerous stromal cells. Two of the isoforms, PI3Kδ and PI3Kγ, which play a known role in immune cell signalling influence carcinogenesis in an indirect way, by shaping the microenvironment surrounding the tumour [88 89]. In the physiological state, Class I PI3K activity is tightly controlled by phosphatases, such as PTEN or INPP4B. In 20% of primary tumours and 40% of CRPC, the most common alterations are; amplifications of, and activating mutations in, PIK3CA; activating mutations of Akt and deactivating mutations of *PTEN*[87 90]. In human cancers, the PIK3CA is the most commonly mutated subunit in the Class I PI3K family, it is also the second most mutated gene across various major cancer types. Particular PIK3CA mutations, such as PI3Kα$^{E542K}$, PI3Kα$^{E545K}$ and PI3Kα$^{H1047R}$ have been detected in prostate directly and correlate with progression of the disease and lower survival rates. Additionally, PI3Kα$^{H1047R}$ can occur along with *PTEN* loss.

Mouse models of prostate cancer progression have shown that combined presence of loss-of-function of *PTEN* and PI3Kα$^{H1047R}$ can greatly speed cancer progression and trigger CRPC, suggesting the coincidence of these mutations in human patients may drive more rapid tumour progression.[91] Mouse models of prostate tumour progression have also indicated that combined inhibition or genetic KO of Class I PI3Ks $\alpha$ and $\beta$ is required to substantially reduce the rate of tumour progression and that inhibition or deletion of either alone had little effect[92]. This conclusion contrasts with that of earlier work from the same group that had argued that ablation of PI3Kβ, but not PI3Kα inhibited progression of *Pten* $^{-/-}$ mouse prostate[93 94 95].

There are difficulties in studying PTEN function using mice as ubiquitous deletion of *Pten* stops development at a very early stage[72]. Mice lacking a single copy of the *Pten* gene in all tissues (*Pten* $^{+/-}$) develop a spectrum of spontaneous tumours in a variety of tissues, such as small and large intestines, lymphoid, mammary, thyroid, endometrial and adrenal glands[96 97 72]. While studying prostate cancer in a *Pten* $^{+/-}$ background model, it was discovered that PIN developed in the prostate organs of all of the affected mice. Interestingly, these mice developed PIN over about 10 months and did not develop

metastatic PC [72].

A number of studies addressed the consequences of introducing further, known oncogenic genetic manipulations in *Pten* $^{+/-}$ mice. *Pten* $^{+/-}$ p27$^{-/-}$ mice develop prostate carcinoma within 3 months after birth with 100% penetratance[98]. *Pten* $^{+/-}$ Nkx3.1$^{-/-}$ develop a high grade PIN, which does not transform to a cancer[99]. Similarly *Pten* $^{+/-}$ Ink4a $^{-/-}$ and *Pten* $^{+/-}$ Ar$^{-/-}$ mice develop PIN in a shorter time than mice that are simply *Pten* $^{+/-}$ [100]. However, none of the models highlighted above developed metastatic cancer. When crossing *Pten* $^{+/-}$ mouse with the well-established TRAMP model (in which expression of oncogenic SV40 T antigen is induced in prostate at puberty), the life span shortens significantly from 245 days to 159 days[101]. In a MPAKT cancer model (where Akt is constitutively active), mice develop PIN in the ventral prostate, without transformation to the metastatic form of cancer [102].

To understand the consequences of deletion of *Pten* in the process of PC progression, a conditional, prostate-specific, *Pten* $^{-/-}$ model was constructed. Pb-Cre4 mice (in which Cre-recombinase was expressed from the ProbasinB promotor which, in males, is active specifically in the prostate epithelium and are henceforth termed PbCre mice) were crossbred with *Pten* $^{loxP/loxP}$ mice, giving rise to males with a homozygous loss of *Pten* in prostate epithelial cells (as a result of broader expression of Cre in PbCre females it is important that males provide the PbCre transgene in crosses with *Pten* $^{loxP/loxP}$ mice[103]). The efficiency of this model was confirmed by an increase in phospho-Akt and elevated cell proliferation in *Pten* $^{-/-}$ compared to *Pten* $^{+/+}$ prostate[72]. In contrast to the *Pten* $^{+/-}$ prostate, PbCre *Pten* $^{loxP/loxP}$ tissue develops PIN within 12 weeks, followed by the emergence of invasive carcinoma at 9-12 months and finally with metastasis, reaching lymph nodes and the lungs at 12-16 months (it is important to note that there is some variation in the trajectory of these events reported by different labs/animal facilities, with some labs, including Babraham, observing no evidence of spread to other tissues) [72]. After castration, regression of PC was only partial, due to residual adenocarcinoma, and gland size and its proliferation index were still higher than in control, indicating it to be a good model of human CRPC[72].

## 1.5 PLEKHS1- a new interactor of Class IA PI3K

A number of studies have catalogued proteins that can be recovered with Class I PI3K subunits, or fragments derived from them, pulled-down from a variety of heterologous expression systems (e.g., proteins recovered with tagged Class I PI3K subunits over-expressed in cancer-derived cell lines[104 105]). Similarly, yeast-2-hybrid approaches have revealed a number of proteins that can interact with Class I PI3K subunits, domains or fragments[106],[107]. Knowledge of proteins that interact with endogenous Class I PI3Ks *in vivo*, is, however, very limited. The primary reasons for this deficiency in knowledge are the lack of efficient immunoprecipitating antibodies, the long-timescale of immunoprecipitation/wash protocols leading to loss of the majority of dynamically interacting proteins and the simple fact that endogenous Class I PI3Ks are very low abundance proteins (5-20nM) in most of the tissues[19].

To address this issue, Dr Tamara Chessa (BI) constructed genetically-modified mouse-models which allowed very efficient pulldown of individual, biotinylated, endogenous subunits of Class IA PI3Ks [19]. To achieve this, a 17aa Avitag, was "knocked-in" to the C-terminus of the endogenous mouse p85α or p85β loci. In a parallel mouse strain, a 'mammalised' (in terms of codon usage) version of the biotin ligase, BirA, was inserted into the endogenous ROSA26 locus, providing developmentally-early, strong, ubiquitous expression of the transgene. BirA recognises a 15aa consensus sequence, contained with the 17aa Avitag, as a substrate and can biotinylate it efficiently. This technology enabled endogenous, Avitagged-p85α and p85β, but not wild-type p85$\alpha$ or p85$\beta$ to become fully biotinylated in the presence, but not the absence of BirA, *in vivo.* Furthermore, biotinylated versions of Avitagged p85$\alpha$ and p85$\beta$, but not wild-type p85$\alpha$ or p85$\beta$ nor unbiotinylated, Avitagged-p85$\alpha$ or p85$\beta$, to be rapidly and efficiently pulled down from tissue or cell lysates with streptavidin agarose (there is a detailed description of the Avitag technology in section 1.6 The Avitag system). Importantly, Avitagged and/or biotinylated versions of p85$\alpha$ or p85$\beta$ were expressed at identical levels to wild-type p85$\alpha$ or p85$\beta$. This system was applied to study the network of Class IA PI3K interactors in healthy prostate and prostate going through tumorigenesis. p85α$^{Avi/Avi}$ BirA$^{+/-}$ and p85β$^{Avi/Avi}$ BirA$^{+/-}$ mice were crossed with a *Pten* $^{loxP/loxP}$ PbCre$^{+/-}$ mouse strain with prostate epithelial cell-specific deletion of *Pten* (*Pten* $^{-/-}$). Comparison of the Class I PI3K

interactomes in healthy and *Pten* $^{-/-}$ prostate revealed striking differences. The insulin receptor substrate 1 (IRS1) showed a marked decrease in interaction with biotinylated p85$\alpha^{Avi/Avi}$ and p85$\beta^{Avi/Avi}$ in *Pten* $^{-/-}$ compared to wild-type prostate. In contrast, interactions between biotinylated p85$\alpha^{Avi/Avi}$ and p85$\beta^{Avi/Avi}$ and Actin Filament Associated Protein 1-Like 2 (Afap1l2), Pleckstrin homology domain-containing family S member 1 (*PLEKHS1*, or C10orf81), B cell adaptor protein (BCAP), Colony stimulating factor 1 receptor (Csf1R) and PI3K$\delta$ were significantly increased in *Pten* $^{-/-}$ compared to wild-type tissue (Figure 1.3 A). Analysis of the cellular distributions of these molecules strongly suggested that BCAP, PI3K$\delta$ and CSF1R are not significantly expressed in prostate epithelial cells but strongly expressed in a variety of immune cells and hence their increased interactions with biotinylated p85$^{Avi/Avi}$ constructs in the absence of PTEN was a result of increased infiltration of immune cells into the *Pten* $^{-/-}$ tissue (note, the BirA and p85$^{Avi}$ constructs were ubiquitously expressed). In contrast, PLEKHS1 and AFAP1L2 are clearly expressed in prostate epithelial cells and more weakly in immune cells and hence their increased recovery with p85$^{Avi/Avi}$ pulldowns from *Pten* $^{-/-}$ tissue

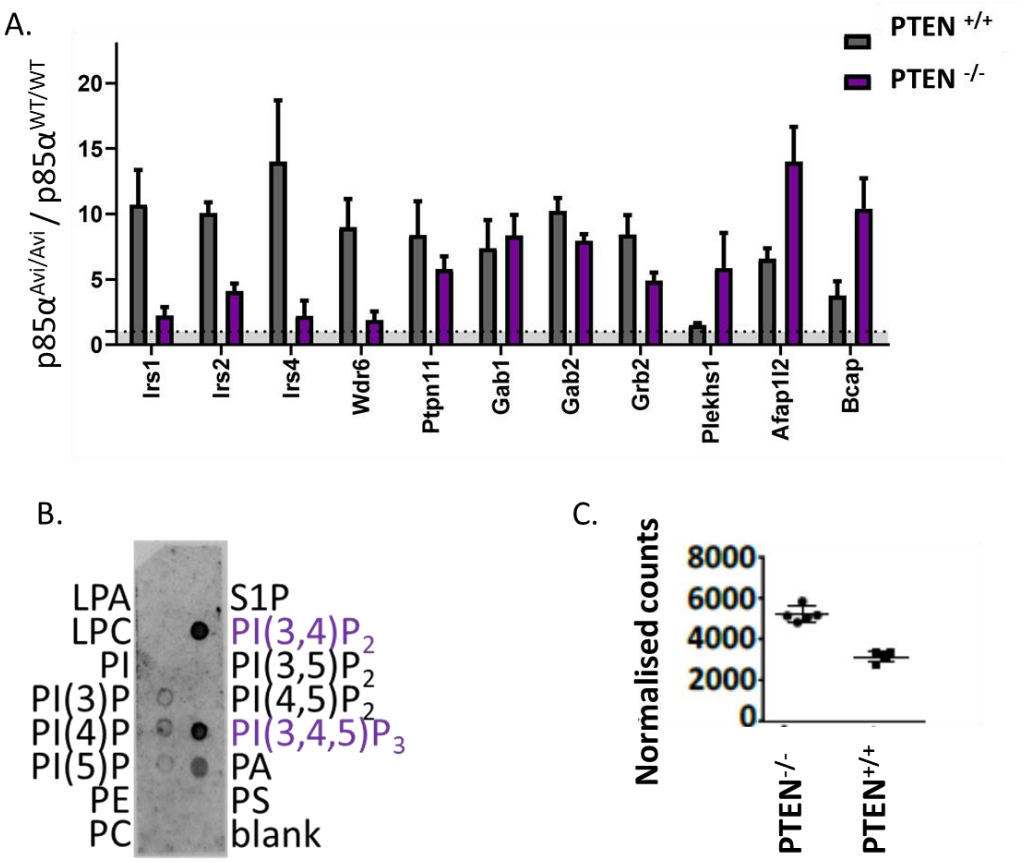

**Figure 1.3 Quantification of the abundance ratios of p85α interactors in $PTEN^{+/+}$ and $PTEN^{-/-}$ mouse prostate and primary characterisation of PLEKHS1**

A. *Mass Spectrometry measurements of proteins recovered in streptavidin-mediated pulldown of biotinylated $p85\alpha^{Avi/Avi}$. Graph shows relative abundance ratios ($^{Avi/Avi}/^{WT/WT}$) of p85α interactors (T. Chessa, unpublished data)*
B. *Lipid blots showing the isolated PH domain of PLEKHS1 (iPH) binds selectively to $PI(3,4)P_2$ and $PI(3,4,5)P_3$ (T. Chessa, M. Wilson, unpublished data)*
C. *Levels of Plekhs1 mRNA in $PTEN^{+/+}$ and $PTEN^{-/-}$ mouse prostate (C. Sandi, S.Pacey, S. Cosulich, unpublished data)*

likely reflects an increase in their association in prostate epithelial cells. One of the hypothesis explaining contrary abundance of Plekhs1 and IRS1 in *Pten*-WT vs *Pten*-KO samples is that PLEKHS1 potentially substitute for IRS in the 'cancerous' sample. To address this question, our lab is planning to use insulin receptor inhibitor and investigate changes in PLEKHS1-PI3K interaction and $PIP_3$ level.

Further studies showed that PLEKHS1 contains a PH domain which can bind to Class I PI3K lipid products: $PI(3,4)P_2$ and $PI(3,4,5)P_3$ (Figure 1.3B) and a conserved YXXM motif (mouse Y258) which when tyrosine phosphorylated could potentially bind to the SH2 domain of the regulatory subunits of Class IA PI3K (section below). Interestingly, the levels *Plekhs1* mRNA decreased in the absence of PTEN, despite PLEKHS1-p85 interaction increasing in *Pten* $^{-/-}$ prostate (Figure 1.3C).

## 1.5.1 PLEKHS1 in physiology

PLEKHS1 is a very poorly characterised protein. There are homologues in human, mice, rats, chicken, and zebrafish (Figure 1.4). In the mouse genome, it is located in chromosome 19 and contains 16 exons[108]. The human analogue of PLEKHS1 contains 8 tyrosine residues at sites 11, 20, 56, 57, 107, 209, 249 and 347, including a canonical ...YXXM... motif (Y249), which can be bound by the SH2 domains of Class IA PI3Ks. Point

mutation of Y249 to F has been shown to inhibit binding of PLEKHS1 to p55γ (PIK3R3). It has also been shown, that point mutation of the C-terminal SH2 domain of p55γ abolishes its ability to bind tyrosine phosphorylated PLEKHS1[109] [108]. PLEKHS1 in mouse is characterised by 11 tyrosine residues at points 17, 26, 61, 62, 113, 133, 217, 218, 258 and 369, where Y258 represents the canonical YXXM motif. In humans, rodents, chicken and zebrafish the PH domain is well conserved, whereas the p85 recognition motif although identical between rat, mouse and chick is not present in zebrafish[108]. This information indicates PLEKHS1 may fulfil quite different roles in particular vertebrate groups.

The closest relatives to PLEKHS1 are the GAB-family of adaptors (GABs1-4)[110]. GAB1 and GAB2 are the best studied and contain a $PIP_3$-binding PH domain and tyrosine within YXXM consensus sequences. They function as adaptor proteins that become tyrosine phosphorylated following growth factor stimulation in many cell types and can bind and activate Class IA PI3Ks via the SH2 domains in the PI3K regulatory subunits[111]. Detailed analysis of the role of GAB1 suggested that binding $PIP_3$ moves it to the plasma membrane and augments its tyrosine phosphorylation. This creates a positive feedback loop that increases the $PIP_3$ levels achieved following receptor activation[112].

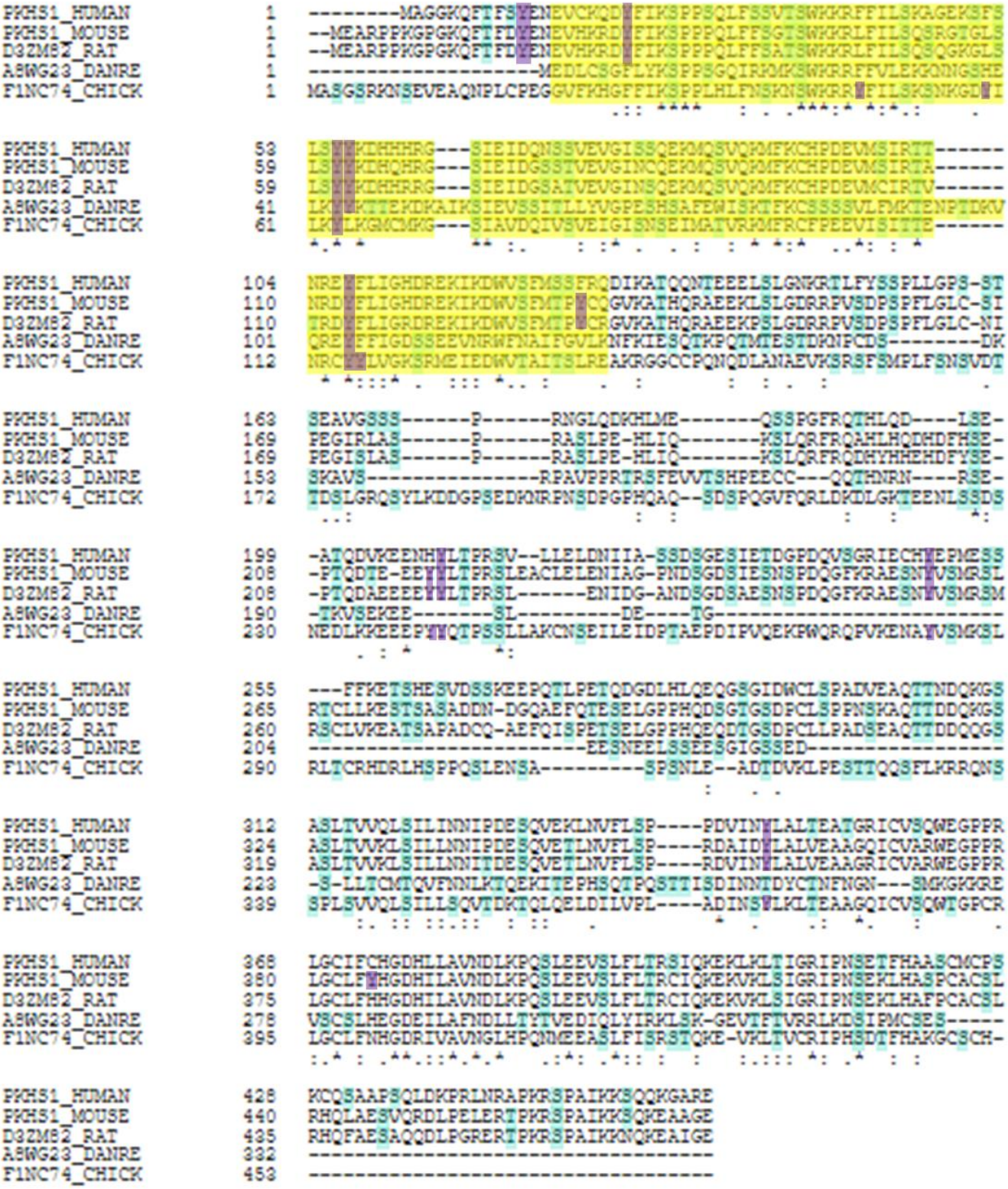
PKHS1_HUMAN
PKHS1_MOUSE
D3ZM82_RAT
A8WG23_DANRE
F1NC74_CHICK

**Figure 1.4 Alignment of Plekhs1 amino acid sequence between human, mouse, rat, zebrafish and chicken**

*Full amino acid sequences of Plekhs1 from 5 species were aligned in order to compare certain regions of the protein. The PH domain is highlighted in yellow, serine/threonine motifs are highlighted in blue and tyrosine motifs are highlighted in purple.*
*Alignment of Plekhs1 sequence was performed in web-based Uniprot software*

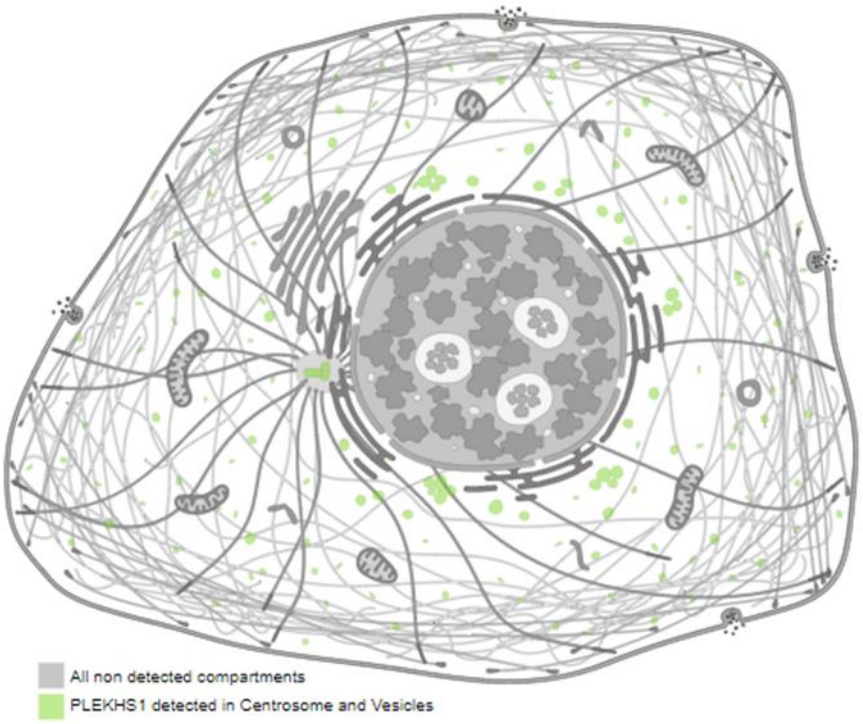


**Figure 1.5 Intracellular localisation of Plekhs1**

*Schematic showing localisation of Plekhs1 based*
*On immuno-localisation approaches in different 3 different human cell lines: A-431, RT4 and U-2 OS (using HPA037583 antibody, Sigma Aldrich). In A-431 (low RNA expression level) and U-2 OS(low RNA expression level) Plekhs1 is localised solely in centrosomes, in RT-4(high RNA expression level) Plekhs1 is localised in centrosomes and vesicles.*
*Adapted from The Human Protein Atlas*

Several human cell lines, including A-431(epidermoid carcinoma), RT4 (urinary balder papilloma cell line) and U-2-OS (osteosarcoma) were observed to be enriched in PLEKHS1 protein in particular organelles: centrosomes and cellular vesicles (Figure 1.5) [113]. A number of publicly-available datasets such as HPA, GTE or Fantom5 include data for PLEKHS1 in their repositories of mRNA levels in different tissues and cell lines. In Figure 1.6 the normalised expression data for human PLEKHS1 is shown that is based on the above-mentioned datasets. Based on this published data, there are six areas with the highest *PLEKHS1* transcript levels in humans: proximal digestive track (especially salivary gland), gastrointestinal track (highest in small intestine, colon and duodenum), female tissues (highest in breast and uterus), pancreas, and male tissues (highest in ductus deferens, seminal vesicles and prostate)[113]. There are no equivalent data sets for mouse *Plekhs1* in the Human Protein Atlas website, therefore we used the BioGPS web-based software along with EMBL database (which include the Fantom5 dataset) to analyse *Plekhs1* transcript levels in various mouse tissues (BioGPS dataset shown in Figure 1.7). Based on the data provided in the above databases, the following tissues could be defined as expressing relatively substantial amounts of *Plekhs1* mRNA: prostate, bladder, genital fat pad, subcutaneous fat, ovaries and uterus. These publicly available data are good indicators of potential protein expression, although inconsistencies between the different datasets and the non-linear correlation between mRNA and protein expression demands wider studies to clarify the relative expression of Plekshs1 across different tissues and cell types[108 114].

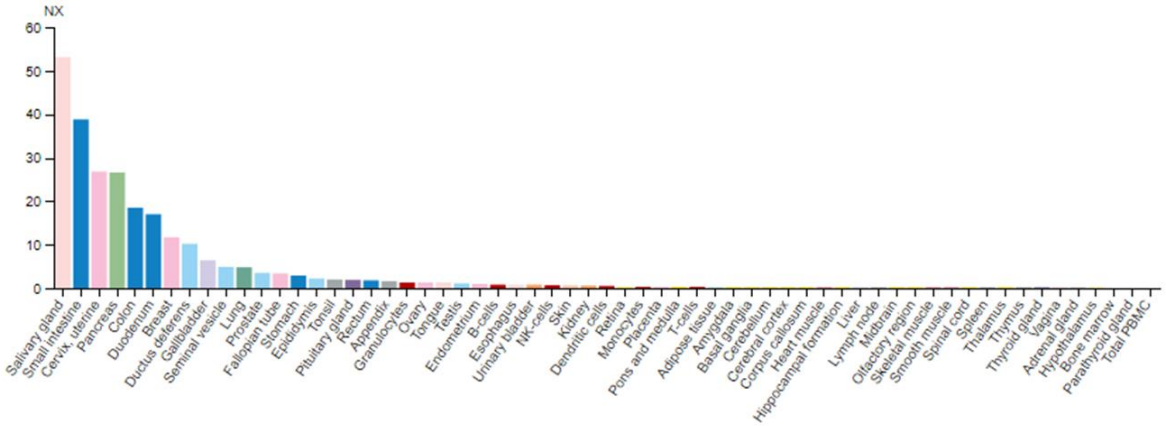

**Figure 1.6 Profiled gene expression from a diverse array of normal tissues, organs and blood cell types in human.**

*Consensus Normalised eXpression (NX)RNA expression levels for 55 tissue types and 6 cell types, created by combining the data from three trasncriptomic datasets (HPA, GTEx and FANTOM5). Color-coding is based on tissue groups, each consisting of tissues with functional features in common.*

*Adapted from The Human Protein Atlas*

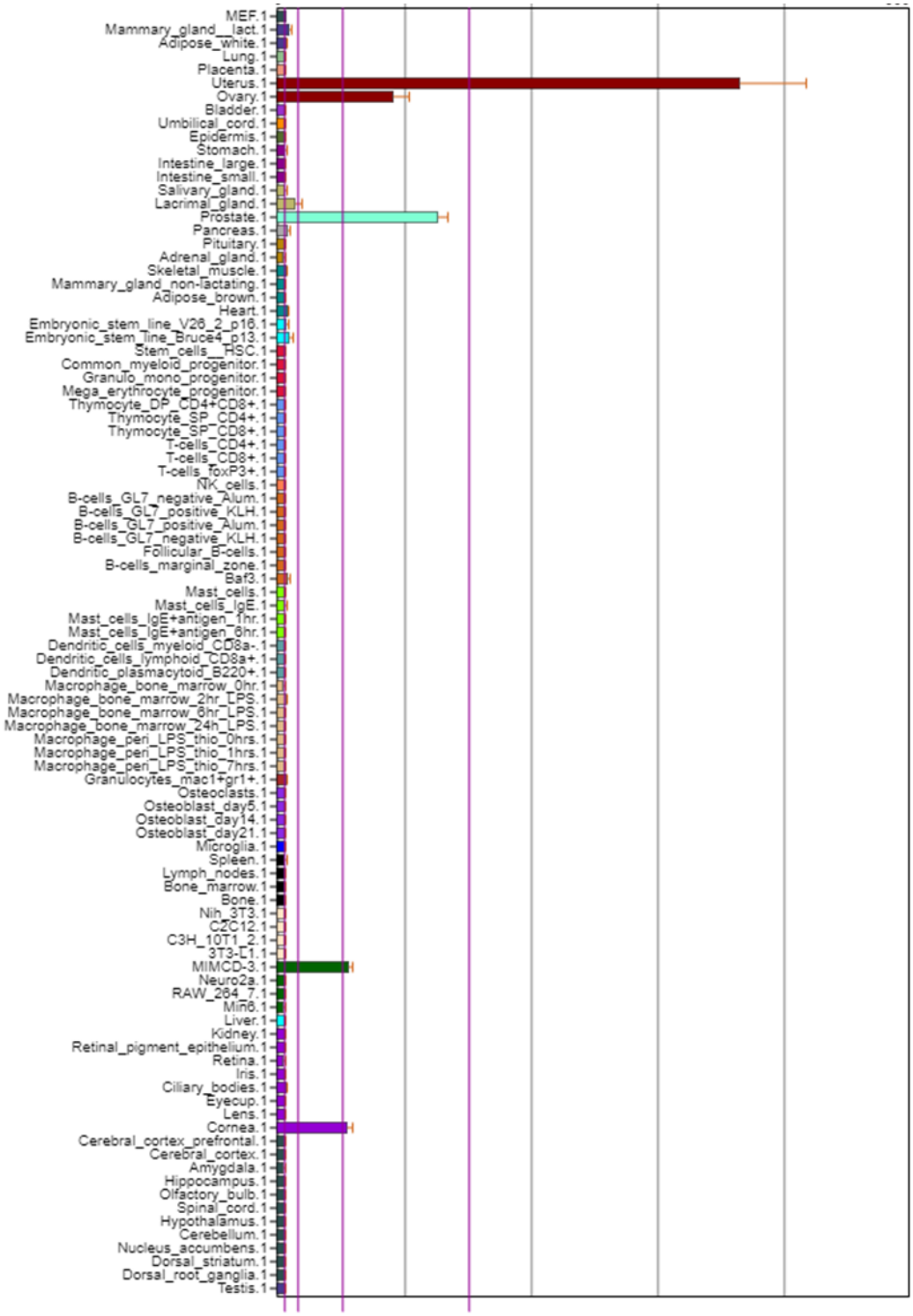
MEF.1
Mammary_gland__lact.1
Adipose_white.1
Lung.1
Placenta.1
Uterus.1
Ovary.1
Bladder.1
Umbilical_cord.1
Epidermis.1
Stomach.1
Intestine_large.1
Intestine_small.1
Salivary_gland.1
Lacrimal_gland.1
Prostate.1
Pancreas.1
Pituitary.1
Adrenal_gland.1
Skeletal_muscle.1
Mammary_gland_non-lactating.1
Adipose_brown.1
Heart.1
Embryonic_stem_line_V26_2_p16.1
Embryonic_stem_line_Bruce4_p13.1
Stem_cells__HSC.1
Common_myeloid_progenitor.1
Granulo_mono_progenitor.1
Mega_erythrocyte_progenitor.1
Thymocyte_DP_CD4+CD8+.1
Thymocyte_SP_CD4+.1
Thymocyte_SP_CD8+.1
T-cells_CD4+.1
T-cells_CD8+.1
T-cells_foxP3+.1
NK_cells.1
B-cells_GL7_negative_Alum.1
B-cells_GL7_positive_KLH.1
B-cells_GL7_positive_Alum.1
B-cells_GL7_negative_KLH.1
Follicular_B-cells.1
B-cells_marginal_zone.1
Baf3.1
Mast_cells.1
Mast_cells_IgE.1
Mast_cells_IgE+antigen_1hr.1
Mast_cells_IgE+antigen_6hr.1
Dendritic_cells_myeloid_CD8a-.1
Dendritic_cells_lymphoid_CD8a+.1
Dendritic_plasmacytoid_B220+.1
Macrophage_bone_marrow_0hr.1
Macrophage_bone_marrow_2hr_LPS.1
Macrophage_bone_marrow_6hr_LPS.1
Macrophage_bone_marrow_24h_LPS.1
Macrophage_peri_LPS_thio_0hrs.1
Macrophage_peri_LPS_thio_1hrs.1
Macrophage_peri_LPS_thio_7hrs.1
Granulocytes_mac1+gr1+.1
Osteoclasts.1
Osteoblast_day5.1
Osteoblast_day14.1
Osteoblast_day21.1
Microglia.1
Spleen.1
Lymph_nodes.1
Bone_marrow.1
Bone.1
Nih_3T3.1
C2C12.1
C3H_10T1_2.1
3T3-L1.1
MIMCD-3.1
Neuro2a.1
RAW_264_7.1
Min6.1
Liver.1
Kidney.1
Retinal_pigment_epithelium.1
Retina.1
Iris.1
Ciliary_bodies.1
Eyecup.1
Lens.1
Cornea.1
Cerebral_cortex_prefrontal.1
Cerebral_cortex.1
Amygdala.1
Hippocampus.1
Olfactory_bulb.1
Spinal_cord.1
Hypothalamus.1
Cerebellum.1
Nucleus_accumbens.1
Dorsal_striatum.1
Dorsal_root_ganglia.1
Testis.1

**Figure 1.7 Profiled gene expression from a diverse array of normal tissues, organs and cell lines in mouse**

*Gene expression profiling of mouse tissue, organs and cell lines based of Gene Atlas database*

*Adapted from The BioGPS database*

### 1.5.2 PLEKHS1 in Pathology

*PLEKHS1* has been repeatedly identified as a very strong hit in genome-wide screens for somatic mutations in non-coding regions of the genome that are potentially driving cancer.[115 116 117 118]. Weinhold et. al.[115] analysed The Cancer Genome Atlas datasets, and focused on mutations in the non-coding genome. They discovered evidence of a "hot spot" of mutations in the first intron of the *PLEKHS1* locus along with other mutational "hot spots" in the none-coding regions in WDR74, SDHD and TERT. There are 2 prominent residues that form the "hot spot" in the regulatory region of *PLEKHS1*. Both of them were observed to be predominantly cytosine to thymidine transitions, furthermore, both of the sites are flanked by 10bp palindromic sequences. This mutational hotspot was identified in 5 different cancer types and was at its most striking in bladder cancer where 40% of the cancers that were analysed carried mutations at this site[116]. Interestingly, in an early study it appeared that hot spot-mutant versions of *PLEKHS1* appeared to have lower expression of *PLEKHS1* mRNA[115]. However, further studies have failed to reproduce this observation and found no correlation between the presence of *PLEKHS1* hot spot mutations and the abundance of its mRNA[116]. Following this study, other groups have investigated *PLEKHS1* association with bladder cancer. Pignot et. al. focused on promoter mutations and *PLEKHS1* mRNA expression in a cohort of 335 bladder tumours. 162 of them represented non-muscle-invasive bladder cancer (NMIBC, 71 males and 91 females) and 173 muscle-invasive bladder cancers (MIBC, 83 males and 90 females). DNA mutational analysis, performed in two series of samples showed that 25% and 33% of NMBIC and 32.2% and 37.8% of MIBC had mutations in *PLEKHS1* in the first and second series respectively. The mutations occurred in two genomic positions, with transitions from G to A/C and C to A/T/G. Importantly, there is no significant change in the type of mutation between NMIBC and MIBC. Additionally,

the mutation profile was not directly correlated with clinical parameters of patients. *PLEKHS1* mRNA levels did not differ between NMBIC and MIBC, although it was significantly higher in bladder cancer vs healthy bladder. Additionally, mRNA levels were not correlated with the presence of mutations in *PLEKHS1* gene in both types of cancer. High *PLEKHS1* mRNA levels were associated with poor survival prognosis of patients with NMIBC. Five and 10-year progression free survival rates (PFC) with high *PLEKHS1* mRNA were 72.4% and 38.8%, whereas with normal *PLEKHS1* mRNA expression they were 88.9% and 88.7 % respectively. This study suggested, that *PLEKHS1* mRNA level could be an independent prognostic factor of progression of NMIBC [116]. By analysing circulation-free DNA (cfDNA) in urine, Dudley, *et al.* found that around 40% of bladder cancer patients show mutations in the promotor region of *PLEKHS1*. They also demonstrated that *PLEKHS1* "hot spot" mutations were amongst the most common somatic mutations in bladder cancer and were shed into the urine[119] and may represent a route to a powerful non-invasive diagnostic tool.

Deep bioinformatics analysis of The Cancer Genome Atlas dataset from the Hepatocellular carcinoma (HCC) cohort analysed differentially expressed genes (DEGs) in this type of cancer. A functional screen of the top candidates, focusing on tumour microenvironment components (TME), revealed that the main candidates are involved in cell adhesion, immune responses and the cellular matrix. Twelve candidates, including *PLEKHS1*, were highlighted to be associated with poor prognosis of HCC. Interestingly, seven out of those twelve candidates could be used as effective prognostic factors for HCC patients, despite the fact they had not been linked to prognosis of HCC previously[120].

In another bioinformatics study, Liu *et. al.* concentrated on differentially expressed genes (between diseased and healthy tissue) associated with pathogenesis and prognosis of gastric cancer in humans. In survival analyses, the *PLEKHS1* was highlighted as one of the protective prognostic genes because higher differential expression of *PLEKHS1* was associated with a better prognosis than relatively lower differential expression [121].

Kotoh et. al. [122], in their studies, used The Otsuka Long-Evans Tokushima Fatty rats (OLETF) [123], which develop symptoms similar to those in type 2 diabetes, and crossed

them with a Leptin receptor null strain of rats ($LepR^{-/-}$). Rats from these crosses that were homozygous for both "mutant loci" were obese and compared with wild-type lean rats. The expression of 41 genes in livers isolated from animals 60min after glucose loading were measured. One of the genes with the most significant differential increase in mRNA levels in obese vs lean animals was *Plekhs1*, along with Prdx, Acs15 and Vtila. In addition, the *Plekhs1* mRNA levels were significantly changed between two obese rat strains but not between lean rat strains, indicating that expression of *Plekhs1* could be correlated with obesity and could be a mediator of obesity-mediated diabetes[122].

Gene Expression Profiling Interactive Analysis (GEPIA) is a web-based RNAseq database, based on two major collaborative data repositories: The Cancer Genome Atlas (TCGA) and The Common Fund's Genotype-Tissue Expression (GTEx) program. GEPIA has become a very powerful tool allowing very easy and effective data mining and provides an opportunity to perform a variety of analyses, such as expression studies, patient survival rate or correlation analyses [124]. Using GEPIA software, we performed an analysis of *PLEKHS1* expression in different cancer types paired with *PLEKHS1* expression in healthy tissue (Figure 1.8). We observed a significant increase in the level of *PLEKHS1* transcript in seven different cancer types: colon adenocarcinoma, esophageal carcinoma, lung adenocarcinoma, ovarian serous cystadenocarcinoma, rectum adenocarcinoma, stomach adenocarcinoma and uterine corpus endometrial carcinoma. Interestingly, in testicular germ cell tumours we observed lower levels of *PLEKHS1* mRNA compared to healthy tissue.

In prostate cancer, which is a subject of interest in my studies, we did not observe any significant difference in *PLEKHS1* transcript levels, although there is a strong trend suggesting higher expression in cancerous tissue. Interestingly, however, the relative levels of *PLEKHS1* mRNA in healthy prostate tissue were very high.

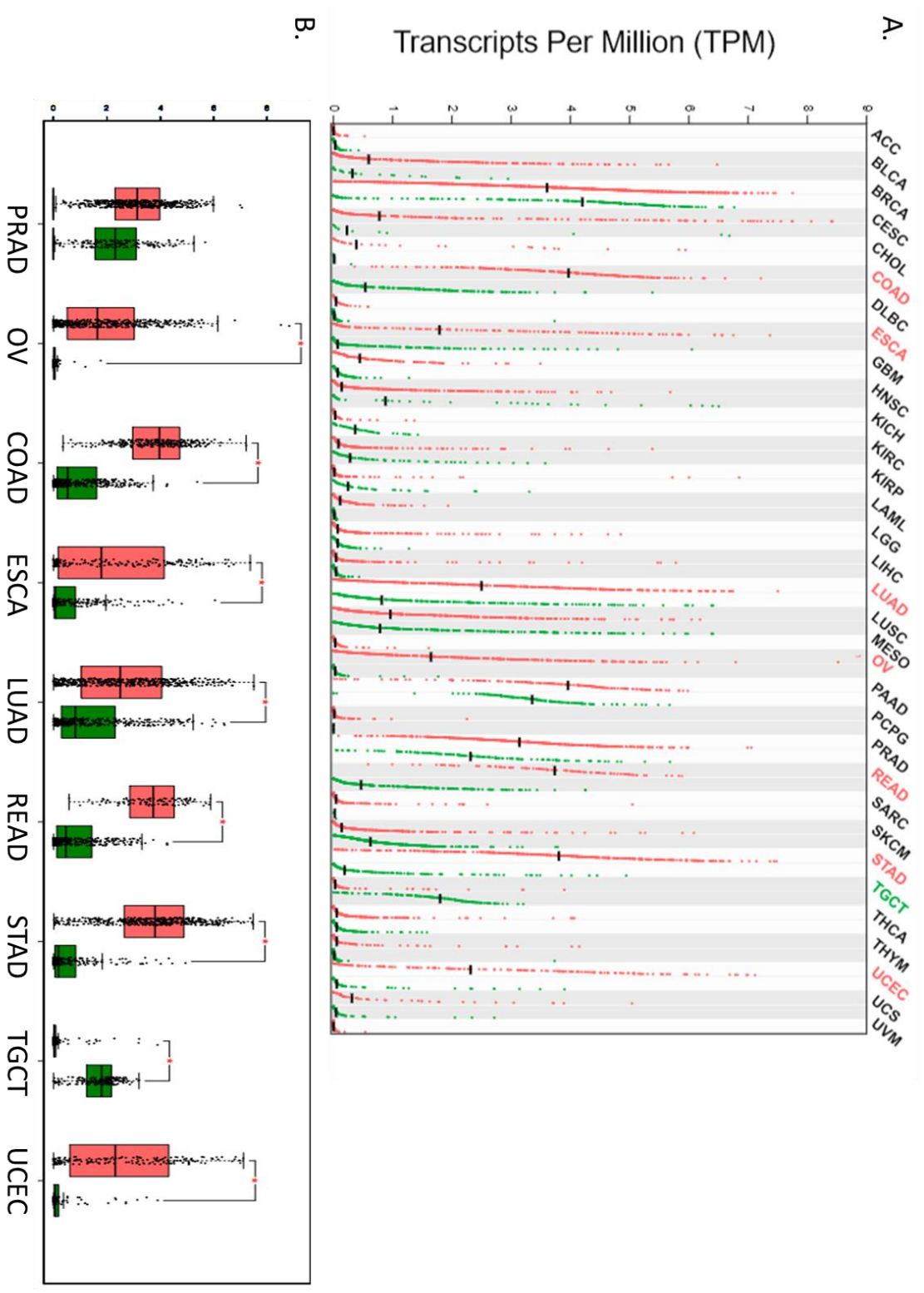
B.
PRAD
OV
COAD
ESCA
LUAD
READ
STAD
TGCT
UCEC
A.
Transcripts Per Million (TPM)
ACC
BLCA
BRCA
CESC
CHOL
COAD
DLBC
ESCA
GBM
HNSC
KICH
KIRC
KIRP
LAML
LGG
LIHC
LUAD
LUSC
MESO
OV
PAAD
PCPG
PRAD
READ
SARC
SKCM
STAD
TGCT
THCA
THYM
UCEC
UCS
UVM

C.

| Abbreviation | Cancer Type | Number of Cancer Samples | Number of Healthy Samples |
|---|---|---|---|
| ACC | Adrenocortical carcinoma | 77 | 128 |
| BLCA | Bladder Urothelial Carcinoma | 404 | 29 |
| BRCA | Breast invasive carcinoma | 1085 | 291 |
| CESC | Cervical squamous cell carcinoma and endocervical adenocarcinoma | 306 | 13 |
| CHOL | Cholangio carcinoma | 36 | 9 |
| COAD | Colon adenocarcinoma | 349 | 275 |
| DLBC | Lymphoid Neoplasm Diffuse Large B-cell Lymphoma | 337 | 47 |
| ESCA | Esophageal carcinoma | 286 | 182 |
| GBM | Glioblastoma multiforme | 207 | 163 |
| HNSC | Head and Neck squamous cell carcinoma | 519 | 44 |
| KICH | Kidney Chromophobe | 66 | 53 |
| KIRC | Kidney renal clear cell carcinoma | 523 | 100 |
| KIRP | Kidney renal papillary cell carcinoma | 286 | 60 |
| LAML | Acute Myeloid Leukemia | 173 | 70 |
| LGG | Brain Lower Grade Glioma | 518 | 207 |
| LIHC | Liver hepatocellular carcinoma | 369 | 160 |
| LUAD | Lung adenocarcinoma | 483 | 347 |
| LUSC | Lung squamous cell carcinoma | 486 | 338 |
| MESO | Mesothelioma | 87 | x |
| OV | Ovarian serous cystadenocarcinoma | 425 | 88 |
| PAAD | Pancreatic adenocarcinoma | 179 | 171 |
| PCPG | Pheochromocytoma and Paraganglioma | 182 | 3 |
| PRAD | Prostate adenocarcinoma | 492 | 152 |
| READ | Rectum adenocarcinoma | 92 | 318 |
| SARC | Sarcoma | 262 | 2 |
| SKCM | Skin Cutaneous Melanoma | 461 | 558 |
| STAD | Stomach adenocarcinoma | 408 | 211 |
| TGCT | Testicular Germ Cell Tumors | 137 | 165 |
| THCA | Thyroid carcinoma | 512 | 337 |
| THYM | Thymoma | 118 | 339 |
| UCEC | Uterine Corpus Endometrial Carcinoma | 174 | 91 |
| UCS | Uterine Carcinosarcoma | 57 | 78 |
| UVM | Uveal Melanoma | 79 | x |

**Figure 1.8 Gene expression profiles across all tumour samples and their paired normal tissues**

A. *Dot plots representing the level of Plekhs1 mRNA in different tumour types in comparison to relevant healthy tissue. Cancerous and healthy tissues are shown in red and green, respectively (in the Figure). Significant over-expression and under-expression of Plekhs1 mRNA in particular cancer types are marked in red and green respectively (to the right of the Figure). The data are combined from the TCGA and GTEx data bases and shown in $log_2$ scale, where each dot represents one sample.*
B. *Box plots representing the level of Plekhs1 mRNA in prostate and tissues with a significant difference in expression between healthy (green) and cancerous (red) samples. The data combined from the TCGA and GTEx data bases and shown in $log_2$ scale, where each dot represents one sample.*
C. *List of cancer types and their abbreviations that were used in the analyses of Plekhs1 expression shown in (A) and (B), with number of samples.*

*Adapted from the GEPIA database*

# 1.6 The Avitag system

## 1.6.1 Avitag Technology

The interaction between streptavidin and biotin is one of the strongest interactions known in nature, which clearly explains why it has been used in research for decades. Its application has increased in recent years due to the discovery of the biotin ligase BirA in Escherichia Coli[125]. BirA has been demonstrated to efficiently and highly selectively biotinylate a 15-amino acid sequence (GLNDIFEAQKIEWHE) that can be fused to other proteins and act as a tag (Avitag)[126]. The biotin-Avitag system has been used in protein detection, protein purification, fluorescence imaging and protein-protein interactions. The technology makes it possible to study protein-protein interactions without using antibody-based methods [127]. Target proteins can be Avitagged on either the N- or C-terminus. In the case of N-terminal fusions a starting codon ATG, which is followed by Ser or Ala to confer protein stability, needs to be included in the coding sequence. It is

very common to add a short linker, preferably Gly-Gly when adding an Avitag to the C-terminus of a target protein[128].

Avitagged proteins can be biotinylated *in vivo* when co-expressed with BirA. Once biotinylated in vivo, the proteins can be retrieved using various forms of streptavidin reagent (including magnetic streptavidin beads), which specifically binds to biotin [129].

#### 1.6.1.1 Biotin

Biotin is a small molecule (244.3 Daltons) classified as a vitamin, widely known as a Vitamin H, Vitamin B7 or Coenzyme R. It is present in most living cells and tissues with corn kernels, egg yolk, liver, blood, and brain being particularly rich sources. Because of its compact size it can be easily conjugated to many proteins and molecules without affecting their functions. The specificity and affinity with which it is bound by streptavidin makes it a very useful tool in research [130] [131] [132].

#### 1.6.1.2 Avidin

Avidin is a 67kDA protein, which plays an antibacterial role in the eggs of birds, amphibians, and reptiles. A characteristic feature of this molecule is its tetrameric structure, based on four 128 amino acid arms, such that the tetramer can bind to a maximum of four molecules of biotin. Once avidin reacts with biotin they make a stable complex resistant to temperature and pH changes. Avidin is widely modified without affecting its function and this adds another major point to its list of advantages. It has become a very useful tool in detecting proteins and their interactors in a variety of conditions [133].

#### 1.6.1.3 Streptavidin

Streptavidin is 60kDA protein, extracted from *Streptomyces avidinii*. Similar to avidin, it has high affinity for biotin, and probably acts as an antibiotic in the eggs of different organisms. It has lower acidic isoelectric point than avidin (PI=5, whilst avidin is pI=10-10.5) and it is characterised by lack of glycosylation, which makes it less prone to problems with proteins none-specifically binding to glycoprotein moieties, and is hence the preferred binding protein in many detection systems [131].

### 1.6.2 Advantages and Disadvantages of the BirA/Avitag system

The BirA/Avitag system has a number of strengths, however, like any other technology this one also has some limitations.

As mentioned previously biotin-streptavidin is one of the strongest non-covalent interactions in biology and the reaction is very rapid, and only weakly affected by temperature and pH changes. The streptavidin-biotin system has many applications beyond pulldowns: ELISA, immunohistochemistry, western, Southern and northern blotting and FACS.

Biotin is an endogenous vitamin, present in most of the tissues, and the presence of endogenous biotin and/or endogenous biotinylated proteins can cause problems with background[134]. However only a relatively small set of well-described proteins are biotinylated in most mammalian cells (e.g. carboxylases). In addition, the strength of the biotin/streptavidin bond can also be a limitation in some settings. For example, it is very difficult to efficiently elute biotinylated proteins from streptavidin reagents without harsh, denaturing reagents like hot SDS-sample buffer. A variety of commercial reagents have been developed that are reputed to allow elution under “native” conditions, but in our labs experience these only allow very small proportions of the bound protein to be eluted. Finally, streptavidin-containing matrices used in pulldown experiments bind none-specifically to a significant number of cellular proteins despite a range of washing protocols. These can be almost entirely removed through use of very stringent washing conditions (e.g., high salt, low concentrations of SDS, detergents like cholate) because of the tenacity of the biotin-streptavidin interaction, however, these conditions would elute all but the most high-affinity potential interactors from the biotinylated target. Hence, in experiments aimed at capturing potentially low-affinity interactors with high on-off rates, it is necessary to use relatively mild washing conditions that will leave a significant number of none-specific background proteins that will be detected by a proteomic analysis. This problem exists with all current pulldown technologies, however, some, e.g. GFP and nano-trap that are reagents based on camelid single chain antibodies; give lower background none-specific binding than streptavidin-based reagents.

A number of differential-labelling techniques have been evolved to mitigate against the

problems created by none-specific recovery of proteins in pulldowns that are to be subject to proteomic analysis. The underlying principle is that experimental samples (e.g. cells expressing an endogenous tagged protein) can be prepared in parallel with controls under exactly the same conditions (e.g. cells expressing the same amount of a wild-type untagged protein) then lysed, mixed and subjected to pulldown, washing and work-up for proteomic analysis in the same tube. By use of bar-coding strategies (most simply in SILAC (Stable Isotope Labelling with Amino Acids in Cell Culture) experiments by growing the cells destined for the control v experimental samples to a state of isotopic equilibrium with "heavy" v "light" non-radioactive isotope-labelled amino acids) all proteins from the control samples can be distinguished from the proteins in the experimental samples by the mass spectrometry step in the proteomics protocol on the basis of their precise mass shift. By analysing the ratio of the abundance of proteins recovered in a pulldown from the experimental v control samples it is possible to identify the target protein (that should only be significantly recovered in the experimental sample) and any specific interactors as significantly enriched compared to none-specific interactors on the basis of a substantial and quantifiable shift in that ratio. Although these types of experiments have proven to be extremely robust and are now the preferred route through which cutting-edge proteomic labs resolve none-specific from specific protein interactions, they can be extremely costly when applied to mice. Some alternative approaches that rely on the same underlying principle of sample-specific bar-coding have been evolved that can be applied in proteomic analyses of protein fractions from tissues. One of these is called TMT labelling.

## 1.7 TMT Labelling

Mass Spectrometry has developed from being a methodology used to perform qualitive analysis of proteins to being a powerful tool for quantification of proteins isolated from tissues or cells[135]. One of the reagents used for quantitative proteomics are isobaric (or Tandem) mass tags (TMT). In 6-plex, 10-plex, 11-plex and 16-plex TMT strategies peptides derived from individual samples are labelled with uniquely-coded probes (unique within the sets of 6, 10, 11 or 16 probes; at the time at which the experiments presented in this thesis were performed the maximum-plex library available was 11) that

all have the same mass and hence can be captured together in the first phase of the mass spectrometry process (MS1).

Before labelling samples with TMT reagents, a sample of cells or tissue are lysed, pulled down with streptavidin beads, eluted, reduced, alkylated and digested to generate peptides. The peptides are then labelled with a selected TMT reagent (e.g., if the experiment is 6-plex it will be with one of family of six isobaric 6-plex probes). The labelled samples are mixed together, fractionated and cleaned-up prior to mass spectrometry. In a sample that is derived from two different samples (experimental/control) that have been generated in parallel and chemically-tagged with unique isobaric reagents, then a specific individual TMT-labelled peptide will have two experimental/control counterparts. The two counterparts will have identical masses (because the underlying peptides are identical and the two unique chemical tags are isobaric) and will hence remain together through the MS1 sector of the mass spectrometer. After MS2 fragmentation each TMT tag gives rise to a specific reporter with a unique mass that allows for separate quantification of the two versions (experimental/control) of the peptide. Quantifying data in terms of the ratios of abundance of the differently tagged versions of a given peptide in a sample gives very robust data that very clearly resolve specific from none-specific interactors in a manner not dissimilar to SILAC-based approaches.

This type of TMT-labelling approach can be used in a number of settings, including; analysis of protein expression levels, protein-protein interactions, chemo-proteomic target studies, cell signalling studies and biomarker studies [136] [137] [138] [139].

## 1.8 Lipidomics and lipid extraction

Individual phosphoinositides, like all phospholipids, are, despite having a single head-group structure, all made up of a collection of molecular species variants based on differing acyl chain compositions. Dogma suggests that stearoyl/arachidonoyl species of phosphoinositides are the most abundant in mammalian tissues. The molecular explanation for this differential accumulation of stearoyl/arachidonoyl-species remains unclear as does its physiological function [140].

It is possible to identify and measure the different molecular species variants of

phosphoinositides, including $PIP_3$, using mass spectrometry-based lipidomics methodologies. When analysed with these techniques molecular variants of a phosphoinositide are most simply defined by the precise mass of their acyl chains and that, combined with knowledge of the underlying biochemistry and data bases of lipid species known to be present in mammalian tissue, allows them to be assigned as containing a number of carbons and double bonds. Hence a stearoyl/arachidonoyl species would be measured as a C38:4 (number of carbons: number of double bonds) in the absence of any further structural information (e.g., from further fragmentation in the mass spectrometer) but could be recognised as very likely to be C18:0/C20:4 (Sn-1, stearoyl/Sn-2, arachidonoyl) on the basis of precedent and much past analytical work. However, when a more unusual molecular species variant is identified, particularly in an unusual biological context, then it is appropriate to rely less on assumptions and adhere to a more limited description of a species (e.g. C34:1) until further work has refined that assignment.

Using these types of methods recent publications have shown that a large variety of molecular species of $PIP_3$ can be detected in cells and tissues and, very broadly, they appear to reflect the molecular species found in the $PIP_2$, PIP and PI species also present in those locations [141] [142]. Unpublished work in our lab, however, has shown that unexpectedly the major species of $PIP_3$ that accumulates in *Pten* $^{-/-}$ mouse prostate tissue is C34:1; other species are present, including C38:4-$PIP_3$, but they are quantitatively more minor[143]. This pattern of enrichment, although less striking can also be seen in $PIP_2$ in *Pten* $^{-/-}$ mouse prostate. The reason for this unusual acyl chain profile remains unclear but is the subject of a major on-going research project in the lab (D.Barneda, unpublished work).

## 1.9 Hypothesis and aim of the project

The primary aim of my project was to understand the functions and interactions of PLEKHS1 through the process of prostate tumorigenesis. My studies predominantly used a mouse model in which tumour progression is driven by conditional deletion of *Pten* in the prostate (PbCre x *Pten* $^{loxP/loxP}$) and focused on 12 week-old animals that are predominantly at a PIN or tissue-hyperplasia stage of carcinogenesis.

To address these aims I attempted to apply Avitag technology and generate mice

expressing endogenous Avitagged *Plekhs1* (*Plekhs1*$^{Avi/Avi}$) and BirA. By integrating these genetic tools into the PbCre x *Pten* $^{loxP/loxP}$ model I planned to define the protein interaction network of PLEKHS1 and how it changed during prostate tumour progression. To study the function of PLEKHS1 I aimed to generate *Plekhs1*$^{-/-}$ mice and again integrate these into the PbCre x *Pten* $^{loxP/loxP}$ model. These powerful tools will give me an opportunity to study the function of PLEKHS1 in Class IA PI3K signalling and more broadly in health and during prostate tumour progression.

The core working hypothesis underpinning my work was that PLEKHS1 plays a dual role in Class IA PI3K signalling pathway. It can act as a classical YXXM-containing adaptor, that, when tyrosine phosphorylated, can bind and activate Class IA PI3Ks. In addition, it contains a PH domain that binds to $PIP_3$. We speculate, on the basis of what is known of signalling via the GAB-family of Class IA PI3K adaptors, that upon $PIP_3$ binding PLEKHS1 is more efficiently tyrosine phosphorylated and hence constitutes a positive-feedback loop driving further activation of $PIP_3$ signalling. Hence, given that the amount of Class IA PI3K-associated PLEKHS1 increases dramatically in *Pten* $^{-/-}$ prostate, in contrast to the major physiological IRS-family adaptors, this could mean that PLEKHS1 becomes a major determinant of $PIP_3$-network activity in the absence of PTEN. This property could drive the Class I PI3K signalling network to be less dependent on cell surface receptor inputs and could constitute a potential advantage for cancer cells.

# 2 MATERIALS AND METHODS

## 2.1 Materials

**Table 2.1 Used Antibodies**

| ANTIBODY | SOURCE | CATALOG # | USED DILUTION |
|---|---|---|---|
| **Anti-phospho-Akt (S473)** | Cell Signaling | 4060 | 1:1000 |
| **Anti-phospho-Akt (T308)** | Cell Signalling | 5106 | 1:1000 |
| **Anti-β-COP** | Babraham Institute | Nick Ktistakis, BI | 1:200 |
| **Anti-Plekhs1** | Santa Cruz | 240003 | 1:200 |
| **Anti-Plekhs1** | Santa Cruz | 240005 | 1:200 |
| **Anti-Akt** | Cell Signalling | 9272S | 1:1000 |
| **Anti-p85 PAN** | Cell Signalling | 19HB | 1:400 |
| **Anti-phospo-Tyrosine** | Cell Signalling | 49411 | 1:1000 |
| **Anti-GFP** | Roche | 11814460001 | 1:2000 |
| **Anti-Avitag** | Genescript | A01738 | 1:2000 |
| **Anti-p38 MAPK** | Cell Signalling | 9212 | 1:1000 |
| **Anti-phospho p70S6K (Thr 389)** | Cell Signalling | 9205 | 1:1000 |
| **Anti-p44/42 MAPK** | Cell Signalling | 91025 | 1:1000 |
| **Anti-phospho-p38 MAPK (Thr180/Tyr182)** | Cell Signalling | 9211 | 1:1000 |
| **Anti-phospho-GSK3 (Ser 21/9)** | Cell Signalling | 9331 | 1:1000 |
| **Anti-phospho-p44/42 MAPK (Thr202/Tyr204)** | Cell Signalling | 9106 | 1:1000 |

| | | | |
|---|---|---|---|
| **Anti-p70 S6K** | Cell Signalling | 9202S | 1:1000 |
| **Anti-phospho-Src (Y416)** | Cell Signalling | 6943 | 1:1000 |
| **Anti-Avitag** | BBT | Custom order | 1:100 |
| **Donkey Anti-Goat IgG (HRP)** | Abcam | 97110 | 1:20000 |
| **Goat Anti-Mouse IgG (HRP)** | Biorad | 1706516 | 1:2500 |
| **Goat Anti-Rabbit IgG (HRP)** | Cell Signalling | 7074s | 1:2500 |
| **Anti-Phospho-Plekhs1 (Y257)** | CRB Cambridge | Custom Order | 1:500 |

**Table 2.2 Reagents**

| REAGENT | SOURCE | CATALOG # |
|---|---|---|
| **2-mercaptoethanol** | Sigma Aldrich | M7522 |
| **Acetone** | VWR chemicals | 20066.33 |
| **Anti-protease Antipain** | Sigma-Aldrich | A6191 |
| **Anti-protease Aprotinin** | Sigma-Aldrich | A1153 |
| **Anti-protease Leupeptin** | Sigma-Aldrich | L8511 |
| **Anti-protease Pepstatin** | Sigma-Aldrich | P5318 |
| **Bovine Serum Albumin** | Sigma-Aldrich | A7906 |
| **Bromophenol Blue** | Sigma-Aldrich | B8026 |
| **C17:0/C16:0-PI** | Biological Chemistry Laboratory, Babraham institute | Dr Jonathan Clark |

| | | |
|---|---|---|
| **C17:0/C16:0-$PIP_3$** | Biological Chemistry Laboratory, Babraham institute | Dr Jonathan Clark |
| **CHAPS** | Merck | CHAPS-RO |
| **Chloroform** | Romil | H140 |
| **ChromoTek GFP-Trap®** | Chromotek | gtma-400 |
| **CS-FBS** | Life Technologies | 12676-029 |
| **d6-SA_$PIP_2$ ISD** | Biological Chemistry Laboratory, Babraham institute | Dr Jonathan Clark |
| **d6-SA_$PIP_3$ ISD** | Biological Chemistry Laboratory, Babraham institute | Dr Jonathan Clark |
| **Dimethyl sulphide** | Sigma-Aldrich | 34869 |
| **Distilled water** | Life Technologies | 15230-089 |
| **DMEM/F12** | Life Technologies | 31330-038 |
| **Dneasy Blood & Tissue Kit** | Qiagen | 69504 |
| **Dulbecco's phosphate buffered saline** | Sigma-Aldrich | D8537 |
| **ECL™ Western Blotting Detection Reagents** | GE Healthcare | RPN2209 |
| **EDTA** | Sigma-Aldrich | E5134 |
| **EGTA** | Sigma-Aldrich | E4378 |
| **Fatty acid free BSA** | Sigma-Aldrich | A7906 |
| **Fetal Bovine Serum** | ThermoFischer | 10270106 |
| **Gelatin** | Sigma-Aldrich | 9391 |
| **GlutaMax/Glutamate** | Invitrogen | 35050061 |
| **Glycerol** | Invitrogen | 15514-011 |
| **Hepes** | Sigma-Aldrich | H3375 |
| **Horse serum** | PAA | B15-021 |
| **HS Polymerase** | Bioline | 21111 |
| **Human EGF** | Sigma-Aldrich | E9644 |

| | | |
|---|---|---|
| **Human insulin** | Sigma-Aldrich | I9278 |
| **KCl** | VWR Chemicals | 26764.26 |
| **KO-DMEM** | GIBCO | 10829-018 |
| **LIF** | Miltenyi Biotech | 130-095-772 |
| **Lipofectamine 2000** | Invitrogen | 11668-019 |
| **Lipofectamine 3000** | Thermo Fisher Scientific | L3000008 |
| **Lipofectamine LTX** | Thermo Fisher Scientific | 15338100 |
| **Methanol** | Romil | H410 |
| **MgCl2** | VWR Chemicals | 25108.295 |
| **Na3VO4** | Sigma-Aldrich | S6508 |
| **Na4P2O7** | Sigma-Aldrich | P8010 |
| **NaCl** | VWR Chemicals | 27810.295 |
| **NaF** | Sigma-Aldrich | S7920 |
| **Optimem** | Life Technologies | 31985-047 |
| **PBS 10x** | Life Technologies | 70011-036 |
| **Penicillin/streptomycin** | Life Technologies | 15140-122 |
| **Pierce™ BCA Protein Assay Kit** | Thermo Fisher Scientific | 23225 |
| **PMSF** | Sigma-Aldrich | 78830 |
| **Proteinase K, recombinant, PCR Grade** | Sigma-Aldrich | 3115879001 |
| **Qiagen Plasmid Plus Midi Kit** | Qiagen | 12943 |
| **QIAquick PCR Purification Kit** | Qiagen | 28104 |
| **Quikchange Lightning Site-directed Mutagenesis kit** | Agilent | 210518 |
| **Random Hexamer Primers** | Thermo Fisher Scientific | S0142 |
| **RPMI-1640** | Sigma-Aldrich | R8758 |
| **RPMI-1640 Medium (ATCC® 30-2001™)** | Sigma-Aldrich | RPMI-1640 |

| | | |
|---|---|---|
| **Src Inhibitor A 419259** | AdooQ Bioscience | A13290 |
| **Streptavidin-coupled dynabeads** | Thermo Fisher Scientific | 65305 |
| **Streptavidin-coupled dynabeads** | Thermo Fisher Scientific | SLM-242 |
| **SuperScript™ II Reverse Transcriptase** | Invitrogen | 18064014 |
| **T7 Endocuclease I** | NEB | E3321 |
| **TMS-diazomethane** | Sigma-Aldrich | 362832 |
| **Tris** | Melford | B2005 |
| **Tris-HCl** | Sigma-Aldrich | T3253 |
| **Triton** | Sigma-Aldrich | T9284 |
| **TRIzol™** | Invitrogen | 15596026 |
| **X-tremeGene 9** | Sigma-Aldrich | XTG9-RO |
| **β- glycerolphosphate** | Calbiochem | 35675 |

**Table 2.3 Resources**

| RESOURCES | MANUFACTURER | CATALOG # |
|---|---|---|
| **1.5 mL, Quick-Seal® Polypropylene Tube** | Beckman Coulter | 357323 |
| **DynaMag™-2 Magnet** | Thermo Fisher Scientific | 12321D |
| **Electroporation Cuvettes** | BTX | 45-0125 |
| **Eppendorf Safe-Lock Tubes, 2.0 mL** | Eppendorf | 30120094 |
| **Eppendorf Tubes® 5.0 mL with snap cap, 5.0 mL** | Eppendorf | 30119401 |
| **Eppendorf® LoBind microcentrifuge tubes** | Eppendorf | Z666505 |
| **GE Healthcare Amersham™** | GE Healthcare | 10534205 |

| | | |
|---|---|---|
| **Hyperfilm™ ECL** | | |
| **Glass Vials** | VWR International Ltd | 1090114 |
| **Mini-Proten Mini Electrophoresis Cell with Transblot module** | Biorad | 1658034 |
| **PVDF membranes (immobilon P)** | Millipore | IPVH00010 |
| **Sep-Pak Aminopropyl (NH2) 1 cc Vac Cartridge** | Waters | WAT023610 |
| **TMT10plex™ Isobaric Label Reagent** | Thermo Fisher Scientific | 90406 |
| **X-ray film** | Scientific Laboratory Supplies Ltd (Sls) | 1110010 |
| **Page Ruler Protein Ladder** | Thermo Fisher Scientific | 26616 |

**Table 2.4 Primers**

| PRIMERS | SEQUENCE 5' -> 3' | MANUFACTURER |
|---|---|---|
| **PLEKHS1-AVI-seq_FV2** | AGAGTCAGAAGGAAGCTGCTGG | Sigma-Aldrich |
| **Plekhs1_Avi-666_Rv** | TGTTCAGCTCACTGCCTCTCTC | Sigma-Aldrich |
| **lacZ_643_FV** | CCCATCTACACCAACGTGACCT | Sigma-Aldrich |
| **LacZ_643_Rv** | CCGCACGATAGAGATTCGGGAT | Sigma-Aldrich |
| **PLEKHS1_818_Sense1** | AGAGAGCCAAGAGGGTAAGA | Sigma-Aldrich |
| **PLEKHS1_818_Antisense1** | GCCTCTCTCTCATTCCTGATTAC | Sigma-Aldrich |
| **PLEKHS1 g1 F** | CACCGGCTGGGGAGTAGGCTACTGC | Sigma-Aldrich |
| **PLEKHS1 g1 R** | AAACGCAGTAGCCTACTCCCCAGCC | Sigma-Aldrich |
| **PLEKHS1 g2 F** | CACCGGAGTAGGCTACTGCAGGCCC | Sigma-Aldrich |
| **PLEKHS1 g2 R** | AAACGGGCCTGCAGTAGCCTACTCC | Sigma-Aldrich |

| | | |
|---|---|---|
| **PLEKHS1 g3 F** | CACCGGAAGGAAGCTGCTGGGGAG T | Sigma-Aldrich |
| **PLEKHS1 g3 R** | AAACACTCCCCAGCAGCTTCCTTCC | Sigma-Aldrich |
| **Plekfor1** | CCGATTCATATGGGCAAACAATTTAC TTTGATTATGAAAATGAAGTCC | Sigma-Aldrich |
| **Plekrev2** | AATCGGGGTACCCTCCCCAGCAGCTT CCTTC | Sigma-Aldrich |
| **Plekhs1 Y257F F** | AAGAGAGCGGAGAGCAATTTCGTGT CAATGAGATCATTG | Sigma-Aldrich |
| **Plekhs1 Y257F R** | CAATGATCTCATTGACACGAAATTGC TCTCCGCTCTCTT | Sigma-Aldrich |
| **Plekfor8** | CCGATTGCGGCCGCCCATGGAAGCC AGACCTCCAAAAGGCCCAGGCAAAC AATTTACATTTGATTATGAAAATGAA GTCC | Sigma-Aldrich |
| **Plekrev4** | GCTACCGCCTCTAGATTACTTGTACA GCTCGTCCATGC | Sigma-Aldrich |

**Table 2.2.5 Cell Lines**

| CELL LINE | SOURCE |
|---|---|
| **HeLa Cells** | Nick Ktistakis lab, Babraham Institute |
| **ES cells** | Dominik Spensberger, Gene Engineering Facility, Babraham Institute |

**Table 2.2.6 Plasmids**

| PLASMID | SOURCE | INFORMATION |
|---|---|---|
| **PCMV3-EE** | Dr Phill Hawkins, Babraham institute | pcDNA3 with and Ampicillin resistance cassette with cloned 'EE' tag |
| **Plekhs1-Wt with mGFP in PCMV3-EE vector** | Dr Tamara Chessa, Babraham Institute | Described in 2.2.8 of Materials and Methods |
| **Plekhs1-Y257F with mGFP in PCMV3-EE vector** | Dr Tamara Chessa, Babraham Institute | Described 2.2.8 of Materials and Methods |

| | | |
|---|---|---|
| **PCMV3-EE-GFP plasmid** | Dr Phill Hawkins, Babraham institute | pcDNA3 with and Ampicillin resistance cassette with cloned 'EE' tag |
| **PLNCX-chick Src K295R** | Addgene | Catalog #13659 |
| **PLNCX-chick Src Y527F** | Addgene | Catalog #13660 |

**Table 2.2.7 Used computer softwares**

| SOFTWARE | UTILITY |
|---|---|
| **Benchling.com** | Oligonucleotides design |
| **Image Studio Lite 5.2** | Western Blots quantification |
| **GraphPad Prism 8** | Statistical Analysis |
| **Proteome Discoverer** | Proteomic data analysis |
| **Perseus** | Proteomic data analysis |
| **Biorender** | Scientific pictures |

## 2.1.1 Mice

PB-Cre4 mice[144] and *Pten* $^{loxP/loxP}$ mice[72] have been described previously. PbCre4 mice and *Pten* $^{loxP/loxP}$ mice were interbred to generate 'WT' (*Pten* $^{loxP/loxP}$, PbCre$^{-/-}$) and *Pten* $^{-/-}$ (*Pten* $^{loxP/loxP}$, PbCre$^{+/-}$) mice and backcrossed to the C57BL/6J strain for at least 4 generations. These mice were then crossed with BirA$^{+/+}$ [19].

*Plekhs1*$^{Avi/Avi}$ mice were generated in the Babraham Institute (BI) Gene Targeting Facility using Crispr/Cas9 technology applied to mouse zygotic embryos. The zygotes used to generate the *Plekhs1*$^{Avi/Avi}$ mouse strain were isolated from *Pten* $^{loxP/loxP}$ x BirA$^{+/+}$ females and then transferred to a WT C57BL/6J foster mother.

The *Plekhs1*$^{-/-}$ mouse strain was generated using genetically engineered embryonic stem (ES) cells clones from Eucomm (two independently derived clones were used, table below). Karyotyped ES cells were injected into zygotes isolated from *Pten* $^{loxP/loxP}$ x BirA$^{+/+}$ females and then transferred to a WT C57BL/6J foster mother. Correctly, targeted

animals were then backcrossed to the C57BL/6J strain for at least 6 generations.
The animals were kept under specific-pathogen-free conditions in the Biological Support Unit at The Babraham Institute and were regularly screened for common pathogens. All animal experiments at The Babraham Institute were reviewed and approved by The Animal Welfare and Ethics Review Body and performed under Home Office Project license PPL 70/8100.

**Table 2.8 ES Plekhs1 'KO-first' clones**

| CLONE ID | ALLELE | MGI ALLELE ID | CELL TYPE | COAT COLOR |
|---|---|---|---|---|
| **HEPDO817_1_F11** | Plekhs1$^{tm2a(EUCOMM)Hmgu}$ | MGI:5511602 | JM8A3.N1.C2 | Agouti |
| **HEPDo817_1_D12** | Plekhs1$^{tm2a(EUCOMM)Hmgu}$ | MGI:5511602 | JM8A3.N1.C2 | Agouti |

# 2.2 Methods

## 2.2.1 Generation of Polyclonal P-Y227 Plekhs1 antibodies

Cambridge Research Biochemical –CRB (https://www.crbdiscovery.com/), generated antibody raised against phosphorylated tyrosine 257 (Y257) residue. Antigen samples were prepared and then injected into rabbit. It evoked high expression level of specific antibodies in the animal serum. After this procedure, blood of the animal is isolated 2 to 3 times and then antibodies are eluted on antigen column using glycine.

## 2.2.2 Generating *Plekhs1*$^{Avi/Avi}$ and *Plekhs1*$^{-/-}$ mice

Chapter 3 describes the details of the gene engineering procedures used to generate the two mouse models.

### 2.2.2.1 Genotyping *Plekhs1*$^{Avi/Avi}$ and *Plekhs1*$^{-/-}$ mice

DNA to perform Polymerase Chain Reaction (PCR) was isolated from mouse ear notches using 50µl of Lysis Buffer with added Proteinase K (table 2.9). After an overnight incubation at 55°C, Proteinase K was deactivated by boiling the sample for 10min at

95°C. Samples were diluted 20 times in MiliQ water and PCR reaction was performed.

**Table 2.9 Lysis buffer used to extract DNA from ear notches**

| **LYSIS BUFFER** | |
|---|---|
| **Tris-HCl pH 8.5** | 100mM |
| **EDTA** | 5mM |
| **SDS** | 0.20% |
| **NaCl** | 200mM |
| **Proteinase K [10mg/ml]** | 10% |

### 2.2.2.2 Genotyping *Plekhs1*$^{Avi/Avi}$

PCR-based genotyping was performed using MyTaq DNA HS polymerase. PCR mix was prepared according to the table 2.9. Parameters used to set up the reaction in the thermocycler are indicated in table 2.10.

**Table 2.10 PCR Components for *Plekhs1*$^{Avi/Avi}$ mice genotyping**

| **PCR COMPONENTS** | **VOL FOR ONE REACTION** |
|---|---|
| **DNA template 100ng** | 2µl |
| **Plekhs1_Avi_666_Rv primer (10uM)** | 1µl |
| **Plekhs1_seq_FV2 primer (10uM)** | 1µl |
| **Mytaq HS DNA polymerase** | 12.5µl |
| **MiliQ Water** | 8.5µl |

**Table 2.11 Thermocycler Program for PCR used to genotype *Plekhs1*$^{Avi/Avi}$ mice**

| **STEP** | **TEMPERATURE** | **TIME** |
|---|---|---|
| **Denature** | 95°C | 1min |
| **Denature** | 95°C | 15s |

35x

| | | |
|---|---|---|
| **Anneal** | 59°C | 15s |
| **Extend** | 72°C | 10s |
| **Hold** | 8°C | Pause |

After the PCR reaction, the resulting DNA was run on a 2% agarose gel and exposed to UV light. 2 products were expected: a 616bp band which represents *Plekhs1* allele with an insertion, and a 565bp band which represents *Plekhs1* allele without an Avitag insert. A typical example of a resulting DNA gel is shown in Figure 2.1.

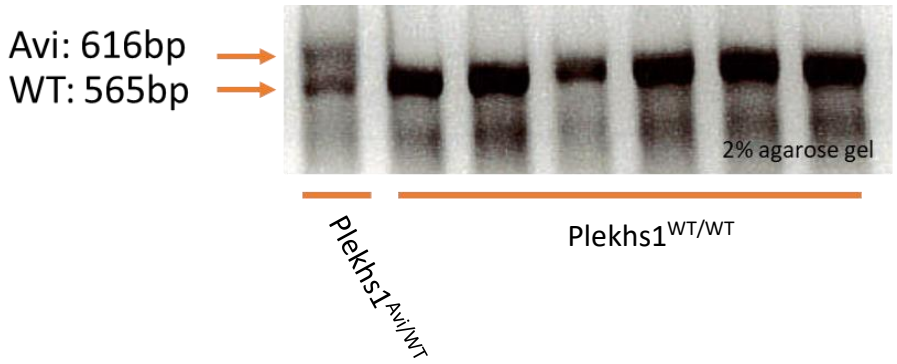


**Figure 2.1 Example of Agarose gel with a PCR product**

### 2.2.2.3 Genotyping *Plekhs1*$^{-/-}$

PCR-based genotyping was performed using MyTaq DNA HS polymerase. ThePCR mix was prepared according to the table 2.11. Parameters used to set up the reaction in Thermocycyler are indicated in table 2.12.

**Table 2.12 PCR Components for *Plekhs1*$^{-/-}$ mice genotyping**

| PCR COMPONENTS | VOL FOR ONE REACTION |
|---|---|
| **DNA template 100ng** | 2µl |
| **LacZ_643_FV primer (10uM)** | 1µl |
| **LacZ_643_Rv primer (10uM)** | 1µl |
| **Mytaq HS DNA polymerase** | 12.5µl |
| **MiliQ Water** | 8.5µl |

**Table 2.13 Thermocycler Program for PCR used to genotype *Plekhs1*$^{Avi/Avi}$ mice**

| STEP | TEMPERATURE | TIME | |
|---|---|---|---|
| **Denature** | 95°C | 1min | |
| **Denature** | 95°C | 15s | 35x |
| **Anneal** | 61.3°C | 15s | |
| **Extend** | 72°C | 10s | |
| **Hold** | 8°C | Pause | |

After the PCR reaction, the resulting DNA was run on a 1.5% agarose gel and exposed to UV light. Two of the primers were flanking part of a unique sequence in the cassette, which do not appear in a 'WT' *Plekhs1* allele. A PCR product of 643bp was only expected to be generated in DNA with the desired mutation.

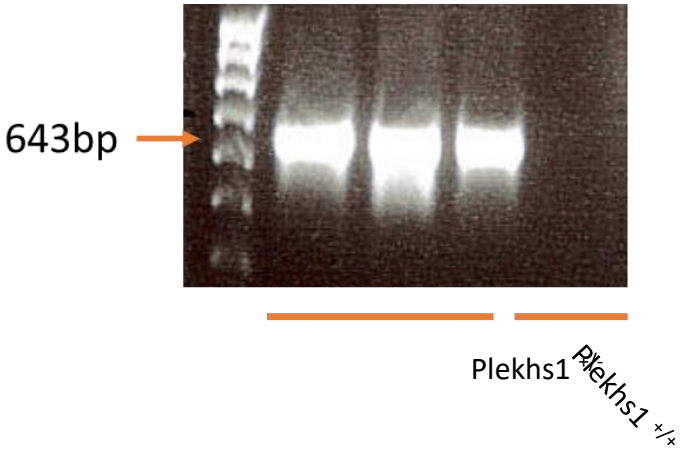


**Figure 2.2 Example of Agarose gel with a PCR product**

## 2.2.3 Tissue Preparation

Tissues were isolated from mice with indicated genotype. Mice were euthanized with $CO_2$ and confirmed dead by cervical dislocation. Mouse prostate as well as other tissues were isolated under a binocular dissecting microscope and the prostate was weighed and photographed. Tissue was rinsed in 1x sterile PBS and snap-frozen in liquid N2. The frozen tissue was pulverized under a continuous flow of N2 and stored at -80°C. Cold lysis buffer (750µl, table 2.14) was added per 50 mg tissue to yield an approximate final protein concentration of 4 mg/ml. Lysates were homogenized by vortexing for 15 sec followed by a extrusion through a 21G syringe needle (3x), followed by a 23G needle (3x). Lysates were then transferred to a 1.7ml ultracentrifuge tubes and cleared by centrifugation for 5min at 75 000g at 4°C. After this process, the cleared lysates were transferred to a fresh, pre-cooled low-protein-binding tube and a small fraction was used to measure the protein concentration using BCA Protein Assay Kit.

**Table 2.2.14 Buffers used for tissue preparation**

| LYSIS BUFFER | SDS BUFFER(4x) | INHIBITOR COCTAIL |
|---|---|---|
| 1% Triton X-100 | 0.2M Tric-HCL | 5mM Sodium Orthovanadate $Na_3VO_4$ |
| 0.4% CHAPS | 0.4M DTT | 5mM β-glycerophosphate |

| | | |
|---|---|---|
| 20MM Tris-HCl pH 7.4 | 8% (w/v) SDS | 10µg/ml Leupepetin, Aprotonin, α-pain, Pepstatin A |
| 150mM NaCl | 6mM Bromophenol Blue | 1mM of PMSF |
| 1mM EDTA | 4.3M Glicerol | |
| 1mM EGTA | | |
| 2.5mM Sodium pyrophosphate $Na_4P_2O7$ | | |
| 25mM NaF | | |

### 2.2.4 Protein Separation by SDS-Page

Aliquots of lysates (of known protein concentration) were mixed with 4xSDS-loading buffer (table 2.14) and heated for 10min at 95°C to denature the protein. After heating, the lysates were centrifuged briefly (30 secs, room temperature, bench top microfuge). Samples were then loaded into 10-well or 15-well 7-8% SDS-PAGE gels. After protein separation, proteins were transferred to PVDF membranes and incubated with the indicated primary antibodies at 4°C overnight. They were then washed with TBS containing 0.1% v/v Tween 20 (3x 10minutes) and incubated for 45min to 1h with HRP-conjugated secondary antibodies (room temperature). After the incubation time membranes were washed with TBS containing 0.1% v/v Tween 20 (3x 10minutes) and incubated for 1min in ECL Western Blotting Detection Reagent. The signal were detected using X-ray film. Signals were quantified using Image Studio Lite software. The amount of protein loaded, antibody dilution as well as exposure times were selected to ensure that signals were linearly related to the amount of input material. During quantitation, the signal intensities of individual bands were corrected for variations in local background followed by normalisation via the signal from “loading controls” (housekeeping proteins) in the same samples.

## 2.2.5 Lipid Extraction

### 2.2.5.1 Ion Exchange Method

Pulverised tissue (5mg) was mixed with the initial organic solvent mix containing H20 (organic mix and H20 in 725:170 ratio, table 2.15). Following this step, 200µl of the resuspended tissue was taken and mixed with initial organic solvent mix: H20 with added standards (table 2.15, 720µl) making a total volume of 920µl. Chloroform (720µl) was added to the resulting solvent mixture, which was then vortexed, centrifuged (5min, 2400 x g at room temperature) and the lower phase was removed carefully and discarded. Chloroform was added again (720µl), the solvent mixture was vortexed and centrifuged (5min at 2400 x g at room temperature) and the organic lower phase was discarded. This was followed by adding 500µl of the initial organic solvent mix. Sep-pak aminopropyl columns were washed 3 times with 1ml initial organic solvent mix: H20. Samples were loaded onto the column and washed twice with organic solvent mix: H20 (1ml at room temperature). Next, samples were washed twice with ammonium acetate wash buffer (1ml) followed by 3 washes with Initial organic solvent Mix: H20 (1ml). Samples were then eluted with acid elution solvent (1ml) followed by chloroform (700µl), collected in 5ml centrifuge tubes and transferred to 2ml safe-lock tubes. After that stage, H20 (340µl) was added, vortexed and centrifuged (5min at 2400 x g at room temperature). After centrifugation, the lower layer was transferred to a fresh tube and mixed with upper, aqueous phase of the Pre-derivatisation wash (table 2.15, 708µl). Samples were vortexed and centrifuged (5min at 2400 x g at room temperature). The lower organic phases of the centrifuged samples were removed and mixed again with fresh aqueous phase of the pre-derivatisation wash (table 2.15, 708µl). The resulting mixture was vortexed and centrifuged (5min at 2400 x g at room temperature). Next, the lower organic phase was transferred to a 2ml centrifuge tube and mixed with 100µl of initial organic solvent mix. TMS (Diazomethyl- trimethylsilane, 50µl) was added to the sample and incubated (10min at room temperature) then neutralised with glacial acetic acid (6µl). After the neutralization step the organic, lower phase was washed twice with final wash upper phase (700µl), vortexed and centrifuged (5min at 2400 x g at room temperature). 90% Methanol in water (700µl) was added and then the samples were dried under a stream of N2 gas (at room temperature), then re-dissolved in 80% Methanol in water (50µl) and sonicated briefly. Samples were run on a mass

spectrometer immediately or stored overnight (-80°C).

**Table 2.15 Buffers used for Lipid Extraction**

| | |
|---|---|
| **PRE-DERIVATISATION WASH** | |
| **Chloroform** | 24ml |
| **Methanol** | 12ml |
| **0.01M Hydrochloric Acid** | 9ml |
| | |
| **FINAL WASH** | |
| **Chloroform** | 24ml |
| **Methanol** | 12ml |
| **Water** | 9ml |
| | |
| **INITIAL ORGANIC SOLVENT MIX** | |
| **Chloroform** | 12ml |
| **Methanol** | 24ml |
| | |
| **ACID EDULTION SOLVENT** | |
| **Methanol** | 48.4ml |
| **Chloroform** | 24.2ml |
| **10M Hydrochloric Acid** | 3.0ml |
| | |
| **INITIAL ORGANIC SOLVENT MIX:H20 WITH ADDED STANDARDS** | |
| **Initial Organic solvent Mix:H20** | 10.08ml |
| **d6_SA_PIP** | 140µl |
| **d6-SA_PIP$_2$** | 140µl |

### 2.2.5.2 Neutral Wash Method

5mg of previously homogenised tissue was resuspended in the initial organic mix (table 2.15, 920µl). Then 92µl transferred to a fresh tube and added Initial organic mix (603µl) and 10µl of each of the following standards: C17:0/C16:0-PI and C17:0/C16:0-$PIP_3$. Sample was vortexed and chloroform was added (725µl). After vortexing lower, organic phase was removed and discarded. In the next step, chloroform was added (725µl) and the sample was vortexed. The lower organic phase was discarded and the Initial Organic Mix (500µl) and of HCl (170µl) was added. This step was followed by adding Chloroform (725µ) and vortexing (5 x 20s) followed by incubation (5min and room temperature). After this time, the sample was centrifuged (5min at 2400x g at room temperature). The lower, organic phase was transferred to a fresh tube containing upper aqueous phase of pre-derivatisation wash (table 2.15, 708µl). The vortexing and centrifugation step was repeated and then the lower, organic phase was transferred to a fresh tube with the initial organic mix (100µl).

TMS (Diazomethyl- trimethylsilane, 50µl) was added to the sample and incubated (10min at room temperature), then neutralised with glacial acetic acid (6µl). After the neutralization step the organic, lower phase was washed twice with final wash upper phase (700µl), vortexed and centrifuged (5min at 2400 x g at room temperature). 90% methanol in water (700µl) was added and then the samples were dried under a stream of N2 gas (at room temperature), then re-dissolved in 80% methanol in water (50µl) and sonicated briefly. Samples were run on a mass spectrometer immediately or stored overnight (-80°C).

### 2.2.5.3 Lipids Mass Spectrometry

Lipid molecules of PtdIns, PI(4,5)$P_2$ and PI(3,4,5)$P_3$ were measured by HPLC-ESI MS/MS, by Jonathan Clark at the Babraham Institute Lipidomics Facility, using an ABSciex Qtrap 4000 mass spectrometer connected to Waters Acquity UPLC system, with duplicate 45µl samples injected as described in Clark et al. 2011[145]. Two technical replicates were routinely analysed for each experiment.

## 2.2.6 Cell Culture

All cells were maintained in an incubator at 37°C with 5% CO2, in medium containing penicillin and streptomycin (10,000Units/ml and 10,000µg/µl).

#### 2.2.6.1 Hela cell line

Hela cells were cultured in Eagle's Minimum Essential Medium. To make the complete growth medium, fetal bovine serum was added to a final concentration of 10%. Cells were passaged 2-3 times a week in the ratio of 1:4. Cells were detached from the bottom of plate using 0.25% (w/v) Trypsin- 0.53mM EDTA for 5-15min.

#### 2.2.6.2 Mouse Embryonic Stem cells (ES cells)

Media, gelatin and trypsin were all kindly made and donated by Dr Dominik Spensberger and the cells were frozen and stored by the Babraham Institute Gene Targeting Facility. The media consisted of knockout DMEM, GlutaMax/Glutamate 2mM, 1x 2-mercaptoethanol, 3ml Penicillin/Streptomycin final 50U/ml, 300µl LIF- from prepared stock 2000U/ml, FBS final 15%. Gelatin was made with 0.1% w/v gelatine in water or 1x PBS.

### 2.2.7 Transient Transfection

#### 2.2.7.1 HeLa Cells

Hela cells were seeded onto 10cm plates and when 70-80% of confluency was achieved, transfected using X-tremeGene reagent.

#### 2.2.7.2 X-tremeGene 9

Before transfection, medium was replaced with fresh medium (9.5ml, stated in section 2.2.6). X-treme gene reagent (30µl) was mixed with Optimem (500µl) and DNA (5µg) and left for incubation (15min at room temperature). After the incubation, the complex was gently dispersed on top of the cells. Transfection efficiency was checked after 24h.

#### 2.2.7.3 Cell stimulation

Used ligands, concentration and time are shown in a table 2.16.

All of the stimulation were performed in a Tissue Culture facility and cells were kept in 37°C during the time of stimulation.

**Table 2.16 Ligands and times used for cell stimulation**

| CELL LINE | LIGAND | CONCENTRATION | TIME OF STIMULATION |
|---|---|---|---|
| **HeLa** | IGF | 100ng/ml | 90s, 5min |

## 2.2.8 Molecular Biology

Cloning of two *Plekhs1* constructs was performed by Dr Tamara Chessa, Babraham Institute according to the described below methods.

Cloning and sequencing of *Mus Musculus Plekhs1* from occurred mouse prostate

RNA was extracted from whole mouse prostate of a C57BL/6J strain using TRIzol™ Reagent, according to manufacturer's instructions. First-Strand cDNA synthesis was performed using SuperScript™ II Reverse Transcriptase in combination with Random Hexamer Primers.

4µl of resulting cDNA was then used to amplify full length *Plekhs1* (nucleotide sequence corresponding to amino acids 9-459), followed by cloning into pRSETB-mEGFP-mEGFP, using primers Plekfor1 and Plekrev2 (detailed sequence Table 2.4 of Materials section); containing engineered restriction sites NdeI (forward primer) and KpnI (reverse primer): Through sequencing of the resulting construct and translation, the following amino acid sequence for mouse *Plekhs1* was obtained:

MEARPPKGPGKQFTFDYENEVHKRDYFIKSPPPQLFFSGTSWKKRLFILSQSRGTGLSLSYYKDHQ
HRGSIEIDGSTVEVGINCQEKMQSVQKMFKCHPDEVMSIRTANRDYFLIGHDREKIKDWVSFMTP
YCQGVKATHQRAEEKLSLGDRRPVSDPSPFLGLCSIPEGIRLASPRASLPEHLIQKSLQRFRQAHLH
QDHDFHSEPTQDTEEEYYLTPRSLEACLELENIAGPNDSGDSIESNSPDQGFKRAESNYVSMRSLRT
CLLKESTSASADDNDGQAEFQTESELGPPHQDSGTGSDPCLSPPNSKAQTTDDQKGNIPDESQVE
TLNVFLSPRDAIDYLALVEAAGQICVARWEGPPRLGCLFYHGDHILAVNDLKPQSLEEVSLFLTRCIQ
KEKVKLSIGRIPNSEKLHASPCACSLRHQLAESVQRDLPELERTPKRSPAIKKSQKEAAGE

The PH domain is highlighted in yellow.

YxxM motif, containing Y257, is highlighted in green.

This sequence differs from the canonical PLEKHS1 sequence (Uniprot Q8BW88), as follows:

Serine 77: missing

Amino acids 323-336: missing

1st 9 amino acids: predicted mouse prostate sequence (not cloned into pRSETB-mEGFP)

#### 2.2.8.1 Generation of PLEKHS1-Y257F in pRSETB-mEGFP

Primers used for site-directed mutagenesis, to generate PLEKHS1-Y257F (in pRSETB-mEGFP): PLEKHS1 Y257F F and PLEKHS1 Y257 R

Site-directed mutagenesis was performed with the Quikchange Lightning Site-directed Mutagenesis kit, according to manufacturer's instructions.

The presence of the mutation was verified using restriction analysis with BsaA1, where Y257F mutation resulted in the removal of the BsaA1 site, as well as sequencing.

#### 2.2.8.2 Cloning of *Plekhs1*-WT and -Y257F into pCMV3-EE

Primers used for cloning of *Plekhs1*-WT and *Plekhs1*-Y257F into PCMV3-EE:

Forward primer: Plekfor8 and reverse primer: Plekrev4

Mouse *Plekhs1*-WT and -Y257F were amplified from above mentioned pRSETB-mEGFP constructs, using primers containing engineered restriction sites NotI (in forward primer; this primer also carries Kozak + sequence encoding amino acids 1-9 that are absent in pRSETB-mEGFP constructs) and XbaI (in reverse primer), and cloned into pCMV3-EE constructed by Dr Phill Hawkins, Babraham Institute [146].

### 2.2.9 GFP-based pull down

To perform this experiment GFP-trap beads (Chromtec) were used. GFP-trap are anti-GFP- Nanobody/ $V_HH$, which are coupled to agarose and magnetic beds, what allows very specific and rapid GFP pulldown.

Before performing GFP-based pulldown cell culture medium was removed and cells were washed with 1x PBS.

Lysis buffer (900µl, Table 2.2.14) was added directly on top of the cell monolayer. 10cm

dishes were incubated on ice (1min) and then cells were scraped and cell lysates moved to ultracentrifuge tube (1.7ml). Cell lysate was spun in an Ultracentrifuge (5min at 75000 x g at 4°C). Meantime, GFP beads (30µl of the slurry per sample) were washed (3x with lysis buffer without added anti-proteinases and anti-phosphatases).

After the ultracentrifuge step, small volume of lysate was saved for BCA Assay and western blot analysis and labelled 'pre'. 600µl of total lysate was used for pulldown. Lysate was transferred to low protein binding tubes and mixed with washed GFP beads. Tubes were incubated with a constant rotation (1h at 4°). After incubation, the mixture of GFP beads and bound proteins were pulled down using DynaMag-2 magnetic rack and small amount of the lysate was collected and labelled as 'post 'lysate. The remaining lysate was discarded and beads were washed (3x with lysis buffer with added anti-proteinases and anti-phosphatases). This was followed by an elution with 1.5x SDS sample buffer (Table 2.2.14, 10min at 95°C). Eluates were snap frozen and kept in -80°C or run immediately on a SDS-page gel.

### 2.2.10 Streptavidin-mediated pull-down of biotinylated Avitagged proteins

Prostates lysates used for the pulldown experiment were prepared based on the method described in section 2.2.3. Taking under consideration the characteristics of Mass Spectrometry, all of the buffers were filtered upon using them in the experiment (3x using 0.2µm filter units). After receiving clear lysate of the estimated protein concentration of 4mg/ml small amount of the total lysate was saved for a BCA assay and Western Blot analysis-labelled 'pre'. 600µl of the Lysate (600µl) was mixed with Dynabeads (30µl of 3 x washed slurry in lysis buffer without added anti-proteinases and anti-phosphatases) in low protein binding tubes. Next, tubes were incubated with a constant rotation (20min at 4°C). After incubation, the mixture of streptavidin beads and bound proteins were pulled down using DynaMag-2 magnetic rack and another small amount of the lysate was collected for further analysis and labelled as 'post'. The remaining lysate was washed (4x with buffer with added anti-proteinases and anti-phosphatases) on the magnetic rack. After the last wash 1.5x loading buffer (table 2.14, 40µl) was added to the beads and boiled (10min at 95°C). After the elution, the lysates

were put on magnetic rack, and the eluates was transferred to a fresh low-binding tube. Remaining beads were boiled again in the same volume of 1.5x SDS loading buffer to confirm the elution efficiency.

### 2.2.11 TMT Labelling and M/S Analysis

Previously eluted proteins in 1.5x loading buffer were 'cleaned' in SDS-page and digested in gel with trypsin. Peptides were labelled in 11-plex TMT reactions and pooled (each 11-plex contained one biological replicate) from each of the 4 genotypes under investigation. The combined samples were fractionated by high pH reverse-phase chromatography prior to LC MS/MS (with online desalting) on a Thermo Q-Exactive Plus. Data analysis was performed using Proteome Discoverer v 2.1. Relative moles of each protein were calculated as follows. For a given target the reporter-ion abundance ratios of PLEKHS1 Avi: no Avi were calculated and normalised by (multiplied by) their precursor-ion areas (average peptide area of the three most abundant peptides for a given target in the PLEKHS1 pull-downs minus the equivalent no-Avi signal (as "non-specific background"). This gives a semi quantitative estimate of the absolute number of moles of a given target recovered in the PLEKHS1 pull-down.

### 2.2.12 Proteomics Analysis

Abundance of protein interactors of PLEKHS1 were primarily analysed by David Oxley and Judith Webster in the Proteomics Facility at the Babraham Institute. A list of normalised proteins over the total mass spec signal for each sample was generated using Proteome Discoverer Software. Anova-based statistical tests were applied to calculate adjusted P value. The data for prostate tissue expressing wild-type PLEKHS1 and PTEN is based on 2 biological replicates (as a result of the restrictions placed by 11-plex TMT labelling that was available at the time). The values plotted are means ± their standard deviations or as means ± range (n=2) and statistical comparisons with prostate samples expressing Avitagged PLEKHS1 in PTEN-wild-type tissue (n=3) (e.g. abundance in PLEKHS1-Avi pulldowns / abundance in PLEKHS1-wild-type pulldowns) use a ANOVA test where the question is: are 3 AviTagged- PLEKHS1 samples significantly higher than the

mean of the PLEKHS1-wild-type samples (ratio greater than 1). Hence to achieve significance in this test requires a substantially greater difference between the tested groups than would be expected if both groups were n=3. Hits with $P \leq 0.05$ between 'Avi'/'No Avi' and/or 'Avi' *Pten* $^{+/+}$/'Avi' *Pten* $^{-/-}$ are shown in Table 5.1-Table 5.3 and Figure 5.4-Figure 5.20 in Chapter 5 of the thesis. Table 5.1, Table 5.3 and Figure 5.4-Figure 5.20 show grouped abundance, where each protein are expressed as a proportion, of the total signal measured for that protein across all 4 genotypes, set to 400. Table 5.2 show raw abundances. All of the histograms were generated using GraphPad Prism 8.

### 2.2.13 Statistics

GraphPad Prism 8 was used to calculate any relevant statistical significance of the research presented in this thesis. Unless stated otherwise, data are presented as means ± Standard Deviation (SD), ns $P > 0.05$, *$P \leq 0.05$, **$P \leq 0.01$, ***$P \leq 0.001$, and ****$P \leq 0.0001$. The type of test and details of each test is given in the results chapters, where appropriate.

# 3 GENERATION AND PRIMARY CHARACTERISATION OF MOUSE MODELS

## 3.1 Introduction

Our laboratory previously set out to determine the endogenous Class IA PI3K interactome in healthy (WT) prostate tissue and in a mouse model harbouring specific deletion of *Pten* in prostate luminal epithelial cells [147] (*Pten* $^{-/-}$, HG-PIN stage of tumorigenesis). This work highlighted a strong increase in association of PLEKHS1 with p85$\alpha$ and –$\beta$ subunits of PI3K in *Pten* $^{-/-}$ prostate.

To confirm this data as well as to elucidate the full PLEKHS1 interactome, we designed a genetically engineered mouse model harbouring an Avitag at the C-terminus of endogenous PLEKHS1. To generate the *Plekhs1*-Avitag knock-in mouse model, we applied CRISPR-Cas9 technology with zygote injection of gRNA and Cas9, as opposed to the more traditional approach of gene-editing embryonic stem (ES) cells followed by the injection of appropriately targeted clones into blastocysts.

The second outstanding question in our studies was; what is the function of PLEKHS1 in prostate and other tissues in health and disease? To address this question, we constructed a genetically engineered mouse model with a '*Plekhs1* KO-first' cassette, in the context of WT (*Pten* $^{+/+}$) and *Pten* $^{-/-}$ prostate luminal epithelium. This model was created by injection of clonal ES cells harbouring the desired genetic modification (obtained from Eucomm) into mouse blastocysts.

In this chapter, we describe the generation of the above-mentioned genetically-engineered mouse models, as well as the validation and characterisation of these two models.

## 3.2 *Plekhs1*$^{Avi/Avi}$ mouse model

### 3.2.1 Using CRISPR-Cas9 technology to generate *Plekhs1*$^{Avi/Avi}$ mice

Genetically modified animals are powerful tools in efforts to understand multiple biological and pathological processes. Information gained from these animal models can

then be used to more quickly understand human physiology. Previously, in the mouse, as well as other rodents, genetic modifications were mostly achieved via homologous recombination in ES cells (Figure 3.1), which is a very time-consuming and laborious process. Development of CRISPR-Cas9 technology shortened and simplified this process. The nuclease Cas9, guided by synthetic single RNAs (sgRNAs), creates precise Double Strand Breaks (DSB) in a defined, guided genomic location[148]. The induced-breaks are repaired by endogenous cell repair mechanisms that can lead to insertions and/or deletions (INDELS) in the target DNA or, when donor DNA is provided, instructed sequence changes, [149].

The efficiency of CRISPR-Cas9 technology raised the realistic possibility of genetically modifying the germ-line and somatic tissues of model animals in a one-step procedure, namely *via* direct modification of the genome of a single-cell embryo, followed by transplantation of the embryo into pseudo-pregnant females. Indeed, this is currently the most effective method by which to generate genetically-modified germline-transmitted animal models for research. This method relies on precise delivery of CRISPR-Cas9 reagents (sgRNAs, Cas9 endonuclease and donor DNA) into the zygote (Figure 3.2). The success of this procedure depends on careful design and preparation of these reagents and selection of the most appropriate delivery method. In our project, we generated gene engineered mice by injection of the reagents into the cytoplasm, without penetrating the pronuclei. Importantly, this particular methodology has been shown to increase the survival rate of the embryos[150].

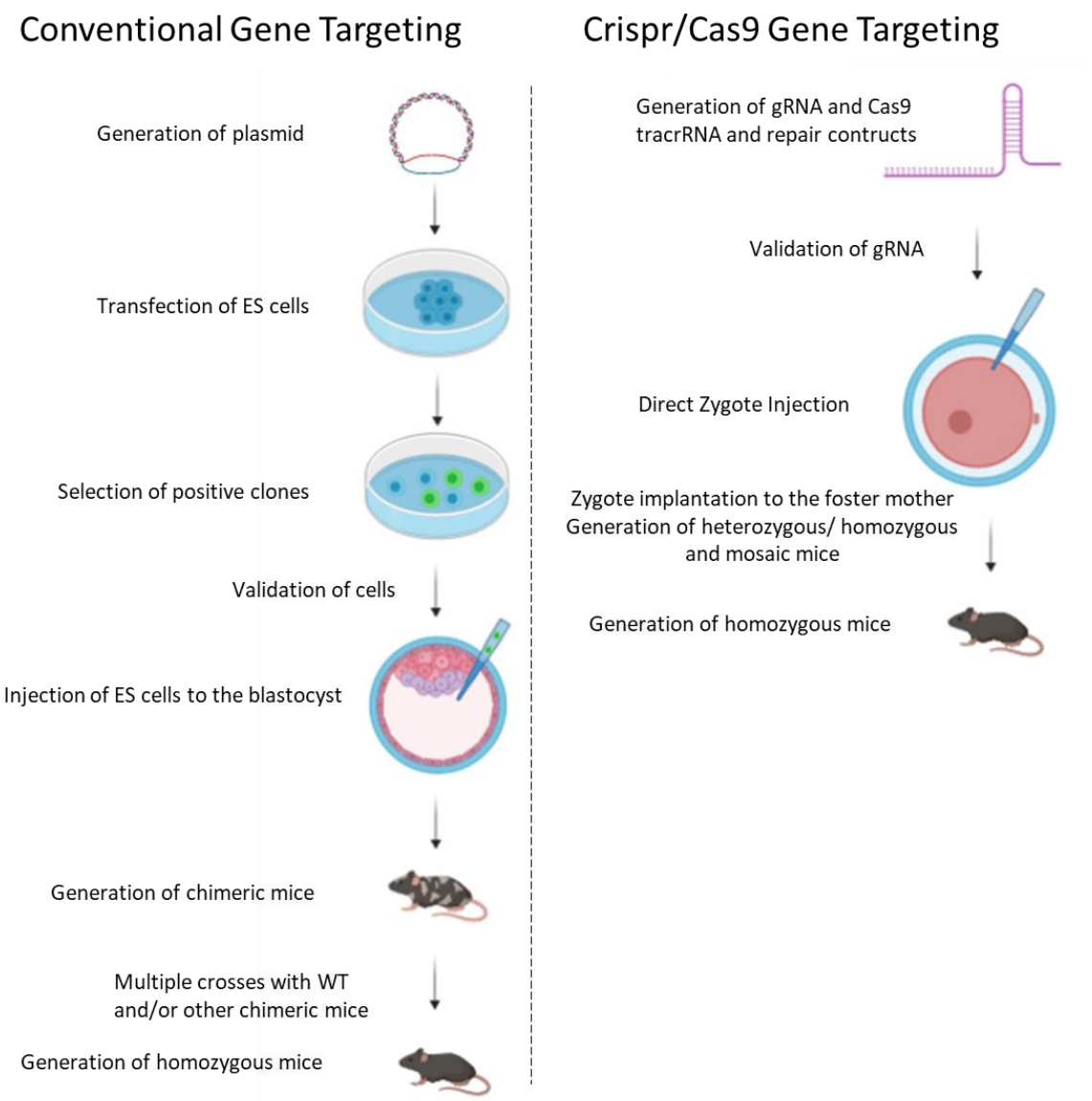
Conventional Gene Targeting
Generation of plasmid
Transfection of ES cells
Selection of positive clones
Validation of cells
Injection of ES cells to the blastocyst
Generation of chimeric mice
Multiple crosses with WT
and/or other chimeric mice
Generation of homozygous mice
Crispr/Cas9 Gene Targeting
Generation of gRNA and Cas9
tracrRNA and repair contructs
Validation of gRNA
Direct Zygote Injection
Zygote implantation to the foster mother
Generation of heterozygous/ homozygous
and mosaic mice
Generation of homozygous mice

**Figure 3.1 Comparison between conventional gene targeting with CRISPR-Cas9 targeting**

*The schematic shows two different strategies of generating genetically engineered mouse models; the traditional method, involving transfection of ES cells, and Crispr/Cas9 targeting of zygotes.*

*The traditional strategy involves constructing a plasmid and transfecting it into ES cells. Following screening of potentially targeted ES clones, successfully targeted ES cells are injected into blastocysts, which are later transferred into pseudo pregnant mothers. From these blastocysts chimeric mice are born. Only chimeric mice that carry the targeted gene in their germline can pass it to their offspring. Chimeric mice are bred to produce heterozygous mice, which are then crossed to produce homozygous mice.*

*Alternatively, Crispr/Cas9 constructs can be injected directly into the mouse zygote. The zygote is then transferred to the pseudo pregnant mother which gives birth to largely heterozygous or homozygous pups. There is a chance that a mosaic mouse will be born, in that situation and only if germ line cells carry the targeted modifications, the offspring have to be bred to generate heterozygous mice and then bred again to yield homozygous mice.*

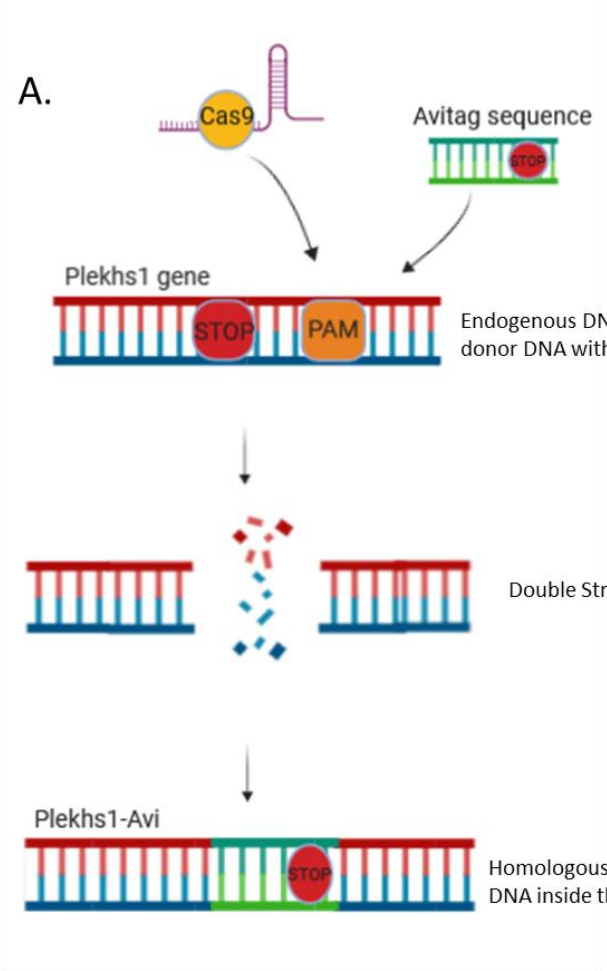
A.
Cas9
Avitag sequence
STOP
Plekhs1 gene
STOP
PAM
Endogenous DNA and injected donor DNA with Cas9-gRNA
Double Strand Breaks induced by Cas9
Plekhs1-Avi
STOP
Homologous Recombination results in the insertion of Donor DNA inside the endogenous DNA

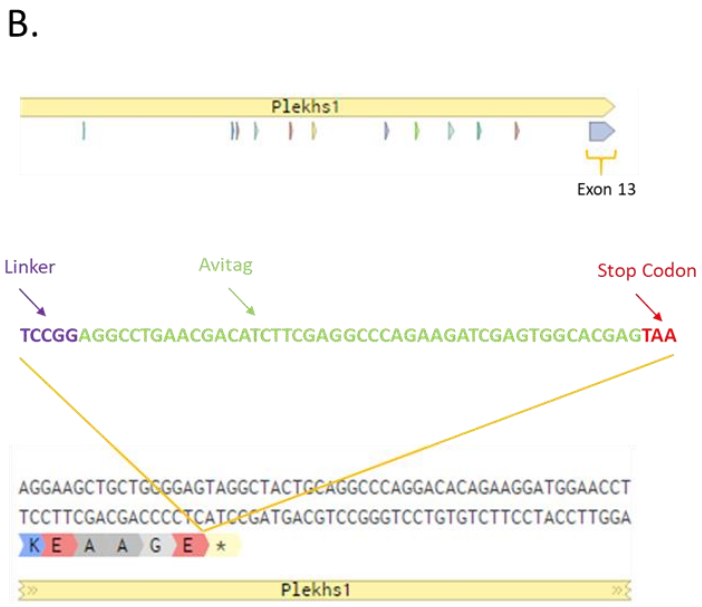
B.
Plekhs1
Exon 13
Linker
Avitag
Stop Codon
TCCGGAGGCCTGAACGACATCTTCGAGGCCCAGAAGATCGAGTGGCACGAGTAA
AGGAAGCTGCTGCGGAGTAGGCTACTGCAGGCCCAGGACACAGAAGGATGGAACCT
TCCTTCGACGACCCCTCATCCGATGACGTCCGGGTCCTGTGTCTTCCTACCTTGGA
K E A A G E *
Plekhs1

**Figure 3.2 Schematic of targeting strategy to generate Plekhs1$^{Avi/Avi}$ mice**

A. *The cartoon shows how Cas9 can introduce a double strand break (DSB) directed by specific gRNAs with complementary sequence to the genome immediately upstream of the protospacer adjacent motif (PAM). Homologous recombination repairs the break using donor DNA including the Avitag sequence.*
B. *Cartoon shows the targeted gene and insert in detail. The sequence of the **linker**, **Avitag** and **stop codon** are highlighted.*

### 3.2.1.1 Crispr Cas 9 guides

The sequence-specificity of the Cas9 nuclease is dependent of the design of sgRNAs. sgRNAs have to be complementary to the 20 nucleotide (nt) sequence upstream of the PAM motif (in this case NGG) in the genomic DNA. The 20nt sgRNAs guide the Cas9 enzyme, that will introduce a DSB ~3bp upstream of the PAM. Importantly, designed sgRNAs have to be directly upstream of the PAM sequence, but they cannot have a sequence that is directly complementary to the PAM. To minimize potential off-target effects of CRISPR-Cas9 targeting, the online Crispr design tool Benchling (www.benchling.org) was used. Benchling software predicts the number of potential off-target sites in the genome of the relevant species, and ranks different sgRNAs based on quantitative estimates of their specificity.

The U5 RNA polymerase III promoter, which drives expression of the designed sgRNAs, shows a large preference for transcripts starting with a guanine (G) nucleotide, therefore adding G at the 5' end of the 20nt sgRNA sequence (when this sequence does not originally begin with G) is recommended. Certain sgRNAs do not guide Cas9 endonuclease efficiently enough to introduce a DSB, and therefore it is considered good-practice to design 2-3 pairs of sgRNAs for each target locus and then validate them in the cell line of choice[151].

### 3.2.1.2 T7 Endonuclease Assay

As stated previously, not all sgRNAs can guide Cas9 with the same efficiency, which can be the outcome of several factors. One of these factors is the sequence context of both the sgRNA as well as the target DNA. In this setting, guanine at position 20 of the gRNA,

as well as cytosine, adenine, or thymidine (C/A/T) following the PAM sequence and cytosine in the PAM sequence may drastically change the efficiency of the system. In addition, particular sequence elements (e.g. GC-content) and chromatin structure can influence sgRNA activity. Therefore, it is standard practice to test the activity and efficiency of a particular sgRNA-Cas9 complex before using it to perform gene-editing in cell lines or model organisms. T7 is a structure-selective endonuclease, which digests DNA heteroduplexes. After successful transfection of CRISPR-Cas9 reagents, genomic DNA surrounding the locus is amplified by PCR (Figure 3.3.). The resulting DNA fragment is denatured, mixed with WT DNA and re-annealed by heating and slow cooling. Heteroduplexes, containing one strand of WT DNA and one strand of modified DNA will be cleaved by T7. The products of these reactions are compared to those of control reactions to estimate the efficiency with which mutations had been introduced (Figure 3.4)[149].

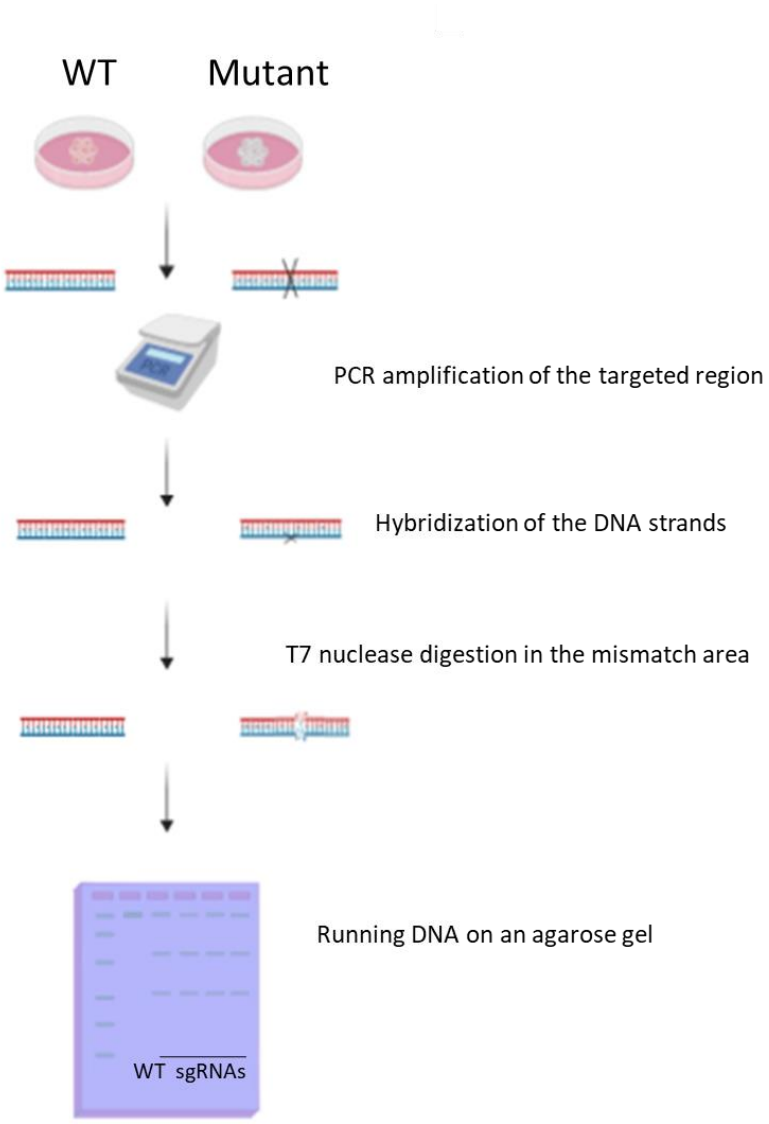


**Figure 3.3 T7 assay used to test the efficiency of induction of double strand breaks (DSB) with different sgRNAs**

*Cells where transfected with Cas9 endonuclease and 3 different sgRNAs. Following PCR amplification of the targeted DNA region, PCR products were annealed together and digested by T7 endonuclease. The resulting fragments were resolved by electrophoresis in an agarose gel.*

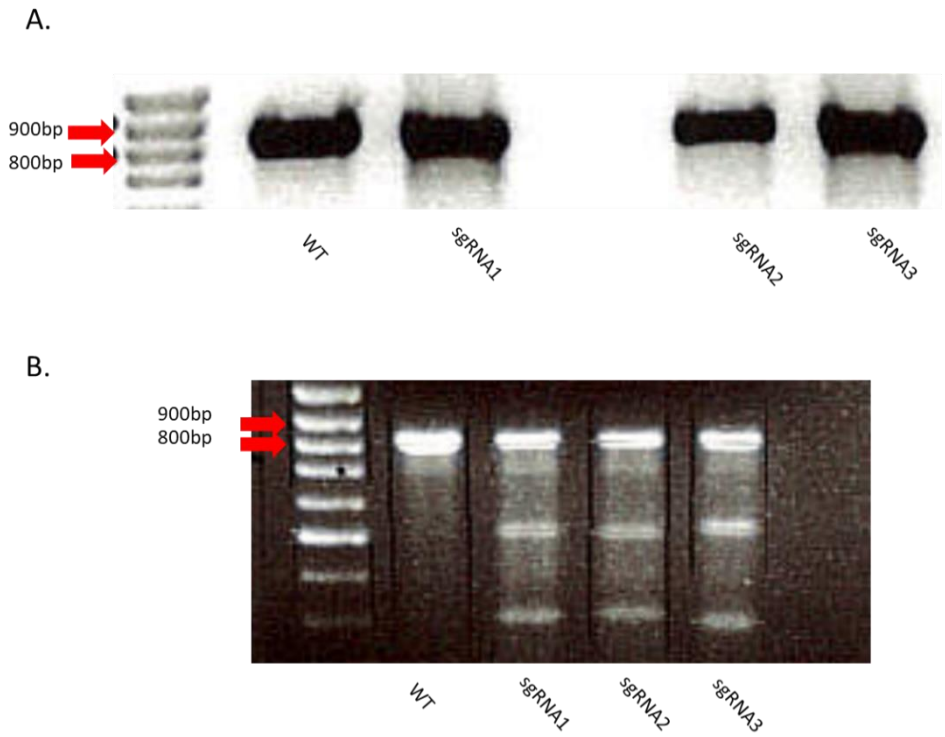


**Figure 3.4 Validation of sgRNAs using T7 assay**

A. *Genomic DNA, isolated from control ES cells and ES cells transfected with complex of Cas9 and sgRNA, was amplified by PCR. Expected product size was 810bp*
B. *200ng of control DNA and 200ng of engineered DNA was annealed together and digested with T7 nuclease. The reaction products were resolved by electrophoresis on a 1.5% agarose gel and visualised with UV light.*

### 3.2.2 Zygote Injection

The donor repair DNA was obtained from the manufacturer as a purified single (ss) or double stranded (ds) DNA, where appropriate. Validated sgRNAs (#2) were obtained from the manufacturer in ssRNA format alongside a TracrRNA sequence that is responsible for forming the secondary structure needed for the guide RNA and Cas9 to form a complex and target the correct DNA locus.

To estimate the efficiency of our gene targeting strategy in mouse zygotes, we first

targeted WT zygotes, through transfection of isolated WT C57BL/6J zygotes with ds donor-repair DNA along with Cas9/sgRNAs (Figure 3.5). Following transfection and 5 days incubation in cell culture, genomic DNA was isolated from 23 zygotes and the targeted sequence was amplified by PCR. Un-transfected zygote DNA was used as a negative control. A PCR product with the desired insert was expected to have been 312bp. Two lanes gave a product of 312bp, indicating that we had correctly targeted at least two zygotes, and hence, that the targeting efficiency was ~8.7%.

In the final gene targeting experiment, from which we ultimately hoped to obtain experimental animals, we used a single-strand (ss) donor-repair DNA, to increase the efficiency with which we obtained mice with the Avitag insert[152 153]. In this project we aimed to generate mice containing biotinylated endogenous PLEKHS1 (*Plekhs1*$^{Avi/Avi}$ BirA$^{+/-}$), in the context of *Pten* $^{+/+}$ and *Pten* $^{-/-}$ prostate luminal epithelium (PbCre, *Pten* $^{loxP/loxP}$). In an attempt to achieve this with maximum efficiency, in the context of our mouse-breeding programme, we aimed to target zygotes that already possessed some of the above genetic features (i.e., BirA, *Pten* $^{loxP}$, and PbCre). Hence, zygotes were retrieved from breeding pairs and trios of C57/BL6 mice of mixed genotypes in terms of BirA, *Pten* $^{loxP}$ and PbCre, in order to obtain experimental animals with the desired genotypes as listed in Figure 3.8.

SsDNA, alongside sgRNAs(#2), TracrRNA and recombinant Cas9 protein were micro-injected into mouse zygotes, to directly edit their genomic DNA, followed by transfer of the zygotes into the uteri of pseudo-pregnant females (this was performed by Dr Dominik Spensberger in BI's Gene Targeting Facility). Our first attempt resulted in only two pups being born, which died shortly after birth. Genotyping of these pups revealed that one of those pups (marked as 1*, Figure 3.6A) had the correct insert and was, hereafter, used as a positive control for successful targeting. Our second attempt resulted in 28 viable pups. Out of those pups, 5 showed evidence that their *Plekhs1* locus had been correctly targeted with an Avitag. One of those (lane nr 1, Figure 3.6A) was suspected to be mosaic and was not taken for further analysis and was not used in further breeding. The efficiency of gene targeting in the zygotes subjected to CRISPR-Cas9 editing in combination with ssDNA was ~22%.

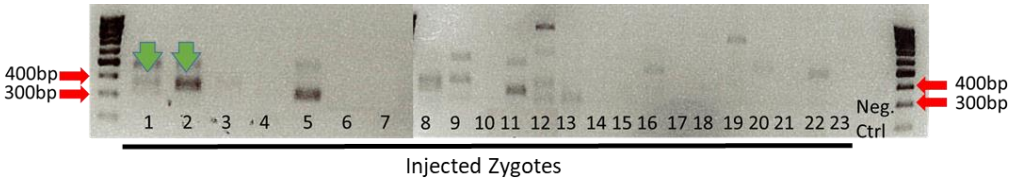


**Figure 3.5 Screening mouse zygotes targeted by injection of Cas9-sgRNA complexes**

*Genomic DNA isolated from 23 zygotes that were injected with Cas9-sgRNA complexes and donor DNA was amplified by PCR. The expected product size was 312bp. The products were resolved by electrophoresis on a 1.5% agarose gel and visualised using UV light. Potentially successfully targeted zygotes are indicated with green arrows.*

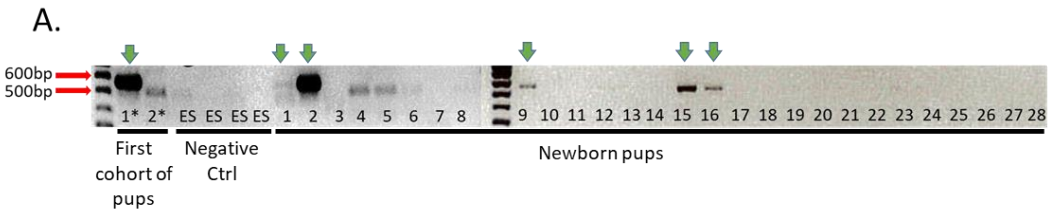


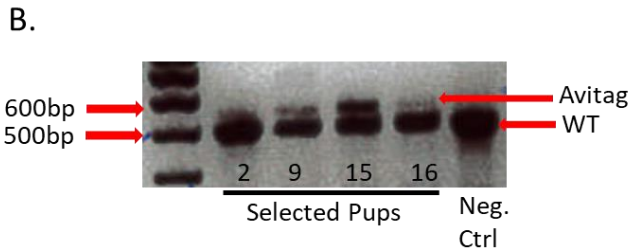


C.

GTCTTAGAAAGTGAAACTCTCCATTGGCCGGATCCCAAACTCAGAGAAGCTCCACGCTTCCCCCTGTGCATGCTCCT
TAAGACACCAGTTGGCTGAGTCTGTCCAGCGGGATTTGCCAGAACTGGAGAGGACACCAAAGAGGAGCCCTGCC
ATCAAAAAGAGTCAGAAGGAAGCTGCTGGGGAGTCCGGAGGCCTGAACGACATCTTCGAGGCCCAGAAGATCG
AGTGGCACGAGTAAGCTACTGCAGGCCCAGGACACAGAAGGATGGAACCTGGGCCACACACAGCCGTGTGACTG
GAGACAAGGCTGCATCTGTCTCTGAGTCACCACTGAATTAACAGTGGGGCCACTGGCCCCACATGAAATAATGACT
AAGGAGTAGAGTTAAAACGGAAGGGCTGATTATCTGAGATTCTGCCCCAGACACGGCAGACATCATTCAGTAAATC
CCTGGTCTAATTAATAGCTGTGTGCTTCCGAGGTCACAGTCCACACAGCTGGCTCTTCGTTAGCCATATCATTTCAGG
GATGCAAGAGAGTGAACGTGTGTCG

**Figure 3.6 Validation of genetically targeted mice**

A. *DNA was isolated from 28 zygotes and PCR was used to amplify DNA fragments containing the targeted site. DNA with the desired mutation should yield a product of 562bp. Products were resolved by electrophoresis on a 1.5% agarose gel and visualised using UV light. Mice with potentially successfully edited DNA are indicated with green arrows.*
B. *PCR fragments were resolved by electrophoresis on 2% agarose gels to distinguish WT and engineered alleles. WT would be expected to give a product of 501bp and edited DNA a product of 533bp*
C. *Original sequence of the amplified 533bp region with the **primers**, the sequence of the **linker**, **Avitag** and **stop codon** highlighted.*

### 3.2.3 Validation of gene engineered mice

The 190bp fragment of genomic DNA isolated from the four positive pups, identified in Figure 3.6A, was amplified by PCR (Figure 3.7) and sent for Sanger sequencing. The sequencing results were then aligned with the designed/theoretical targeted sequence using Nucleotide Blast. Importantly, the correct sequence, including linker, Avitag and new stop codon, was found in all 4 genetically modified mice, and no additional indels were observed in the locus. The resulting mice were used as founders of the *Plekhs1*$^{Avi/Avi}$ colony.

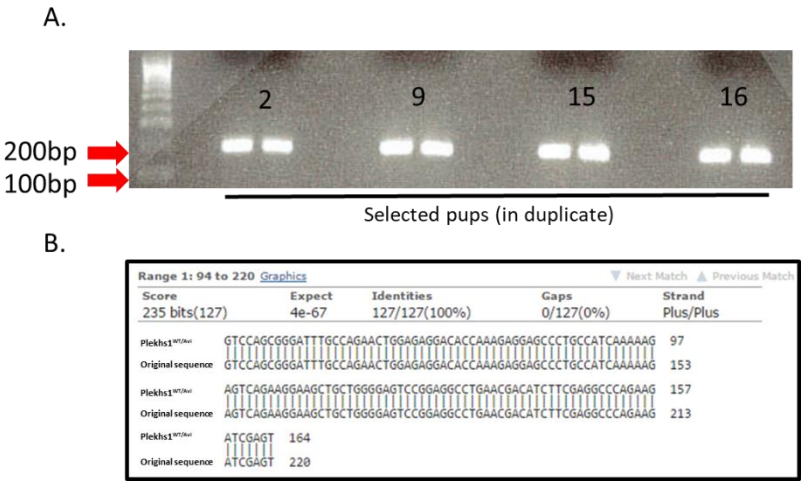


**Figure 3.7 Sequencing and validation of gene targeted mice**

A. *Genomic DNA from selected mice was amplified by PCR, resolved by electrophoresis on 1.5% agarose gels, and visualised using UV light (in duplicates). The expected product size is 190bp*
B. *Genomic DNA was isolated from newborn pups and amplified by PCR. The sequence of the amplified region was aligned using Nucleotide Blast.*

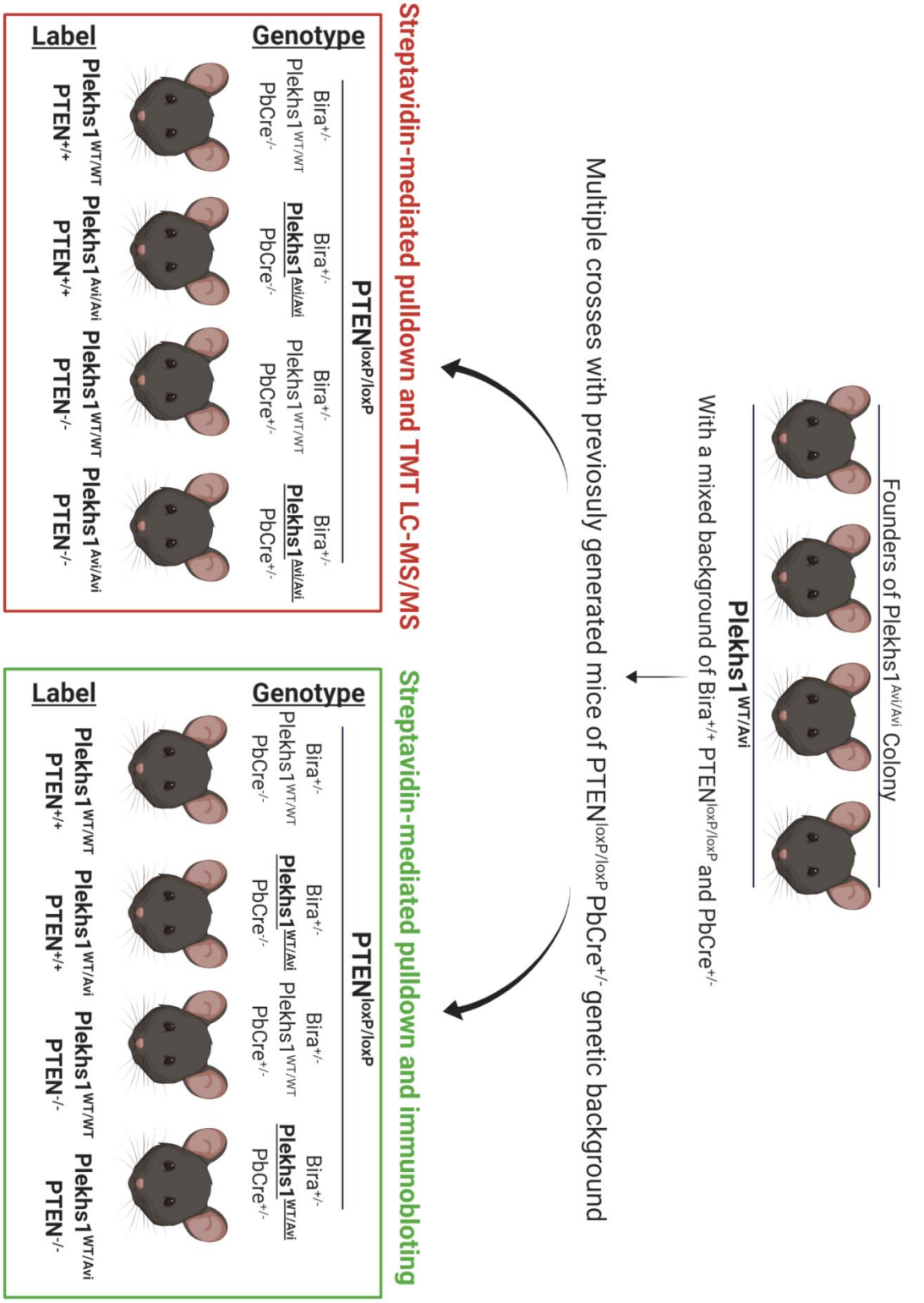
Founders of Plekhs1Avi/Avi Colony
Plekhs1WT/Avi
With a mixed background of Bira+/+ PTENloxP/loxP and PbCre+/-
Multiple crosses with previosuly generated mice of PTENloxP/loxP PbCre+/- genetic background
Streptavidin-mediated pulldown and TMT LC-MS/MS
Streptavidin-mediated pulldown and immunobloting
PTENloxP/loxP
Genotype
Label
Bira+/- Plekhs1WT/WT PbCre-/-
Bira+/- Plekhs1Avi/Avi PbCre-/-
Bira+/- Plekhs1WT/WT PbCre+/-
Bira+/- Plekhs1Avi/Avi PbCre+/-
Plekhs1WT/WT PTEN+/+
Plekhs1Avi/Avi PTEN+/+
Plekhs1WT/WT PTEN-/-
Plekhs1Avi/Avi PTEN-/-
Bira+/- Plekhs1WT/WT PbCre-/-
Bira+/- Plekhs1WT/Avi PbCre-/-
Bira+/- Plekhs1WT/WT PbCre+/-
Bira+/- Plekhs1WT/Avi PbCre+/-
Plekhs1WT/WT PTEN+/+
Plekhs1WT/Avi PTEN+/+
Plekhs1WT/WT PTEN-/-
Plekhs1WT/Avi PTEN-/-

**Figure 3.8 Model of breeding strategy to produce a Plekhs1 $^{Avi/Avi}$ mouse colony**

*The schematic shows the breeding strategy used to generate the Plekhs1$^{Avi/Avi}$ mouse colony. Founders (Plekhs1$^{WT/Avi}$) of the colony with a mixed background and a combination of the following alleles: BirA, PTEN$^{loxP}$, PbCre were crossed with mice having a PTEN$^{loxP/loxP}$ PbCre$^{+/-}$ background to generate mice of genotypes indicated in the Figure.*

### 3.2.3.1 Genotyping and breeding strategy

Founder pups (three males and one female), at 8 weeks of age, were crossed with *Plekhs1*$^{WT/WT}$ mice. The results of genotyping the resulting pups are shown in Figure 3.9. Four independent founder pups were interbred to obtain mice with genotypes indicated in Figure 3.8. We considered it important that the mice were out-crossed six times to minimize the consequences of any off-target mutations introduced by the process [154] [155].

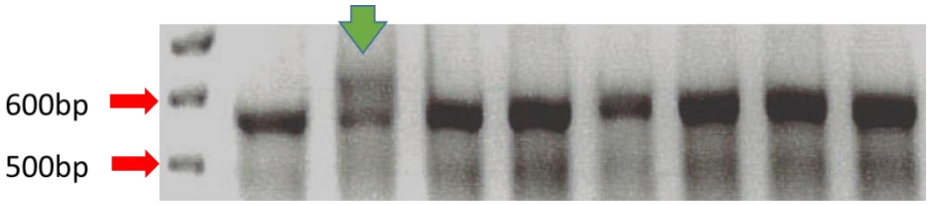


**Figure 3.9 Original Genotyping of first generation of pups from *Plekhs1*$^{Avi/WT}$ x *Plekhs1*$^{WT/WT}$ crosses**

*DNA was isolated from 8 ear clips and PCR was used to amplify a DNA fragment containing the targeted site. WT should give a product of 565bp and edited DNA should give a product of 616bp. The products were resolved by electrophoresis on a 2.0% agarose gel and visualised using UV light. An example of a mouse with successfully edited DNA is indicated with a green arrow.*

### 3.2.4 Validation of protein expression in *Plekhs1*-Avitag mice

We decided to attempt to validate the genetic targeting of *Plekhs1* at a protein level and to test the impact of Avi-tagging on the expression and interactions of PLEKHS1 by immuno-blotting aliquots of prostate lysates, from relevant genetically modified or control mice, with anti-Avi and anti- PLEKHS1 antibodies.

Previous work in the laboratory had demonstrated that the PLEKHS1-Class IA PI3K interaction is strongly enhanced in *Pten* $^{-/-}$ mouse prostate (T. Chessa, unpublished and see The Introduction). Furthermore, although the levels of *Plekhs1* mRNA were reduced in *Pten* $^{-/-}$ prostate it remained unclear whether the amount of PLEKHS1 protein changed. Hence, we attempted to address these questions at the same time as we validated our Avitagging strategy.

Mice with three different genotypes (*Plekhs1*$^{WT/WT}$, *Plekhs1*$^{WT/Avi}$ and *Plekhs1*$^{Avi/Avi}$, in the absence of BirA) were probed for PLEKHS1 and the Avitag, using antibodies directed against mouse PLEKHS1 and the Avitag, respectively, in the context of *Pten* $^{+/+}$ and *Pten* $^{-/-}$ prostate. A representative blot is shown in Figure 3.10 and the quantification in Figure 3.11.

We noted that the presence of the Avitag conferred the expected shift in the apparent size of PLEKHS1 of approximately 2.3 kD. Interestingly, we also observed the PLEKHS1 signal appeared as doublet, irrespective of the presence of the tag. This observation could indicate the existence of post-translational modifications (PTMs) or alternatively spliced forms of PLEKHS1 in mouse prostate. Additionally, PLEKHS1 ran at a much higher apparent size (~70kDa) than previously predicted (~50kDa). The reason for the difference in apparent size remains unknown.

Importantly, the Avitag does not affect expression of PLEKHS1 protein. Interestingly, the relative levels of PLEKHS1 protein are increased in *Pten* $^{-/-}$ prostate compared to *Pten* $^{+/+}$ prostate.

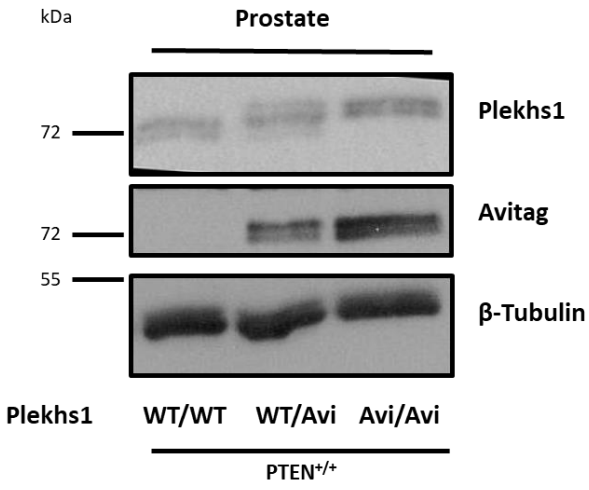


**Figure 3.10 Probing for the expression of endogenous Avi-tagged PLEKHS1**

*Prostate tissue was rapidly dissected from mice (12-15w) with the genotypes indicated in the Figure lysed and aliquots (30μg protein) were immuno-blotted with antibodies directed against the epitopes shown (right of the Figure) (all mice were BirA$^{+/-}$, PbCre$^{-/-}$, Pten $^{loxP/loxP}$). The primary antibodies were visualised with HRP-labelled 2$^{0}$-antibodies. β-Tubulin was used as a loading control.*

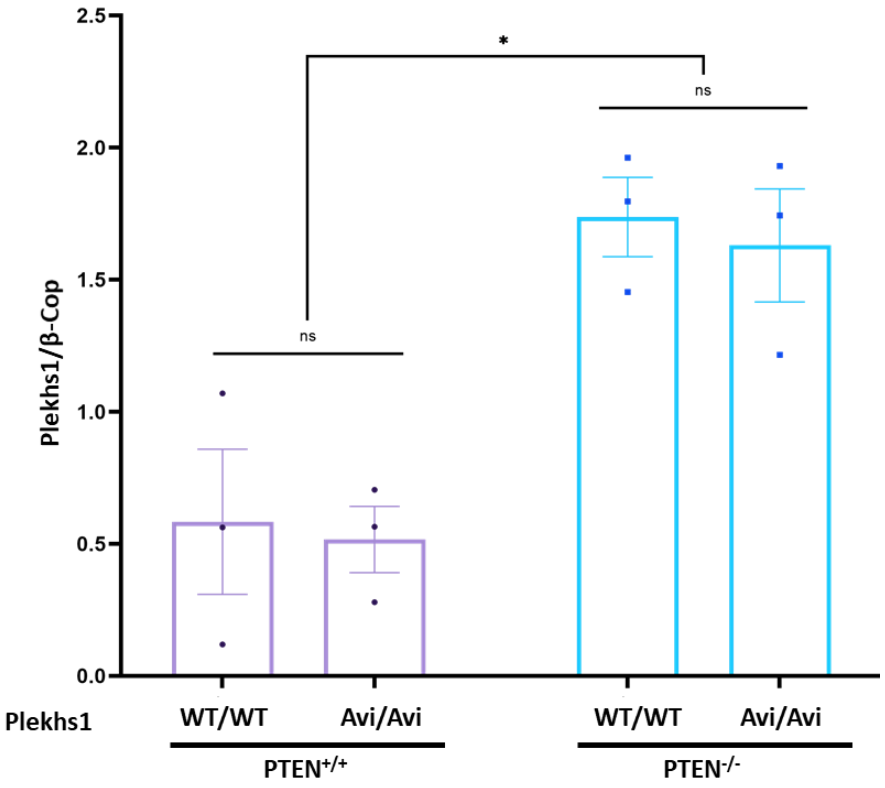


**Figure 3.11 Plekhs1 expression in control and PTEN$^{-/-}$ and/or Plekhs1$^{Avi/Avi}$ mouse prostate**

*Immuno-blots were quantified using Image Studio Lite software. The signal intensity of individual bands was normalized to the β-Cop (loading control) band in the same sample (all mice were BirA$^{+/-}$, mice described as PTEN$^{-/-}$ were PbCre$^{+/-}$, PTEN$^{loxP/loxP}$, PTEN$^{+/+}$were PbCre$^{-/-}$, PTEN$^{loxP/loxP}$). Statistical significance was tested with a multi-comparison two-way Anova test. Data represent means ± SD of 3 independent replicated experiments; each independent replicate experiment contained 6 separate biological samples.*

The BioGPS and EMBL databases provided us with information regarding levels of *Plekhs1* mRNA across different human and mouse tissues (see the *PLEKHS1* RNAseq data in the Introduction chapter). We hypothesised that prostate, bladder, genital fat pad and subcutaneous fat have high levels of expression of PLEKHS1 protein and liver, heart, skeletal muscle, brain, lungs and kidney have low levels of PLEKHS1 expression.

We isolated a panel of tissues from *Plekhs1*$^{WT/WT}$ and *Plekhs1*$^{Avi/Avi}$ mice and immuno-blotted for both PLEKHS1 and the Avitag, in whole tissue lysates (Figure 3.12). Surprisingly, we observed a PLEKHS1 band in both *Plekhs1*$^{WT/WT}$ and *Plekhs1*$^{Avi/Avi}$

prostate, but did not detect any PLEKHS1 expression in the other tissues in this panel, indicating that expression of PLEKHS1 is restricted to the prostate.

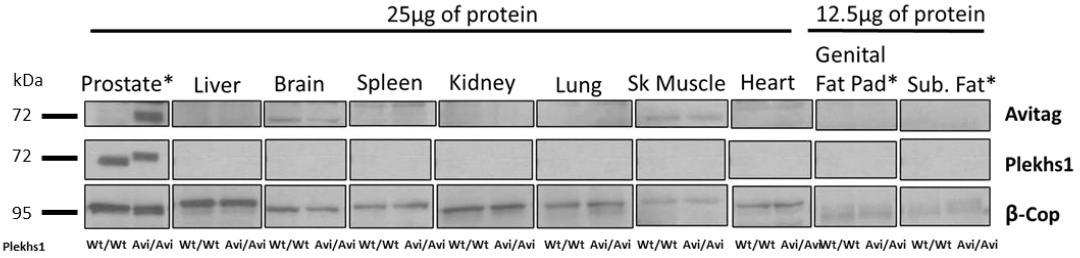


**Figure 3.12 Expression of PLEKHS1 in different mouse tissues**

*Tissues were rapidly dissected from mice (12-15w) with the genotypes indicated in the Figure, lysed and aliquots (25µg or 12.5µg protein, indicated in the Figure, this difference between some tissues was for technical reasons) were immuno-blotted with antibodies directed against the epitopes shown (right of the Figure). All mice were BirA$^{+/-}$, PbCre$^{-/-}$, Pten$^{loxP/loxP}$. The primary antibodies were visualised with HRP-labelled 2$^{0}$-antibodies. β-Cop was used as a loading control. Tissues with high mRNA (based on BioGPS and EMBL databases) level are marked *.*

The BioGPS database indicates the levels of *Plekhs1* mRNA in certain tissues of the female reproductive system; ovaries and uterus are high. To assess the levels of expression of PLEKHS1 protein in these tissues, as well as in oviducts, which are not listed on BioGPS, we immuno-blotted for the Avitag and PLEKHS1, using *Plekhs1*$^{WT/WT}$ and *Plekhs1*$^{Avi/Avi}$ mice. An aliquot prostate lysate was used as a positive control.

Intriguingly, there was no detectable expression of PLEKHS1 protein in ovaries, but high expression in oviducts and uterus (Figure 3.13). Our results suggested stronger expression of PLEKHS1 in uterus and oviducts, compared to the prostate, but further experiments are required to accurately quantify the expression level and function of PLEKHS1 in these tissues.

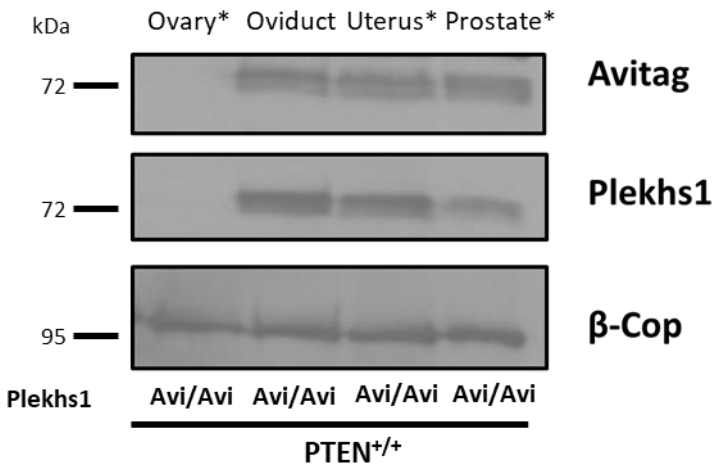


**Figure 3.13 Expression of Plekhs1 in the female reproductive system**

*Tissues were rapidly dissected from Plekhs1$^{Avi/Avi}$ mice (12-15w), lysed and aliquots (30µg protein) were immuno-blotted with antibodies directed against the epitopes shown (right of the Figure) (all mice were BirA$^{+/-}$, PbCre$^{-/-}$, PTEN$^{loxP/loxP}$). The primary antibodies were visualised with HRP-labelled 2$^{0}$-antibodies. β-Cop was used as a loading control. Tissues with high mRNA (based on BioGPS and EMBL databases) level are marked *. Prostate tissue was used as a positive control.*

## 3.2.5 Characterisation of *Plekhs1*$^{Avi/Avi}$ mice

To establish whether the presence of the Avitag on the C-terminus of the PLEKHS1 interfered with any major biological functions some basic measurements were performed. The total body weights of both female and male mice were compared (Figure 3.14). There were no significant differences observed between female *Plekhs1*$^{Avi/Avi}$ and *Plekhs1*$^{WT/WT}$ mice (BirA$^{+/-}$). In a group of males, weights of mice with four genotypes were analysed: control, *Pten* $^{-/-}$ with or without *Plekhs1*$^{Avi/Avi}$. There were no significant differences noticed between those groups.

The wet-weights of the tissues, which we had found expressed relatively large amounts of PLEKHS1, were also measured (Figure 3.15) in Pleksh1$^{WT/WT}$ and *Plekhs1*$^{Avi/Avi}$ mice. The weights of these tissues did not show any significant differences. However, there is a trend indicating a decrease in the weight of the tissues in mice with a tagged version of PLEKHS1, similar to that seen in total body weight.

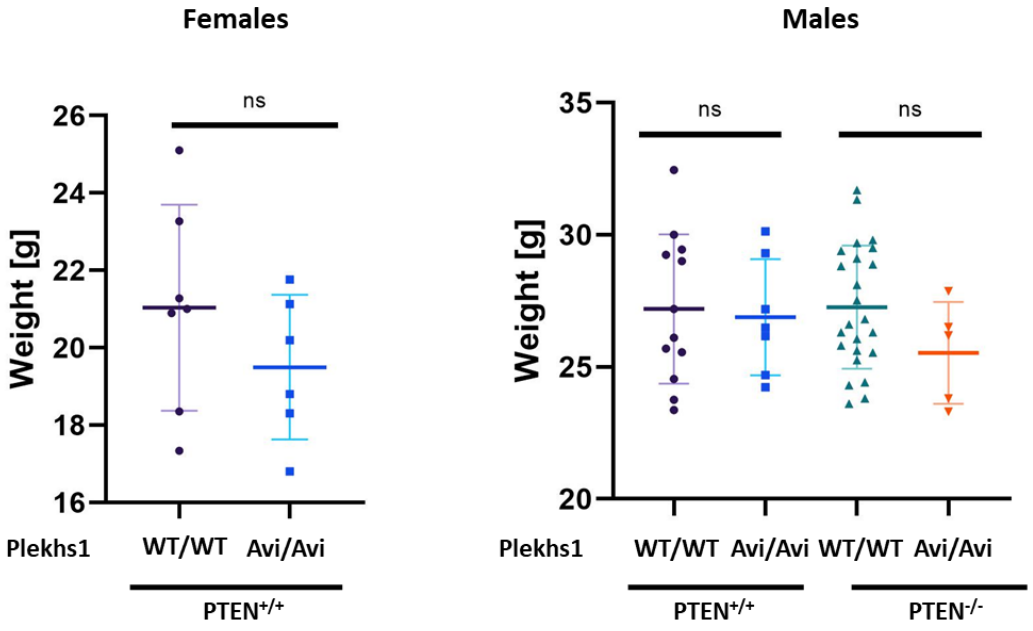


**Figure 3.14 Weights of control, PTEN$^{-/-}$ and/or Plekhs1$^{Avi/Avi}$ mice**

*Male and female mice (12w-15w) of the genotypes indicated were weighed (note the y-axes do not start at 0) (all mice were BirA$^{+/-}$, mice described as PTEN$^{-/-}$ were PbCre$^{+/-}$, PTEN$^{loxP/loxP}$, PTEN$^{+/+}$ were PbCre$^{-/-}$, PTEN$^{loxP/loxP}$). To test statistical significance, a multi-comparison on-way Anova test was appliedData represent means ± SD of minimum 5 biological replicates. Each symbol represents an individual mouse.*

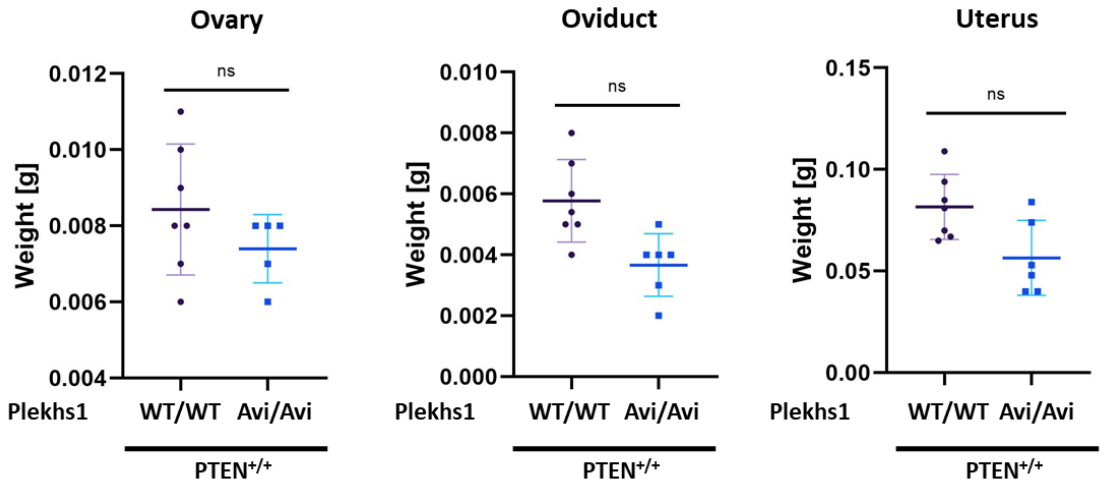


**Figure 3.15 Weights of ovaries, oviducts and uteri isolated from control or *Plekhs1*$^{Avi/Avi}$ mice**

*Ovaries, oviducts and uteri were rapidly dissected from mice (12-15w) with the genotypes indicated and weighed (note the y-axis of the graph showing ovary weights does not start at 0) (all mice were BirA$^{+/-}$, PbCre$^{-/-}$, Pten $^{loxP/loxP}$). To test statistical significance a multi-comparison one-way Anova test was applied. Data represent means ± SD of minimum 5 biological replicates. Each symbol represents an individual mouse.*

Figure 3.16 shows the weights of prostates isolated from control and *Pten* $^{-/-}$ mice, either expressing Avitagged, or wild type, PLEKHS1. The *Pten* $^{-/-}$ mouse model of prostate cancer, described in section 1.4 and 1.5, is a well-established model to study prostate tumorigenesis. Not surprisingly, and similarly to studies published by other groups, we noticed a significant difference in the size of prostates of mice with *Pten* $^{+/+}$ or *Pten* $^{-/-}$ genotypes[156]. Our results also strongly indicate that the presence of the Avitag does not affect weight of prostate tissues in *Plekhs1*$^{Avi/Avi}$ mice.

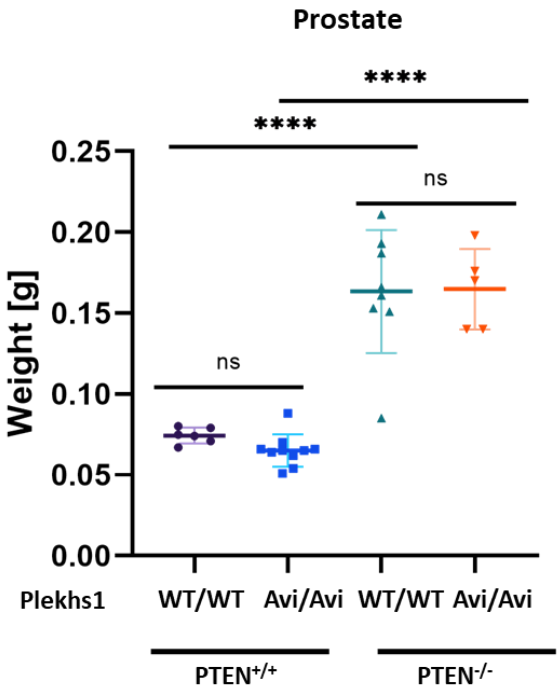


**Figure 3.16 Weights of prostates isolated from control, PTEN$^{-/-}$ and/or Plekhs1$^{Avi/Avi}$ mice**

*Prostate tissue was rapidly dissected from mice (12-15w) with genotypes indicated in the Figure and weighed (all mice were BirA$^{+/-}$, mice described as PTEN$^{-/-}$ were PbCre$^{+/-}$, PTEN$^{loxP/loxP}$, PTEN$^{+/+}$ were PbCre$^{-/-}$, PTEN$^{loxP/loxP}$). To test significance a multi-comparison one-way Anova test was applied. Data represent means ± SD of minimum 5 biological replicates. Each symbol represents an individual mouse.*

# 3.3 *Plekhs1*$^{-/-}$ mouse model

## 3.3.1 KO- first gene editing strategy


**Figure 3.17 Schematic representation of the genetic strategy applied to target the *Plekhs1* locus in mouse ES cells**

*A schematic representation of the Plekhs1 'KO-first' construct transfected into ES cells. Two independent clones were obtained from Eucomm. The 'knockout-first' allele, contains a lacZ reporter/trapping cassette and a floxed promoter-driven neo-selection-cassette inserted into the intron (between exons 4 and 5 in Plekhs1), is predicted to disrupt gene function. Flp converts the 'knockout-first' allele to a conditional allele, restoring gene activity and establishing the potential for Cre-mediated conditional expression of Plekhs1. Exposure to Cre following exposure to Flp deletes the floxed exon of the Plekhs1 allele to disrupt expression. SA, Splice Acceptor; pA, poly-Adenylation signal; FRT, Flippase Recombination Target (for the Flp recombinase); neo, neomycin selection cassette; lacZ, an enzymatic reporter construct based on β-galactosidase*.

To analyse the function of PLEKHS1 in prostate, as well as other mouse tissues, we generated *Plekhs1*$^{-/-}$ mice using conventional gene targeting methodology with ES cells (two clones were obtained from Eucomm, Figure 3.17).

The knockout-first gene editing strategy combines reporter-tagged and conditional expression systems. The initial, unrecombined allele is predicted to be dysfunctional due to the forced heterologous expression, via powerful splice acceptor and polyadenylation sequences (mouse En2 SA), of a lacZ, and not *Plekhs1*, mRNA[157 158]. Conditional KO alleles are created by the activity of a Flp recombinase, which mediates recombination between FRT sites and hence removes the gene-trap cassette, resulting in normal gene

expression. After Flp-mediated recombination, the remaining loxP sites still flank a critical exon. Exposure to Cre recombinase results in deletion of a critical exon and enforces a frameshift between the preceding and following exons ensuring a functional protein cannot be expressed. Usually, loxP sites are positioned in gene introns, in order to preserve normal transcription and translation of the gene. It is important to mention, that both the loxP and FRT sites are situated in positions, which should not interfere with the splice sites of the critical exon[159].

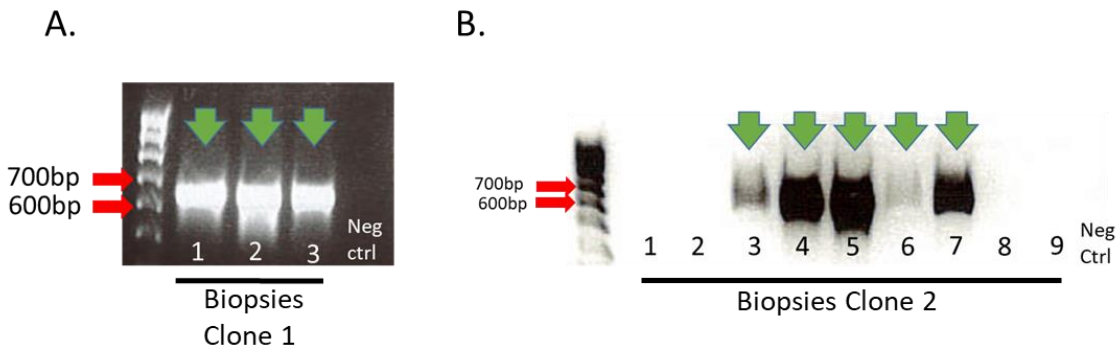


**Figure 3.18 Validation of Plekhs1 gene-targeting in mice**

*(A-B) DNA was isolated from ear clips (3 clips from mice derived from ES cell clone 1 in A and 9 clips from mice derived from ES cell clone 2 in B) and PCR was used to amplify a DNA fragment containing the targeted site. DNA with the desired mutation should give a product of 643bp. The PCR products were resolved by electrophoresis on a 1.5% agarose gel and visualised using UV light. Mice with successfully targeted DNA are indicated with green arrows.*

### 3.3.2 Validation of gene engineered mouse

Two independent clones (see Materials and Methods and Table 2.8 ES *Plekhs1* 'KO-first' clones) of ES cells (C57BL/6N) transfected with *Plekhs1* 'KO-first' constructs were injected into blastocysts produced from an already established colony of *Pten* $^{-/-}$ mice (*Pten* $^{loxP/loxP}$ PbCre). A specific fragment of the genomic DNA isolated from newborn pups, encompassing part of the lacZ construct, was amplified by PCR. Both the forward and the reverse primers used in the genotyping PCR annealed specifically to the lacZ locus, which made the PCR product specific for the *Plekhs1* KO-first allele. Three out of three mice generated from ES clone 1, were born with the mutation (100% efficiency), and five out of nine mice generated using ES clone 2 were born with the desired genetic modification (~55% efficiency).

### 3.3.3 Genotyping and breeding strategy

Resulting chimeric mice were crossed with *Pten* $^{-/-}$ mouse strain (*Pten* $^{loxP/loxP}$ PbCre). The first genotyping results are shown in Figure 3.19. 6 pups were born, and 4 of these showed the presence of the PCR band specific to the targeted allele, indicating that those pups carried the *Plekhs1* KO-first cassette, and that the mutation was carried in the germline. Founders of the new *Plekhs1*$^{-/-}$ colony were interbred with mice from the *Pten* $^{-/-}$ colony on a C57BL/6J genetic background indicated in Figure 3.20.

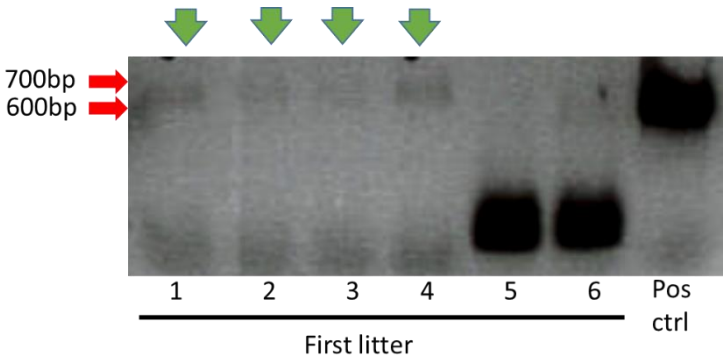

**Figure 3.19 Original Genotyping of first generation of pups from Plekhs1$^{-/+}$ x Plekhs1$^{+/+}$ crosses**

*DNA was isolated from 6 ear clips and PCR was used to amplify a DNA fragment containing the targeted site. DNA with the desired mutation should give a product of 643bp. Mice with successfully edited DNA are indicated with green arrows.*

Founders of Plekhs1-/- Colony
Plekhs1+/-
C57BL6J/N chimeric mice
With a mixed background of Bira+/+ PTENloxP/loxP and PbCre+/-
Multiple crosses with previosuly generated mice of PTENloxP/loxP PbCre+/- genetic background
Backcrossing to C57BL6J
Analysis of prostate cancer progression and activation of PI3K signalling pathway
PTENloxP/loxP
Genotype
Label
Plekhs1+/+ PbCre-/-
Plekhs1+/+ PTEN+/+
Plekhs1+/- PbCre-/-
Plekhs1+/- PTEN+/+
Plekhs1-/- PbCre-/-
Plekhs1-/- PTEN+/+
Plekhs1+/+ PbCre+/-
Plekhs1+/+ PTEN-/-
Plekhs1+/- PbCre+/-
Plekhs1+/- PTEN-/-
Plekhs1-/- PbCre+/-
Plekhs1-/- PTEN-/-

**Figure 3.20 Breeding strategy to produce *Plekhs1* $^{-/-}$ mouse colony**

*The schematic shows breeding strategy of mouse colony. Founders (Plekhs1$^{+/-}$) of the colony with a mixed background and combination of the following alleles: BirA, PTEN, PbCre were crossed with previously generated mice of PTEN$^{loxP/loxP}$ PbCre$^{+/-}$ background to generate mice of C57BL6J background and the genotypes indicated in the Figure.*

### 3.3.4 Validation of Plekhs1$^{-/-}$ mice

After at least four out-crosses, the first cohort of mice with different combinations of genotypes (Plekhs1$^{+/+}$ *Pten* $^{loxP/loxP}$, Plekhs1$^{+/-}$ *Pten* $^{loxP/loxP}$ and Plekhs1$^{-/-}$ *Pten* $^{loxP/loxP}$, all with or without PbCre) were obtained and analysed to validate the efficiency of the Plekhs1 knockout strategy (Figure 3.21). As expected, there was a noticeable band (a doublet), recognised by an anti-Plekhs1 antibody, in prostate isolated from the Plekhs1$^{+/+}$ mouse and ~50% reduction of the intensity of this band in the heterozygous mouse. In the Plekhs1$^{-/-}$ prostate sample, there was no detectable expression of Plekhs1.

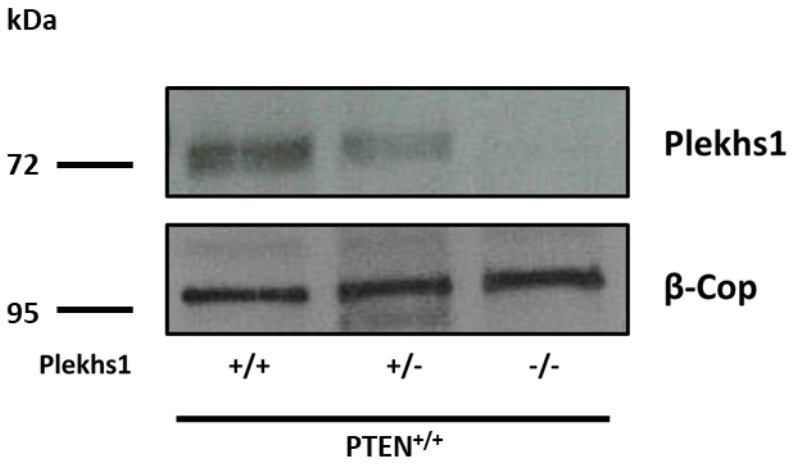


**Figure 3.21 Probing expression of PLEKHS1 in control, *Plekhs1*$^{+/-}$ and *Plekhs1*$^{-/-}$ mouse prostate**

*Prostate tissue was rapidly dissected from mice (12-15w) with genotypes indicated in the Figure, lysed and aliquots (30μg protein) were immuno-blotted with antibodies directed against the epitopes shown (right of the Figure) (all mice were PbCre$^{-/-}$, PTEN$^{loxP/loxP}$). The primary antibodies were visualised with HRP-labelled 2$^{0}$-antibodies. β-Cop was used as a loading control.*

### 3.3.5 Characterisation of Plekhs1 $^{-/-}$ mice

The combination of the genotypes listed in the Section Validation of gene engineered mouse (Section 3.3.2) were subjected to a primary characterisation and the data are shown below.

Figure 3.22 shows lateral and dorsal views of female mice with the genotypes indicated. The animals were all between 15 and 16cm in length, which is considered standard for 12-15 week-old mice. There were no abnormalities or overt phenotypes observed.


**Figure 3.22 Picture of control, *Plekhs1*$^{+/-}$ and *Plekhs1*$^{-/-}$ female mice**

*Lateral and dorsal view of the female mice (12-15w), euthanized with $CO_2$ and cervical dislocation, with genotypes indicated in the Figure (all mice PbCre$^{-/-}$, PTEN$^{loxP/loxP}$).*

The body weights of female *Plekhs1*$^{+/+}$, *Plekhs1*$^{+/-}$ and *Plekhs1*$^{-/-}$ mice were measured (Figure 3.23); there were no significant differences.

After the whole-body measurements the ovaries with attached oviducts and uteri were isolated, the supportive fat layer was removed to expose the tissues of interest, and they were photographed (Figure 3.24). The size and morphology of these tissues from mice with the three different genotypes were compared. We observed no overt differences in the morphology of these tissues between the different genotypes.

Tissues from the female reproductive system were also weighed after dissection (Figure

3.25). Three genotypes: control (*Plekhs1*$^{+/+}$), *Plekhs1*$^{+/-}$ and *Plekhs1*$^{-/-}$ were compared. According to our observations, there was no significant difference in the weight of *Plekhs1*$^{-/-}$ ovaries compared to *Plekhs1*$^{+/+}$ ovaries. In addition, there was no significant difference in the weight of the uteri. However, we observed a trend towards decreased weights of uteri from Pleksh1-null compared to *Plekhs1*-wild-type mice. Surprisingly, there was a significant reduction in the weight of oviducts from *Plekhs1*-null compared to *Plekhs1*-wild-type mice. To understand the function of *Plekhs1* in oviduct development and (patho-) physiology, further investigations will be required.

We performed a similar primary phenotypic characterisation of male *Plekhs1*-manipulated mice. Figure 3.24 shows lateral and dorsal views of male mice with six different genotypes (indicated in the figure). No significant differences in the size, gross morphology (Figure 3.24) and weight (Figure 3.26) between the different genotypes of those mice were observed.

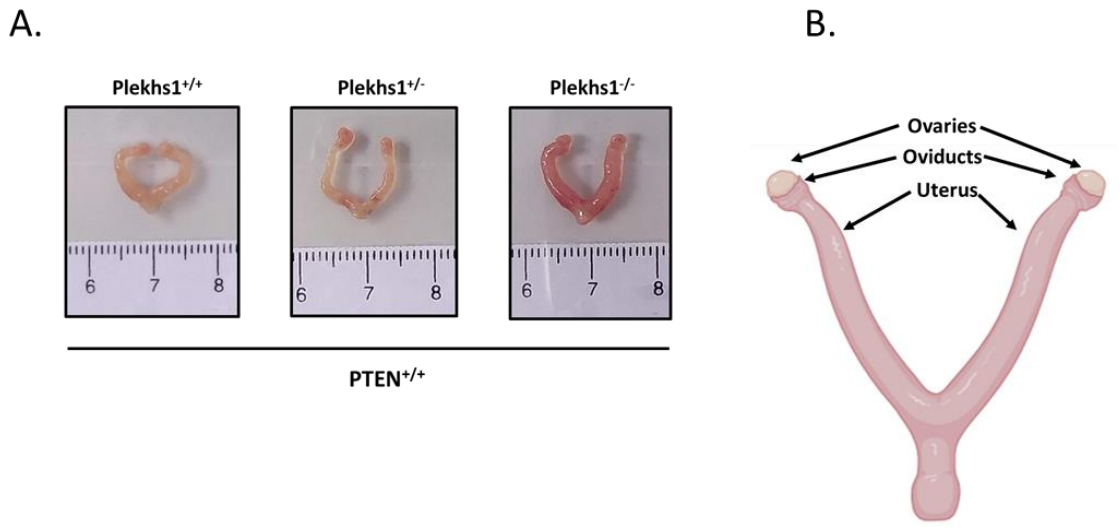


**Figure 3.23 Picture of control, *Plekhs1*$^{+/-}$ and *Plekhs1*$^{-/-}$ female reproductive systems**

*A. Female reproductive system: ovaries, oviducts and uteri were rapidly dissected from mice (12-15w) with genotypes indicated in the Figure (all mice were PbCre*$^{-/-}$*, PTEN*$^{loxP/loxP}$*).*

*B. Schematic showing the structure of female mouse reproduction system*

Prostate tissue, which is an example of tissue with very high expression of Plekhs1, was isolated from mice with the indicated genotypes. In Figure 3.25, representative pictures are shown. There is a significant change in the size of the prostate comparing WT mice and mice lacking expression of *Pten* in prostate luminal epithelium (*Pten* $^{-/-}$), which has been previously described in the literature[160] and is also in accordance with our previous observations at this stage of tumorigenesis (T. Chessa, unpublished). Interestingly, we observed a striking phenotype in the *Pten* $^{-/-}$ *Plekhs1* $^{-/-}$ prostate, namely that the size and wet weight of *Pten* $^{-/-}$ *Plekhs1* $^{-/-}$ prostates were significantly smaller compared to *Pten* $^{-/-}$ *Plekhs1* $^{+/+}$ prostates. In the PbCre, *Pten* $^{loxP/loxP}$ mouse model of prostate tumour progression the dorsal-lateral prostate (DLP) characteristically displays evidence of the greatest relative rate of tumour progression followed by anterior prostate (AP) and ventral prostate (VP)[161]. However, it was impossible to directly visualise the DLP in my photographs of the organ. The AP is the most visible structure in mouse prostate and the most prominent and consistently aligned in the photographs. Following the photography, the weights of the micro-dissected, pooled prostate lobes were measured from mice with indicated genotypes (Figure 3.28). As observed previously, whole prostate weights are significantly higher in mice without a functional *Pten* gene (T. Chessa, unpublished). This data is in agreement with photographs displayed in Figure 3.16 and Figure 3.25, as well as with previously published studies by other groups[162 156]. We observed a striking reduction in the weights of *Plekhs1* $^{-/-}$ *Pten* $^{-/-}$ pooled prostate lobes, compared to *Plekhs1* $^{+/-}$ *Pten* $^{-/-}$ and *Plekhs1* $^{+/+}$ *Pten* $^{-/-}$ prostates. Histological analysis of this phenotype is currently underway.

These results indicate that Plekhs1 is required for tumour progression in a *Pten* $^{-/-}$, mouse-model of prostate tumorigenesis.

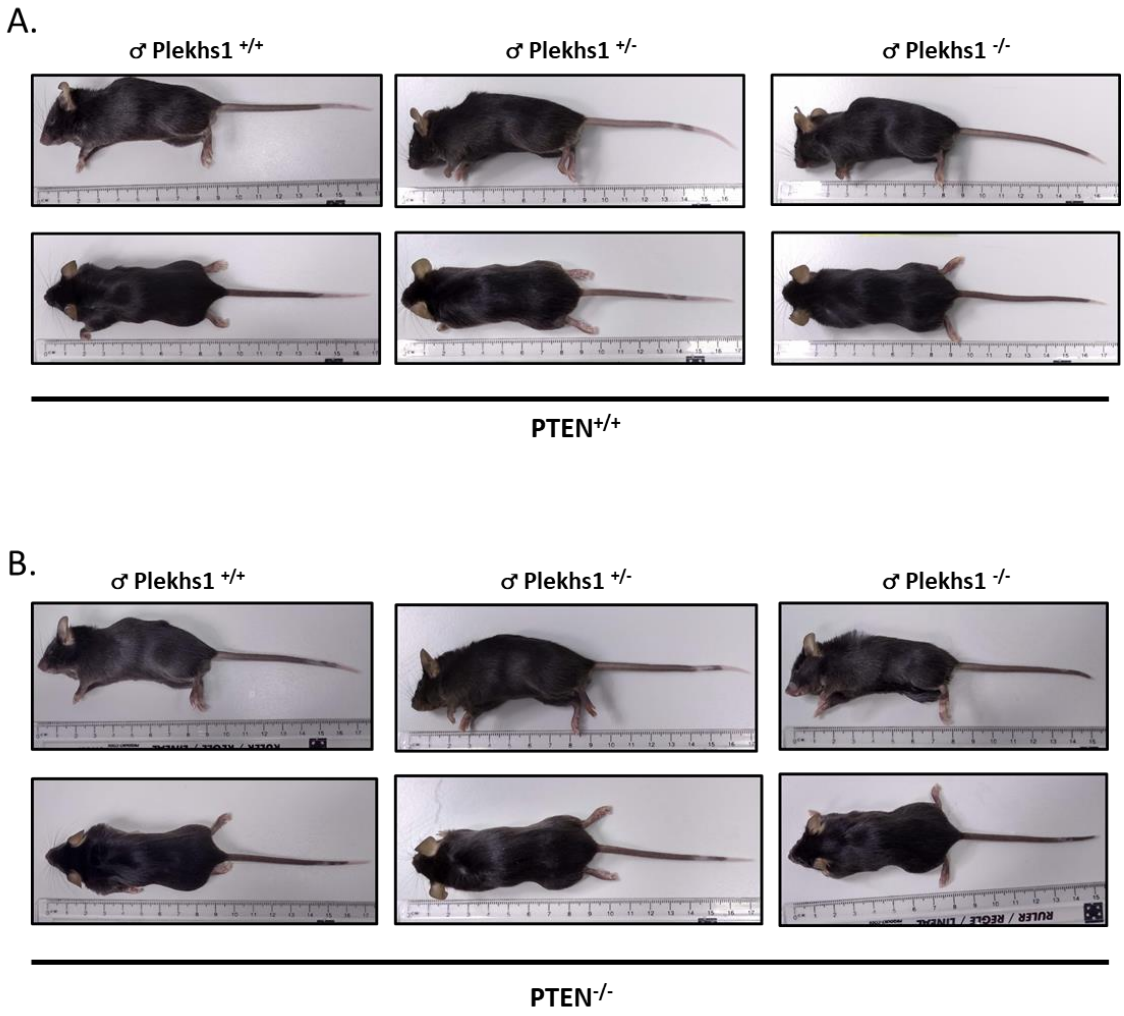


**Figure 3.24 Picture of control, PTEN$^{-/-}$ and/or *Plekhs1*$^{-/-}$ male mice**

(*A-B) Lateral and dorsal view of the male mice (12-15w), euthanized with $CO_2$ and cervical dislocation, with genotypes indicated in the Figure (mice described as PTEN$^{-/-}$ were PbCre$^{+/-}$, PTEN$^{loxP/loxP}$, PTEN$^{+/+}$ were PbCre$^{-/-}$, PTEN$^{loxP/loxP}$)*

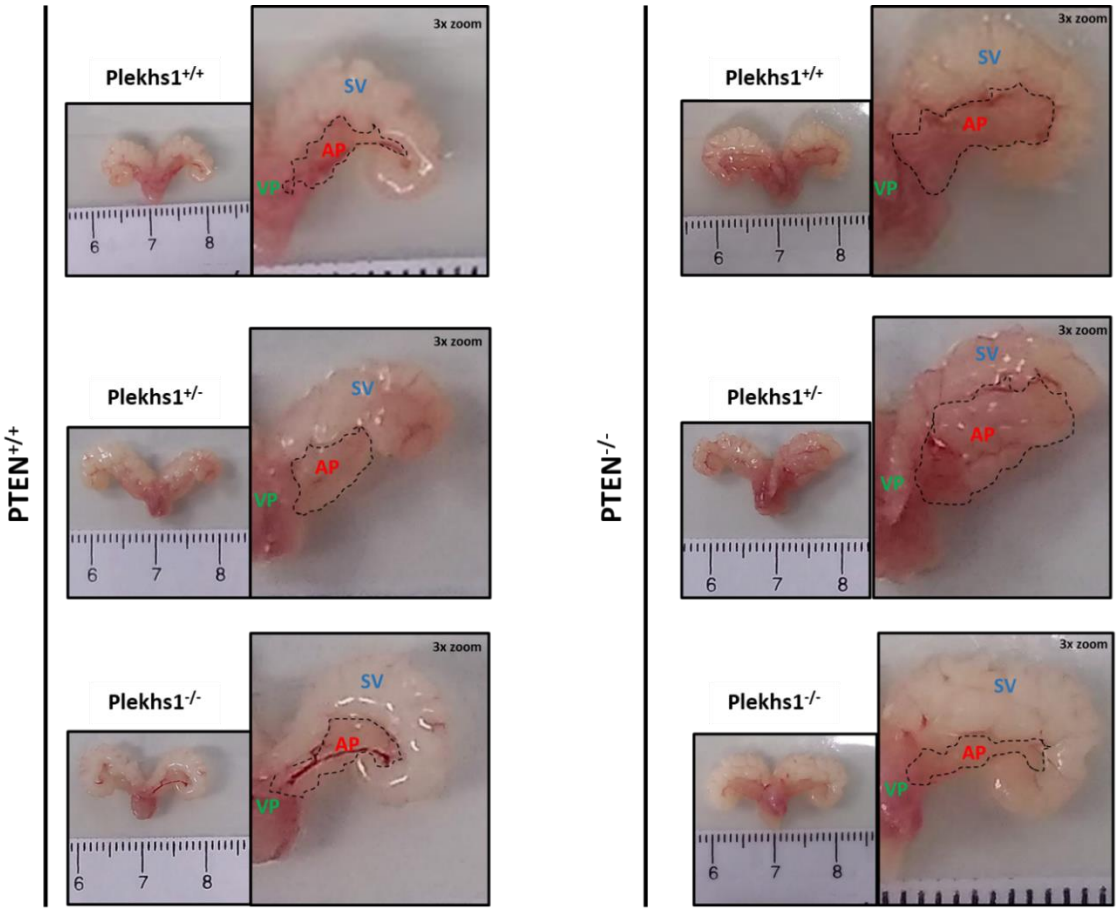


**Figure 3.25 Pictures of control, PTEN$^{-/-}$ and/or *Plekhs1*$^{-/-}$ mouse prostates**

*Prostate tissue was rapidly dissected from mice (12-15w) with genotypes indicated in the Figure (mice described as PTEN$^{-/-}$ were PbCre$^{+/-}$, PTEN$^{loxP/loxP}$, PTEN$^{+/+}$ were PbCre$^{-/-}$, PTEN$^{loxP/loxP)}$. Magnified pictures highlight ventral prostate- **VP**, seminal vesicles-**SV** and anterior prostate- **AP** (also outlined).*

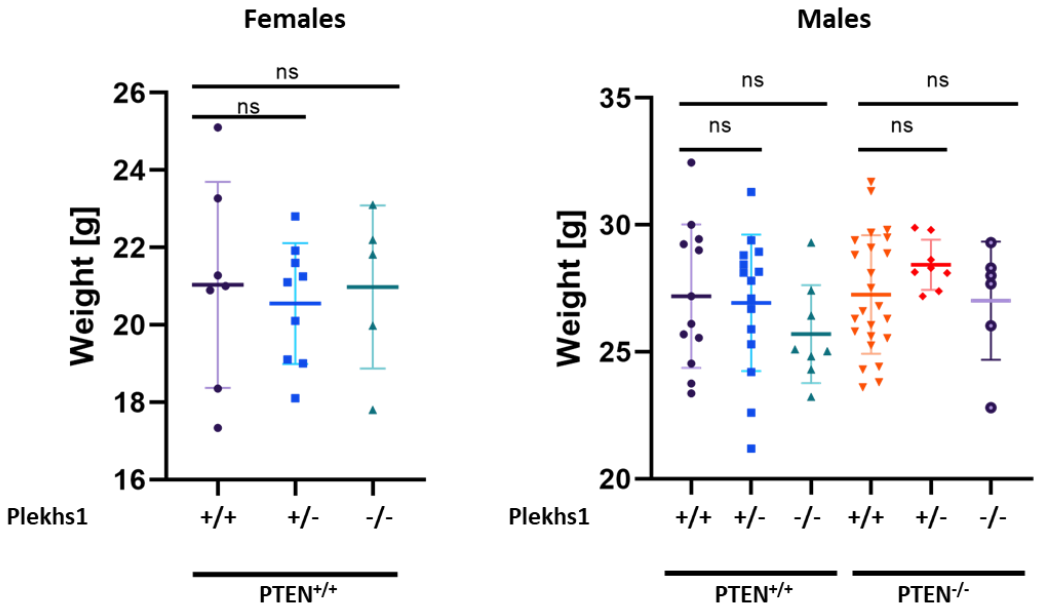


**Figure 3.26 Weights of control, PTEN$^{-/-}$ and/or *Plekhs1*$^{-/-}$ mice**

*Male and female mice (12w-15w) of the genotypes indicated in the Figure were weighed (mice described as PTEN$^{-/-}$ were PbCre$^{+/-}$, PTEN$^{loxP/loxP}$, PTEN$^{+/+}$ were PbCre$^{-/-}$, PTEN$^{loxP/loxP}$) (note the y-axes do not start at 0). To calculate significance, a multi-comparison one-way Anova test has been applied. Data represent means ± SD of minimum 5 biological replicates. Each symbol represents individual mouse.*

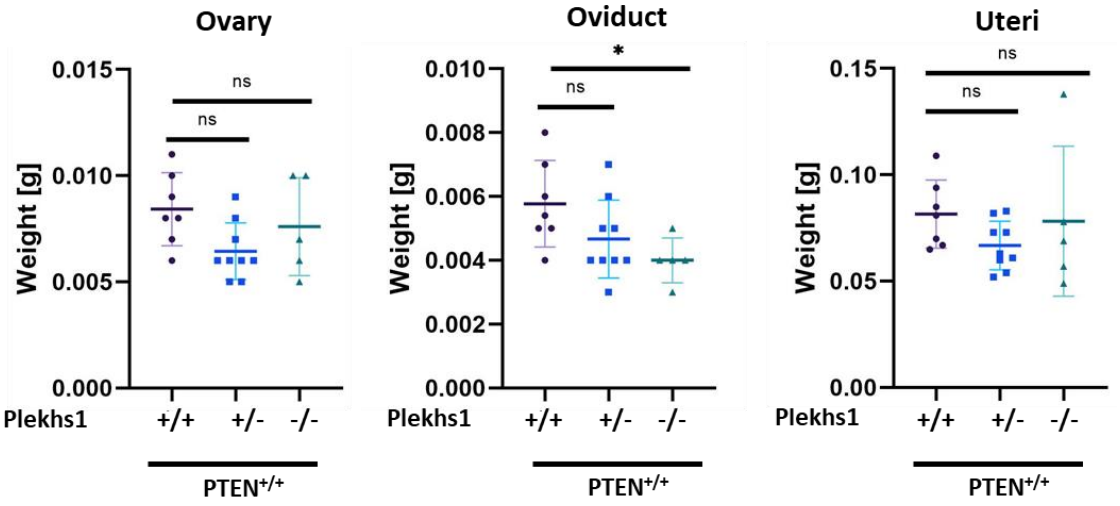

**Figure 3.27 Weights of ovaries, oviducts and uterus isolated from control and *Plekhs1*$^{-/-}$ mice**

*Ovaries, oviducts and uteri issue were rapidly dissected from mice (12-15w) with genotypes as indicated in the Figure (all mice were PbCre$^{-/-}$, PTEN$^{loxP/loxP}$).*
*To test statistical significance a multi-comparison one-way Anova test was applied. Data represent means ± SD of minimum 5 biological replicates. Each symbol represents individual mouse.*

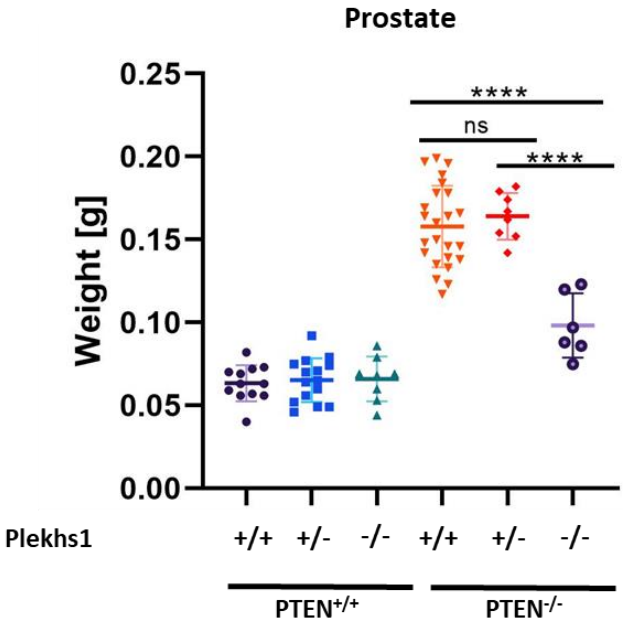


**Figure 3.28 Weights of prostates isolated from control, PTEN$^{-/-}$ and/or *Plekhs1*$^{-/-}$ mice**

*Prostate tissue was rapidly dissected from mice (12-15w) with genotypes (mice described as PTEN$^{-/-}$ were PbCre$^{+/-}$, PTEN$^{loxP/loxP}$, PTEN$^{+/+}$ were PbCre$^{-/-}$, PTEN$^{loxP/loxP}$) as indicated in the Figure and weighed. To calculate significance, a multi-comparison one-way Anova test was applied. Data represent means ± SD of minimum 5 biological replicates. Each symbol represents individual mouse.*

## 3.4 Discussion

In this chapter, I described the development and primary characterisation of mice generated by two mouse gene-targeting projects; *Plekhs1*$^{Avi/Avi}$ and *Plekhs1*$^{-/-}$.

We chose to generate the *Plekhs1*$^{Avi/Avi}$ mouse model to enable us to perform highly efficient and specific streptavidin-mediated pulldown of endogenous PLEKHS1, followed by identification of its interactors in the context of healthy and *Pten* $^{-/-}$ prostate tissue (results from these experiments are described in Chapter 5).

Ubiquitous expression of the Avitagged-*Plekhs1* construct in all mouse tissues enabled us to perform a cross-validated screen of PLEKHS1 expression in a panel of different tissues. We immunoblotted tissue lysates using both anti- PLEKHS1 and anti-Avitag antibodies, and we were able to demonstrate that PLEKHS1 is expressed strongly in the prostate in male mice, and in the oviduct and uterus of female mice. In recent years, several publications highlighted a role for Class I PI3K signalling network in the female reproductive system. Mutations in Class I PI3K signalling network genes have been observed in carcinosarcomas of the uterus and ovaries[163].

We successfully demonstrated that the Avitag does not affect the expression of endogenous PLEKHS1 protein. We also noted that the full body weight and broad appearance of both male and female mice does not significantly change in the presence of the Avitagged- PLEKHS1 compared to controls. In addition, we demonstrated that there are no significant changes in the weight of the male or female reproductive tissues in the presence of endogenously Avitagged PLEKHS1.

The *Plekhs1*$^{-/-}$ mouse model that we generated is an outstanding tool to define PLEKHS1 function in healthy tissue as well as during prostate tumour progression. In the next Chapter 1, describe our investigation of the function and phosphorylation of PLEKHS1 in healthy prostate and prostate going through hyperplasia. In this chapter, my work showed that *Plekhs1*$^{-/-}$ mice are viable and have normal total body size and weight. I found no convincing evidence suggesting that were changes in fertility of either males or females, although more experiments will need to be pursued to verify this with high confidence. Female *Plekhs1*$^{-/-}$ mice showed a significant reduction in the weight of their oviducts, but not in any of the other tissues analysed. Given the trend towards a decrease in uterine weight in *Plekhs1*$^{-/-}$ females, more experiments will be needed to

establish whether the absence of PLEKHS1 affects uterine growth. Similarly, further investigation is required to establish whether PLEKHS1 plays a broader role in the development and (patho-) physiology of the female reproductive system.

The most striking observations were observed when comparing the total weight of prostate tissue isolated from WT and *Pten* $^{-/-}$ tissues with or without PLEKHS1. Previous unpublished work from our laboratory, as well as much published work, has shown that the prostate expands significantly when PTEN is absent from the prostate epithelium; both at the age of 12-weeks, when tumour progression has reached the stage of prostate intraepithelial neoplasia (PIN), as well as in later stages of tumour progression[156]. We demonstrated that when both PLEKHS1 and PTEN are absent the size of the prostate is significantly smaller compared to the *Pten* $^{-/-}$ *Plekhs1* $^{+/+}$ prostate. This discovery suggests a non-redundant role for *Plekhs1* in *Pten* $^{-/-}$ mediated prostate tumorigenesis. These findings open a major opportunity to study the role of PLEKHS1 in physiology and pathology of the prostate, in the context of Class I PI3K signalling, and possibly other cell signalling pathways.

# 4 PLEKHS1, A MAJOR REGULATOR OF PI3K SIGNALLING IN THE PTEN$^{-/-}$ MOUSE MODEL FOR PROSTATE CANCER

## 4.1 Introduction

We have established a role for PLEKHS1 in prostate growth in the context of prostate intraepithelial neoplasia (PIN) in the PbCre x *Pten* $^{loxP/loxP}$ mouse model of prostate cancer. Unpublished data from our laboratory also indicated that the interaction between PLEKHS1 and Class IA PI3K subunits increased significantly when PTEN is absent (T. Chessa, unpublished data, Section 1.5 PLEKHS1- a new interactor of Class IA PI3K). The mouse PLEKHS1 sequence contains a tyrosine residue, Y257, which resides in an YxxM motif, a consensus for binding to the SH2 domains of PI3K regulatory subunits. Indeed, a study by Grossman et al[109] showed a direct interaction between human PLEKHS1, when phosphorylated on the equivalent residue (Y248xxM), and the class I PI3K regulatory subunit p55ɣ, in transiently transfected cells. Hence, we hypothesise that phosphorylation of mouse PLEKHS1 on Y257 enables its interaction with, and activation of, class IA PI3Ks. We propose that increased tyrosine phosphorylation of PLEKHS1 and its association with class IA PI3Ks in *Pten* $^{-/-}$ prostate leads to this becoming a major driver of the $PIP_3$ network in this cancer model.

In the first part of this chapter I present data from studies performed *"in transfecto"*, where we attempted to elicit phosphorylation of PLEKHS1 on Y257 through the expression of a constitutively active Src kinase, or upon receptor stimulation, and measured the interaction between mouse PLEKHS1 and the regulatory subunits of PI3K under these experimental conditions.

Next, in order to address whether PLEKHS1-PI3K interaction is dependent on the phosphorylation status of PLEKHS1 *in vivo*, and whether phosphorylation of PLEKHS1 is enhanced in *Pten* $^{-/-}$ prostates, we measured phosphorylation of endogenously Avitagged PLEKHS1, in the context of *Pten* $^{+/+}$ or *Pten* $^{-/-}$ prostates.

Finally, we set out to define the function of PLEKHS1 in PI3K signalling in healthy prostate and in prostate intra-epithelial neoplasia.

## 4.2 Interaction between PI3K and PLEKHS1 *in transfecto* in the presence of constitutively active Src

Src-family kinases are a group of non-receptor tyrosine kinases containing nine members: Lck, Hck, Fyn, Blk, Lyn, Fgr, Yes, Yrk and Src itself. They function to regulate various cellular processes in response to growth factors, cytokines, adhesion and antigen receptors. In the Src domain structure, we can distinguish consecutive SH3 (Src homology 3 domain), SH2 domain (Src homology 2 domain) as well as the catalytic tyrosine kinase region (Figure 4.1). There is also a divergent region ('Var'), containing 50-70 amino acids that differ between members of the family. A central characteristic of the Src-family kinases is that they can be phosphorylated near the C-terminus (Y527 in Src) by Csk (C-terminal Src kinase). When Y527 is phosphorylated it forms an intramolecular association with Src's SH2 domain and keeps the catalytic region in a closed, inactive conformation. Following dephosphorylation of the Y527 site, Y416 is auto-phosphorylated leading to Src adopting a catalytically active conformation (Figure 4.1C) [164].

A.

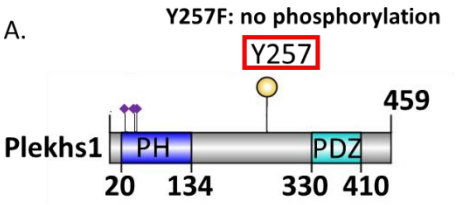
Y257F: no phosphorylation
Y257
459
Plekhs1
PH
PDZ
20
134
330
410

B.

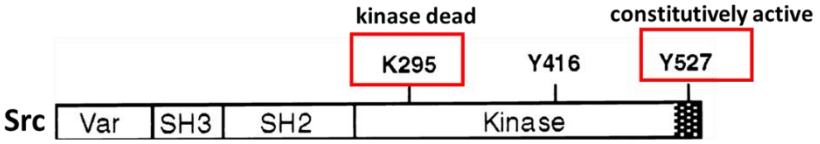
kinase dead
constitutively active
K295
Y416
Y527
Src
Var
SH3
SH2
Kinase

C.

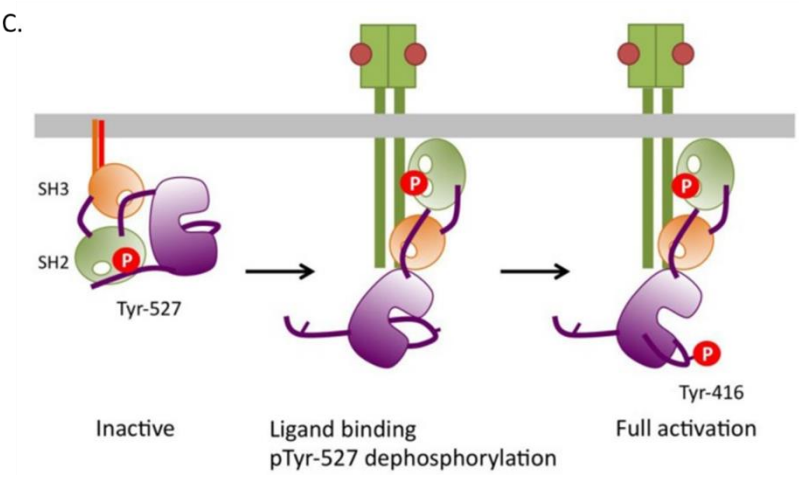
SH3
SH2
P
Tyr-527
P
P
Tyr-416
Inactive
Ligand binding
pTyr-527 dephosphorylation
Full activation

**Figure 4.1 Schematic of the domain organisation of Plekhs1 and Src and mechanism of Src activation**

A. *Schematic of Plekhs1 domain organisation with highlighted PH (Plekstrin homology domain) and PDZ domain and the YxxM motif (Y257) that was targeted. The Y257F (in red frame) mutant was used to pursue experiments shown in Figure 4.2*
B. *Schematic of Src domain organisation. Y416 is a target of the A-419259 inhibitor. K295 and Y527 residues mutants were used to pursue experiments showed in Figure 4.2 (adapted from Xu et al., PNAS 1999).*
C. *Schematic models of inactive and active forms of Src. Inactive Src is phosphorylated at Y527 and adopts a closed conformation. It is stabilised by two interactions: 1) binding to Y527 to its own SH2 domain and 2) binding of the SH2 domain to the SH3 domain. Once Y527 is dephosphorylated, the inactive conformation is disrupted. Active Src can auto-phosphorylate Y416 which locks the enzyme in an active conformation (adapted from Okada, Int J Biol Sci 2012).*

It has previously been shown that human PLEKHS1, once phosphorylated by Src kinase, interacts via Y248xxM (equivalent to mouse Y257xxM; Figure 4.1A) with class IA PI3K regulatory subunits[109].

We performed experiments to test the ability of mouse PLEKHS1 to interact with regulatory subunits of class IA PI3K *"in transfecto"*. We hypothesised that this interaction is mediated by phosphorylation of the Y-257-xxM motif of PLEKHS1 and subsequent binding to the SH2 domain of p85s [165] (Figure 4.2). We transfected HeLa cells, which do not contain detectable endogenous PLEKHS1, with plasmids carrying monomeric-EGFP-tagged WT-*Plekhs1* (cDNA cloned from mouse prostate) or EGFP-Y257F-*Plekhs1*. Cells were co-transfected with plasmids expressing constitutively active Y527F-Src or kinase-dead K295R-Src. Following transfection cells were incubated with a selective Src-family kinase inhibitor, A-419259, or its vehicle. After performing GFP-trap mediated pulldown (immuno-blots of the lysates before (pre) and after (post) pulldown showed that the GFP-trap pulldowns had worked efficiently), bead eluates were immunoblotted using a custom-made anti-phospho-Y257- PLEKHS1 antibody (P-PLEKHS1 in Figure 4.2 ) and an anti-pan-p85 antibody. Immunoblot of 'Pre' and 'Post' pulldown samples were probed for P-Src (Y416) and total Src. Surprisingly, we observed Src416Y phosphorylation in both closed (K295R) and open (Y257F) confirmation of the enzyme, which was reduced by the inhibitor treatment. Higher phosphorylation level of Src Y416 in 'kinase dead' comparing to Y257F construct might be due to different abilities of phosphatases to bind to distinct mutants. To validate these unexpected results, more replicates of the experiment will be required. We detected a strong band with the anti-phospho-Y257- PLEKHS1 antibody, at approximately 90-100kD, consistent with the size of EGFP- PLEKHS1, and a strong band at approximately 85kD with the anti-pan-p85 antibody, consistent with p85αand/or p85β being present in the pulldowns. Both of these bands appeared only when the cells were transfected with the WT form of EGFP-*Plekhs1* and the constitutively active form of Src, in the absence of the Src-family kinase inhibitor. Therefore, we can conclude that PLEKHS1 interacts with p85 subunits upon phosphorylation on Y257, through the action of Src, *in transfecto*. This is entirely consistent with previous work[109]. In future work we aim to identify the kinase that phosphorylates Y257- PLEKHS1 *in vivo.*

To determine whether phosphorylation of PLEKHS1 is elicited upon growth factor stimulation, we stimulated HeLa cells, transiently expressing EGFP-WT- PLEKHS1, with Insulin-like Growth Factor (IGF), at a dose known to elicit near-maximal effects (100ng/ml) (Figure 4.3). The cells were lysed and subjected to GFP-trap mediated pulldown, (which was demonstrated to be efficient, Figure 4.3A) and the eluates were immuno-blotted with anti-pan-p85 antibodies (as this was more sensitive than the anti-phospho-Y257- PLEKHS1 antibody). To ensure the IGF stimulation had elicited activation of the class I PI3K pathway, we immuno-blotted total cell lysates with an anti-phospho-Ser473-Akt antibody. That revealed a clear IGF-stimulated increase in phosphorylation of Ser473-Akt (Figure 4.3B). However, we were not able to detect an IGF-stimulated increase in p85 interaction with PLEKHS1 (Figure 4.3B). Hence, we can conclude that IGF cannot stimulate an increase in the interaction of class IA PI3Ks with heterologous PLEKHS1 in Hela cells. Future works aims to investigate a wider range of agonists and in

cells expressing endogenous PLEKHS1.

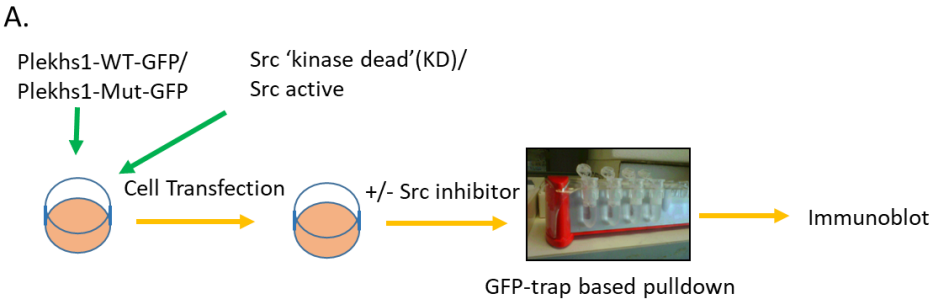


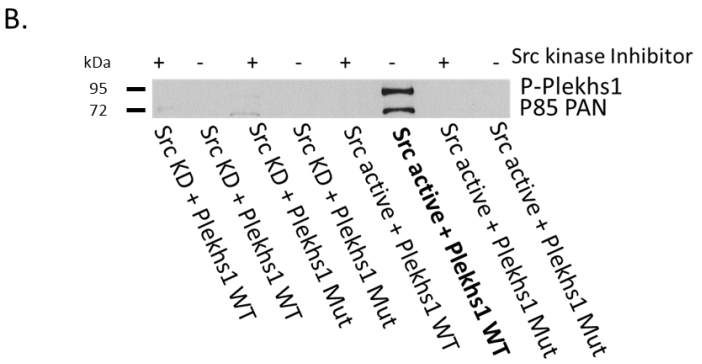


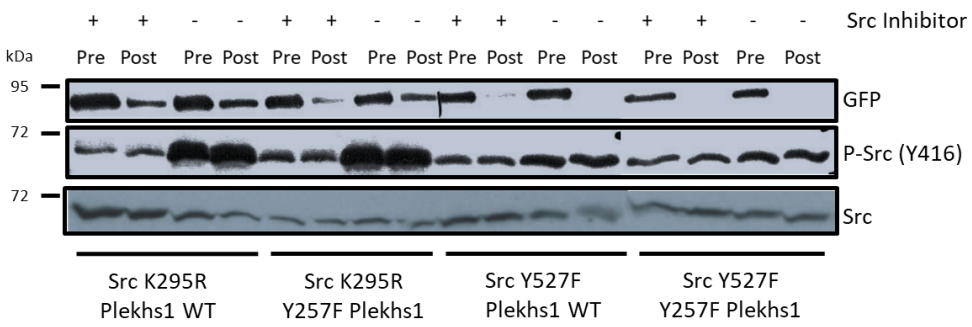

**Figure 4.2 The interaction between Plekhs1 and p85 in the presence or absence of active Src in transfected cells.**

A. *Schematic representation of the workflow. Hela Cells were transfected with the plasmids indicated in the Figure; EGFP-WT-Plekhs1, EGFP-Y257F-Plekhs1, kinase-dead K295R-Src or constitutively active Y527F-Src. The cells were incubated with or without the Src-inhibitor A-419259 (1μM for 1h), lysed and mixed with GFP-trap beads. The beads were washed and eluted with SDS-PAGE sample buffer.*
B. *GFP-trap pulldowns (1.5mg input protein) were performed as in (A). Bead eluates (100% of input) were immuno-blotted with the indicated $1^0$-antibodies (right of Figure), HRP-linked $2^0$-antibodies and visualised.*
C. *Total cell lysates were collected before ('pre') and after ('post') GFP-trap pulldown. Aliquots (50μg protein) were immuno-blotted with antibodies directed against the epitopes shown (right of the Figure). The primary antibodies were visualised with HRP-labelled $2^0$-antibodies. β-Cop was used as a loading control. The results were obtained in 1 experiment.*

A.

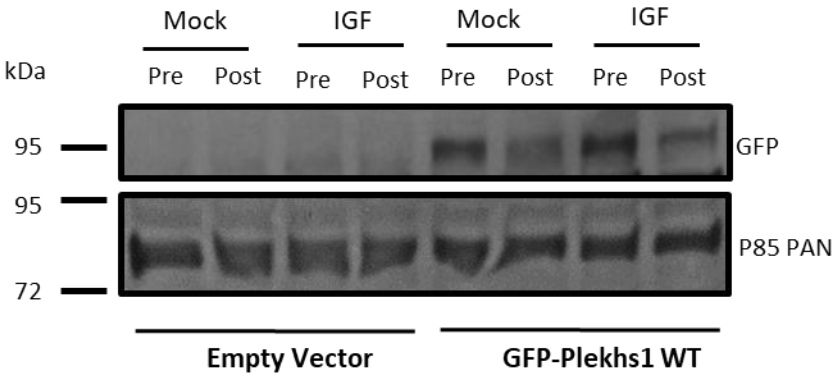
Mock
IGF
Mock
IGF
kDa
Pre
Post
Pre
Post
Pre
Post
Pre
Post
95
95
72
GFP
P85 PAN
Empty Vector
GFP-Plekhs1 WT

B.

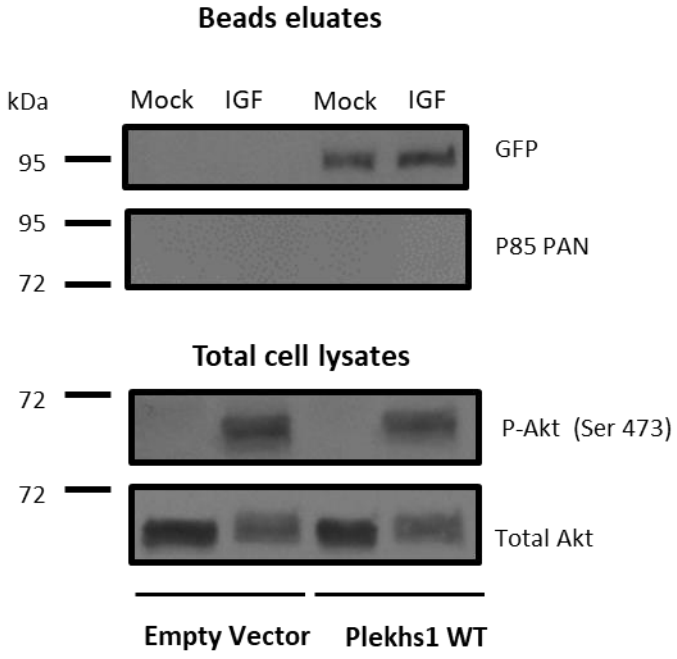
Beads eluates
kDa
Mock
IGF
Mock
IGF
95
95
72
GFP
P85 PAN
Total cell lysates
72
72
P-Akt (Ser 473)
Total Akt
Empty Vector
Plekhs1 WT

**Figure 4.3 Testing the interaction of heterologous GFP-Plekhs1 with p85s in IGF-stimulated HeLa cells**

*HeLa cells were transfected with the plasmids indicated in the Figure, stimulated with IGF (100ng/ml for 90s) or its vehicle, lysed, mixed with GFP-trap beads, washed and the eluates were immuno-blotted with primary antibodies directed at the epitopes indicated on the right. Following incubation with HRP-linked $2^0$-antibodies the blots were visualised.*

A. *Aliquots of the total cell lysates (30μg protein, collected before ('pre') or after ('post') pulldown) were immuno-blotted with anti-GFP (upper panel) and anti-pan-p85 (lower panel) antibodies. Demonstrating the GFP-trap pulldowns and PAN-p85-immuno-blots had worked efficiently.*
A. *Bead eluates; aliquots of the eluates (100% of input) were immuno-blotted with anti-GFP and anti-pan-p85 antibodies. Demonstrating the EGFP-Plekhs1 had been pulled down but that there was no IGF-stimulated increase in interaction of EGFP-Plekhs1 with p85s.*

*Total cell lysates; aliquots of the total cell lysates (30μg protein, after (post) pulldown) were immuno-blotted with anti-phospho-S473-Akt antibodies (upper panel) or anti-total-Akt antibodies (lower panel) as a loading control. Demonstrating IGF had stimulated phosphorylation of Akt in this experiment.*

*The results were obtained in 1 experiment.*

## 4.3 PLEKHS1 phosphorylation on Y257 is enhanced in PTEN$^{-/-}$ prostates

Previous work from our laboratory has indicated that an interaction between PLEKHS1 and class I PI3K p85 subunits is strongly enhanced in *Pten* $^{-/-}$ mouse prostate (T. Chessa, unpublished and see the Introduction). The work presented above, demonstrated that phosphorylation of PLEKHS1 on Y257 is necessary for interaction with p85s. We hypothesised that phosphorylation of this residue is enhanced in *Pten* $^{-/-}$ prostate, compared to *Pten* $^{+/+}$ prostate.

To investigate whether the phosphorylation status of PLEKHS1 is indeed altered in the

absence of PTEN, we performed streptavidin-mediated pulldown of Avitagged PLEKHS1 (*Plekhs1*$^{Avi/WT}$) from *Pten* $^{+/+}$ and *Pten* $^{-/-}$ prostate lysates (Figure 4.4) and immuno-blotted the resulting bead-eluates with antibodies against phospho-Y257- PLEKHS1 (P-PLEKHS1), total PLEKHS1, the Avitag and pan-p85s.

The results to these experiments also served to validate a number of aspects of the methodologies we employed and the endogenous Avitagged *Plekhs1* construct. The Avitag and total Plekhs1 immuno-blots in Figure 4.4B show that the Avitagged PLEKHS1 is both completely biotinylated *in vivo* and then completely captured by streptavidin pulldown (quantification in Figure 4.6). The lack of WT- PLEKHS1 in streptavidin pulldowns shows the process is specific. The biotinylated PLEKHS1 is then efficiently eluted in a first wash with SDS-sample buffer (Figure 4.6A).

The results indicate that a specific interaction between endogenous PLEKHS1 and p85 proteins in mouse prostate can be detected *via* pulldown of PLEKHS1 and that interaction is increased in *Pten* $^{-/-}$ compared to WT prostate. These results represent independent confirmation of the unpublished work of Tamara Chessa, presented in the Introduction.

It is clear that there is an increase in phospho-Y257- PLEKHS1 in *Pten* $^{-/-}$ compared to *Pten* $^{+/+}$ prostate (Figure 4.4A). The results of the experiments immuno-blotting tissue lysates from *Pten* $^{-/-}$ compared to *Pten* $^{+/+}$ for the Avitag and total PLEKHS1 (Figure 4.4B) indicate that the expression of both Avitagged and WT PLEKHS1 had increased similarly in *Pten* $^{-/-}$ prostate. Quantification of the change in P- PLEKHS1/total PLEKHS1 shows a 2-fold increase from *Pten* $^{+/+}$ to *Pten* $^{-/-}$ prostate (measured as P- PLEKHS1 /Avitag- PLEKHS1, Figure 4.5). These observations suggest that the stoichiometry of phosphorylation of Y257- PLEKHS1 had increased in *Pten* $^{-/-}$ compared to *Pten* $^{+/+}$ prostate. The increased stoichiometry of phosphorylation of Y257- PLEKHS1 combines with the increased levels of PLEKHS1 protein in *Pten* $^{-/-}$ prostate to yield a large overall increase in the amount of phosphorylated Y257- PLEKHS1 per unit of tissue. Our results have shown that phosphorylated Y257- PLEKHS1 is a potential binding site for class IA PI3K regulatory subunits and hence the increase its concentration could drive an increase in their association.

Unpublished work from Tamara Chessa (part of which is presented in the Introduction) has shown that the expression of p85$\alpha$ and p85$\beta$ is similar in *Pten* $^{+/+}$ and *Pten* $^{-/-}$ prostate

from 12-15w mice and that there is a substantial molar excess of p85 proteins compared to their bound, tyrosine-phosphorylated adaptors, including PLEKHS1, in 12-15w *Pten* $^{-/-}$ or *Pten* $^{+/+}$ mouse prostate. These results are compatible with the idea that an increase in the concentration of phosphorylated Y257- PLEKHS1 in *Pten* $^{-/-}$ prostate could drive its increased association with class IA PI3Ks.

These conclusions were supported by further, unpublished experiments conducted by Tamara Chessa (to which I made some small contributions); in which lysates of *Pten* $^{-/-}$ and *Pten* $^{+/+}$ 12-15w mouse prostate were immuno-precipitated with anti-phosphotyrosine antibodies (Figure 4.7). By immuno-blotting the tissue lysates and anti-phosphotyrosine pulldowns with anti- PLEKHS1 antibodies it was clear there had been a substantial increase in the amount of phosphotyrosine-associated PLEKHS1 in *Pten* $^{-/-}$ compared to *Pten* $^{+/+}$ prostate. These results do not show that the PLEKHS1 was the direct target of the anti-phosphotyrosine antibodies and was itself tyrosine phosphorylated. They could also be explained by increased association of PLEKHS1 with other tyrosine-phosphorylated proteins. In the context of the apparently greater relative increase in association of PLEKHS1 with anti-phosphotyrosine antibodies in *Pten* $^{-/-}$ prostate compared to my results, the simplest explanation is that there is an increase in both the direct tyrosine phosphorylation of PLEKHS1, at least in part at Y257- PLEKHS1 but potentially at further tyrosines (see Chapter 5), and increased association of PLEKHS1 with tyrosine phosphorylated proteins.

A.

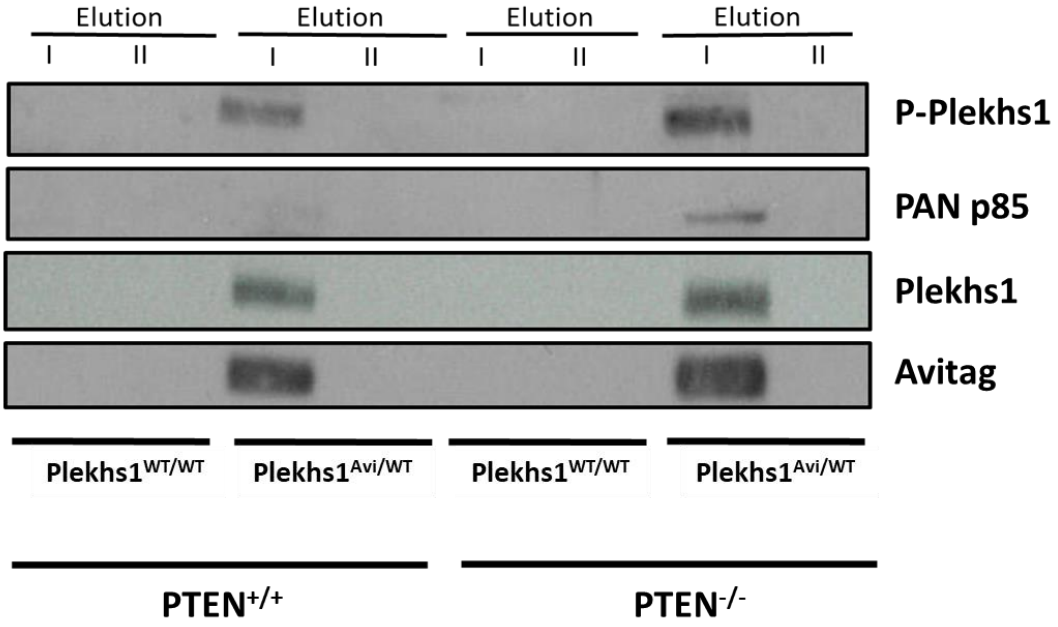
Elution
Elution
Elution
Elution
I
II
I
II
I
II
I
II
P-Plekhs1
PAN p85
Plekhs1
Avitag
Plekhs1WT/WT
Plekhs1Avi/WT
Plekhs1WT/WT
Plekhs1Avi/WT
PTEN+/+
PTEN-/-

B.

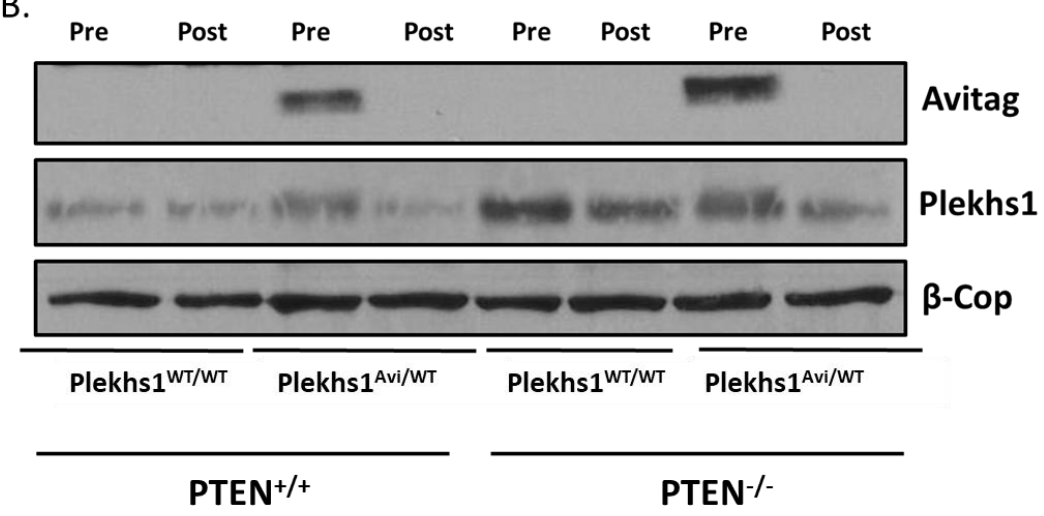
Pre
Post
Pre
Post
Pre
Post
Pre
Post
Avitag
Plekhs1
β-Cop
Plekhs1WT/WT
Plekhs1Avi/WT
Plekhs1WT/WT
Plekhs1Avi/WT
PTEN+/+
PTEN-/-

**Figure 4.4 The tyrosine phosphorylation of Plekhs1 and its interaction with p85 in control and PTEN$^{-/-}$ mouse prostate**

*Prostate tissue was rapidly dissected from mice (12-15w), with genotypes indicated in the Figure, lysed and mixed with streptavidin beads to pull-down biotinylated proteins (all mice were BirA$^{+/-}$, mice described as PTEN$^{-/-}$ were PbCre$^{+/-}$, PTEN$^{loxP/loxP}$, PTEN$^{+/+}$were PbCre$^{-/-}$, PTEN$^{loxP/loxP}$). The beads were washed and eluted with SDS-sample buffer twice.*

A. *Aliquots of prostate lysates (1.5mg input protein) were subjected to streptavidin-pull down and eluted. Half of the total eluate was immuno-blotted with anti- P-Plekhs1 and pan-p85 antibodies and half with anti- Plekhs1 and Avitag antibodies (as indicated in the right of the Figure). The primary antibodies were visualised with HRP-labelled 2$^0$-antibodies.*
B. *Lysates were collected before ('pre') and after ('post') the pulldown. Aliquots (50µg protein) were immuno-blotted with antibodies directed against the epitopes shown (right of the Figure). The primary antibodies were visualised with HRP-labelled 2$^0$-antibodies. β-Cop was used as a loading control.*

*These results are typical of those obtained in 2 independent experiments. Plekhs1 phosphorylation status was quantified and the results are shown in Figure 4.5. The efficiency of bead-elution into fraction I compared to II and of Plekhs1-depletion were calculated and shown in Figure 4.6.*

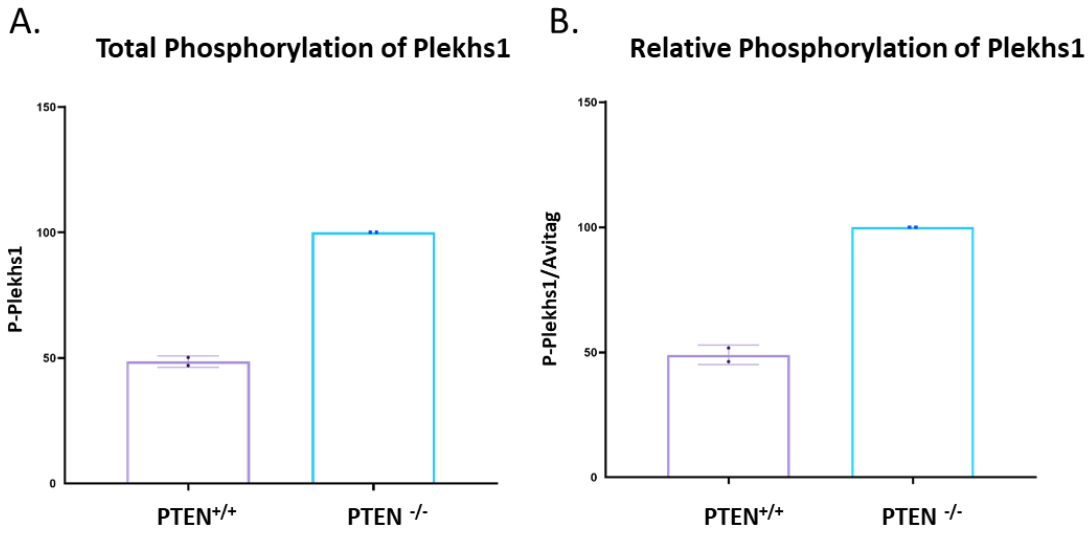


**Figure 4.5 Tyrosine phosphorylation of Plekhs1 in WT and PTEN$^{-/-}$ mouse prostate**

*Immuno-blots (shown in Figure 4.4) were quantified using Image Studio Lite software (using baseline correction). (A) Quantification of total phosphorylation of Plekhs1. (B) Quantification of relative phosphorylation of Plekhs1 signal normalized to the Avitag signal. Data represent means ± range from 2 biological replicates.*

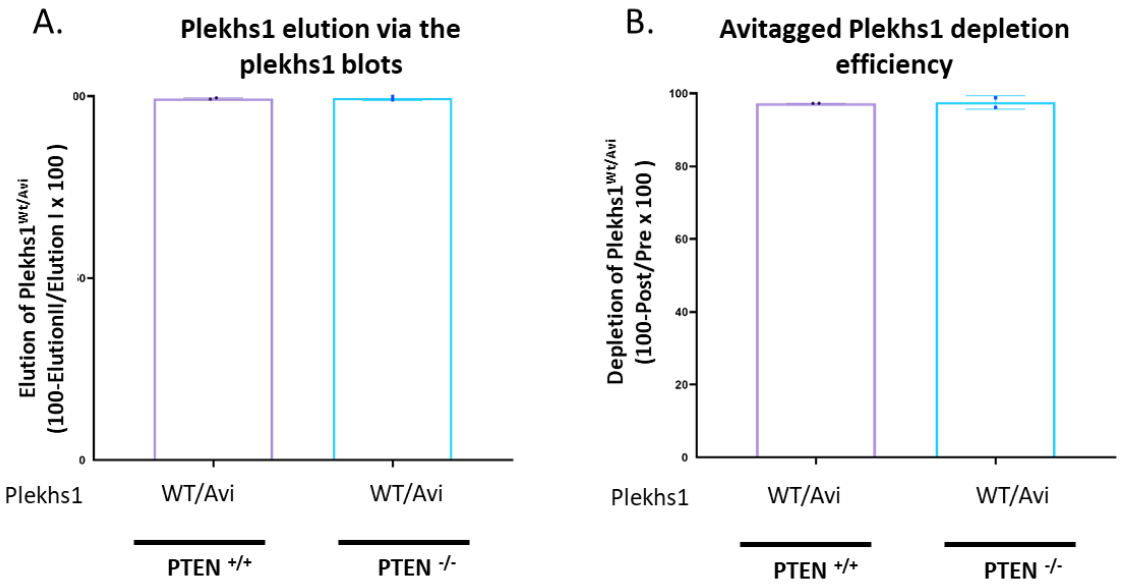


**Figure 4.6 Quantification of the efficiency of Plekhs1 elution and depletion by pull-down**

*Immuno-blots (Figure 4.4) were quantified using Image Studio Lite software (baseline correction was applied). The efficiency of Plekhs1 elution was calculated via the Plekhs1 immuno-blots and the efficiency of Avitagged Plekhs1 depletion was calculated via the Avitag immuno-blots.*

*(A-B) The signal intensity of individual bands was normalized to the $\beta$-Cop signal in the*

A.

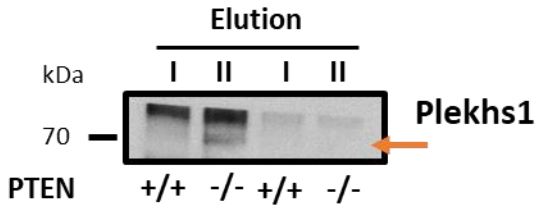
Elution
kDa
I II I II
70
Plekhs1
PTEN +/+ -/- +/+ -/-

B.

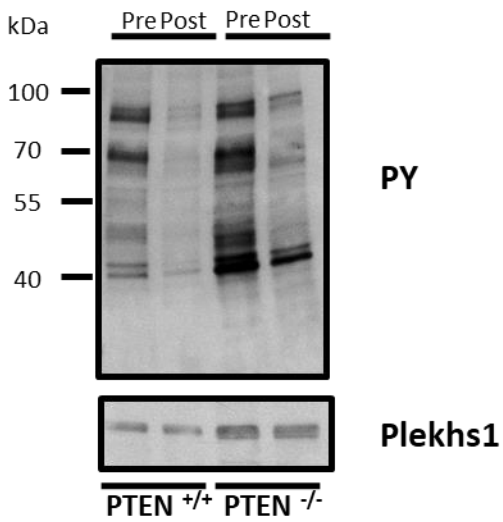
kDa
Pre Post Pre Post
100
70
55
40
PY
Plekhs1
PTEN +/+ PTEN -/-

C.

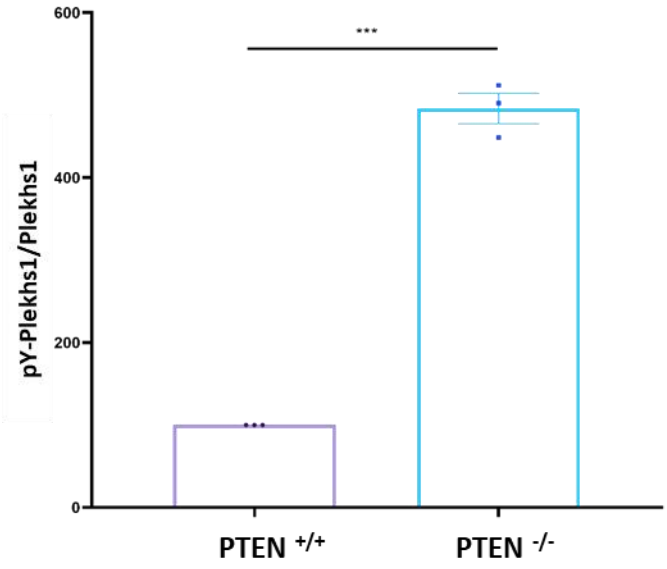
600
400
200
0
***
***
pY-Plekhs1/Plekhs1
PTEN +/+
PTEN -/-

**Figure 4.7 The tyrosine phosphorylation of Plekhs1 in control and PTEN$^{-/-}$ mouse prostate**

*Prostate tissue was rapidly dissected from mice (12-15w) with genotypes indicated in the Figure (mice described as PTEN$^{-/-}$ were PbCre$^{+/-}$, PTEN$^{loxP/loxP}$, PTEN$^{+/+}$were PbCre$^{-/-}$, PTEN$^{loxP/loxP}$), lysed (750µl lysis buffer/50mg frozen pulverised prostate) and incubated with beads conjugated with anti-P-tyrosine antibodies to immuno-precipitate proteins with phosphorylated tyrosine residues. The beads were washed and eluted with SDS-sample buffer twice (I and II, the experiment was performed by Dr Tamara Chessa, Babraham Institute)*

A. *Lysates (2 mg of total input protein) were mixed with anti-phospho-tyrosine antibody conjugated beads, washed and eluted. The eluates (100% of total) were immuno-blotted with antibodies directed against Plekhs1 (right of the Figure). The primary antibodies were visualised with HRP-labelled 2$^0$ antibodies.*
B. *Lysates collected before ('pre') and after ('post') the pulldown and aliquots (25µg protein) were immuno-blotted with antibodies directed against the epitopes shown (right of the Figure). The primary antibodies were visualised with HRP-labelled 2$^0$-antibodies.*
C. *Immuno-blots were quantified using Image Studio Lite software. Data are presented as a ratio of pY-Plekhs1 (IP eluates): total Plekhs1 (total lysate). To test significance a paired T-Test with baseline correction was applied. Data represent means ± SD from 3 biological replicates.*

## 4.4 Activation of PI3K signalling pathway in *Plekhs1*$^{-/-}$ mouse prostate

One of the outstanding scientific questions which we aimed to address was the role of PLEKHS1 during prostate tumorigenesis *in vivo*. We anticipated that, at least, a substantial part of any role would be mediated *via* impacts on the class I PI3K network. A prime tool through which we planned to address this was the *Plekhs1*$^{-/-}$ mouse model. The class I PI3K network is based on a huge series of regulatory interactions that translate $PIP_3$ signals and integrate them with many other intracellular signalling networks to shape cell behaviour at many levels but including metabolism, cell architecture and survival. The protein kinase Akt is a primary target of $PIP_3$ signalling, its activation can be monitored by measuring the phosphorylation of key sites such as T308-Akt, the target of the $PIP_3$-sensitive phosphorylation by PDK-1, and S473-Akt, the target of the mTORC2 complex (mammalian Target of Rapamycin Complex 2, a kinase that is subject to complex but poorly understood control by growth factors and mTORC1-see below). Akt can phosphorylate and regulate a large set of proteins and through them control a number of further signalling cascades, e.g., GSK3 (Glycogen Synthetase Kinase) a prime regulator of carbohydrate metabolism and development. Similarly, Akt can phosphorylate the TSC complex (Tuberous Sclerosis Complex) and through that modulate a network centred around the mTORC1 complex, that is the central integrator collating a wide range of nutrient-sensing mechanisms to determine the metabolic state of the cell. A prime substrate of mTORC1 in these pathways is the protein kinase p70-S6K (also called ribosomal protein S6 kinase $\beta$1) that controls, amongst many things, protein translation. Hence Akt, GSK3 and p70$^{S6K}$ are all regulated by class I PI3K signalling and that regulation can be read-out by monitoring phosphorylation of key residues using specific anti-phospho-peptide antibodies (T-308-Akt, S-473-Akt, S9/S21-GSK3$\beta$/$\alpha$, T389-p70$^{S6K}$). They experience increasingly indirect control by $PIP_3$ and are subject to coordinated control by an increasingly large number of other signalling pathways. In contrast, the p42/p44 MAPK pathway (Microtubule Associated Protein kinase, or ERK, Extracellular signal Regulated Kinase) is a protein kinase-based signalling cascade that is primarily controlled, and resolved from other receptor proximal signalling, by activation of the Ras/Raf/MEK pathway. The p42/p44 MAPK pathway controls many aspects of cell

behaviour but particularly cell cycle progression. Activation of the p42/p44-MAPK is typically insensitive to $PIP_3$ signalling and can be monitored *via* the phosphorylation status of key sites using specific anti-phospho-peptide antibodies (T202/Tyr204). The p38 MAPK pathway is a cytokine/stress sensitive signalling cascade that controls a variety of transcription factors, like ATF2, and cell stress responses. Again, p38 MAPK activity can be monitored through use of specific anti-phospho-peptide antibodies (T180/Tyr182) and is typically found to be insensitive to class I PI3K signalling. Through this suite of read-outs it should be possible to profile the primary signalling mechanisms operating in *Pten* $^{-/-}$ and *Pten* $^{+/+}$ prostate that are dependent on PLEKHS1.

Lysates were prepared from prostates rapidly isolated from *Pten* $^{-/-}$ or *Pten* $^{+/+}$ and/or *Plekhs1*$^{-/-}$ 12w mice (also expressing PbCre$^{+/-}$). In Figure 4.8 we show immuno-blots with antibodies directed against T308-Akt, S473-Akt, S9/21-GSK3$\beta/\alpha$, T202/Tyr204-p42/p44-MAPK, T180/Tyr182-p38-MAPK and T389-p70$^{S6K}$ (along with the respective total protein-directed antibodies). All of these immuno-blots were quantified normalised to $\beta$-Cop expression in the same samples and that data is summarised in Figure 4.9.

There was no significant effect of loss of PTEN and/or loss of PLEKHS1 on phosphorylation of T202/Tyr204-p42/p44-MAPK or T180/Tyr182-p38-MAPK. In contrast, there was a striking increase in phosphorylation of T308-Akt, S473-Akt, S9/21-GSK3$\beta/\alpha$ and T389-p70$^{S6K}$ in *Pten* $^{-/-}$ compared to *Pten* $^{+/+}$ prostate. This was most clear for both phosphorylation sites on Akt. Given the known sensitivity of all of these enzymes to class I PI3K signalling and the fact that Akt phosphorylation is regulated by $PIP_3$ directly these results are consistent with understanding of these signalling networks and past work showing Akt phosphorylation is increased in response to deletion of *Pten* [167] [168] [143] including mouse prostate [144].

Importantly, there was a substantial, clear reduction in Akt phosphorylation on both T308 and S473 in *Pten* $^{-/-}$ prostate upon deletion of *Plekhs1* with an intermediate reduction in *Plekhs1*$^{+/-}$ tissue. These results show that activation of Akt in *Pten* $^{-/-}$ mouse prostate requires PLEKHS1. Although deletion of *Plekhs1* did not cause a significant reduction in phosphorylation of GSK3 nor p70$^{S6K}$ there is a trend suggesting that further experiments may reveal the phosphorylation of these sites depends on PLEKHS1 and thus the dependency on PLEKHS1 may extend down the class I PI3K signalling network.

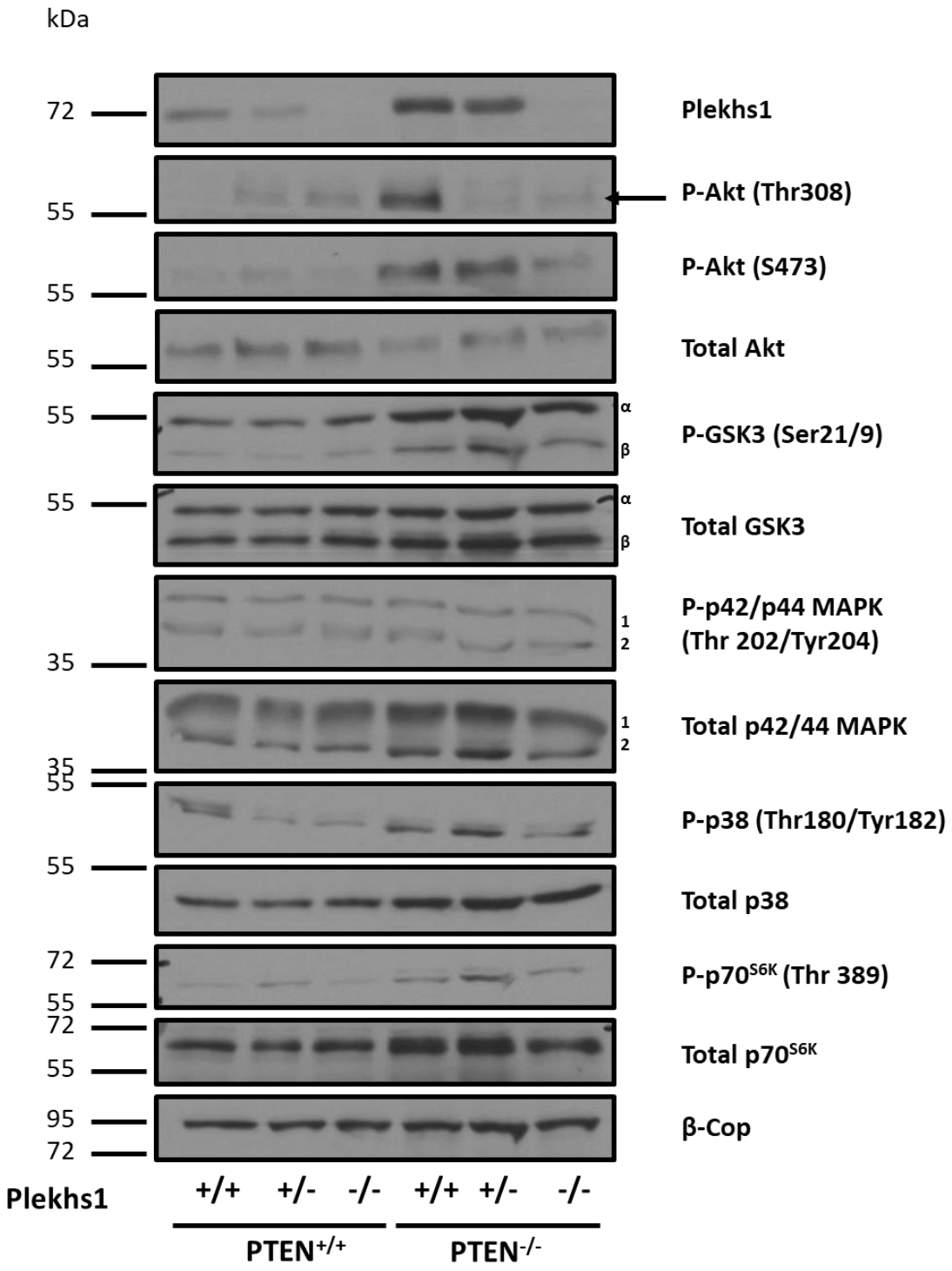
kDa
72
55
55
55
55
55
35
35
55
55
72
55
72
55
95
72
Plekhs1
Plekhs1
P-Akt (Thr308)
P-Akt (S473)
Total Akt
P-GSK3 (Ser21/9)
Total GSK3
P-p42/p44 MAPK (Thr 202/Tyr204)
Total p42/44 MAPK
P-p38 (Thr180/Tyr182)
Total p38
P-p70S6K (Thr 389)
Total p70S6K
β-Cop
+/+ +/- -/- +/+ +/- -/-
PTEN+/+
PTEN-/-

**Figure 4.8 The phosphorylation status of Akt, GSK3β, p42/44 MAPK, p38 and p70$^{S6K}$ in control, PTEN$^{-/-}$ and/or Plekhs1$^{-/-}$ mouse prostate**

*Prostate tissue was rapidly dissected from mice (12-15w) with genotypes indicated in the Figure (mice described as PTEN$^{-/-}$ were PbCre$^{+/-}$, PTEN$^{loxP/loxP}$, PTEN$^{+/+}$were PbCre$^{-/-}$, PTEN$^{loxP/loxP}$), lysed and aliquots (30$\mu$g protein) were immuno-blotted with antibodies directed against the epitopes shown (right of the Figure). The primary antibodies were visualised with HRP-labelled 2$^{0}$-antibodies. $\beta$-Cop was used as a loading control. The results are typical of those obtained in a minimum of 3 independent experiments. The images from all experiments were quantified and the results are shown in Figure 4.9*

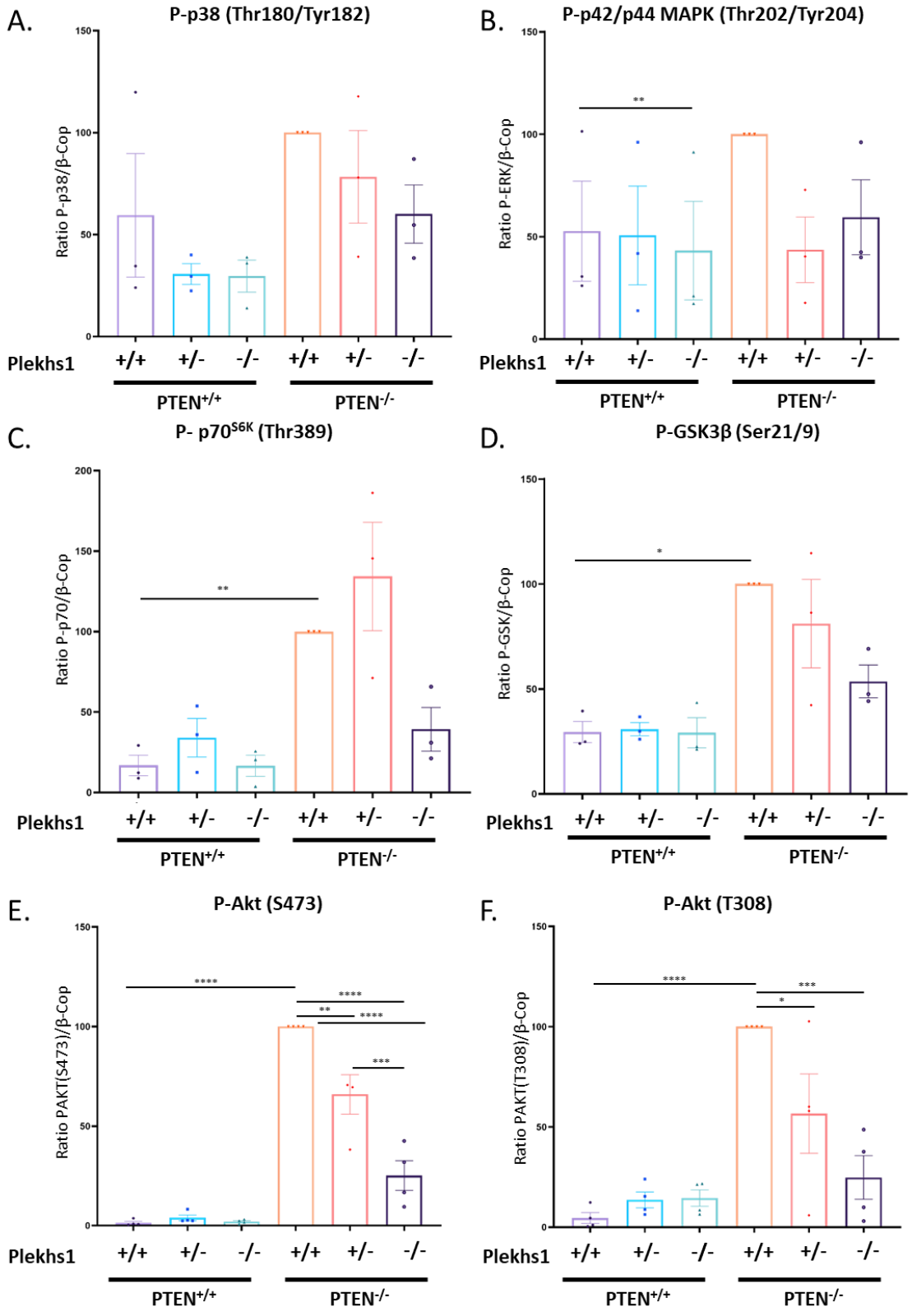
A.
P-p38 (Thr180/Tyr182)
Ratio P-p38/β-Cop
B.
P-p42/p44 MAPK (Thr202/Tyr204)
Ratio P-ERK/β-Cop
C.
P- p70S6K (Thr389)
Ratio P-p70/β-Cop
D.
P-GSK3β (Ser21/9)
Ratio P-GSK/β-Cop
E.
P-Akt (S473)
Ratio PAKT(S473)/β-Cop
F.
P-Akt (T308)
Ratio PAKT(T308)/β-Cop
Plekhs1
+/+ +/- -/- +/+ +/- -/-
PTEN+/+
PTEN-/-

**Figure 4.9 Quantification of immuno-blots measuring phosphorylation of Akt, GSK3β, p42/p44-MAPK, p38 and p70$^{S6K}$**

*(A-F) Immuno-blots in were quantified using Image Studio Lite software. The signal intensity of individual bands was normalized to the $\beta$-Cop signal in the same sample. To test statistical significance a multi-comparison Anova test with baseline correction was applied. Data represent means ± SD of a minimum 3 biological replicates.*

PTEN is a $PIP_3$ and $PI(3,4)P_2$ 3-phosphatase[169] [143]. In its absence the levels of $PIP_3$ and $PI(3,4)P_2$ increase dramatically, this is believed to be the primary oncogenic impetus that follows its deletion and leads to the activation of a number of $PIP_3$/$PI(3,4)P_2$-sensors, like Akt, directly. The levels of $PIP_3$ and $PI(3,4)P_2$ have been shown to rise substantially in *Pten* $^{-/-}$ mouse prostate[143] [144].

We used mass spectrometry-based lipidomics methodologies to measure the levels of $PIP_3$ in *Pten* $^{+/+}$ and *Pten* $^{-/-}$ and/or *Plekhs1*$^{-/-}$ 12-15w mouse prostate samples (also expressing PbCre$^{+/-}$). As explained in the Introduction, these lipidomics approaches can identify and quantify molecular species variants of $PIP_3$ and other phosphoinositides. The molecular origin of these species and their specific functions, if any, are currently unknown.

Strikingly, total-$PIP_3$ and all of its species we detected, except C34:2-$PIP_3$ which is of very low abundance and its data had a substantial variance, increased substantially in the absence of PTEN (Figure 4.10 and Figure 4.11). Importantly, loss of PLEKHS1 significantly reduced the accumulation of C34:1-, C36:1-, C36:2- C38:3, C38:4- and total-$PIP_3$ in *Pten* $^{-/-}$ prostate, in a dose-of- PLEKHS1 -dependent fashion. This result aligns with my evidence that loss of PLEKHS1 substantially reduces Akt phosphorylation (T308 and S473) in *Pten* $^{-/-}$ mouse prostate (Figure 4.8 and Figure 4.9).

When the relative abundances of different $PIP_3$ species were calculated on a common scale to enable their relative amounts to be compared directly (the relative abundance of a given molecular species of $PIP_3$/ the relative total abundance of all $PIP_2$ species; Figure 4.10) it was clear that the major molecular species of $PIP_3$ in *Pten* $^{-/-}$ prostate was C34:1-$PIP_3$. There is a larger variance in some of the data presented in Figure 4.11, than

the data presented in Figure 4.10 presumably because there is some additional variation in the proportion of the different molecular species of $PIP_3$ between samples that is naturally corrected in the data shown in Figure 4.10. Furthermore, although quantification of $PIP_3$ in *Pten* $^{+/+}$ tissue is more challenging because of its relatively low levels, it was clear that C34:1-$PIP_3$ was not the major species in *Pten* $^{+/+}$ prostate and thus it had increased substantially as a result of deletion of *Pten*. Unpublished earlier work in our lab (D. Barneda, A. Kielkowska, M. Malek, J. Clark), described in the Introduction, had also found that C34:1-$PIP_3$ appeared to be the most abundant species present in *Pten* $^{-/-}$ mouse prostate.

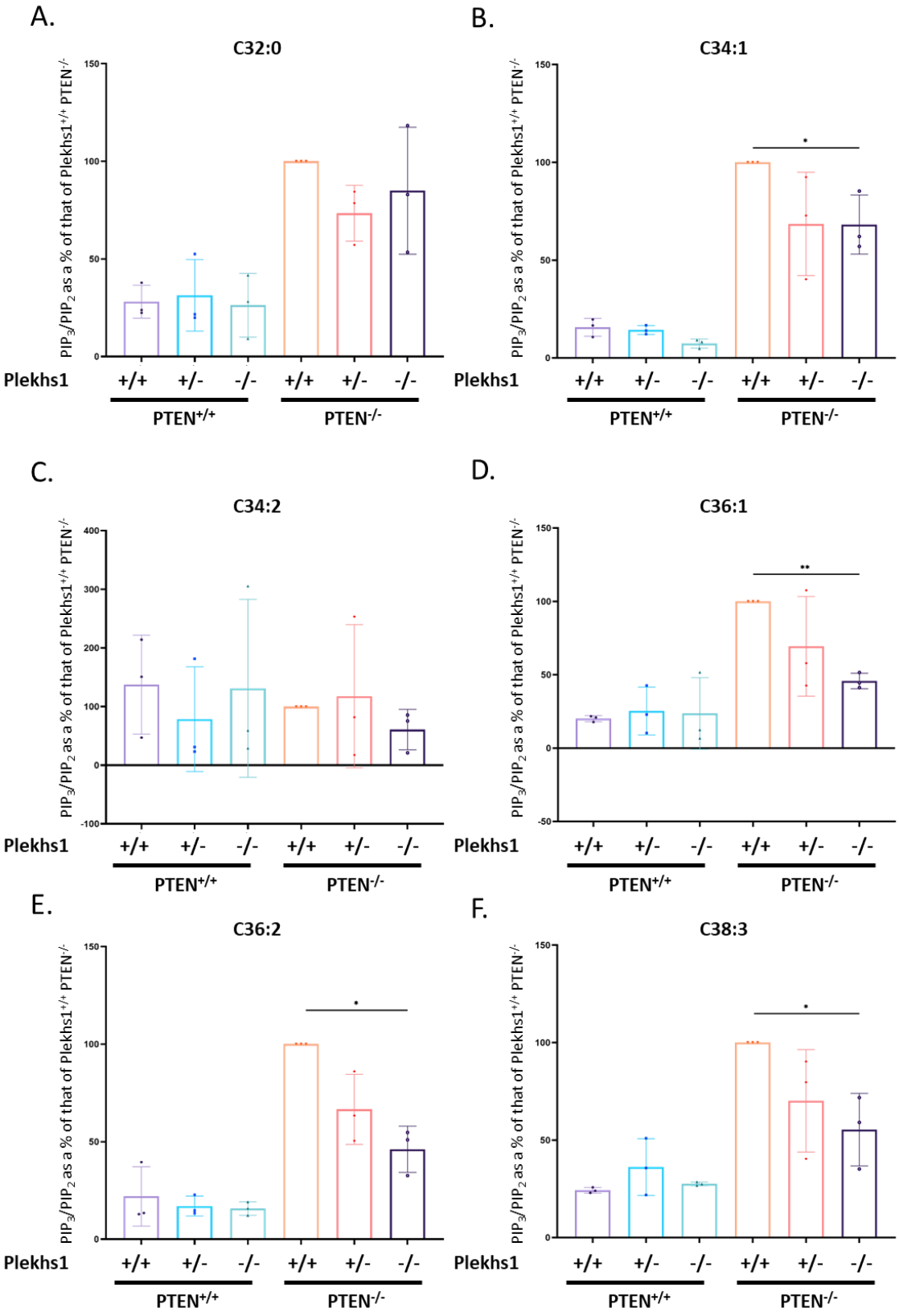
A.
C32:0
B.
C34:1
C.
C34:2
D.
C36:1
E.
C36:2
F.
C38:3
PIP3/PIP2 as a % of that of Plekhs1+/+ PTEN-/-
Plekhs1
+/+ +/- -/- +/+ +/- -/-
PTEN+/+
PTEN-/-
*
**

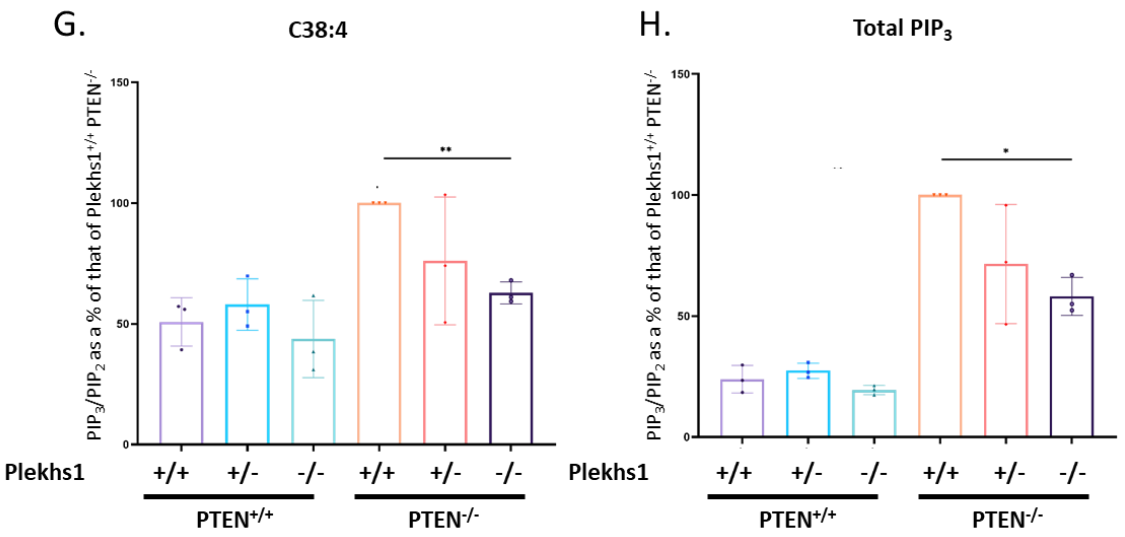


**Figure 4.10 $PIP_3$ levels in control, $PTEN^{-/-}$ and/or $Plekhs1^{-/-}$ mouse prostate**

*(A-H) Prostate tissue was rapidly dissected from mice (12-15w) with genotypes indicated in the Figure (mice described as $PTEN^{-/-}$ were $PbCre^{+/-}$, $PTEN^{loxP/loxP}$, $PTEN^{+/+}$were $PbCre^{-/-}$, $PTEN^{loxP/loxP}$), lysed and aliquots (1mg protein) were extracted to recover membrane lipids. The levels of $PIP_3$ and $PIP_2$ molecular species (as specified in the Figure) were quantified by mass spectrometry using HPLC-ESI MS/MS in conjunction with internal standards and are presented as the ratio of the relative abundance of a molecular species of $PIP_3$/ the relative abundance of the same molecular species of $PIP_2$ as a % of that of the $PTEN^{-/-}$ $Plekhs1^{+/+}$ tissue. The total $PIP_3$ data was calculated as the sum of the abundances of the different molecular species of $PIP_3$/the sum of the abundances of the different molecular species of $PIP_2$. To test significance a paired T-Test with baseline correction was applied. Data represent means ± SD of 3 biological replicates, each of which was an average of 2 technical replicates*

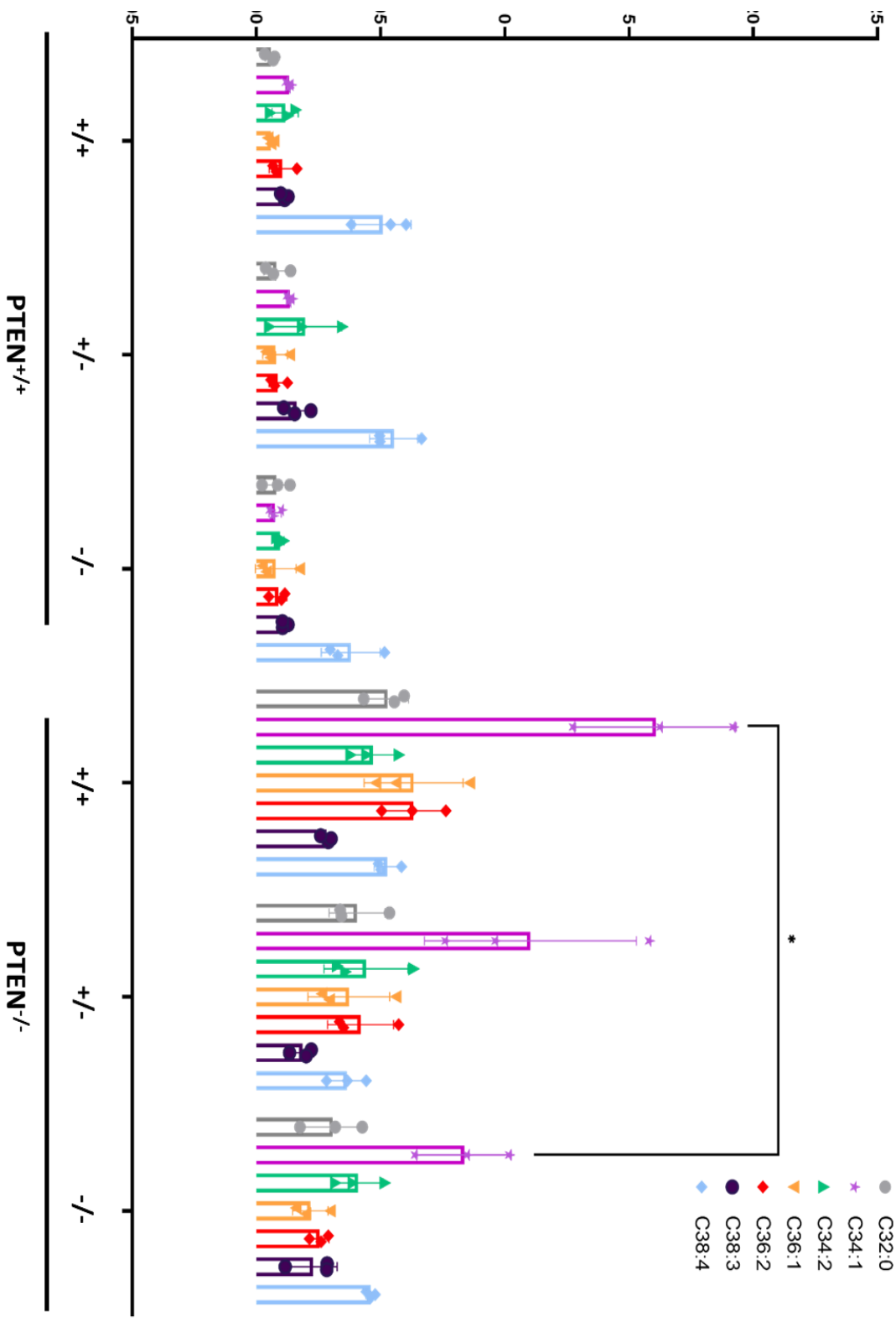
PTEN+/+
PTEN-/-
+/+
+/-
-/-
+/+
+/-
-/-
*
C32:0
C34:1
C34:2
C36:1
C36:2
C38:3
C38:4

**Figure 4.11 $PIP_3$ levels in control, $PTEN^{-/-}$ and/or $Plekhs1^{-/-}$ mouse prostate with all species plotted on a common scale**

*Prostate tissue was rapidly dissected from mice (12-15w) with genotypes indicated in the Figure (mice described as $PTEN^{-/-}$ were $PbCre^{+/-}$, $PTEN^{loxP/loxP}$, $PTEN^{+/+}$were $PbCre^{-/-}$, $PTEN^{loxP/loxP}$), lysed and aliquots (1mg protein) were extracted to recover membrane lipids. The levels of $PIP_3$ and $PIP_2$ molecular species (as specified in the Figure) were quantified by mass spectrometry using HPLC-ESI MS/MS in conjunction with internal standards and are presented as the ratio of the relative abundance of a molecular species of $PIP_3$/ the sum of the abundances of different molecular species of $PIP_2$. To test significance a paired T-Test with baseline correction was applied. Data represent means ± SD of 3 biological replicates, each of which was an average of 2 technical replicates.*

## 4.5 Discussion

In this chapter I have described experiments aimed at understanding the molecular interactions of PLEKHS1 "*in transfecto*" and the abundance, tyrosine phosphorylation, interactions with class IA PI3K regulatory subunits and functions of PLEKHS1 in a mouse model of *Pten* $^{-/-}$ prostate tumour progression.

We confirmed the ability of Src kinase to phosphorylate PLEKHS1 in its conserved YxxM motif. We also observed that upon phosphorylation of PLEKHS1 in this motif it becomes able to bind class IA PI3K regulatory subunits. Using two different approaches, we demonstrated that the relative tyrosine phosphorylation of PLEKHS1 is increased in the absence of PTEN in mouse prostate. This appeared to be a result of increases in both the stoichiometry of tyrosine phosphorylation and an increase in the levels of PLEKHS1 in *Pten* $^{-/-}$ prostate.

The kinase(s) that phosphorylate Y257- PLEKHS1 in vivo is unclear. Clearly, Src-family kinases can perform this job in transfected cells and are expressed in prostate tissue, however, there are many examples where kinases with those types of characteristics have subsequently been shown not to perform the role *in vivo*[170]. This question will need to be addressed by a combination of genetic and inhibitor studies *in vivo*.

The increase in phosphorylation of Y257- PLEKHS1 in *Pten* $^{-/-}$, compared to WT, mouse prostate could be mediated by either an increase in the activity of the relevant kinase(s) and/or a reduction in the activity of the phosphatase that is responsible for its dephosphorylation. Currently the identity of the phosphatase(s) that mediates dephosphorylation of this site remains unclear.

I found that deletion of *Plekhs1* substantially reduced the phosphorylation of both T308 and S473-sites in Akt in *Pten* $^{-/-}$ prostate. It is interesting that both sites in Akt were similarly suppressed, given that PDK-1 is responsible for phosphorylation of T308-Akt and mTORC2 is responsible for phosphorylation of S473-Akt. The implication is that both "upstream" and "downstream" parts of the $PIP_3$ network have been similarly impacted. This is in contrast to the fact that deletion of *Plekhs1* did not appear to have a significant impact on $p70^{S6K}$ phosphorylation, despite the fact that this kinase could be described as similarly "downstream" in the $PIP_3$ cascade. This apparent contradiction may be a result of the fact that mTORC2 is regulated differently to mTORC1 and/or the large

variance in the $p70^{S6K}$ phosphorylation data masking a potentially biologically significant effect and/or the fact that activation of Akt is a complex process and that the extent of S473-Akt phosphorylation does not simply reflect the activity of mTORC2 but is also determined by the availability of Akt as a substrate.

The scale of increase in phosphorylation of Akt induced by loss of PTEN and, possibly, the scale of impact of deletion of *Plekhs1* on that, appears to be greater than the respective changes in molecular species of, or total, $PIP_3$. This is a common observation in class I PI3K signalling, and signalling pathways more generally, and is a result of the poise of the sensitivity of the Akt phosphorylation mechanisms to $PIP_3$. The $PIP_3$-sensing mechanism have evolved to be fully activated by only a part of the range of $PIP_3$ concentrations that occur in the cell and provide a form of sensitivity-amplification into the pathway.

The different patterns of change in the molecular species of $PIP_3$ we detected in prostate are extremely interesting but currently very difficult to interpret. Similar observations have been made in neutrophils, various cell lines and platelets, where very strikingly differential changes in different molecular species of $PIP_3$ have been observed but not explained or understood[141 142]. To fully understand the implications of these results it will be necessary to resolve whether the different molecular species of $PIP_3$ have distinct signalling properties; e.g., are more potent or selective activators of $PIP_3$-sensors such as Akt. There is already some *in vitro* data indicating this is possible, e.g., suggesting that Akt phosphorylation by PDK-1 can be more potently activated by stearoyl/arachidonoyl-$PIP_3$ than dipalimitoyl-$PIP_3$ [171]. However, the potential pitfalls in interpreting those types of *in vitro* experiments, where minor changes in acyl change composition could very easily alter the precise molecular-level distribution of a $PIP_3$ between artificial liposomes and hence give different apparent potencies, are very substantial when trying to project what happens in biological membranes. This will require sophisticated *in vitro* and cell-based experiments, with chemically synthesised versions of the relevant $PIP_3$ species, to be conducted.

These results are also difficult to understand without a complete understanding of the relative cellular/tissue distribution of the different molecular species of $PIP_3$ and $PIP_2$. For example, it is possible that C34:1-$PIP_2$ and C34:1-$PIP_3$ are unexpectedly, particularly

enriched in cell types that are expanded in *Pten* $^{-/-}$ prostate (e.g. prostate epithelial luminal cells). This would mean that their increased abundance in *Pten* $^{-/-}$ prostate is not ENTIRELY a result of a change in $PIP_2$ and/or $PIP_3$ accumulation in ALL of the cells as a DIRECT result, for example, of the substrate selectivity of PTEN. This problem may be addressed by use of mass-spectrometry-based imaging technologies; that can resolve cell-level differences in the relative abundance of the different molecular species of phospholipids[172]and/or use of cell-sorting techniques to separate different populations of cells from enzymatically-dispersed prostate tissue; that can then be analysed similarly to the whole prostate tissue.

# 5 PROTEOMICS

## 5.1 Introduction

The proteome is a global set of proteins produced by an organism or a set of protein in certain state and time, where proteomics technology defines the proteome. Proteins dynamically interact witch each other in order to facilitate plethora of cellular processes. Over the last years, numbers of biophysical and biochemical methods have been developed to elucidate the identities, structure and function of proteins. This approaches became a very powerful tool do understand roles of proteins in complex biological systems[173]. The traditional techniques include ion exchange chromatography (IEC), size exclusion chromatography (SEC) and affinity chromatography[174]. ELISA and western blotting techniques are usually applied to analysis of already selected proteins. To separate a complex protein samples SDS-PAGE method, two-dimensional electrophoresis (2-DE) and two-dimensional gel electrophoresis (2-DIGE) are used[175] [176] [177]. Very sensitive approaches based on Mass Spectrometry (MS) has been developed to analyse and identify a complex protein mixture in cells or tissues. Several technologies, like Isotope-coded affinity tag (ICAT) labelling, stable isotope labelling (SILAC) and isobaric tagging (iTRAQ, TMT) have been recently developed to allow to achieve quantitate proteomics[178] [179]. Protein structural studies are most of the times based on two high-throughput techniques: X-ray crystallography and magnetic resonance (NMR) [178] [180].

For the purpose of our studies, we used mass spectrometry and TMT labelling along with Avitag technology (described in the Introduction chapter). After protein isolation, several steps are undertaken to prepare the samples for mass spec analysis, like: denaturation, reduction, alkylation, and tryptic digest. Samples then are labelled with an isobaric tag, fractionated, cleaned up and analysed on mass spectrometer. In the isobaric tags we can distinguish three main components: the mass reporter, the mass normalizer and the reactive group [137] [181] [182]. After mass spec analysis relative abundances of reporter ions are quantified.

In this chapter, we described our proteomic results. To perform this complex analysis we used prostates tissues isolated from *Plekhs1*$^{Avi/Avi}$ mice (described in Chapter 3). Using Avitag technology and streptavidin-mediated pulldown along with TMT/MS methodology we were able to dissect the interactome of Plekhs1 in *Pten*$^{+/+}$ and *Pten* $^{-/-}$ mouse tissues.

## 5.2 Experimental set up and workflow

Prostates were rapidly isolated from mice with relevant genotypes (see later and as indicated in Figure 5.1) and flash frozen. Frozen prostate tissue was pulverised and lysates were prepared as described (section 2.2.4 of Materials and Methods). Small amounts of the total lysates were kept for further analysis ("pre"-pulldown samples in immuno-blots) but the majority was mixed with streptavidin beads. After 20min mixing, a small aliquot of the lysates was kept for further analysis ("post"-pulldown samples in immuno-blots). The streptavidin beads were collected with a magnetic rack, washed quickly and eluted with warm SDS sample buffer (Figure 5.1). Eluted proteins were then processed by David Oxley and Judith Webster in the Babraham Institute Proteomics Facility. In the Proteomics Facility, proteins were cleaned and digested with trypsin. The resulting peptides were labelled with one of the probes from an 11-plex TMT reagent set (section 2.2.12 of Materials and Methods). Samples prepared from other individual mice that had been processed in parallel, and each individually labelled with one of the set of 11-plex probes, were pooled together for analysis by LC-MS/MS. The resulting PLEKHS1 interactomes were analysed using Proteome Discoverer and Perseus software. Several features of this protocol represented tactical decisions or choices over alternatives, where we attempted to best fit the experiments to the aims of the work and the constraints we were working with.

The time over which the proteins were pulled down (20mins) and the amount of streptavidin beads that we used per mg of lysate protein, were chosen on the basis of prior work in the lab using this pulldown technology that suggested under our conditions near to 100% of the Avi-tagged constructs should be depleted from the lysates, with the least beads possible to reduce non-specific binding, and within a time that was minimal,

to limit degradation and dissociation of complexes of proteins following the dilution caused by lysis. However, there was little to be gained by reducing the time of the pulldowns further as the samples had to be dissolved into lysis buffer, centrifuged and sampled prior to pulldown down and, under optimal conditions, about 90% of an Avi-tagged protein can be pulled down in 8 mins.

We washed the beads as quickly as possible, whilst efficiently removing non-specifically interacting proteins, to minimize loss of PLEKHS1-interacting proteins. Further, we washed the beads with a buffer that represented a compromise between very stringent washing conditions to minimise non-specific background, made possible by the use of a streptavidin/biotin interaction to retain PLEKHS1, and the risk of driving the dissociation of potentially important interactors that we aimed to identify.

Our elution strategy, with warm SDS-sample buffer, was also a compromise based on many trials. Our efforts to elute captured proteins with non-denaturing buffers or proprietary elution buffers failed to reproducibly elute more than 10-20% of the specifically bound proteins. Another alternative would have been to subject the pulldowns to proteolytic digestion directly. The problem with this approach was that we obtained poorly reproducible digestion/recovery and the technical challenges, raised by the large quantities of peptides released from the streptavidin, compromised the sensitivity of our analysis for some proteins (in our experiments the streptavidin was covalently conjugated to the magnetic beads and hence was not significantly eluted with SDS sample buffer). In a setting where it was important we retained high reproducibility and sensitivity, elution with SDS-sample buffer was our preferred method, as in trials we had reproducibly recovered greater than 95% of the Avi-tagged target and we did not experience problems with peptides generated from any streptavidin that had been eluted.

We elected to perform these experiments with an 11-plex TMT library. At the time this was the maximum degree of multiplexing that was available, and our lab had not previously used an 11-plex library, however, advice from the Proteomics Facility indicated this would be the most robust approach available to us.

Aliquots of the lysates from before (“pre”) and after (“post”) pulldown were analysed by immuno-blotting with anti-Avitag and anti- PLEKHS1 antibodies (Figure 5.2). The

results confirmed the Avi-tagged construct had been expressed and efficiently and specifically biotinylated (i.e., only when the Avi-tagged construct and BirA were expressed) *in vivo* and, finally, that the Avi-tagged PLEKHS1 could be efficiently eluted and recovered from the streptavidin beads (Figure 5.3).

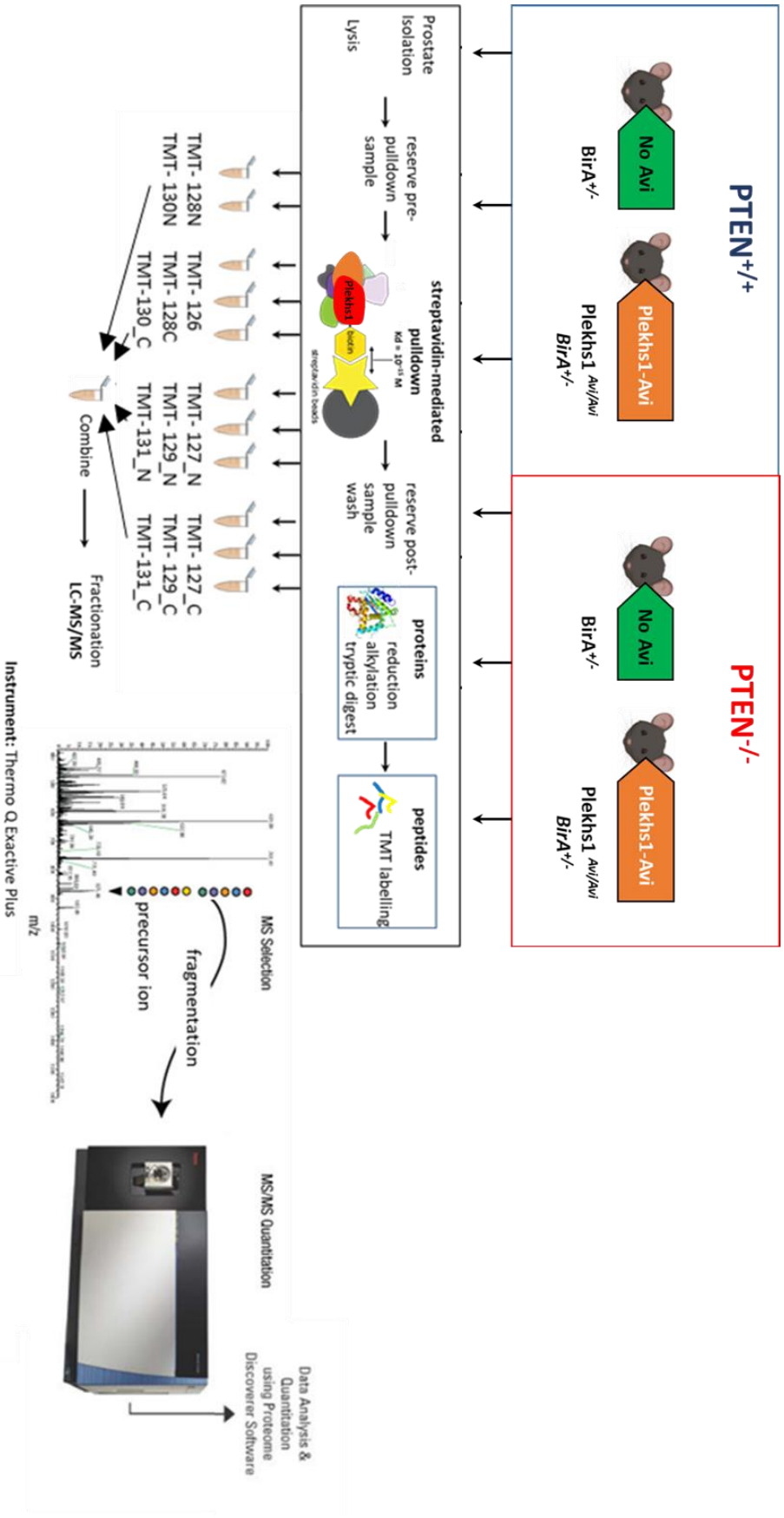
PTEN+/+
PTEN-/-
No Avi
Plekhs1-Avi
BirA+/-
Plekhs1 Avi/Avi BirA+/-
Prostate Isolation
Lysis
reserve pre-pulldown sample
streptavidin-mediated pulldown
reserve post-pulldown sample wash
proteins
reduction alkylation tryptic digest
peptides
TMT labelling
Combine
Fractionation LC-MS/MS
TMT- 128N
TMT- 130N
TMT- 126
TMT- 128C
TMT-130_C
TMT-131_C
TMT- 127_N
TMT- 129_N
TMT-131_N
TMT- 127_C
TMT- 129_C
MS Selection
precursor ion
fragmentation
MS/MS Quantitation
Instrument: Thermo Q Exactive Plus
m/z
Data Analysis & Quantitation using Proteome Discoverer Software

**Figure 5.1 Workflow of streptavidin-based protein pulldown and LC-MS/MS with TMT labelling for mapping the composition of the Plekhs1 interactome in mouse prostate**

*Prostate tissue was rapidly dissected from mice (12-15w) with genotypes indicated in the figure, lysed and incubated with streptavidin beads to perform pulldown. Eluted proteins were 'cleaned' via SDS-page and digested in-gel with trypsin. Peptides were labelled in 11-plex TMT reactions and pooled (each 11-plex reaction contained one biological replicate) from each of the four genotypes under investigation (as described in section 2.2.12 of Materials and Methods). The combined samples were fractionated by high pH reverse-phase chromatography prior to LC MS/MS (with online desalting) on a Thermo Q-Exactive Plus. The resulting data were used to build a Plekhs1-interactor-specific library in Proteome Discoverer. Analysis and visualisation of TMT data were performed in Proteome Discoverer and GraphPad Prism 8.*

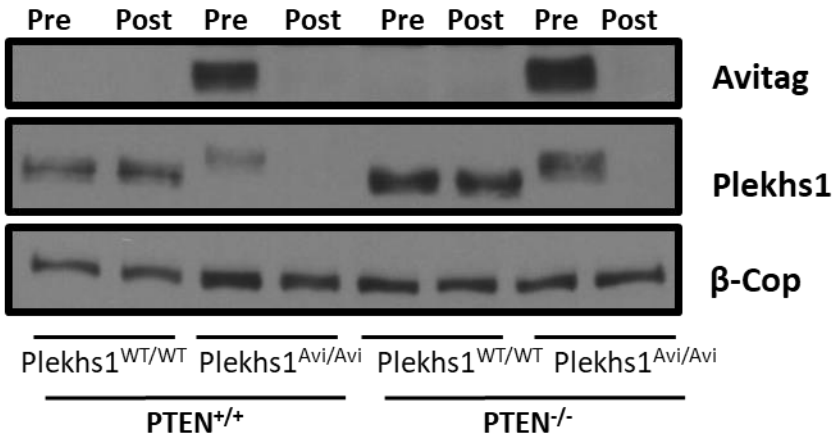


**Figure 5.2 Streptavidin-mediated Plekhs1 pulldown of PTEN$^{+/+}$ and PTEN$^{-/-}$ mouse prostate**

*Prostate tissue was rapidly dissected from mice (12-15w) with genotypes indicated in the figure (that were all BirA$^{+/-}$), lysed and incubated with Streptavidin beads to perform pulldowns. Aliquots (30µg protein) of the total lysates collected before ('pre') and after ('post') the pulldown were immunoblotted with antibodies directed against the epitopes shown (right of the figure). The primary antibodies were visualised with HRP-labelled 2$^{0}$-antibodies. β-Cop was used as a loading control. The results are typical of those obtained in 3 independent experiments using a different set of biological replicates in each experiment. The efficiency of pulldown was quantified and shown in Figure 5.3.*

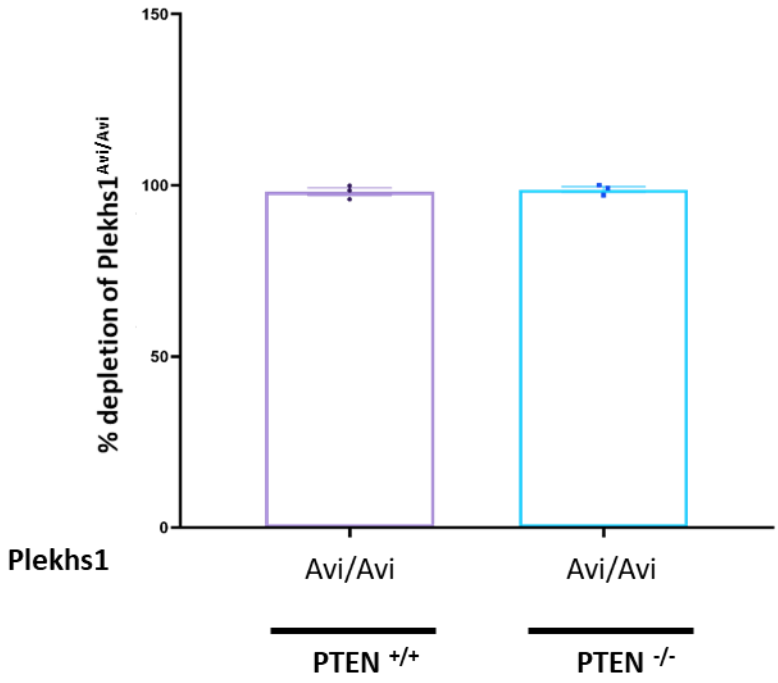


**Figure 5.3 Quantification of the efficiency of Plekhs1 pulldown**

*Immunoblots (as described in Figure 5.2) were quantified using Image Studio Lite software. Signal intensity of individual bands was normalized to the β-Cop band in the same sample, to correct for loading. The efficiency of depletion was calculated as a % as follows; 100 - (normalised "post pulldown" signal/normalised "pre pulldown" signal x 100). Data represent means ± SD of 3 biological replicates.*

## 5.3 Identification of PLEKHS1-interacting proteins

Approximately 3450 proteins were identified in the streptavidin-bead eluates from the Avi-PLEKHS1/BirA-expressing mouse prostate samples using Proteome Discoverer. These identifications are based by precise mass-matching, with greater than threshold confidence, of detected peptides against the known and predicted mouse proteome. The majority of these proteins are very likely to be based on very small numbers of peptides and present as a result of non-specific interactions with the streptavidin-beads, PLEKHS1, its interactors or other non-specifically associated proteins. To identify proteins that might be specifically interacting with PLEKHS1, including those that might change between *Pten* $^{+/+}$ and *Pten* $^{-/-}$ prostate tissue, we searched for proteins in the data that were significantly enriched in Avi-pulldowns from prostate that expressed Avi-tagged PLEKHS1 and BirA, either in the presence or absence of PTEN, compared to wild-type PLEKHS1.

This approach led to the identification of a total of 69 proteins that were enriched in either (or both) *Pten* $^{+/+}$ or *Pten* $^{-/-}$ prostate samples (Table 5.1). The approach that was used to normalise the raw data for analysis was to use the total peptide mass spec signal detected for each sample as measure of "total input". The normalised data were subsequently analysed and presented using a standard option in Proteome Discoverer termed grouping. In this approach the abundance of the protein in a given sample is expressed as a proportion of the total mass spec signal for that protein across all 4 conditions (genotypes), set at 400 (i.e., the sum of the normalised grouped abundances for a given protein across the 4 conditions is always 400). This approach significantly reduced the overall variance of the data. The weaknesses of this approach, however, is that it obscures the actual relative abundance of different interactors. However, it is important to acknowledge that the best approaches to estimating the actual relative abundances of proteins in these types of proteomic experiment still have major limitations and are best seen as semi-quantitative. The only way of making proteomic data genuinely quantitative is to use "synthetic peptides", that are identical to the peptides used to measure a given protein, in accurately quantified amounts as standards. To provide a guide to the relative abundances of the proteins recovered in

the PLEKHS1 pulldowns I have presented the normalised, but not grouped, abundances of the proteins we identified (Table 5.2) These data have a greater variance than the grouped data, as explained above. However, it is clear that, as expected, by far the most abundant protein in the pulldowns was PLEKHS1. A number of other proteins clearly reach relatively substantial levels, particularly in the case of 14-3-3 proteins in *Pten* $^{-/-}$ prostate samples. Interestingly, the overall abundance of proteins recovered with PLEKHS1 was 3.1x-greater in the *Pten* $^{-/-}$ samples, and 2.2x-greater when corrected for the amount of PLEKHS1, compared to *Pten* $^{+/+}$ prostate. I will return to the subject of the potential significance of the different classes of proteins that are recovered in these samples, later in the chapter.

To identify those proteins recovered with PLEKHS1 that changed between wild-type and *Pten* $^{-/-}$ prostate, proteins whose normalised, grouped abundances in the pulldowns from prostates expressing Avi-tagged- PLEKHS1 were significantly different between *Pten* $^{-/-}$ and *Pten* $^{+/+}$ prostate samples were identified (Table 5.1). The initial set of 240 proteins identified is significantly bigger than that identified as significantly different between the respective Avi- PLEKHS1/wild-type- PLEKHS1 conditions in either *Pten* $^{+/+}$ or *Pten* $^{-/-}$ samples (69, Table 5.3). This is because there a large number of proteins captured in this analysis that show a striking differences in their normalised grouped abundances between the wild-type- PLEKHS1-expressing prostate samples in either a *Pten* $^{+/+}$ or *Pten* $^{-/-}$ backgrounds (Table 5.1); i.e., they are likely non-specifically associated proteins that are probably expressed at very different levels in *Pten* $^{+/+}$ compared to *Pten* $^{-/-}$ prostate and hence “contaminate” the pulldowns differently. A clear example of this behaviour is Cse1L (Chromosome Segregation 1 Like, see Figure 5.20). There is clear and significant difference in recovery between tissues expressing Avi- PLEKHS1 in a *Pten* $^{-/-}$ or *Pten* $^{+/+}$ background; however, that is mirrored in the wild-type- PLEKHS1-expressing controls, indicating Cse1L is non-specifically associated with the PLEKHS1 pulldowns but is probably more highly expressed in *Pten* $^{-/-}$ mouse prostate. The data shown in Table 5.1 was filtered to remove these types of false-positives, resulting in the identification of 52 proteins that were deemed to have significantly and meaningfully changed their association with PLEKHS1 between *Pten* $^{+/+}$ and *Pten* $^{-/-}$ prostate. Although there are many overlaps with the proteins identified in Table 5.3 there are also some differences

as a result of the different comparison being applied between prostate tissues either expressing, or not, PTEN.

The data compiled in Table 5.1, Table 5.2 and Table 5.3 represents a broad summary and compact way of presenting the range and significance of various proteins interactions with PLEKHS1 that were the result of a systematic analysis of all of the interactors that were detected in any of the PLEKHS1 pulldowns. As revealed by the data presented in histogram form for Cse1L (Figure 5.20) however, it is important to understand the changes in the amount of an interactor recovered in a specific pulldown in the context of all 4 of the genetic conditions and that is best done *via* histogram plots for each interactor, although they are space consuming. As a result, a series of histograms have been constructed for each interactor of interest, that were identified in at least one of the analyses presented in Table 5.1 and Table 5.3. To simplify the process of presenting and discussing this data the interactors have been assembled into sets of similar function or homology and, in some cases, those sets include related proteins, with marginal or no statistical significance in our data, for reference (Figure 5.4-Figure 5.20).

## 5.4 Data that addresses existing results or hypotheses

There are a number of features of these results that represent tests of hypotheses arising from unpublished, past work in the lab (described in the Introduction) and of work presented earlier in this thesis.

These include data, primarily based on proteomic studies of pulldowns of Avi-p85 subunits from *Pten* $^{+/+}$ or *Pten* $^{-/-}$ mouse prostate, that p85s can interact with PLEKHS1 and that is increased substantially in the absence of PTEN. Clearly, the data presented in Table 5.1, Table 5.2, Table 5.3, and Figure 5.14 support that idea. None of the class IA PI3K subunits are identified as significantly interacting with PLEKHS1 in *Pten* $^{+/+}$ prostate tissue. However, p110$\alpha$, p110$\beta$, p85$\alpha$, p85$\beta$ and p55$\gamma$ all become significantly associated with PLEKHS1 in *Pten* $^{-/-}$ prostate and, indeed, become the second most abundant class of interactors (normalised, not grouped abundances in Table 5.2), behind the 14-3-3 proteins, under those conditions. There are some interesting details in these results. It is clear p55$\gamma$ becomes a substantial interactor with PLEKHS1 in *Pten* $^{-/-}$ prostate,

although there is no evidence that its expression at an mRNA level is increased under these conditions[183] nor that it is significantly expressed in mouse prostate; indicating that it might preferentially associate with PLEKHS1. It is also noteworthy that the sole study of interactions between PLEKHS1 and class IA PI3K[109] focused on p55γ in their study.

In earlier work in the lab, conducted by Tamara Chessa, in which the Avi-p85α or Avi-p85β interactomes in *Pten* $^{-/-}$ or *Pten* $^{+/+}$ mouse prostate were defined, found that the recovery of p110δ in those pulldowns was dramatically increased in *Pten* $^{-/-}$ prostate. The observation was rationalised, in the context that p110δ expression in mouse prostate appears to be relatively low, by speculating that this was a result of hugely increased immune infiltration into the *Pten* $^{-/-}$ prostate and that those immune cells were enriched in p110δ (noting that the Avi-p85 and BirA were ubiquitously expressed and that a variety of similar immune-cell-specific, PI3K-interacting proteins like BCAP behaved similarly). It is notable that p110δ is not significantly enriched in any of the PLEKHS1 interactomes described here. That maybe a result of the fact that PLEKHS1 is relatively more weakly expressed in immune cells compared to prostate epithelial cells than p85s and/or a result of preferential binding of PLEKHS1 to p110α- and p110β-containing PI3Ks.

Earlier work in the lab and work performed and presented as part of this thesis has indicated that expression of PLEKHS1 protein is increased in *Pten* $^{-/-}$ compared to *Pten* $^{+/+}$ mouse prostate. The proteomics data shown here is consistent with that conclusion, although the increase in PLEKHS1 is not statistically significant (Table 5.1 and Figure 5.4). Given the expected precision and reproducibility of the different methods, there is no doubt that the results obtained by immuno-blotting (against either PLEKHS1 or the AviTag) of whole tissue lysates are the most reliable estimates. The fact there is no significant difference in the levels of PLEKHS1 recovered between wild type and *Pten* $^{-/-}$ prostate in the proteomics data led us to present our data comparing the abundance of different interactors between conditions without correcting for the amount of PLEKHS1; however, this factor should be borne in mind when considering these results.

## 5.5 Identification of PLEKHS1 interactors

In this section, I will consider groups of proteins with similar cell functions and/or homology.

### 5.5.1 Chaperones

A large number of proteins belonging to the protein quality control apparatus of the cell were identified (Figure 5.5). These included components and regulators of the Hsp40, 70 and 90 complexes.

Broadly, these proteins are understood to bind to "mis-folded" proteins and use ATP to fold them into an active conformation. Some of this activity is focused on the initial, primary folding of proteins during their synthesis and/or maturation but some functions to retrieve protein that has become unfolded following maturation. The different chaperone complexes have different client-proteins and/or operate in different cellular contexts[184].

A number of the proteins from this family that are identified in the data presented in Table 5.1, Table 5.2, Table 5.3 and Figure 5.5 are members of well-described protein complexes where several members of the complex are detected, e.g. Bag6:Ubl4:GET4 (cytosolic protein quality control) or Hspa2:Hspa8 along with other members of the family such as Hsp90aa1, Hspa1A and Hsp90ab1. The DNAJ-family proteins (A2, A4 and C7) are also identified in our pulldowns as significant, specific interactors of PLEKHS1 and also known to associate and share common functions with the chaperones described above (these interactions are annotated in the STRING databases[185]). In these cases, where a group of proteins that are already known to interact, are identified as potential PLEKHS1 interactors it is unclear which protein(s) mediate(s) the interaction. Nevertheless, the parallel identification of different member of these known complexes adds confidence that they are genuine interactors.

Strikingly, all of the members of the protein quality control apparatus that were identified as significant PLEKHS1 interactors were only recovered in pulldowns from *Pten* $^{+/+}$, and not *Pten* $^{-/-}$, prostate lysates (this is seen in both the "absolute" and "grouped" abundances shown in Table 5.1 and Table 5.2, respectively; the only exception is Hspa8 that is also found, with marginal statistical significance, in pulldowns

from *Pten* $^{-/-}$ samples). It is not clear from this data whether the expression of all of these proteins (or at least those interacting directly with PLEKHS1) had been dramatically reduced in *Pten* $^{-/-}$ prostate, although it would appear unlikely.

There is a significant body of data describing mRNA abundances in mouse prostate from *Pten* $^{+/+}$ and *Pten* $^{-/-}$ prostate (data that overlapped with proteins identified in our screen are summarised in Table 5.4. That data suggests that the mRNA levels of the majority of the group of protein quality control-related hits are actually increased in *Pten* $^{-/-}$ prostate and hence our observation that their interaction with PLEKHS1 in *Pten* $^{-/-}$ prostate is plausibly a result of a change in their "affinity" and/or local availability and/or competition with other interactors. Clearly, as the correlation between mRNA and protein levels is not strong, these observations need to develop by measurements of the relevant protein concentrations. There are some proteomic and multi-omics studies of *Pten* $^{+/+}$ and *Pten* $^{-/-}$ prostate[186] , that had the potential to directly define any differences in the whole-tissue abundance of members of the PLEKHS1 interactome between these genotypes. However, those results are quite restricted and presented data for only four proteins we have mapped into the PLEKHS1 interactome. This may be partly a result of the fact that at least some of the proteins we have identified are relatively low abundance in whole tissue lysates.

Some of the proteins in the chaperone family are well recognised members of the "crapome"[187]; proteins that are regularly identified in a variety of affinity-pulldown-based proteomic experiments. This is particularly the case for Hspa2, Hspa8 and Hspa1A in our data but other chaperones we detect (e.g. the Bag6 complex, above) are not well-recognised members of the Crapome. This problem is reported to be worse in contexts where the tagged proteins have been "over-expressed" and may have over-loaded the cells protein folding machinery; something that should not be a problem in our experiments where we are working with endogenous PLEKHS1 and its levels are unchanged by tagging.

A significant number of proteins in the Crapome are features of the pulldown strategy applied (e.g. always appear in GFP-tag-based pulldowns but not FLAG-tag pulldowns). Our approach has not been sufficiently widely applied for a clear family of potential methodology-related false-positives to be defined. However, our overall proteomic

strategy (use of TMT-labelling that allows direct internal comparison between proteins recovered in specific v control pulldowns), controls (e.g. streptavidin pulldowns from tissues where the only difference is the expression of the AviTag on PLEKHS1), the small tag and the fact that the key biotin moiety has to be bound by a very tight interaction with streptavidin, meaning a protein binding to the biotin moiety is very unlikely to be retrieved, suggest our approach should minimise these problems; and that is supported by our results.

It seems likely that some of the chaperones that appear in the Crapome, and in our experiments, are actually recognising proteins that are tagged, and partially "misfolded" as a result, *in vivo*. It is also possible that some of the chaperones detected in our experiments may be recognising PLEKHS1 or its associated proteins as "misfolded" during the freezing/lysis/pulldown protocol and do not interact *in vivo*. It is not possible to distinguish these alternatives with our data. It could be possible to partially address this question by performing experiments in which differentially labelled tissues (e.g., with non-radioactive isotope-labelled metabolites) are mixed at lysis (e.g., by lysing one batch of cells and then using that lysate to solubilise the other sample). By looking for evidence that proteins in the lysate, that was added to the second tissue, became incorporated into complexes retrieved from the second tissue it might be possible to establish whether at least some protein complexes were forming post-lysis.

Finally, it is likely some of these proteins are involved in the normal, primary folding or refolding of PLEKHS1 of one or more of its interactors. In that context, the reductions in binding in *Pten* $^{-/-}$ prostate may represent an important redirection of function.

### 5.5.2 Proteins involved in ubiquitination

Proteins can be post translationally modified by ubiquitination in a variety of positions and patterns. Broadly, the modification is put in place by E3 ligase complexes in a cascade of reactions involving proteins that recognise, bind and present the substrates for the E3 ligase to modify. Those protein ubiquitin residues are then either recognised by a diverse family of "sensors" that direct further trafficking of the host protein, typically for degradation by a variety of mechanisms; or alternatively are removed by

de-ubiquitinylating enzymes.

Key ubiquitination-related proteins that appear to be members of the PLEKHS1-interactome are Stub1 (an E3 ligase), Maged1 (an activator of E3 ligases), Sqstm1 (also commonly called p62, a sensor of ubiquitinylated proteins that also binds LC3 and hence can recruit ubiquitinylated proteins to autophagosomes), Nbr1 (a functional relative of Sqstm1, and also known to bind the peroxisomal protein, Pex5, see below), Keap1 (a substrate-specific adaptor of E3 ligases and known to be tightly linked to Sqstm1 in the STRING data base[185]), Dacf11 (interacts with and stimulates E3 ligases) and Ddb1 (contains a domain that presents specific substrates to an E3 ligase).

Again, the recovery of the majority of these proteins in PLEKHS1 pulldowns is reduced in both absolute and grouped terms (Table 5.1, Table 5.2, Table 5.3 and Figure 5.6) from *Pten* $^{-/-}$ prostate compared to *Pten* $^{+/+}$ prostate.

It is possible some of the family of ubiquitination-related PLEKHS1-interactors bind to Plekhs1 and/or interactome following disruption of the tissue as a result of their ability to detect “damaged” protein, however, this is probably less of an issue than with the group of interactors that regulate protein quality control.

There is some published data available describing changes in the abundance of mRNA coding for proteins involved in ubiquitination processes. Some of that data is summarised in Table 5.4. The mRNA levels of one of our hits is increased in *Pten* $^{-/-}$ prostate whilst three others are decreased by relatively small amounts. Again, suggesting that the reduction in their recovery with PLEKHS1 in *Pten* $^{-/-}$ tissue is possibly a result of a change in their “affinity” and/or local availability and/or competition with other interactors, rather a simple reduction in their levels.

It remains likely that some of this sub-family of PLEKHS1 interactors are physiological determinants of PLEKHS1 and/or its interactome’s degradation and turnover *in vivo*. Furthermore, this data suggests that loss of *Pten* expression in the prostate leads to a functionally significant reshaping of ubiquitin-directed protein turnover within the PLEKHS1 interactome that might be relevant to the broader phenotype of *Pten* $^{-/-}$ tissues.

### 5.5.3 Centrosomal components and/or regulators.

Four proteins in the PLEKHS1-interactomes described in Table 5.1, Table 5.2, Table 5.3 and Figure 5.11 are known components or regulators of centrosomes (Cep97, Cep170b, Cep192 and Pcm1). None of these interactions are increased by loss of PTEN and two are clearly decreased in that context. The relevant mRNA-seq data for these proteins indicates the levels of their mRNA are either reduced (Cep97) or not changed between *Pten* $^{+/+}$ and *Pten* $^{-/-}$ prostate (Table 5.4), implying that their reduced recovery in PLEKHS1-pulldowns from *Pten* $^{-/-}$ tissue for at least some of these interactors may not be a result of a reduction in their expression. It is difficult to understand the implications of these connections without knowing more about the precise functions of these centrosomal proteins and how they are influenced by their connection to PLEKHS1 and/or its interactors. Nevertheless, on the basis of these three functionally inter-related hits it would appear that this is a physiological role for the PLEKHS1interactome in control of centrosomes or alternatively that centrosomes control aspects of the function of the PLEKHS1 interactome. It would appear this connection is reduced or lost in *Pten* $^{-/-}$ prostate tissue and that may be an important feature of the loss-of-PTEN phenotype.

### 5.5.4 Autophagy-related proteins

Six proteins belonging to this broad grouping are found in the PLEKHS1 interactome defined in Table 5.1, Table 5.2, Table 5.3 and Figure 5.7. Interestingly, ATG101 is a known interactor and stabilises the key autophagy protein ATG13, also recovered with PLEKHS1 in these experiments. This connection obscures which protein is responsible for their recovery with the PLEKHS1 interactome. Other hits include the proteins Sqstm1 and Nbr1 that both bind ubiquitinated proteins and direct them to autophagosomes *via* their additional ability to bind LC3 (and are also listed under ubiquitination-related proteins). Pik3r4 (Vps15) is the protein kinase-like adaptor found in Vps34 complexes related to its autophagy functions. The majority of this set (5/6) are recovered in relatively smaller amounts (in either grouped Table 5.1 or absolute terms Table 5.2) from *Pten* $^{-/-}$ prostate. The relevant published mRNA-seq data for members of this set of proteins shows that, for the majority the levels of their mRNAs are reduced in *Pten* $^{-/-}$ prostate (Table 5.4). The

implication of these results is that the reduced association of autophagy-related proteins with the PLEKHS1 interactome in the absence of PTEN may be driven by a reduction in their expression. Collectively, this data indicates a physiologically important connection between autophagy and the PLEKHS1 interactome, the directionality (does PLEKHS1 control autophagy and/or *vice versa*?) and impact of these interactions remains unclear but appears to be reduced in *Pten* $^{-/-}$ prostate and that could have relevance to the phenotype.

### 5.5.5 PIP4K2C

One of the lipid kinases that were recovered in PLEKHS1-pulldowns in our experiments was PIP4K2C (PI5P4K2γ; the other lipid kinases were all class IA PI3K subunits and were considered above) (Table 5.1, Table 5.2, Table 5.3 and Figure 5.14). Notably, PIP4K2C was recovered very similarly from both *Pten* $^{+/+}$ and *Pten* $^{-/-}$ prostate. It is a lipid kinase with a number of interesting connections to nuclear and stress signalling pathways. It is unclear whether the interaction with PLEKHS1 is direct and what the respective impacts on the partners and their functional implications are.

### 5.5.6 Protein kinases

A total of five protein kinases were identified in PLEKHS1-pulldowns from mouse prostate (Table 5.1, Table 5.2, Table 5.3 and Figure 5.13). The recovery of none of these protein kinases is increased in *Pten* $^{-/-}$ prostate compared to wild-type prostate tissue. Although one or more of these kinases may have the potential to phosphorylate PLEKHS1 (see later in the phospho-proteomics in results in Section 5.6), at this point, that remains unclear and whether any of the members of the PLEKHS1 interactome are physiological substrates or these are entirely regulatory interactions will only be resolved by further work.

### 5.5.7 14-3-3 proteins

The most striking and unexpected feature of all of the proteomic results presented in this chapter is the recovery of substantial amounts of a number of 14-3-3 proteins in

association with PLEKHS1, in a manner that is dramatically increased in *Pten* $^{-/-}$ prostate (Table 5.1, Table 5.2, Table 5.3 and Figure 5.15).

14-3-3 proteins are relatively abundant 7-member family of scaffolding proteins[188]. The canonical model by which they are understood to function is mediated by their ability, thought to be manifest when they are homo- or hetero-dimerised, to bind to proteins phosphorylated within local sequence motifs (classically RXXpS/TXP). Often 14-3-3 binding depends on 2 adjacent phospho-sites. The association of 14-3-3 proteins can lead to the initiation of a wide variety of molecular mechanisms. 14-3-3 binding can block nuclear export or localization signals, link 2 phosphorylated proteins together (through 14-3-3 dimerization), can displace or block other proteins interactions and they can cause conformational changes that activate or inhibit other domains (e.g., catalytic) in the protein.

Mouse PLEKHS1 houses at least one, and possibly four, 14-3-3 binding sites, predicted by the 14-3-3 Pred webserver (in order of decreasing confidence); S157, S256 (that is very close to the PI3K-YXXM-binding site at Y258), S180 (forming a possible tandem 14-3-3 binding site with S157) and S167. Analysis of phospho-peptides released from PLEKHS1-pulldowns shows that the three highest-confidence sites are phosphorylated *in vivo* (there is possibly low-level phosphorylation of S167 but it is near borderline) and, furthermore, the stoichiometry of phosphorylation at all three high-confidence sites is increased in *Pten* $^{-/-}$ prostate (see later, section 5.6). Analysis of published mRNA-seq data (Table 5.4) suggests that the levels of the majority of 14-3-3 mRNAs are significantly increased in *Pten* $^{-/-}$ prostate, indicating their increased association may be driven, in part, by increased protein expression.

Collectively, these data indicate that 14-3-3 proteins can interact with PLEKHS1 in prostate and that association is increased substantially in the absence of PTEN. The increased interaction might be driven by increased phosphorylation and expression of PLEKHS1 (see work presented in 5.6). The kinase responsible is unclear (see section 5.5.6). Not only does the interaction of PLEKHS1 with 14-3-3 proteins indicate the molecular properties and functions of PLEKHS1 have been modulated directly, but the absolute amounts of 14-3-3 proteins recovered (Table 5.2) also suggest they may have "displaced" other PLEKHS1-interactors, in line with observations about, for example, the

reduced recovery of protein quality control-related and ubiquitination-related PLEKHS1 interactors.

### 5.5.8 Other proteins that increase their association with PLEKHS1 in *Pten* $^{-/-}$ prostate

Only a very small number of proteins, that are not class IA PI3K subunits nor 14-3-3 proteins, are recovered in greater amounts in PLEKHS1 pulldowns from *Pten* $^{-/-}$ prostate. These are PhldB2 (Pleckstrin Homology like Domain family B member 2, LL5β), Gpx2 (Glutathione Peroxidase 2), Memo1 (Mediator Of cell Motility 1), Stat3 (Signal Transducer and Activator of Transcription 3), Xaf1 (Xiap Associated Factor 1) and Ly6C1 (Lymphocyte antigen 6 complex, locus C1).

In this family Gpx2 is a peroxidase that protects cells against oxidative damage and is known to be up-regulated in a number of cancer types[186]. Published data indicates the mRNA coding for Gpx2 is substantially up regulated by loss of PTEN in the prostate (Table 5.4). It is clear that the association of Gpx2 with PLEKHS1-pulldowns in *Pten* $^{-/-}$ prostate is specific as it is dramatically reduced in control tissues that express wild type, as opposed to Avi-tagged PLEKHS1. Nevertheless, the increase in association could be driven by the increased expression of Gpx2. The consequences of this change in molecular co-localisation of Gpx2 and PLEKHS1 could be significant for the *Pten* $^{-/-}$ phenotype.

Ly6C1 is an endothelial and immune cell expressed GPI-anchored cell surface protein. It is one of the more unexpected members of the PLEKHS1 interactome but it remains possible it associates at some point in its trafficking prior to arrival at the plasma membrane. There is a large increase in Ly6c1 mRNA detected in *Pten* $^{-/-}$ prostate compared to *Pten* $^{+/+}$ prostate; that could be a result of immune cell infiltration. However, for an increase in the number of immune cells rich in Ly6C1 to lead to an increase in recovery with PLEKHS1, the simplest explanation would be that PLEKHS1 is also expressed in those cells. That explanation is not simply consistent with our failure to detect p110δ in the PLEKHS1 interactome (see above). The potential implications of this interaction between Ly6C1 and the PLEKHS1 interactome remains unclear.

PhldB2 (LL5β) houses a PH domain capable of binding $PIP_3$ with high selectivity and a distinct domain that can bind the cytoskeletal proteins, Filamin A and C, with high affinity and specificity[189]. The physiological functions of PhldB2 are poorly understood generally, and could be summarised as supporting translocation of the actin-crosslinking protein, Filamin A, to sites of $PIP_3$ and this is required for lamellipodia formation in response to agonists. The ability of the $PIP_3$-phosphatase, SHIP2, to bind Filamin A, and through these contacts move to sites of $PIP_3$, may contribute the local dynamics of these $PIP_3$/actin cytoskeleton interactions[190]. However, nothing is known of its functions in the prostate and we did not detect significant association of either Filamin A or SHIP2 with the PLEKHS1-pulldowns. There is no data available describing changes in the levels of mRNA encoding PhldB2, or of the protein, between wild-type and *Pten* $^{-/-}$ prostate so it is difficult to predict what drives the increased association with the PLEKHS1 interactome that occurs in *Pten* $^{-/-}$ prostate observed in our data.

Memo1 is an interesting signalling molecule that has been mapped downstream of ErbB2 (part of the Epidermal growth factor family of receptor tyrosine kinases) and upstream of a RhoA-DiaPH1 transduction cassette that controls microtubules[191 192]. Recent work suggests it has a unique phosphor-protein binding domain that allows it to interact with ErbB2 and Irs1[193].

The levels of mRNA encoding Memo1 is significantly increased in *Pten* $^{-/-}$ prostate (Table 5.4) indicating that an increase in Memo expression may be involved in driving the increase in association of Memo1 with the PLEKHS1 interactome, although its phospho-peptide binding domain might be involved (as the presence of Irs1 in PLEKHS1 pulldowns is reduced in *Pten* $^{-/-}$ prostate it is unlikely to the connection). However, with its network of ErbB2 signalling interactions controlling the cytoskeleton and cell migration, Memo1 is well placed to have an important role in the *Pten* $^{-/-}$ phenotype of prostate.

The Stat family of proteins, of which Stat3 is a member, are phosphorylated by activated cytokine receptor-associated kinases and then dimerise and move to the nucleus where their activity as transcription factors become manifest. The expression of Stat3 mRNA is increased in *Pten* $^{-/-}$ prostate (Table 5.4) suggesting increased expression may be one of the potential factors underlying its increased association with the PLEKHS1-interactome. There are no outstanding, known, binding-partners of Stat3 also found significantly

enriched in the PLEKHS1-pulldowns that offer a molecular explanation for their association. Interestingly, Stat5a is also significantly enriched in PLEKHS1-pulldowns but only from *Pten* $^{+/+}$, and not *Pten* $^{-/-}$, prostate (Table 5.1, Figure 5.16). However, it remains possible that the increased presence of Stat3 in the PLEKHS1 interactome from *Pten* $^{-/-}$ prostate is functionally important.

| | | Abundances(grouped) | | | | Adjusted p value |
|---|---|---|---|---|---|---|
| Gene Symbol | Unique Peptides | Plekhs1$^{WT/WT}$ PTEN$^{+/+}$ | Plekhs1$^{Avi/Avi}$ PTEN$^{+/+}$ | Plekhs1$^{WT/WT}$ PTEN$^{-/-}$ | Plekhs1$^{Avi/Avi}$ PTEN$^{-/-}$ | Plekhs1$^{Avi/Avi}$ PTEN$^{-/-}$/ Plekhs1$^{Avi/Avi}$ PTEN$^{+/+}$ |
| **Chaperones** | | | | | | |
| Bag2 | 9 | 45.5 | 215.6 | 53.7 | 85.2 | 0.0121 |
| Bag6 | 15 | 60.3 | 191.3 | 63.8 | 84.6 | 0.0108 |
| Dnaja4 | 14 | 76.1 | 185.4 | 55.1 | 83.4 | 0.0212 |
| Dnajc7 | 17 | 69.8 | 199.8 | 59.7 | 70.7 | 0.0080 |
| Get4 | 5 | 57.3 | 186.4 | 67.6 | 88.7 | 0.0178 |
| Hspa1a | 1 | 78.8 | 189.4 | 50.9 | 80.8 | 0.0137 |
| Hspa1b | 1 | 58.7 | 208.2 | 44.9 | 88.2 | 0.0195 |
| Hspa2 | 19 | 74.1 | 145.9 | 72.5 | 107.5 | 0.0344 |
| Stub1 | 8 | 40.5 | 233.2 | 46.1 | 80.2 | 0.0143 |
| Ubl4 | 6 | 68.5 | 191.5 | 65 | 74.9 | 0.0020 |
| Zswim8 | 6 | 56.5 | 182.6 | 58 | 102.9 | 0.0417 |
| **Ubiquitination** | | | | | | |
| Maged1 | 19 | 67.7 | 183 | 69.1 | 80.2 | 0.0164 |
| Nbr1 | 5 | 61 | 196.8 | 62 | 80.3 | 0.0150 |
| Stub1 | 8 | 40.5 | 233.2 | 46.1 | 80.2 | 0.0143 |
| Sqstm1 | 3 | 85.2 | 151.7 | 73.5 | 89.6 | 0.0239 |
| **Autophagy** | | | | | | |
| Atg101 | 1 | 63.9 | 186.9 | 75 | 74.1 | 0.0164 |
| Atg13 | 1 | 80.5 | 151.4 | 85.9 | 82.2 | 0.0383 |
| Atp6v1c2 | 2 | 75.1 | 228.6 | 37.8 | 58.5 | 0.0121 |
| Nbr1 | 5 | 61 | 196.8 | 62 | 80.3 | 0.0150 |
| Sqstm1 | 3 | 85.2 | 151.7 | 73.5 | 89.6 | 0.0239 |
| **Peroxisomes** | | | | | | |
| Nbr1 | 5 | 61 | 196.8 | 62 | 80.3 | 0.0150 |
| Pex5 | 2 | 80.8 | 169.8 | 69.4 | 80 | 0.0248 |
| **Glutathione Peroxidases** | | | | | | |
| Gpx2 | 5 | 38 | 46.8 | 83.4 | 231.9 | 0.0181 |
| **Golgi** | | | | | | |
| Gga2 | 4 | 89.5 | 154.8 | 81.1 | 74.7 | 0.0233 |
| **Centrosome** | | | | | | |
| Cep97 | 1 | 83.3 | 177.5 | 73.8 | 65.4 | 0.0197 |
| Pcm1 | 5 | 95.4 | 146.3 | 79.5 | 78.7 | 0.0203 |
| **Cytoskeleton** | | | | | | |
| Phldb2 | 2 | 41.6 | 43.9 | 82.7 | 231.8 | 0.0108 |
| **Protein kinases** | | | | | | |
| Camk2d | 12 | 63.7 | 176.3 | 68.3 | 91.7 | 0.0080 |
| Camk2g | 10 | 83.8 | 189.5 | 52.8 | 73.9 | 0.0150 |
| Irak1 | 6 | 75.5 | 166.6 | 69 | 88.9 | 0.0406 |
| Map3k7 | 1 | 64.1 | 143.5 | 96.8 | 95.7 | 0.0474 |
| **Lipid kinases** | | | | | | |
| Pik3cb | 12 | 47.8 | 96.5 | 45.9 | 209.8 | 0.0202 |
| Pik3r1 | 27 | 34.7 | 71.2 | 27.5 | 266.5 | 0.0143 |
| Pik3r2 | 15 | 41.9 | 75 | 34.3 | 248.7 | 0.0197 |
| **14-3-3** | | | | | | |
| Sfn | 9 | 20 | 47 | 57.6 | 275.4 | 0.0137 |
| Ywhab | 13 | 13.9 | 84.1 | 12.7 | 289.2 | 0.0164 |
| Ywhae | 28 | 20.3 | 94.2 | 15.7 | 269.8 | 0.0099 |
| Ywhah | 24 | 15.9 | 74.9 | 10.3 | 299 | 0.0137 |

| | | | | | | |
|---|---|---|---|---|---|---|
| **Signalling near receptors** | | | | | | |
| **Irak1** | 6 | 75.5 | 166.6 | 69 | 88.9 | 0.0406 |
| **Irs1** | 1 | 94.1 | 209.1 | 33.7 | 63.1 | 0.0143 |
| **Map3k7** | 1 | 64.1 | 143.5 | 96.8 | 95.7 | 0.0474 |
| **Memo1** | 3 | 67.8 | 77.5 | 68 | 186.7 | 0.0164 |
| **Phldb2** | 2 | 41.6 | 43.9 | 82.7 | 231.8 | 0.0108 |
| **Pik3cb** | 12 | 47.8 | 96.5 | 45.9 | 209.8 | 0.0202 |
| **Pik3r1** | 27 | 34.7 | 71.2 | 27.5 | 266.5 | 0.0143 |
| **Pik3r2** | 15 | 41.9 | 75 | 34.3 | 248.7 | 0.0197 |
| **Stat3** | 11 | 60.5 | 78.9 | 81.8 | 178.8 | 0.0080 |
| **Stat5a** | 3 | 82.7 | 155 | 66.1 | 96.2 | 0.0198 |
| **Ttc7** | 2 | 81.3 | 145.6 | 80.8 | 92.3 | 0.0189 |
| **General signalling** | | | | | | |
| **Ttc7** | 2 | 81.3 | 145.6 | 80.8 | 92.3 | 0.0189 |
| **NF-κB signalling** | | | | | | |
| **Map3k7** | 1 | 64.1 | 143.5 | 96.8 | 95.7 | 0.0474 |
| **Others** | | | | | | |
| **Ankhd1** | 8 | 86.1 | 146.3 | 80.8 | 86.8 | 0.0080 |
| **Atf6** | 3 | 80.3 | 167.5 | 72.5 | 79.7 | 0.0178 |
| **Cse1l** | 11 | 64.4 | 68.4 | 132.7 | 134.5 | 0.0212 |
| **D6Wsu116e** | 10 | 69.2 | 178.3 | 70.6 | 81.9 | 0.0164 |
| **Dnajb5** | 1 | 78.6 | 184.8 | 59.9 | 76.6 | 0.0226 |
| **Eef2k** | 2 | 83.4 | 141.4 | 81.8 | 93.3 | 0.0320 |
| **Gramd3** | 4 | 83.1 | 226 | 32.3 | 58.5 | 0.0236 |
| **Krt23** | 3 | 68.3 | 175.1 | 75.7 | 80.8 | 0.0150 |
| **Ly6c1** | 2 | 60.8 | 57.5 | 90 | 191.7 | 0.0367 |
| **Mkl2** | 6 | 72.7 | 149.6 | 86.4 | 91.2 | 0.0263 |
| **Tcp11l2** | 3 | 38.1 | 222.4 | 49.9 | 89.6 | 0.0236 |
| **Tgm4** | 58 | 113.2 | 219.6 | 27.1 | 40.1 | 0.0417 |
| **Xaf1** | 1 | 30.1 | 36.1 | 123 | 210.9 | 0.0099 |
| **Zc3h7a** | 7 | 67.6 | 153.7 | 83.4 | 95.3 | 0.0382 |

**Table 5.1 Plekhs1-interacting proteins significantly differentially recovered from PTEN$^{+/+}$ or PTEN$^{-/-}$ mouse prostate**

*Prostates from 12-15w mice were rapidly dissected and frozen (all mice were BirA$^{+/-}$, mice described as PTEN$^{-/-}$ were PbCre$^{+/-}$, PTEN$^{loxP/loxP}$, PTEN$^{+/+}$were PbCre$^{-/-}$, PTEN$^{loxP/loxP}$). Lysates were prepared, subjected to streptavidin-pulldown and the associated proteins were quantified by TMT- proteomics techniques. The data were analyzed and presented as normalized (to the total peptide mass spec signal for each sample), but NOT grouped, abundances using Proteome Discoverer software and the replication and statistics are as explained in the Methods. Proteins are identified by their gene names and the number of unique peptides upon which the data are based are indicated. Selected proteins, presented in* Figure 5.5-Figure 5.20*) are shown in this format, which enables the relative abundance of different Plekhs1 interactors to be compared.*

| | | Abundances(absolute) | | | |
|---|---|---|---|---|---|
| Gene Symbol | Unique Peptides | Plekhs1$^{WT/WT}$ PTEN$^{+/+}$ | Plekhs1$^{Avi/Avi}$ PTEN$^{+/+}$ | Plekhs1$^{WT/WT}$ PTEN$^{-/-}$ | Plekhs1$^{Avi/Avi}$ PTEN$^{-/-}$ |
| **Chaperones** | | | | | |
| Bag6 | 15 | 265 | 858 | 287 | 364 |
| Get4 | 5 | 145 | 480 | 161 | 229 |
| Stub1 | 8 | 38 | 244 | 48 | 75 |
| Ubl4 | 6 | 294 | 797 | 277 | 322 |
| **Ubiquitination** | | | | | |
| Klhl22 | 1 | 49 | 130 | 42 | 64 |
| Maged1 | 19 | 985 | 2889 | 1121 | 1141 |
| Nbr1 | 5 | 115 | 378 | 116 | 149 |
| Pja2 | 1 | 15 | 68 | 18 | 21 |
| Sqstm1 | 3 | 56 | 104 | 50 | 60 |
| Stub1 | 8 | 38 | 244 | 48 | 75 |
| Zer1 | 3 | 60 | 96 | 58 | 72 |
| **Autophagy** | | | | | |
| Atg13 | 1 | 49 | 89 | 48 | 50 |
| Nbr1 | 5 | 115 | 378 | 116 | 149 |
| Sqstm1 | 3 | 56 | 104 | 50 | 60 |
| **Peroxisomes** | | | | | |
| Nbr1 | 5 | 115 | 378 | 116 | 149 |
| Pex1 | 5 | 225 | 429 | 247 | 281 |
| Pex5 | 2 | 86 | 177 | 70 | 83 |
| **Glutathione Peroxidases** | | | | | |
| Gpx2 | 5 | 188 | 207 | 435 | 1238 |
| **Golgi** | | | | | |
| Gga2 | 4 | 71 | 125 | 65 | 60 |
| Golga3 | 11 | 106 | 344 | 124 | 154 |
| **Centrosome** | | | | | |
| Cep97 | 1 | 38 | 79 | 33 | 32 |
| Pcm1 | 5 | 120 | 192 | 98 | 96 |
| **Cytoskeleton** | | | | | |
| Phldb2 | 2 | 10 | 10 | 19 | 52 |
| Spg20 | 2 | 53 | 111 | 61 | 62 |
| **Protein kinases** | | | | | |
| Camk2d | 12 | 904 | 2535 | 980 | 1308 |
| Map3k7 | 1 | 48 | 105 | 72 | 71 |
| **Lipid kinases** | | | | | |
| Pik3ca | 14 | 310 | 699 | 299 | 1682 |
| Pik3cb | 12 | 267 | 517 | 251 | 1318 |
| Pik3r1 | 27 | 667 | 1250 | 500 | 5173 |
| Pik3r2 | 15 | 226 | 392 | 187 | 1310 |
| Pik3r3 | 13 | 207 | 598 | 165 | 3057 |

| | | | | | |
|---|---|---|---|---|---|
| **14-3-3** | | | | | |
| **Sfn** | 9 | 117 | 251 | 306 | 1411 |
| **Ywhab** | 13 | 248 | 1561 | 250 | 5012 |
| **Ywhae** | 28 | 2701 | 12371 | 2075 | 35662 |
| **Ywhag** | 17 | 874 | 5151 | 621 | 13052 |
| **Ywhah** | 24 | 1289 | 6129 | 761 | 25479 |
| **Ywhaq** | 24 | 1208 | 6090 | 942 | 16089 |
| **Ywhaz** | 20 | 1389 | 8363 | 1143 | 25623 |
| **Signalling near receptors** | | | | | |
| **Irs1** | 1 | 37 | 90 | 14 | 23 |
| **Map3k7** | 1 | 48 | 105 | 72 | 71 |
| **Memo1** | 3 | 84 | 104 | 83 | 239 |
| **Phldb2** | 2 | 10 | 10 | 19 | 52 |
| **Sqstm1** | 3 | 56 | 104 | 50 | 60 |
| **Ttc7** | 2 | 96 | 176 | 95 | 111 |
| **General signalling** | | | | | |
| **Bin3** | 1 | 101 | 246 | 118 | 158 |
| **Tbc1d17** | 2 | 34 | 74 | 41 | 48 |
| **Ttc7** | 2 | 96 | 176 | 95 | 111 |
| **NF-κB signalling** | | | | | |
| **Map3k7** | 1 | 48 | 105 | 72 | 71 |
| **Others** | | | | | |
| **Ankhd1** | 8 | 629 | 1047 | 597 | 633 |
| **Atf6** | 3 | 257 | 536 | 220 | 239 |
| **D6Wsu116e** | 10 | 456 | 1143 | 483 | 543 |
| **Eef2k** | 2 | 101 | 170 | 98 | 112 |
| **Gramd1b** | 2 | 25 | 56 | 27 | 29 |
| **Ly6c1** | 2 | 59 | 55 | 83 | 173 |
| **Mkl2** | 6 | 91 | 189 | 112 | 118 |
| **Pja1** | 1 | 8 | 43 | 9 | 13 |
| **Rundc1** | 2 | 18 | 45 | 22 | 25 |
| **Tcp11l2** | 3 | 22 | 137 | 27 | 51 |
| **Zc3h7a** | 7 | 46 | 109 | 56 | 62 |

**Table 5.2 The absolute abundances of proteins selectively recovered with Avi-tagged Plekhs1 pulled down from $PTEN^{+/+}$ or $PTEN^{-/-}$ mouse prostate**

*Prostates from 12-15w mice were rapidly dissected and frozen (all mice were $BirA^{+/-}$, mice described as $PTEN^{-/-}$ were $PbCre^{+/-}$, $PTEN^{loxP/loxP}$, $PTEN^{+/+}$were $PbCre^{-/-}$, $PTEN^{loxP/loxP}$). Lysates were prepared, subjected to streptavidin-pulldown and the associated proteins were quantified by TMT- proteomics techniques. The data were analyzed and presented as normalized (to the total peptide mass spec signal for each sample), grouped (data for each protein are expressed as a proportion, of the total signal measured for that protein across all 4 genotypes, set to 400) abundances using Proteome Discoverer software and the replication and statistics are as explained in the Methods. Proteins are identified by their gene names and the number of unique peptides upon which the data are based are indicated. All proteins that were significantly differently recovered from $PTEN^{+/+}$ compared to $PTEN^{-/-}$ prostate were identified (240). This list of proteins was filtered to remove those that were different due to changed non-specific recovery (defined by recovery from $Plekhs1^{WT/WT}$ tissue) probably resulting from differential expression between $PTEN^{+/+}$ and $PTEN^{-/-}$ tissues; to leave the 52 proteins shown in the table. Those whose recovery were increased from $PTEN^{-/-}$ prostate are green, those whose recovery were decreased from $PTEN^{-/-}$ are red.*

| | | Abundances(grouped) | | | | Adjusted p value | |
|---|---|---|---|---|---|---|---|
| Gene Symbol | Unique Peptides | Plekhs1$^{WT/WT}$ PTEN$^{+/+}$ | Plekhs1$^{Avi/Avi}$ PTEN$^{+/+}$ | Plekhs1$^{WT/WT}$ PTEN$^{-/-}$ | Plekhs1$^{Avi/Avi}$ PTEN$^{-/-}$ | PTEN$^{+/+}$ AVI/WT | PTEN$^{-/-}$ AVI/WT |
| **Chaperones** | | | | | | | |
| Bag2 | 9 | 45.5 | 215.6 | 53.7 | 85.2 | 0.0026 | 0.2562 |
| Bag6 | 15 | 60.3 | 191.3 | 63.8 | 84.6 | 0.0036 | 0.9999 |
| Dnaja2 | 21 | 69.8 | 150.9 | 79.1 | 100.2 | 0.0206 | 0.9999 |
| Dnaja4 | 14 | 76.1 | 185.4 | 55.1 | 83.4 | 0.0410 | 0.7651 |
| Dnajc7 | 17 | 69.8 | 199.8 | 59.7 | 70.7 | 0.0045 | 0.9999 |
| Get4 | 5 | 57.3 | 186.4 | 67.6 | 88.7 | 0.0065 | 0.7089 |
| Hsp90aa1 | 38 | 60.8 | 130.4 | 86.5 | 122.3 | 0.0025 | 0.0784 |
| Hsp90ab1 | 45 | 64.5 | 135.1 | 87 | 113.4 | 0.0143 | 0.6094 |
| Hspa1a; Hspa1b | 1 | 78.8 | 189.4 | 50.9 | 80.8 | 0.0239 | 0.3511 |
| Hspa1b | 1 | 58.7 | 208.2 | 44.9 | 88.2 | 0.0112 | 0.1846 |
| Hspa2 | 19 | 74.1 | 145.9 | 72.5 | 107.5 | 0.0065 | 0.1015 |
| Hspa8 | 43 | 56.9 | 155.9 | 65.8 | 121.4 | 0.0059 | 0.0458 |
| Stub1 | 8 | 40.5 | 233.2 | 46.1 | 80.2 | 0.0053 | 0.8397 |
| Ubl4 | 6 | 68.5 | 191.5 | 65 | 74.9 | 0.0025 | 0.9999 |
| **Ubiquitination** | | | | | | | |
| Dcaf11 | 3 | 44.1 | 151.2 | 45.1 | 159.5 | 0.0191 | 0.0171 |
| Ddb1 | 40 | 69.9 | 126.9 | 88.5 | 114.6 | 0.0349 | 0.5474 |
| Fam175b | 3 | 82.5 | 116.3 | 94.7 | 106.6 | 0.0294 | 0.9999 |
| Keap1 | 10 | 75.3 | 131 | 84.2 | 109.6 | 0.0029 | 0.0458 |
| Maged1 | 19 | 67.7 | 183 | 69.1 | 80.2 | 0.0239 | 0.9999 |
| Nbr1 | 5 | 61 | 196.8 | 62 | 80.3 | 0.0142 | 0.9999 |
| Rps27a | 4 | 67.1 | 146.4 | 80.6 | 105.9 | 0.0025 | 0.1811 |
| Stub1 | 8 | 40.5 | 233.2 | 46.1 | 80.2 | 0.0053 | 0.8397 |
| Usp4 | 7 | 64.5 | 107.1 | 102.1 | 126.4 | 0.0028 | 0.1846 |
| **Autophagy** | | | | | | | |
| Atg101 | 1 | 63.9 | 186.9 | 75 | 74.1 | 0.0239 | 0.9999 |
| Nbr1 | 5 | 61 | 196.8 | 62 | 80.3 | 0.0142 | 0.9999 |
| Pik3r4 | 5 | 68.8 | 137.6 | 82.2 | 111.4 | 0.0244 | 0.6320 |
| **Peroxisomes** | | | | | | | |
| Nbr1 | 5 | 61 | 196.8 | 62 | 80.3 | 0.0142 | 0.9999 |
| **Glutathione Peroxidases** | | | | | | | |
| Gpx1 | 8 | 43 | 86.9 | 47.6 | 222.6 | 0.4630 | 0.0469 |
| **Centrosome** | | | | | | | |
| Cep170b | 13 | 68 | 137 | 79.6 | 115.4 | 0.0239 | 0.8875 |
| Cep192 | 1 | 65.5 | 152.4 | 61.9 | 120.1 | 0.0125 | 0.0458 |
| **Cytoskeleton** | | | | | | | |
| Kif16b | 6 | 77.8 | 137 | 98.2 | 87 | 0.0244 | 0.9999 |
| Lrch3 | 3 | 73.5 | 117.1 | 82.9 | 126.5 | 0.0357 | 0.0458 |
| Rufy3 | 6 | 55.1 | 166.4 | 61.6 | 116.9 | 0.0294 | 0.4582 |
| **Protein kinases** | | | | | | | |
| Camk2d | 12 | 63.7 | 176.3 | 68.3 | 91.7 | 0.0025 | 0.2202 |
| Map3k4 | 2 | 67.4 | 104 | 60.5 | 168.1 | 0.6709 | 0.0308 |
| Map3k7 | 1 | 64.1 | 143.5 | 96.8 | 95.7 | 0.0118 | 0.9999 |
| **Lipid kinases** | | | | | | | |
| Pik3ca | 14 | 42.5 | 95.8 | 42.4 | 219.3 | 0.3050 | 0.0214 |
| Pik3cb | 12 | 47.8 | 96.5 | 45.9 | 209.8 | 0.1932 | 0.0059 |
| Pik3r1 | 27 | 34.7 | 71.2 | 27.5 | 266.5 | 0.5736 | 0.0046 |
| Pik3r2 | 15 | 41.9 | 75 | 34.3 | 248.7 | 0.7195 | 0.0074 |
| Pik3r3 | 13 | 20.1 | 62.7 | 16.4 | 300.8 | 0.7750 | 0.0214 |
| Pik3r4 | 5 | 68.8 | 137.6 | 82.2 | 111.4 | 0.0244 | 0.6320 |
| Pip4k2c | 15 | 38.8 | 146.4 | 52.1 | 162.7 | 0.0025 | 0.0033 |

| | | | | | | | |
|---|---|---|---|---|---|---|---|
| **14-3-3** | | | | | | | |
| Sfn | 9 | 20 | 47 | 57.6 | 275.4 | 0.4673 | 0.0458 |
| Ywhab | 13 | 13.9 | 84.1 | 12.7 | 289.2 | 0.0063 | 0.0006 |
| Ywhae | 28 | 20.3 | 94.2 | 15.7 | 269.8 | 0.0025 | 0.0002 |
| Ywhag | 17 | 18.4 | 104.7 | 14.1 | 262.8 | 0.0143 | 0.0013 |
| Ywhah | 24 | 15.9 | 74.9 | 10.3 | 299 | 0.0194 | 0.0006 |
| Ywhaq | 24 | 20.2 | 93.2 | 17.5 | 269.1 | 0.0753 | 0.0069 |
| Ywhaz | 20 | 15.3 | 90.2 | 11.2 | 283.3 | 0.0502 | 0.0047 |
| **Signalling near receptors** | | | | | | | |
| Map3k4 | 2 | 67.4 | 104 | 60.5 | 168.1 | 0.6709 | 0.0308 |
| Map3k7 | 1 | 64.1 | 143.5 | 96.8 | 95.7 | 0.0118 | 0.9999 |
| Memo1 | 3 | 67.8 | 77.5 | 68 | 186.7 | 1.0000 | 0.0179 |
| Pik3ca | 14 | 42.5 | 95.8 | 42.4 | 219.3 | 0.3050 | 0.0214 |
| Pik3cb | 12 | 47.8 | 96.5 | 45.9 | 209.8 | 0.1932 | 0.0059 |
| Pik3r1 | 27 | 34.7 | 71.2 | 27.5 | 266.5 | 0.5736 | 0.0046 |
| Pik3r2 | 15 | 41.9 | 75 | 34.3 | 248.7 | 0.7195 | 0.0074 |
| Pik3r3 | 13 | 20.1 | 62.7 | 16.4 | 300.8 | 0.7750 | 0.0214 |
| Stat3 | 11 | 60.5 | 78.9 | 81.8 | 178.8 | 0.4005 | 0.0059 |
| Stat5a | 3 | 82.7 | 155 | 66.1 | 96.2 | 0.0197 | 0.3511 |
| Traf2 | 5 | 52.3 | 104.7 | 68.2 | 174.7 | 0.1663 | 0.0458 |
| Ttc7 | 2 | 81.3 | 145.6 | 80.8 | 92.3 | 0.0192 | 0.9999 |
| **General signalling** | | | | | | | |
| Pik3r4 | 5 | 68.8 | 137.6 | 82.2 | 111.4 | 0.0244 | 0.6320 |
| Pip4k2c | 15 | 38.8 | 146.4 | 52.1 | 162.7 | 0.0025 | 0.0033 |
| Rufy3 | 6 | 55.1 | 166.4 | 61.6 | 116.9 | 0.0294 | 0.4582 |
| Ttc7 | 2 | 81.3 | 145.6 | 80.8 | 92.3 | 0.0192 | 0.9999 |
| **NF-κB signalling** | | | | | | | |
| Map3k7 | 1 | 64.1 | 143.5 | 96.8 | 95.7 | 0.0118 | 0.9999 |
| Traf2 | 5 | 52.3 | 104.7 | 68.2 | 174.7 | 0.1663 | 0.0458 |
| **Others** | | | | | | | |
| A9C474 (Uniprot) | 1 | 53.6 | 135.8 | 81.8 | 128.8 | 0.0197 | 0.4582 |
| Ankhd1 | 8 | 86.1 | 146.3 | 80.8 | 86.8 | 0.0065 | 0.9999 |
| Ankrd27 | 1 | 58.8 | 142.4 | 90.4 | 108.4 | 0.0375 | 0.9979 |
| Atp6v1c2 | 2 | 75.1 | 228.6 | 37.8 | 58.5 | 0.0415 | 0.7636 |
| D6Wsu116e | 10 | 69.2 | 178.3 | 70.6 | 81.9 | 0.0194 | 0.9999 |
| Epm2aip1 | 2 | 58.6 | 149.8 | 84.8 | 106.8 | 0.0476 | 0.9999 |
| Gstm6 | 1 | 47.8 | 173.2 | 58.3 | 120.7 | 0.0025 | 0.0308 |
| Krt23 | 3 | 68.3 | 175.1 | 75.7 | 80.8 | 0.0143 | 0.9999 |
| Mkl2 | 6 | 72.7 | 149.6 | 86.4 | 91.2 | 0.0191 | 0.9999 |
| Mlf2 | 3 | 47.5 | 154.6 | 55.2 | 142.7 | 0.0065 | 0.0184 |
| Phldb3 | 4 | 55.7 | 150 | 80.2 | 114.1 | 0.0065 | 0.3849 |
| Plekhs1 | 46 | 21.5 | 150.4 | 15.8 | 212.3 | 0.0063 | 0.0015 |
| Polr2b | 12 | 72.1 | 125.6 | 81.8 | 120.5 | 0.0344 | 0.4093 |
| Polr2c | 2 | 67.5 | 121.8 | 92.8 | 117.8 | 0.0415 | 0.9999 |
| Tcp11l2 | 3 | 38.1 | 222.4 | 49.9 | 89.6 | 0.0063 | 0.4582 |
| Zc3h7a | 7 | 67.6 | 153.7 | 83.4 | 95.3 | 0.0244 | 0.9999 |
| Zwism8 | 6 | 56.5 | 182.6 | 58 | 102.9 | 0.0130 | 0.3511 |

**Table 5.3 Proteins selectively interacting with Plekhs1 in either PTEN$^{+/+}$ or PTEN$^{-/-}$ mouse prostate**

*Prostates from 12-15w mice were rapidly dissected and frozen (all mice were BirA$^{+/-}$, mice described as PTEN$^{-/-}$ were PbCre$^{+/-}$, PTEN$^{loxP/loxP}$, PTEN$^{+/+}$were PbCre$^{-/-}$, PTEN$^{loxP/loxP}$). Lysates were prepared, subjected to streptavidin-pulldown and the associated proteins were quantified by TMT- proteomics techniques. The data were analyzed and presented as normalized (to the total peptide mass spec signal for each sample), grouped (data for each protein are expressed as a proportion, of the total signal measured for that protein across all 4 genotypes, set to 400) abundances using Proteome Discoverer software and the replication and statistics are as explained in the Methods. Proteins are identified by their gene names and the number of unique peptides upon which the data are based are indicated. All proteins (69) that were significantly enriched in pulldowns (abundance in pulldowns from Plekhs1$^{Avi/Avi}$ prostate/abundance in Plekhs1$^{WT/WT}$ prostate, significantly greater than 1) from PTEN$^{+/+}$ and/or PTEN$^{-/-}$ prostate are shown in the figure.*

| Gene Symbol | WT AP(mean) | PIN AP(mean) | P-values |
|---|---|---|---|
| **Chaperones** | | | |
| Bag2 | 4.08020556 | 4.799879075 | 0.000466 |
| Bag6 | 6.79540655 | 6.99053365 | 0.422470 |
| Dnaja4 | 4.9697805 | 5.330910525 | 0.000932 |
| Dnajc7 | 7.119181025 | 6.9187331 | 0.013030 |
| Get4 | 6.24610225 | 5.2112303 | 0.000029 |
| Hspa1a | 1.03725219 | 1.162885963 | 0.544845 |
| Hspa1b | 3.159738175 | 3.478182175 | 0.253553 |
| Hspa2 | 4.58683855 | 5.1201231 | 0.002509 |
| Stub1 | 7.751568575 | 7.49930455 | 0.022955 |
| Zswim8 | 6.01623845 | 6.474191 | 0.025633 |
| **Ubiquitination** | | | |
| Maged1 | 8.15460975 | 8.21127105 | 0.941098 |
| Nbr1 | 7.9066753 | 7.505490575 | 0.011022 |
| Stub1 | 7.751568575 | 7.49930455 | 0.022955 |
| Sqstm1 | 8.7491935 | 8.210807625 | 0.000516 |
| **Autophagy** | | | |
| Nbr1 | 7.9066753 | 7.505490575 | 0.011022 |
| Atg13 | 6.717036775 | 5.82731625 | 0.000034 |
| Atp6v1c2 | 9.44295775 | 4.732305725 | 0.000005 |
| Nbr1 | 7.9066753 | 7.505490575 | 0.011022 |
| Sqstm1 | 8.7491935 | 8.210807625 | 0.000516 |
| **Peroxisomes** | | | |
| Nbr1 | 7.9066753 | 7.505490575 | 0.011022 |
| Pex5 | 6.114801175 | 5.106869 | 0.000011 |
| **Glutathione Peroxidases** | | | |
| Gpx2 | -0.435303593 | 5.556058675 | 0.000005 |
| **Golgi** | | | |
| Gga2 | 6.283689 | 4.885881425 | 0.000216 |
| **Centrosome** | | | |
| Cep97 | 4.90895325 | 1.609970575 | 0.000004 |
| Pcm1 | 6.23443915 | 6.2739294 | 0.820689 |
| **Cytoskeleton** | | | |
| Phldb2 | 3.500264475 | 5.536074675 | 0.000009 |
| **Protein kinases** | | | |
| Camk2d | 5.924432775 | 6.163664925 | 0.164297 |
| Camk2g | 5.6058501 | 4.8599155 | 0.004325 |
| Irak1 | 6.82169325 | 6.623809775 | 0.006240 |
| Map3k7 | 5.473881925 | 5.807345575 | 0.019374 |
| **Lipid kinases** | | | |
| Pik3cb | 5.903596775 | 4.97921375 | 0.000059 |
| Pik3r1 | 6.7682504 | 7.6416309 | 0.000721 |
| Pik3r2 | 5.607625575 | 6.1654317 | 0.002379 |

| | | | |
|---|---|---|---|
| **14-3-3** | | | |
| Sfn | 0.59773986 | 3.062934675 | 0.000243 |
| Ywhab | 7.3136443 | 7.964395 | 0.000025 |
| Ywhae | 8.637941375 | 8.990574125 | 0.000022 |
| Ywhah | 5.489704825 | 5.945857825 | 0.005255 |
| **Signalling near receptors** | | | |
| Irak1 | 6.82169325 | 6.623809775 | 0.006240 |
| Irs1 | 7.058754975 | 1.777406285 | 0.000014 |
| Map3k7 | 5.473881925 | 5.807345575 | 0.019374 |
| Memo1 | 3.45036305 | 5.570651375 | 0.000000 |
| Phldb2 | 3.500264475 | 5.536074675 | 0.000009 |
| Pik3cb | 5.903596775 | 4.97921375 | 0.000059 |
| Pik3r1 | 6.7682504 | 7.6416309 | 0.000721 |
| Pik3r2 | 5.607625575 | 6.1654317 | 0.002379 |
| Sqstm1 | 8.7491935 | 8.210807625 | 0.000516 |
| Stat3 | 6.174676 | 7.533415 | 0.000001 |
| Stat5a | 8.1402145 | 5.7191255 | 0.000016 |
| Ttc7 | 5.67478075 | 5.741540825 | 0.610973 |
| **General signalling** | | | |
| Ttc7 | 5.67478075 | 5.741540825 | 0.610973 |
| **Nfkb signalling** | | | |
| Map3k7 | 5.473881925 | 5.807345575 | 0.019374 |
| **Others** | | | |
| Ankhd1 | 5.9721975 | 6.13545835 | 0.164984 |
| Atf6 | 8.4154255 | 5.9200572 | 0.000001 |
| Cse1l | 4.86894355 | 5.426153925 | 0.002191 |
| Dnajb5 | 2.777083775 | 3.06512965 | 0.177591 |
| Eef2k | 6.880467625 | 5.6029499 | 0.000120 |
| Gramd3 | 6.9280045 | 4.6232384 | 0.000000 |
| Ly6c1 | 3.7014432 | 6.43544775 | 0.000001 |
| Tcp11l2 | 6.134402575 | 5.18309025 | 0.000338 |
| Tgm4 | 15.75078275 | 7.368728025 | 0.000000 |
| Xaf1 | 1.256285095 | 4.20951985 | 0.000442 |
| Zc3h7a | 6.339927075 | 7.2561485 | 0.005132 |

**Table 5.4 Transcriptomic analysis of anterior prostates (AP) of control ($PTEN^{+/+}$) and $PTEN^{-/-}$ mouse**

*Prostates from 17-28w mice (FVB strain) were rapidly dissected and frozen (mice described as $PTEN^{-/-}$ were $PbCre^{+/-}$, $PTEN^{loxP/loxP}$, $PTEN^{+/+}$ were $PbCre^{-/-}$, $PTEN^{loxP/loxP}$). mRNA expression profiles of prostate/prostate during PIN stage of tumorigenesis were analysed assessed by RNA sequencing. Table represents $log_2$ values for gene of interest.*

*Above experiments were performed in five ($PTEN^{+/+}$) or four ($PTEN^{-/-}$) replicates.*

*Re-analysing of published dataset (Jurimeister et al., EMBO Molecular Medicine, 2018) was performed by Dr Felix Krueger and Dr Tamara Chessa, Babraham Institute using SeqMonk software*

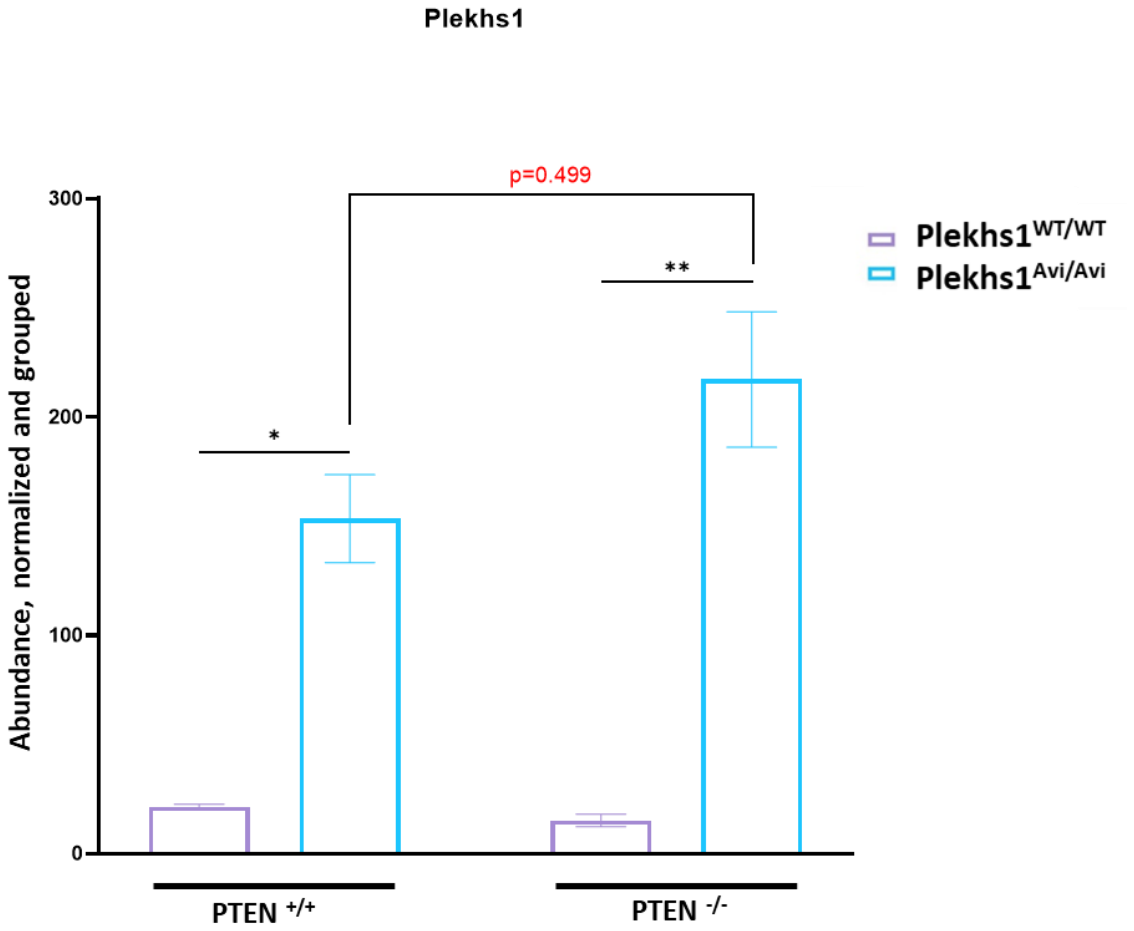


**Figure 5.4 The relative abundance of Plekhs1 in Avi-pulldowns from mouse prostate**

*Prostates from 12-15w mice were rapidly dissected and frozen (genotypes; Plekhs1$^{WT/WT}$, PTEN$^{+/+}$; Plekhs1$^{Avi/Avi}$, PTEN$^{+/+}$; Plekhs1$^{WT/WT}$, PTEN$^{-/-}$; Plekhs1$^{Avi/Avi}$, PTEN$^{-/-}$; and all PbCre$^{+/-}$). Lysates were prepared, subjected to streptavidin-pulldown and the associated proteins were quantified by TMT- proteomics techniques. The data were analyzed and presented as normalized (to the total peptide mass spec signal for each sample), grouped (data for each protein are expressed as a proportion, of the total signal measured for that protein across all 4 genotypes, set to 400) abundances using Proteome Discoverer software and the replication and statistics are as explained in the Methods. P-values in red are not significant.*

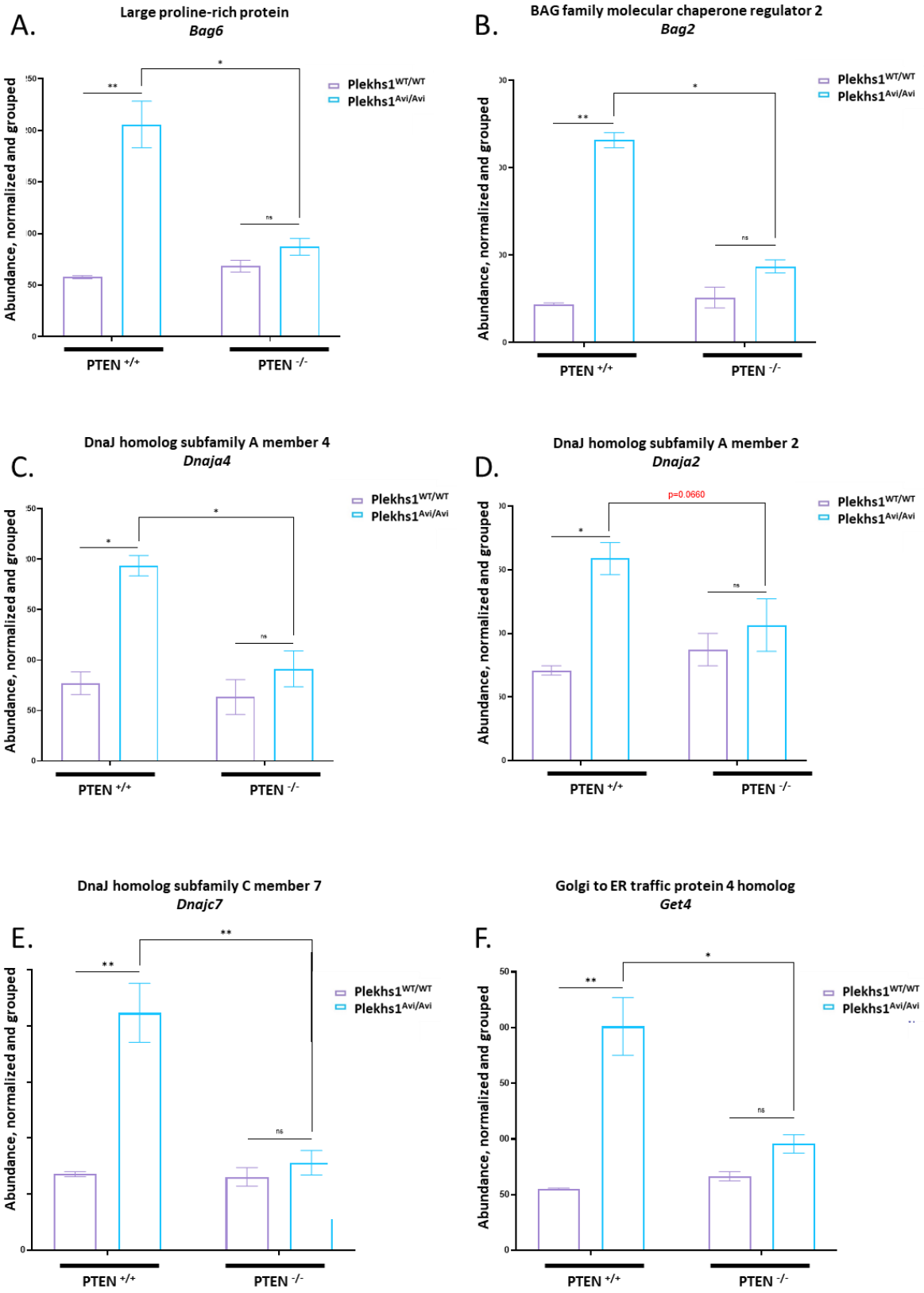
A.
Large proline-rich protein
Bag6
B.
BAG family molecular chaperone regulator 2
Bag2
C.
DnaJ homolog subfamily A member 4
Dnaja4
D.
DnaJ homolog subfamily A member 2
Dnaja2
p=0.0660
E.
DnaJ homolog subfamily C member 7
Dnajc7
F.
Golgi to ER traffic protein 4 homolog
Get4
Abundance, normalized and grouped
Plekhs1WT/WT
Plekhs1Avi/Avi
PTEN +/+
PTEN -/-
ns

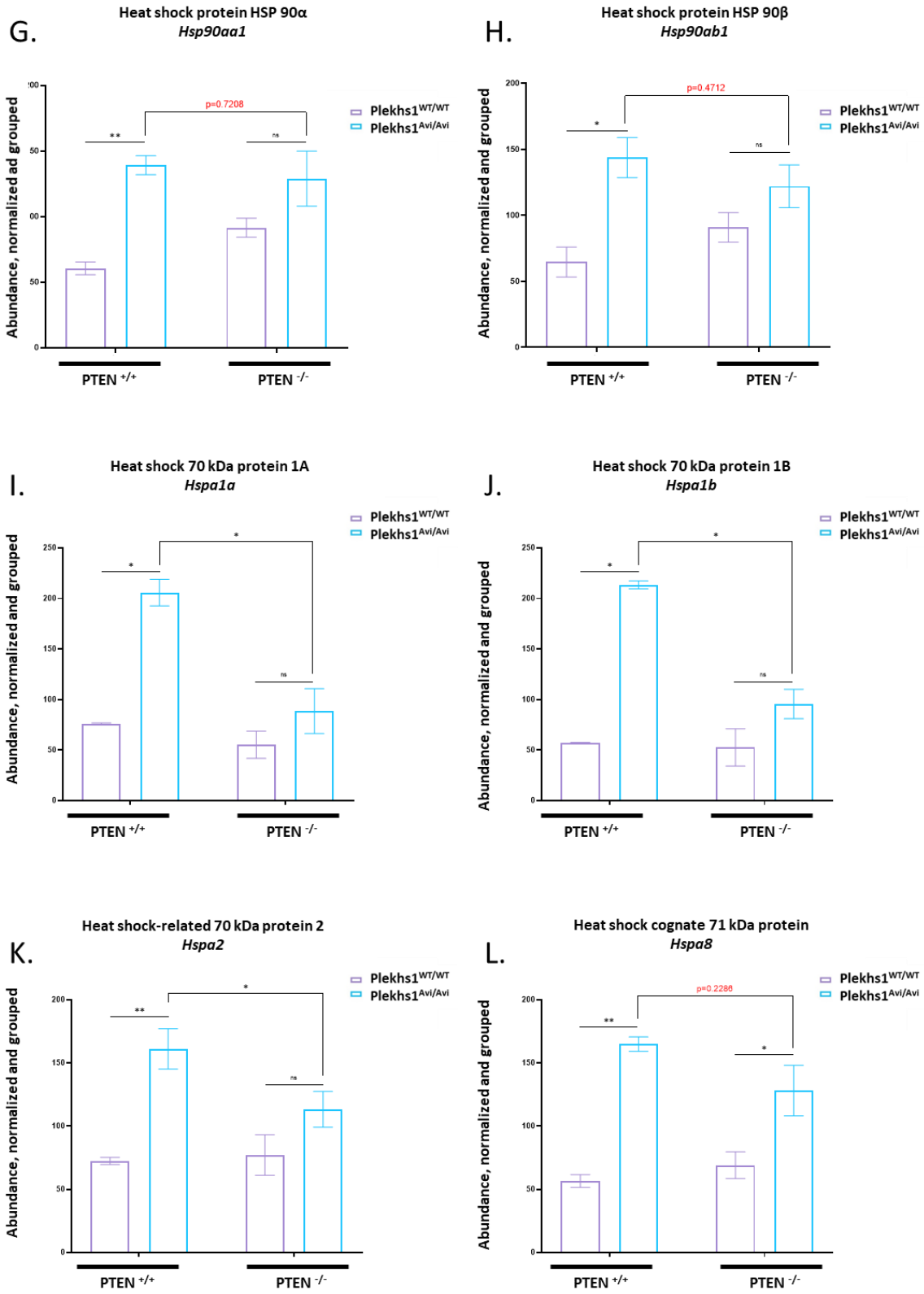
G.
Heat shock protein HSP 90α
Hsp90aa1
p=0.7208
**
ns
Abundance, normalized ad grouped
Plekhs1WT/WT
Plekhs1Avi/Avi
PTEN +/+
PTEN -/-
H.
Heat shock protein HSP 90β
Hsp90ab1
p=0.4712
*
ns
Abundance, normalized and grouped
Plekhs1WT/WT
Plekhs1Avi/Avi
PTEN +/+
PTEN -/-
I.
Heat shock 70 kDa protein 1A
Hspa1a
*
*
ns
Abundance, normalized and grouped
Plekhs1WT/WT
Plekhs1Avi/Avi
PTEN +/+
PTEN -/-
J.
Heat shock 70 kDa protein 1B
Hspa1b
*
*
ns
Abundance, normalized and grouped
Plekhs1WT/WT
Plekhs1Avi/Avi
PTEN +/+
PTEN -/-
K.
Heat shock-related 70 kDa protein 2
Hspa2
**
*
ns
Abundance, normalized and grouped
Plekhs1WT/WT
Plekhs1Avi/Avi
PTEN +/+
PTEN -/-
L.
Heat shock cognate 71 kDa protein
Hspa8
p=0.2286
**
*
Abundance, normalized and grouped
Plekhs1WT/WT
Plekhs1Avi/Avi
PTEN +/+
PTEN -/-

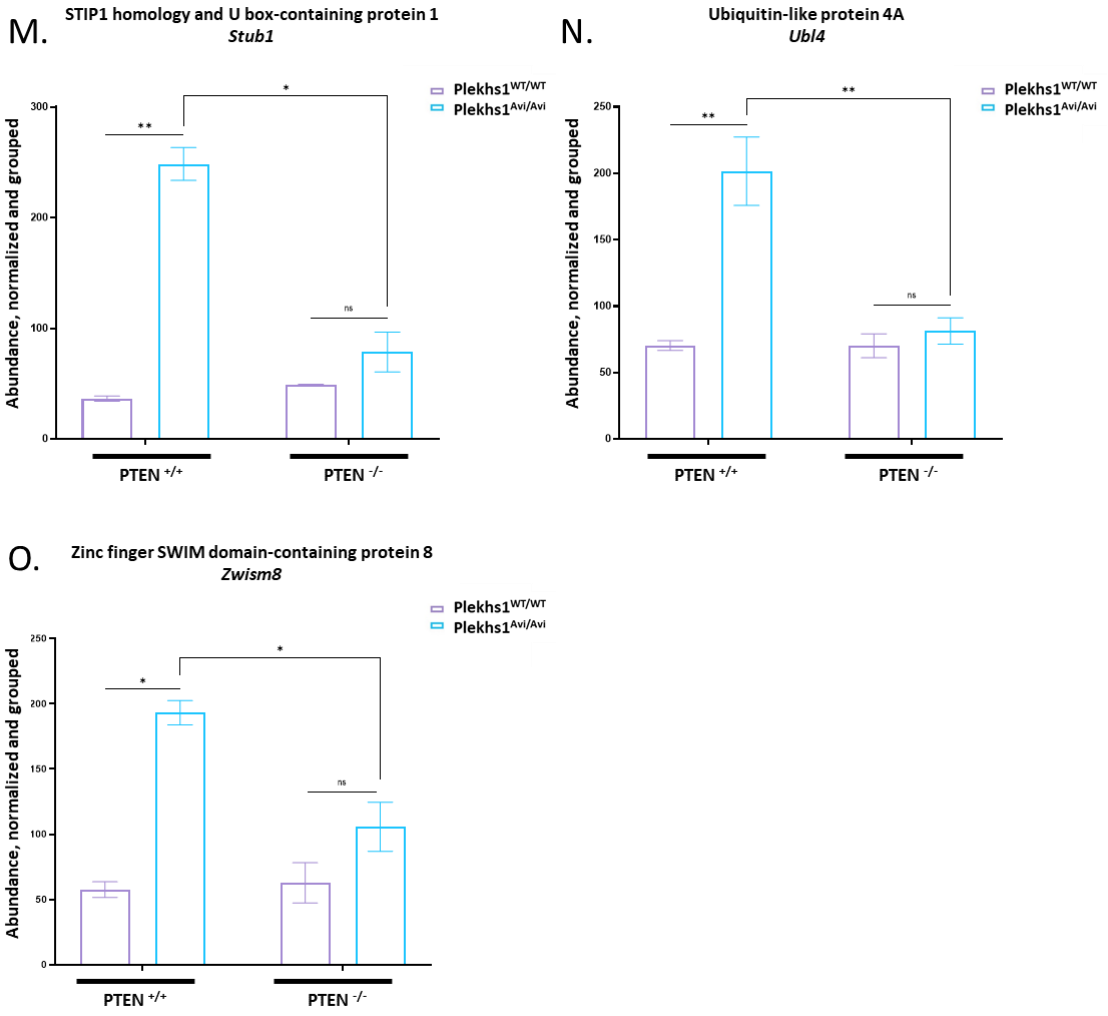


**Figure 5.5 The relative abundance of chaperone proteins in Avi-pulldowns from mouse prostate**

*Refer to the legend of Figure 5.4 for an explanation of this figure.*

*Some proteins are presented in more than one of the classes of protein types presented in the following figures.*

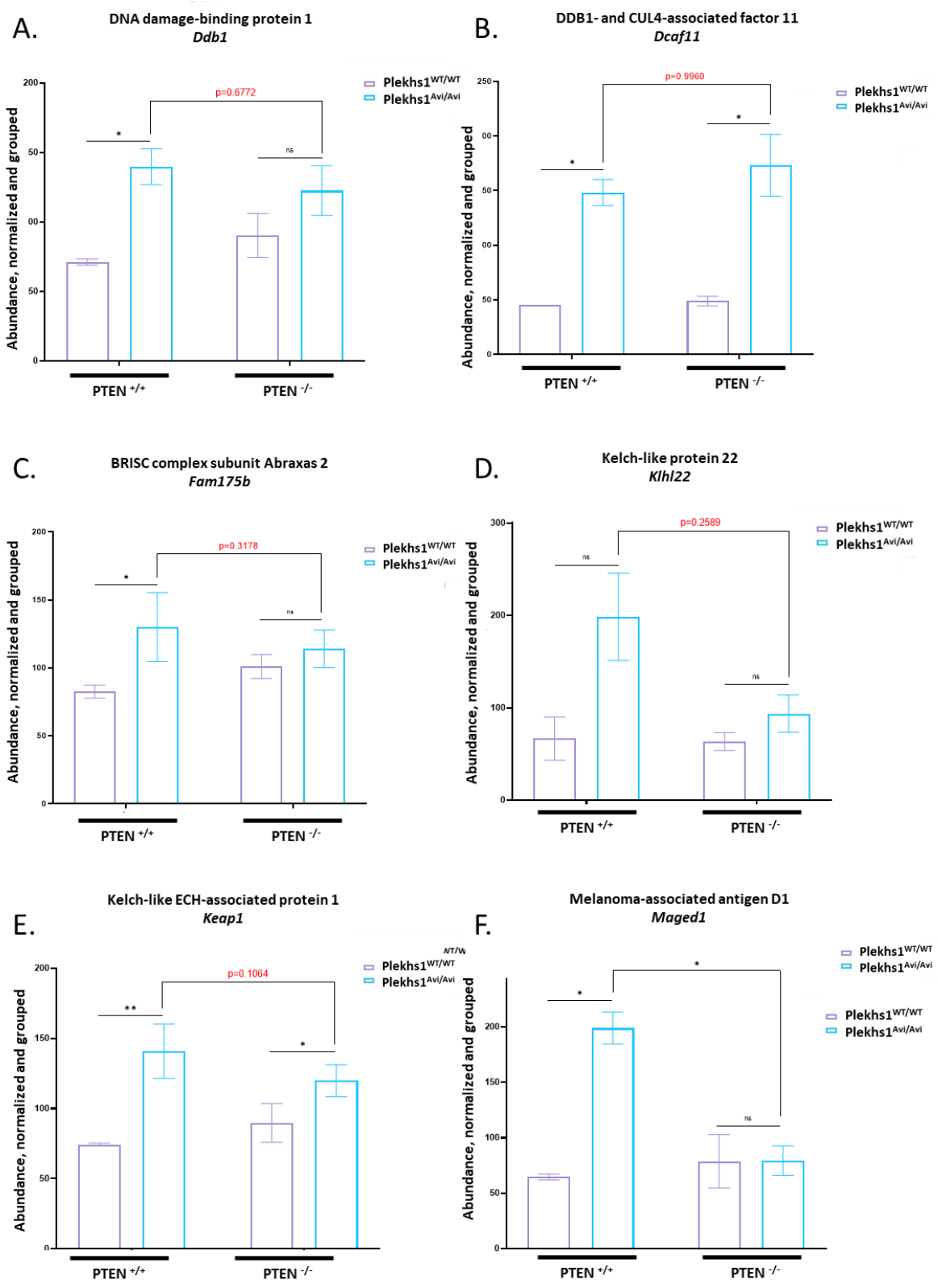
A.
DNA damage-binding protein 1
Ddb1
B.
DDB1- and CUL4-associated factor 11
Dcaf11
C.
BRISC complex subunit Abraxas 2
Fam175b
D.
Kelch-like protein 22
Klhl22
E.
Kelch-like ECH-associated protein 1
Keap1
F.
Melanoma-associated antigen D1
Maged1
Abundance, normalized and grouped
Plekhs1WT/WT
Plekhs1Avi/Avi
PTEN +/+
PTEN -/-
p=0.6772
p=0.9960
p=0.3178
p=0.2589
p=0.1064
ns

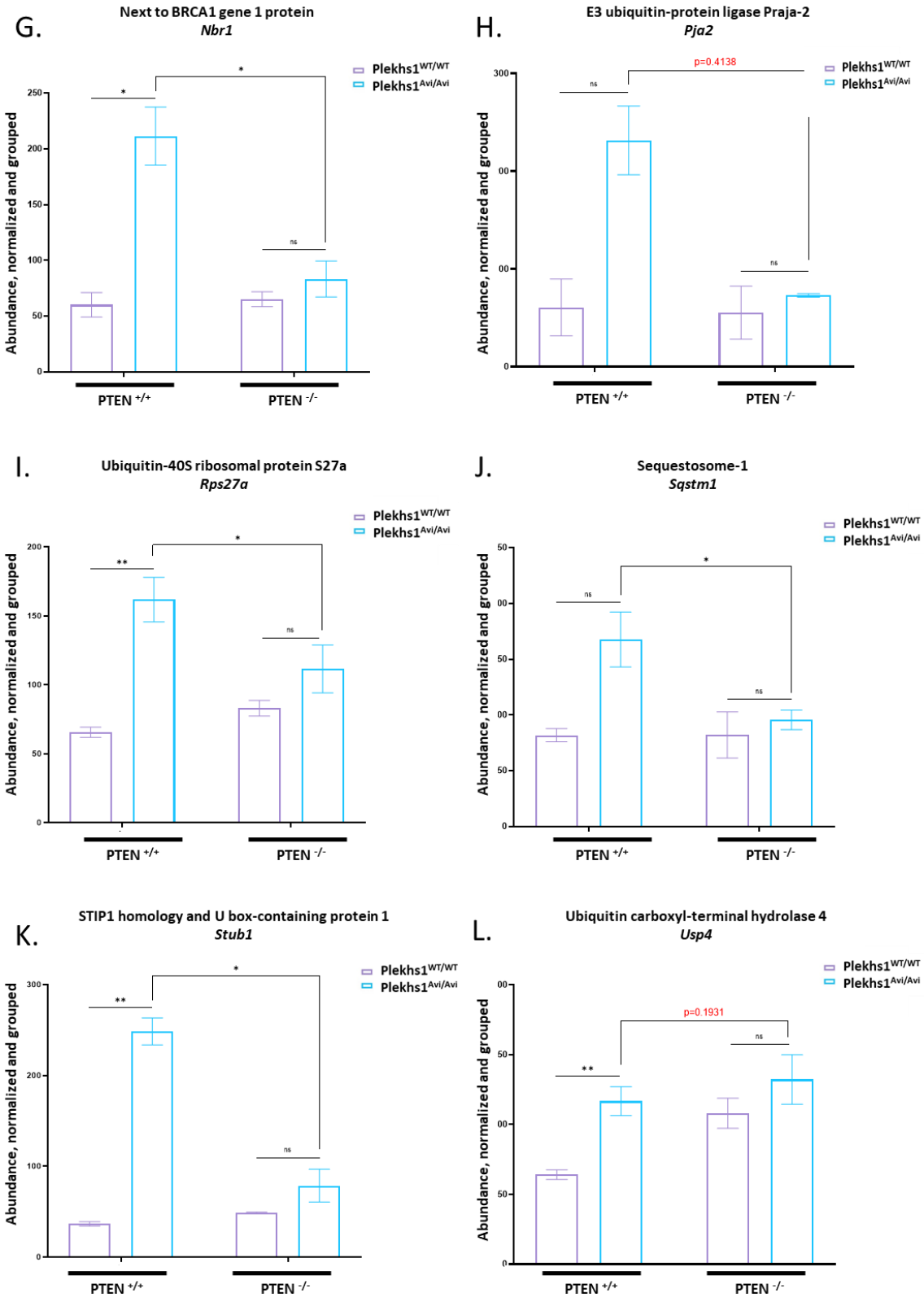
G.
Next to BRCA1 gene 1 protein
Nbr1
H.
E3 ubiquitin-protein ligase Praja-2
Pja2
p=0.4138
I.
Ubiquitin-40S ribosomal protein S27a
Rps27a
J.
Sequestosome-1
Sqstm1
K.
STIP1 homology and U box-containing protein 1
Stub1
L.
Ubiquitin carboxyl-terminal hydrolase 4
Usp4
p=0.1931
Plekhs1WT/WT
Plekhs1Avi/Avi
Abundance, normalized and grouped
PTEN +/+
PTEN -/-
ns

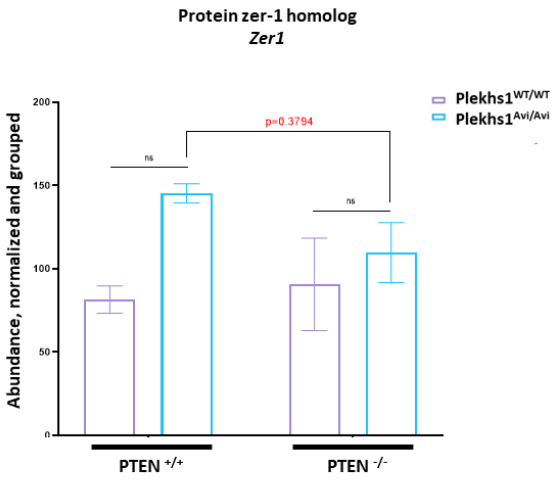


**Figure 5.6 The relative abundance of proteins associated with ubiquitination processes in Avi-pulldowns from mouse prostate**

*Refer to the legend of Figure 5.4 for an explanation of this figure.*

*Some proteins are presented in more than one of the classes of protein types presented in the following figures.*

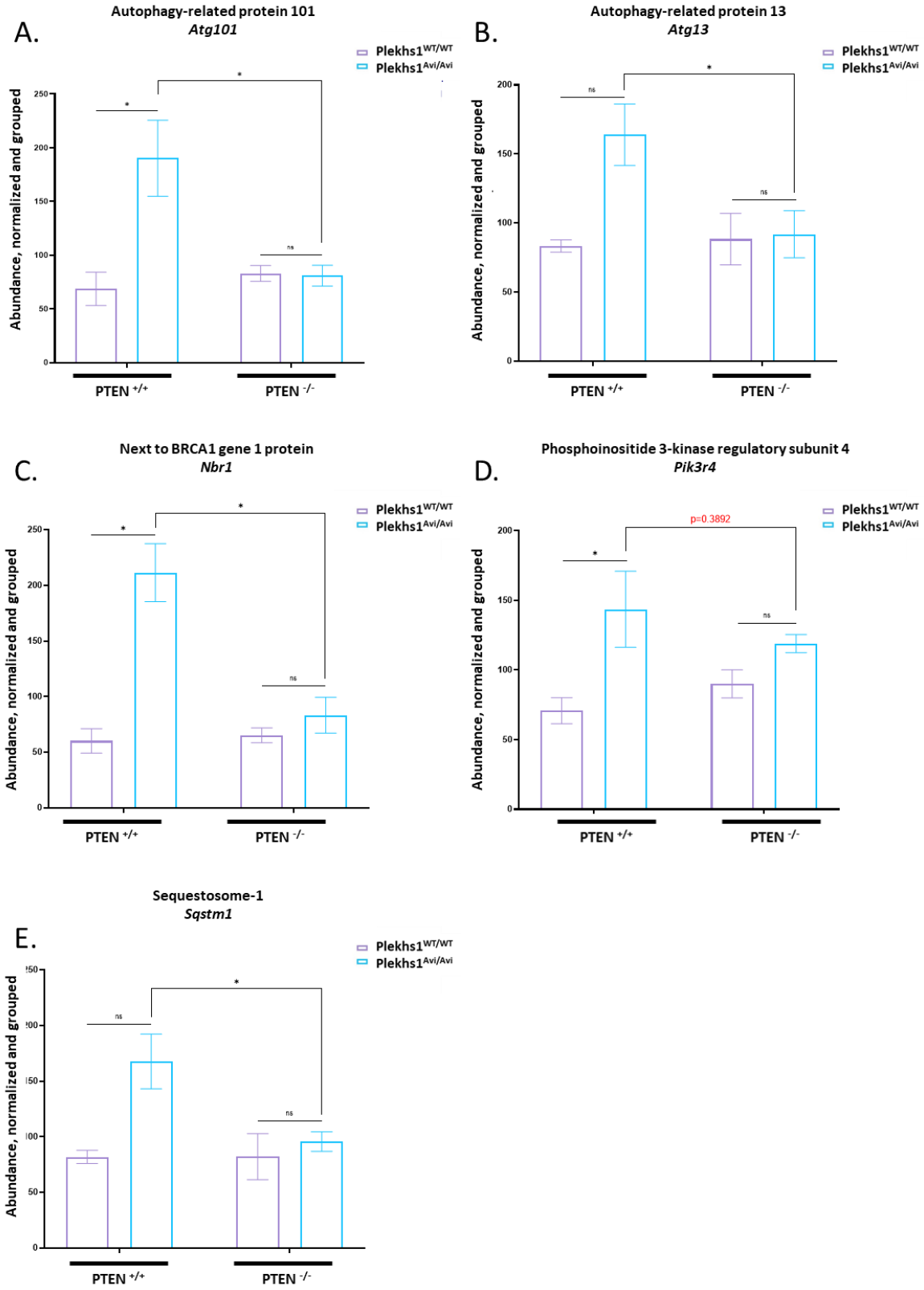
A.
Autophagy-related protein 101
Atg101
Plekhs1WT/WT
Plekhs1Avi/Avi
Abundance, normalized and grouped
PTEN +/+
PTEN -/-
B.
Autophagy-related protein 13
Atg13
C.
Next to BRCA1 gene 1 protein
Nbr1
D.
Phosphoinositide 3-kinase regulatory subunit 4
Pik3r4
p=0.3892
E.
Sequestosome-1
Sqstm1

**Figure 5.7 The relative abundance of proteins associated with autophagy in Avi-pulldowns from mouse prostate**

*Refer to the legend of Figure 5.4 for an explanation of this figure.*
*Some proteins are presented in more than one of the classes of protein types presented in the following figures.*

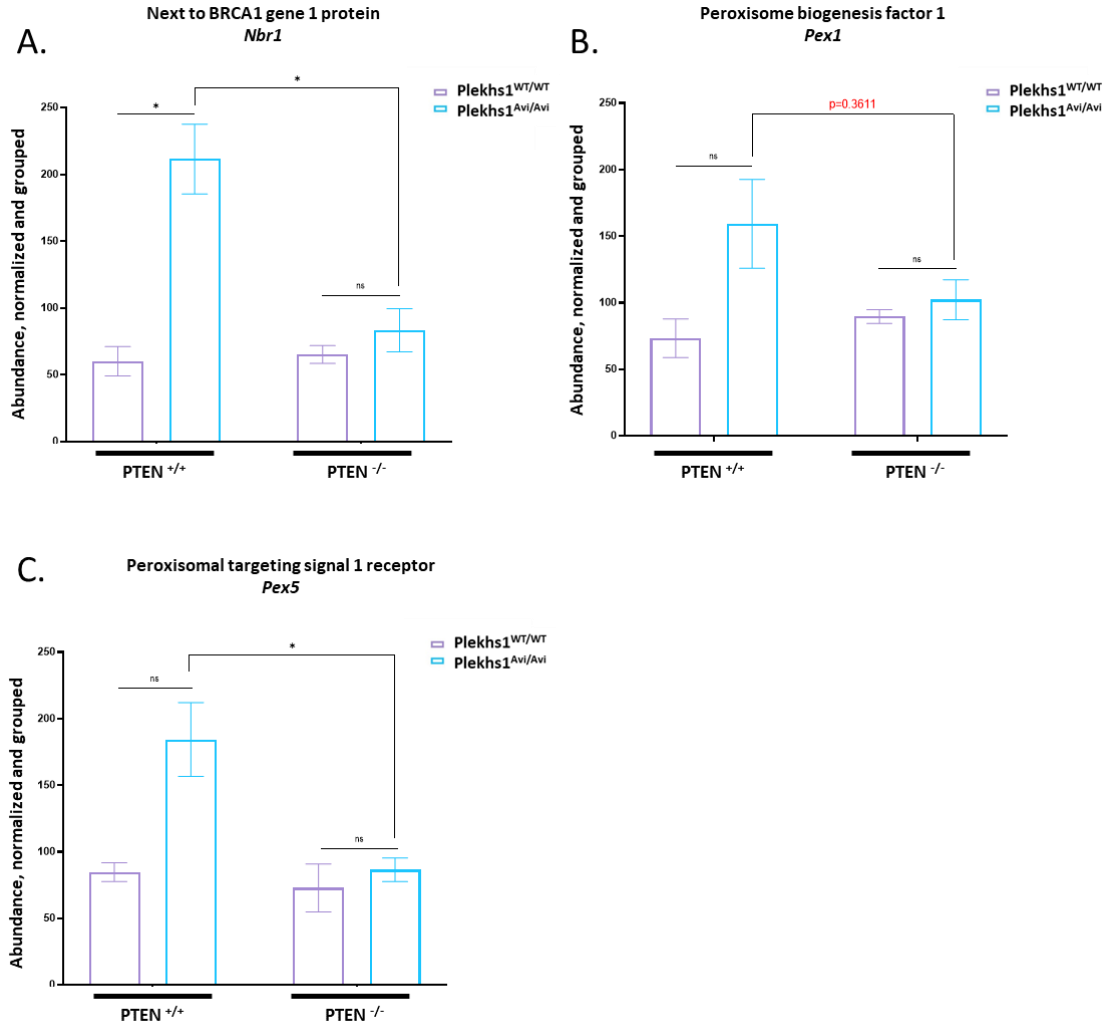


**Figure 5.8 The relative abundance of proteins associated peroxisomes in Avi-pulldowns from mouse prostate**

*Refer to the legend of Figure 5.4 for an explanation of this figure.*

*Some proteins are presented in more than one of the classes of protein types presented in the following figures.*

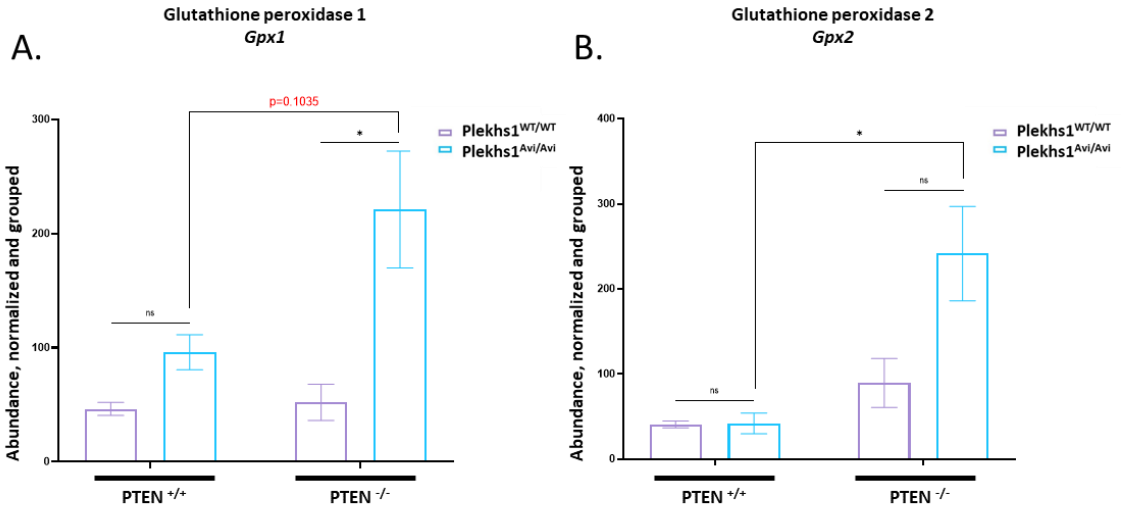


**Figure 5.9 The relative abundance of glutathione peroxidases**

*Refer to the legend of Figure 5.4 for an explanation of this figure.*

*Some proteins are presented in more than one of the classes of protein types presented in the following figures.*

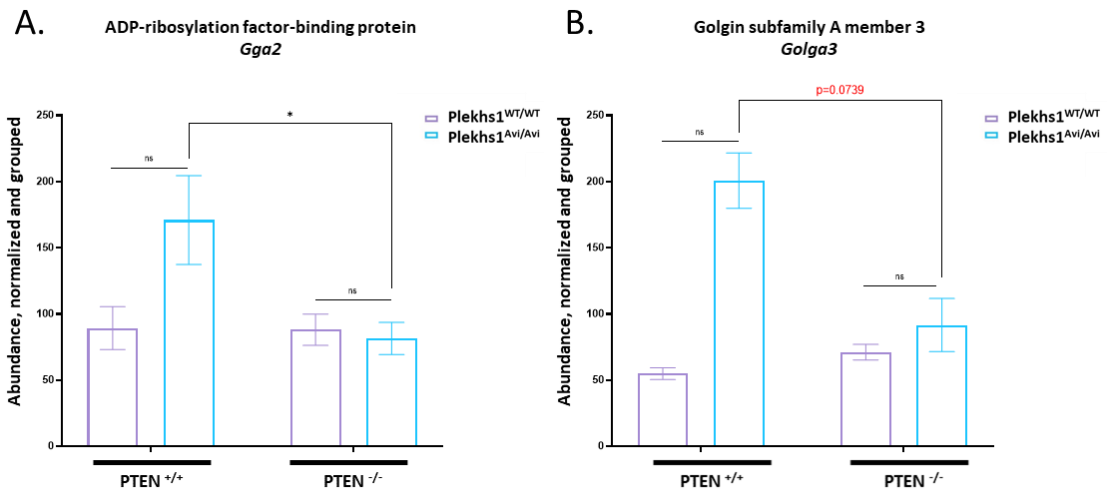


**Figure 5.10 The relative abundance of proteins associated with the Golgi in Avi-pulldowns from mouse prostate**

*Refer to the legend of Figure 5.4 for an explanation of this figure.*

*Some proteins are presented in more than one of the classes of protein types presented in the following figures.*

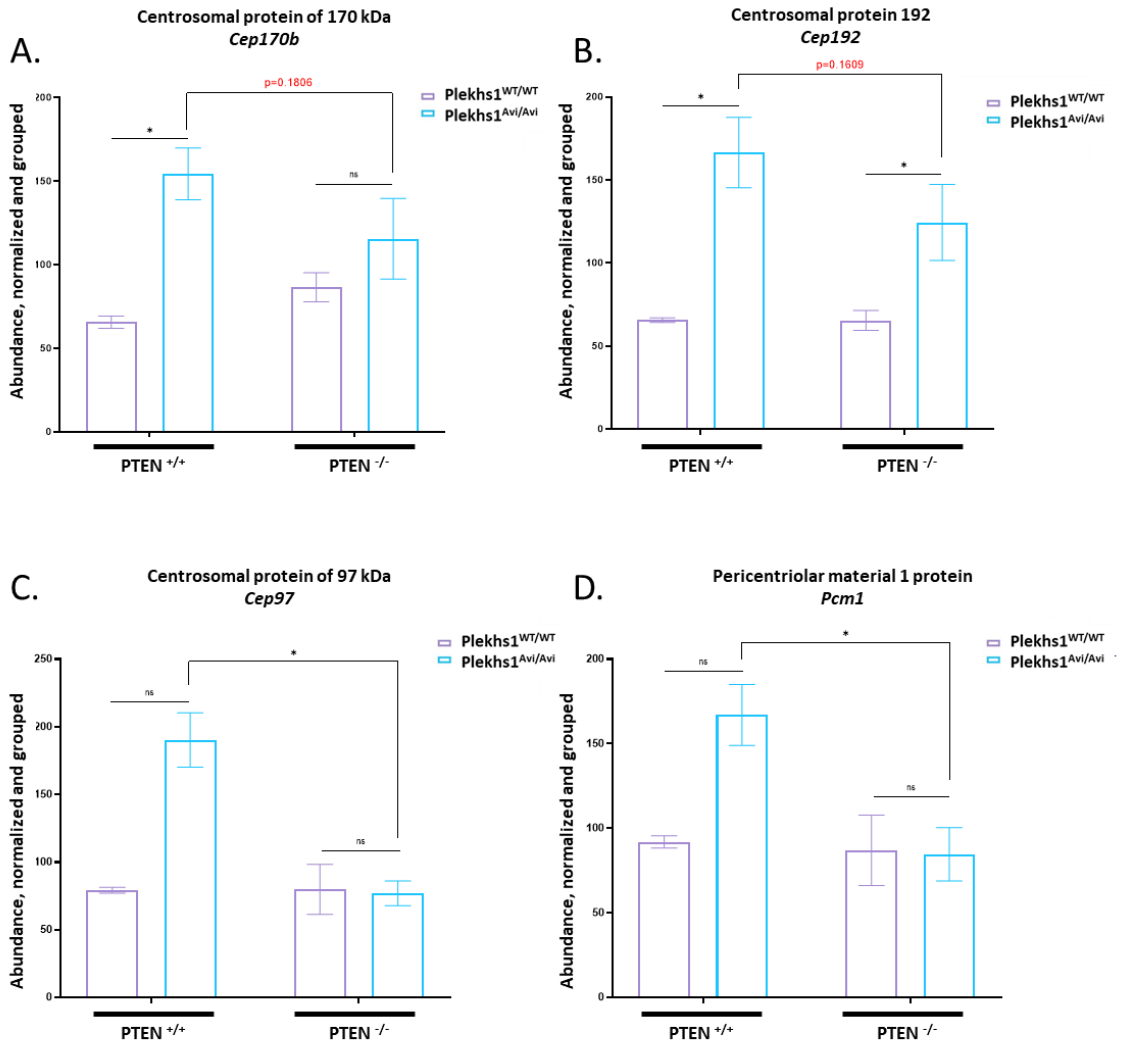


**Figure 5.11 The relative abundance of proteins associated with centrosomes in Avi-pulldowns from mouse prostate**

*Refer to the legend of Figure 5.4 for an explanation of this figure.*

*Some proteins are presented in more than one of the classes of protein types presented in the following figures.*

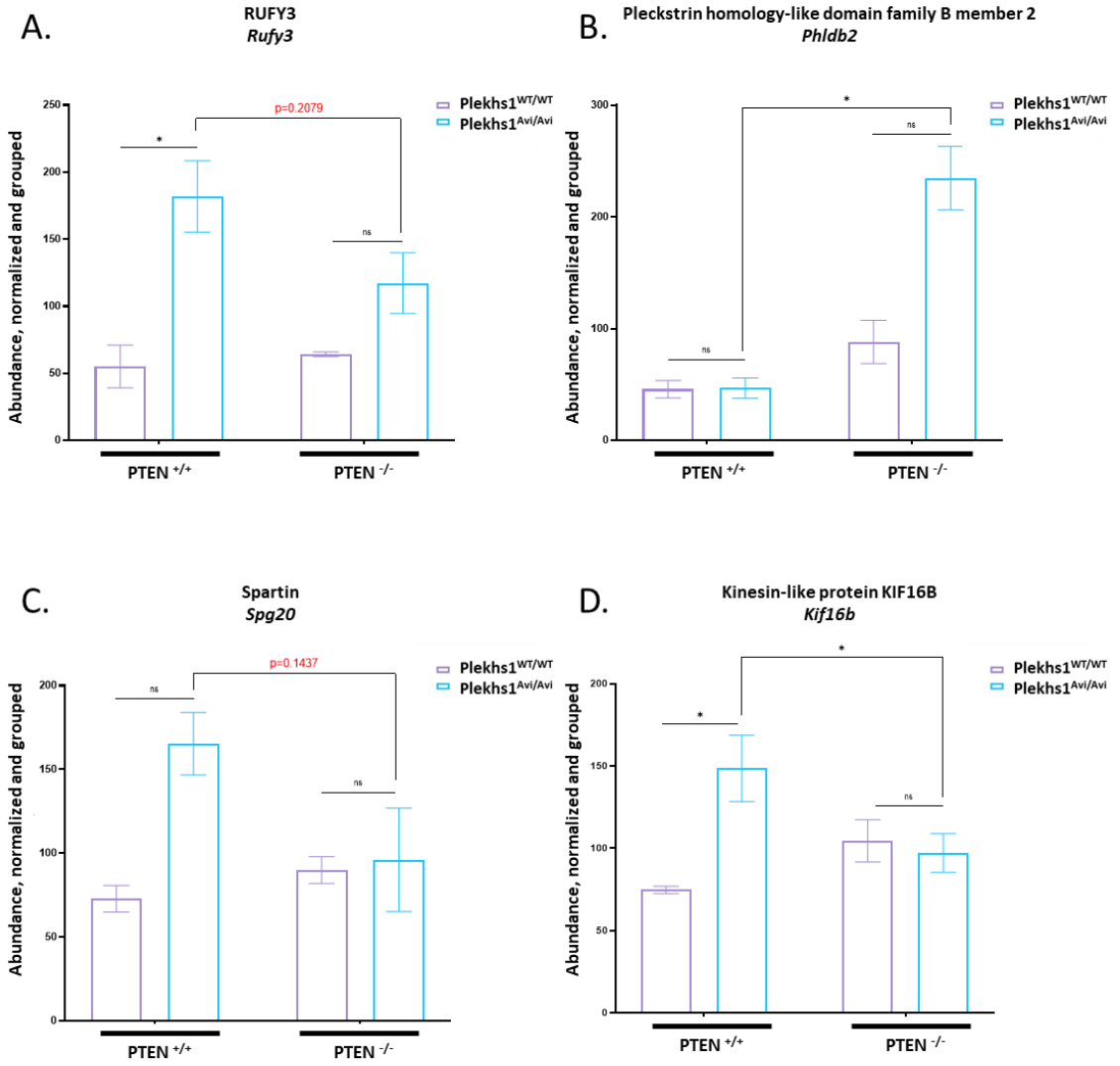


**Figure 5.12 The relative abundance of proteins associated with cytoskeleton in Avi-pulldowns from mouse prostate**

*Refer to the legend of Figure 5.4 for an explanation of this figure.*

*Some proteins are presented in more than one of the classes of protein types presented in the following figures.*

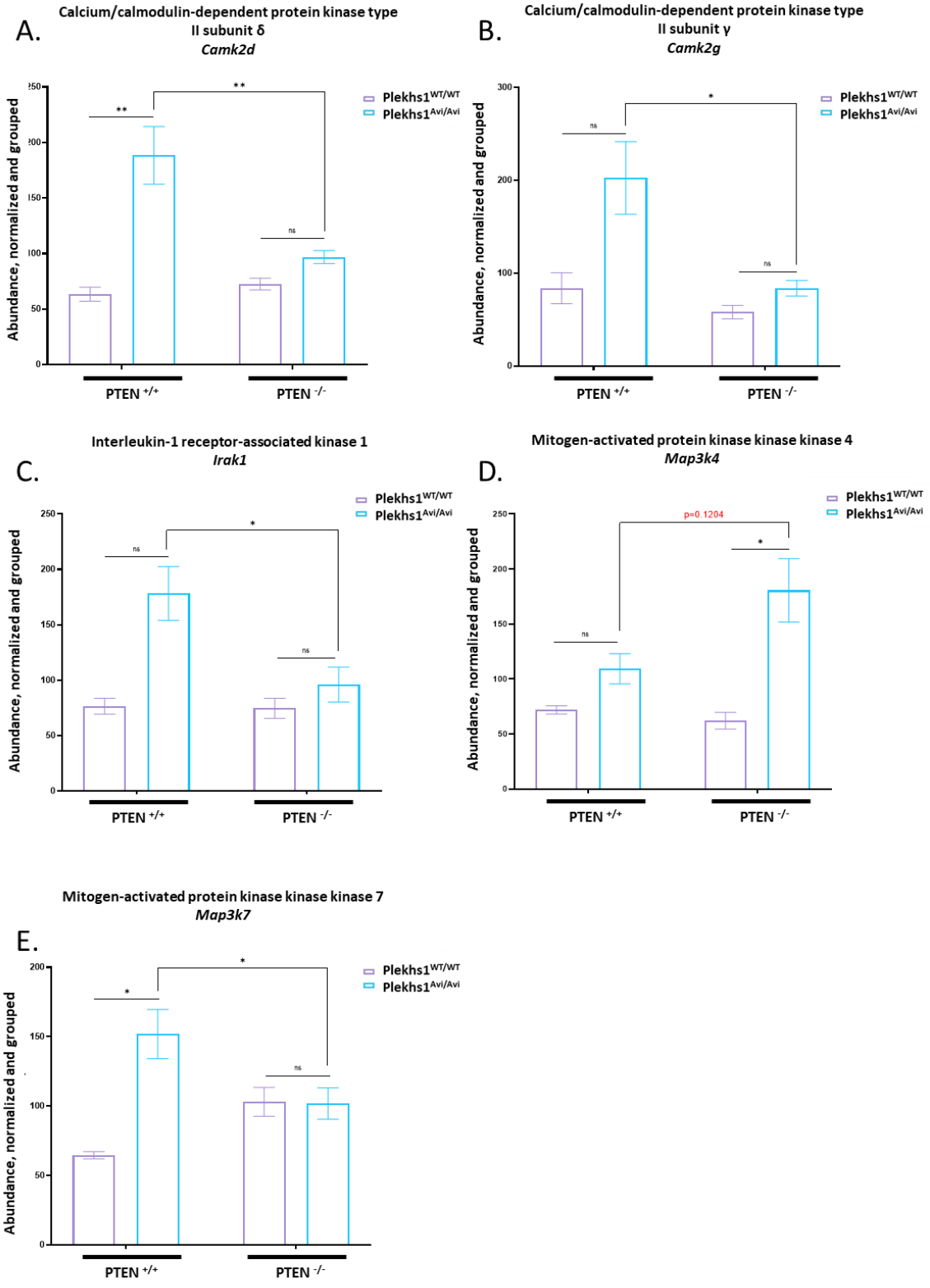
A.
Calcium/calmodulin-dependent protein kinase type II subunit δ
Camk2d
B.
Calcium/calmodulin-dependent protein kinase type II subunit γ
Camk2g
C.
Interleukin-1 receptor-associated kinase 1
Irak1
D.
Mitogen-activated protein kinase kinase kinase 4
Map3k4
E.
Mitogen-activated protein kinase kinase kinase 7
Map3k7
Abundance, normalized and grouped
Plekhs1WT/WT
Plekhs1Avi/Avi
PTEN +/+
PTEN -/-
ns
p=0.1204

**Figure 5.13 The relative abundance of protein kinases in Avi-pulldowns from mouse prostate**

*Refer to the legend of Figure 5.4 for an explanation of this figure.*
*Some proteins are presented in more than one of the classes of protein types presented in the following figures.*

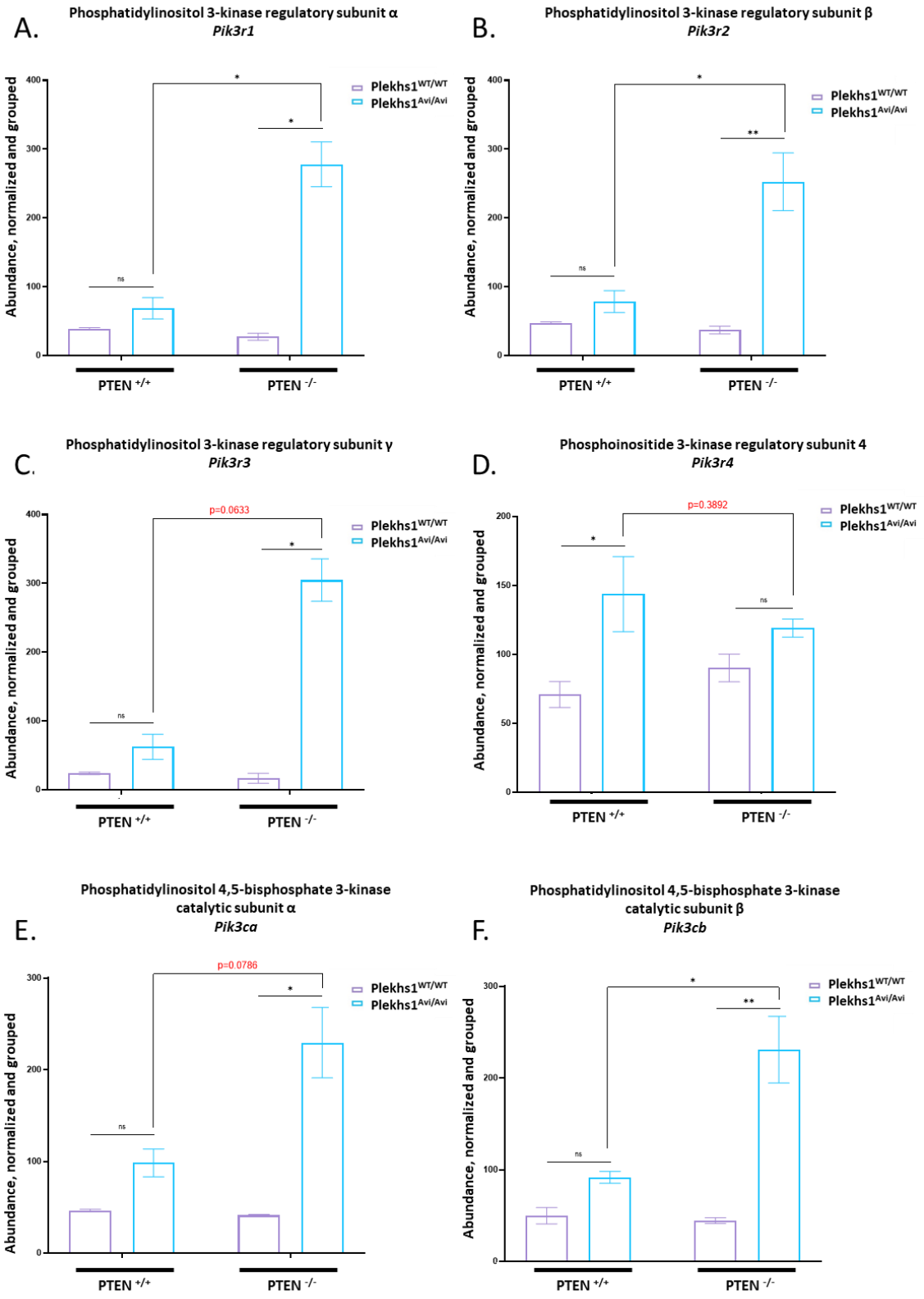
A.
Phosphatidylinositol 3-kinase regulatory subunit α
Pik3r1
B.
Phosphatidylinositol 3-kinase regulatory subunit β
Pik3r2
C.
Phosphatidylinositol 3-kinase regulatory subunit γ
Pik3r3
D.
Phosphoinositide 3-kinase regulatory subunit 4
Pik3r4
E.
Phosphatidylinositol 4,5-bisphosphate 3-kinase catalytic subunit α
Pik3ca
F.
Phosphatidylinositol 4,5-bisphosphate 3-kinase catalytic subunit β
Pik3cb
Abundance, normalized and grouped
Plekhs1WT/WT
Plekhs1Avi/Avi
PTEN +/+
PTEN -/-
ns
*
**
p=0.0633
p=0.3892
p=0.0786

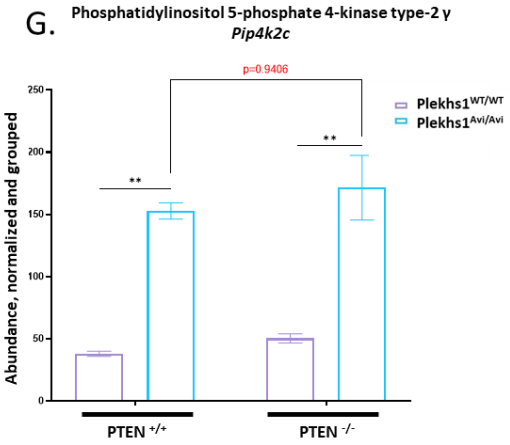


**Figure 5.14 The relative abundance of lipid kinases in Avi-pulldowns from mouse prostate**

*Refer to the legend of Figure 5.4 for an explanation of this figure.*

*Some proteins are presented in more than one of the classes of protein types presented in the following figures.*

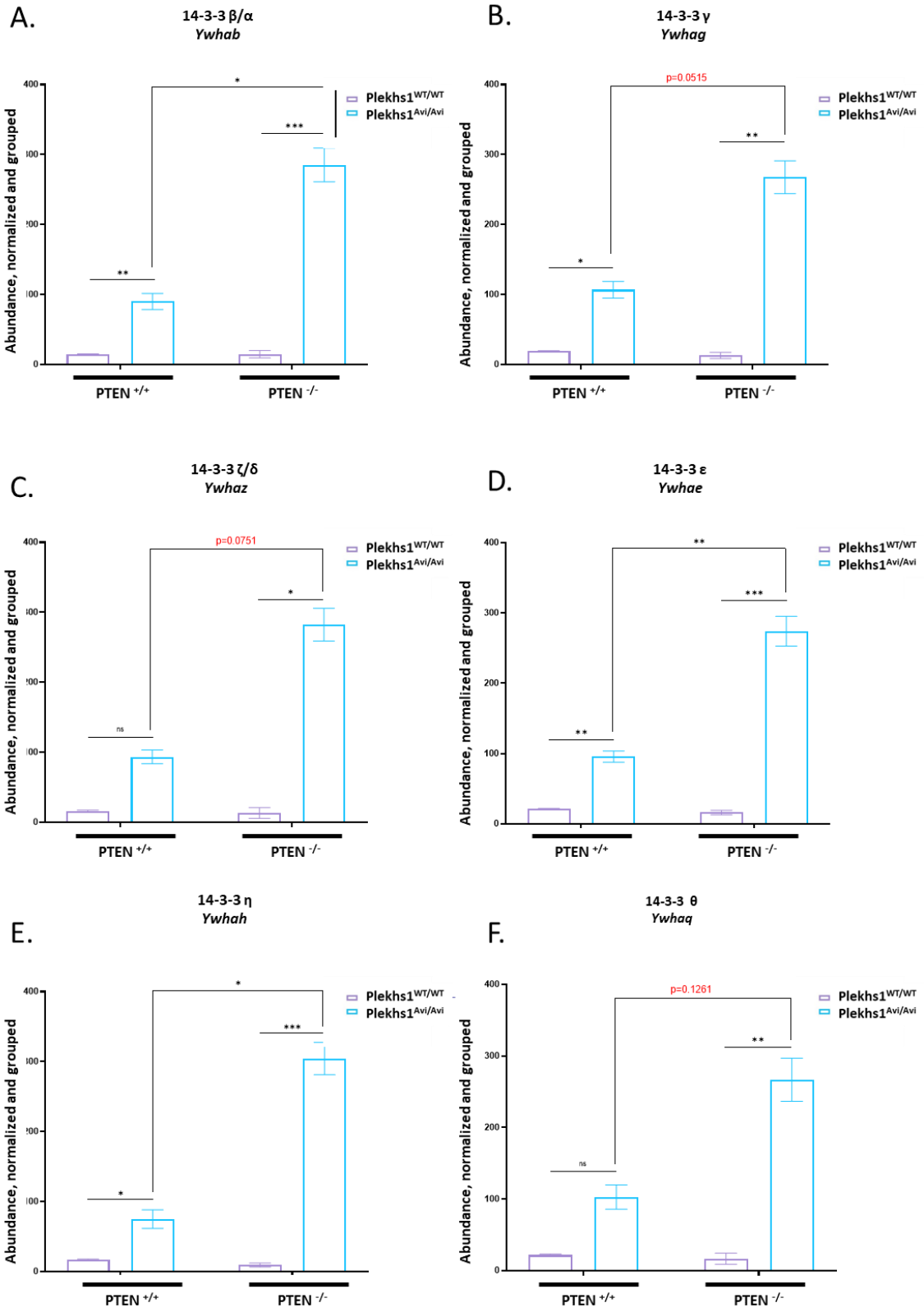
A.
14-3-3 β/α
Ywhab
B.
14-3-3 γ
Ywhag
p=0.0515
C.
14-3-3 ζ/δ
Ywhaz
p=0.0751
D.
14-3-3 ε
Ywhae
E.
14-3-3 η
Ywhah
F.
14-3-3 θ
Ywhaq
p=0.1261
Abundance, normalized and grouped
Plekhs1WT/WT
Plekhs1Avi/Avi
PTEN +/+
PTEN -/-
ns

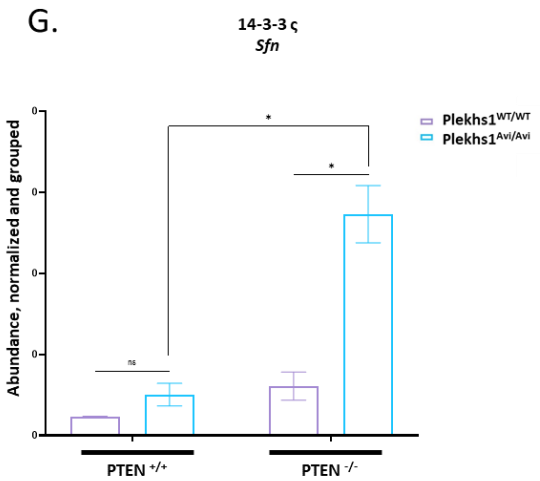


**Figure 5.15 The relative abundance of 14-3-3 proteins in Avi-pulldowns from mouse prostate**

*Refer to the legend of Figure 5.4 for an explanation of this figure.*
*Some proteins are presented in more than one of the classes of protein types presented in the following figures.*

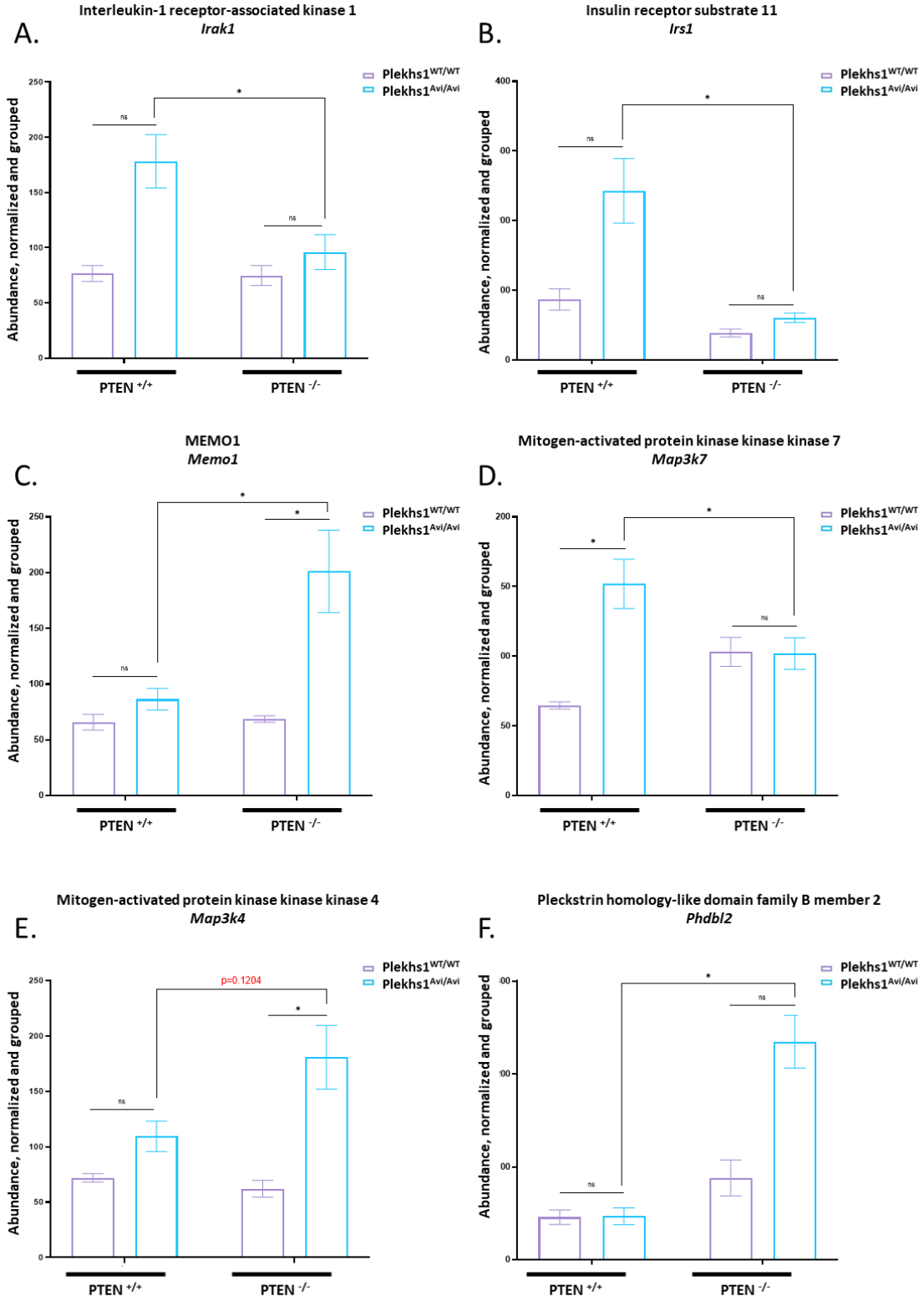
A.
Interleukin-1 receptor-associated kinase 1
Irak1
B.
Insulin receptor substrate 11
Irs1
C.
MEMO1
Memo1
D.
Mitogen-activated protein kinase kinase kinase 7
Map3k7
E.
Mitogen-activated protein kinase kinase kinase 4
Map3k4
p=0.1204
F.
Pleckstrin homology-like domain family B member 2
Phdbl2
Abundance, normalized and grouped
Plekhs1WT/WT
Plekhs1Avi/Avi
PTEN +/+
PTEN -/-
ns
*

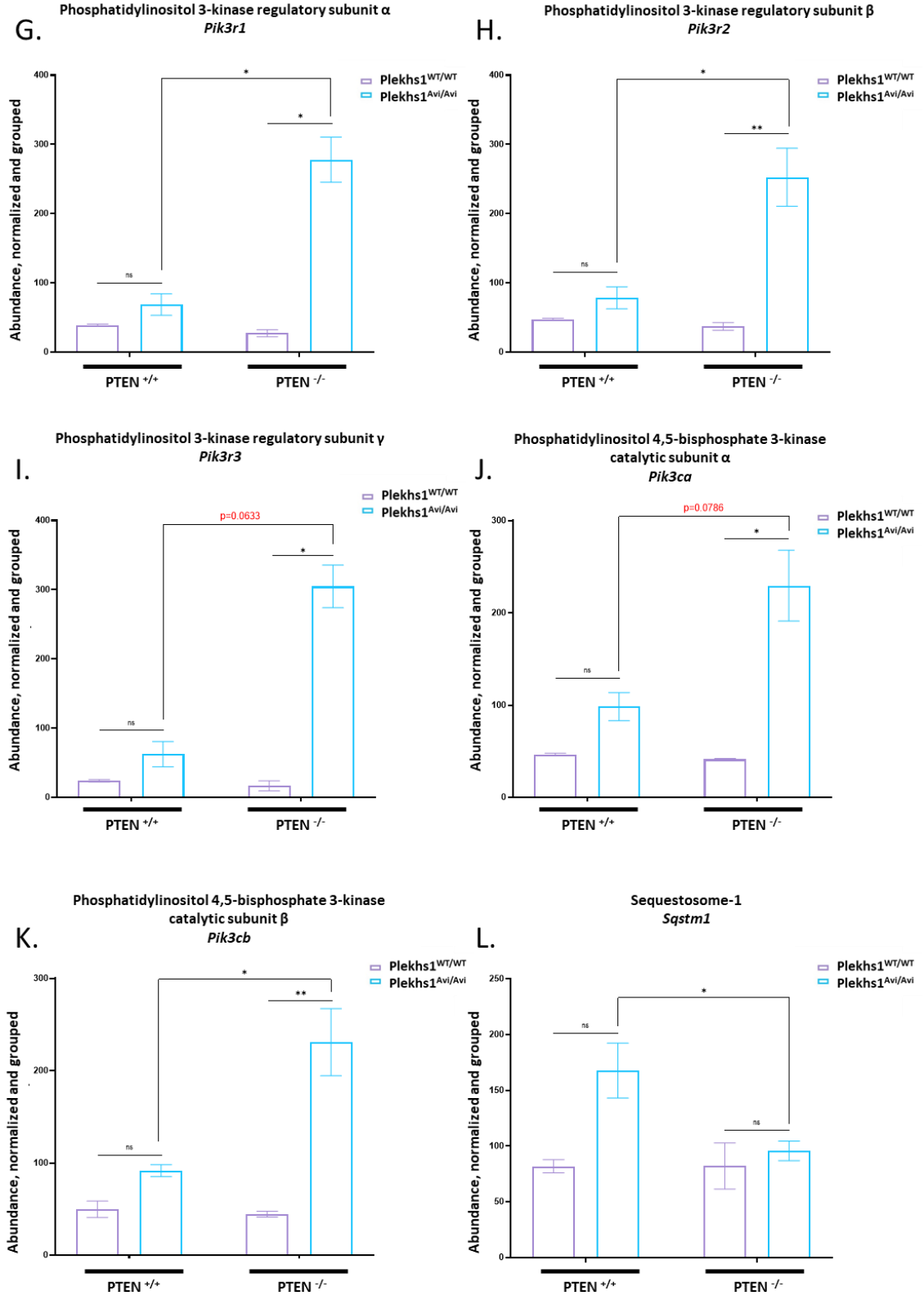
G.
Phosphatidylinositol 3-kinase regulatory subunit α
Pik3r1
H.
Phosphatidylinositol 3-kinase regulatory subunit β
Pik3r2
I.
Phosphatidylinositol 3-kinase regulatory subunit γ
Pik3r3
p=0.0633
J.
Phosphatidylinositol 4,5-bisphosphate 3-kinase catalytic subunit α
Pik3ca
p=0.0786
K.
Phosphatidylinositol 4,5-bisphosphate 3-kinase catalytic subunit β
Pik3cb
L.
Sequestosome-1
Sqstm1
Abundance, normalized and grouped
Plekhs1WT/WT
Plekhs1Avi/Avi
PTEN +/+
PTEN -/-
ns

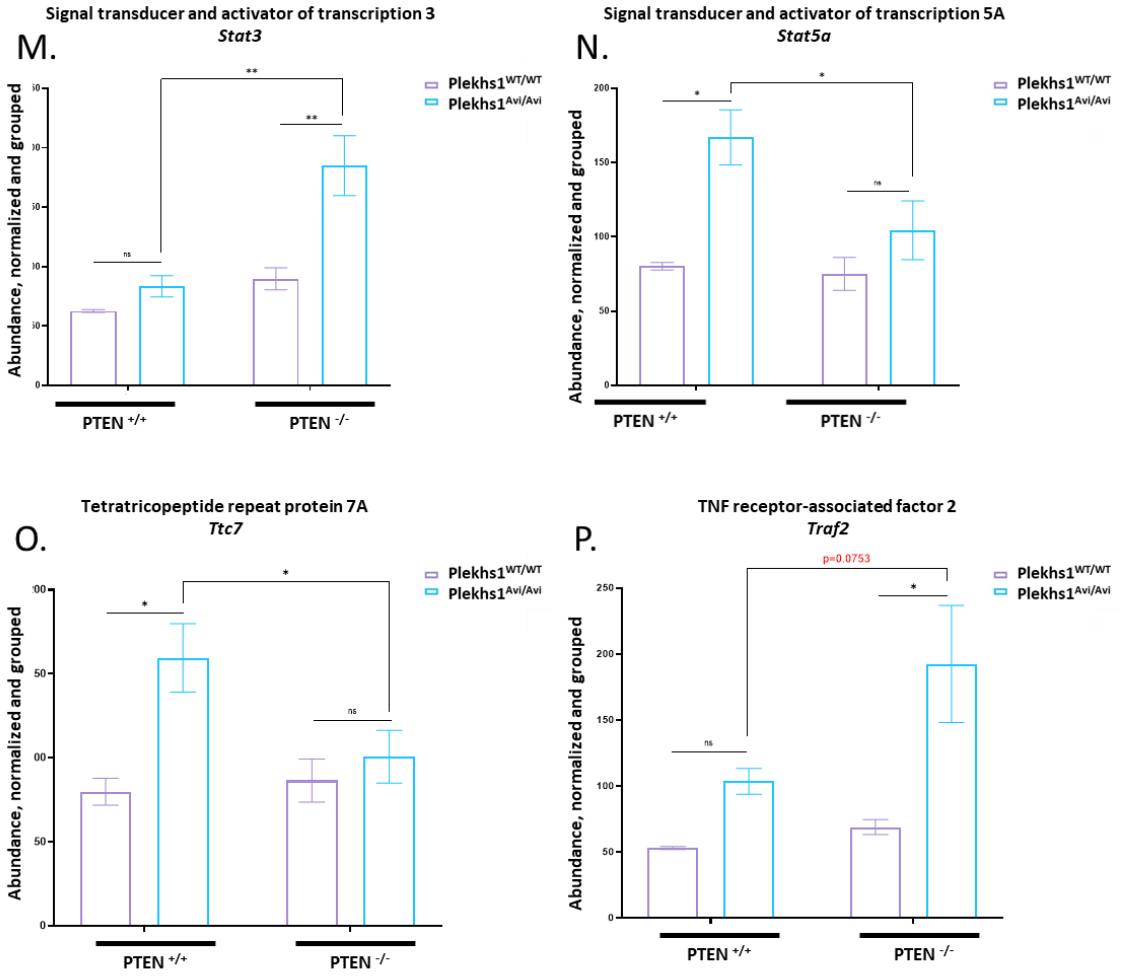


**Figure 5.16 The relative abundance of proteins associated with near-receptor cell signalling in Avi-pulldowns from mouse prostate**

*Refer to the legend of Figure 5.4 for an explanation of this figure.*

*Some proteins are presented in more than one of the classes of protein types presented in the following figures.*

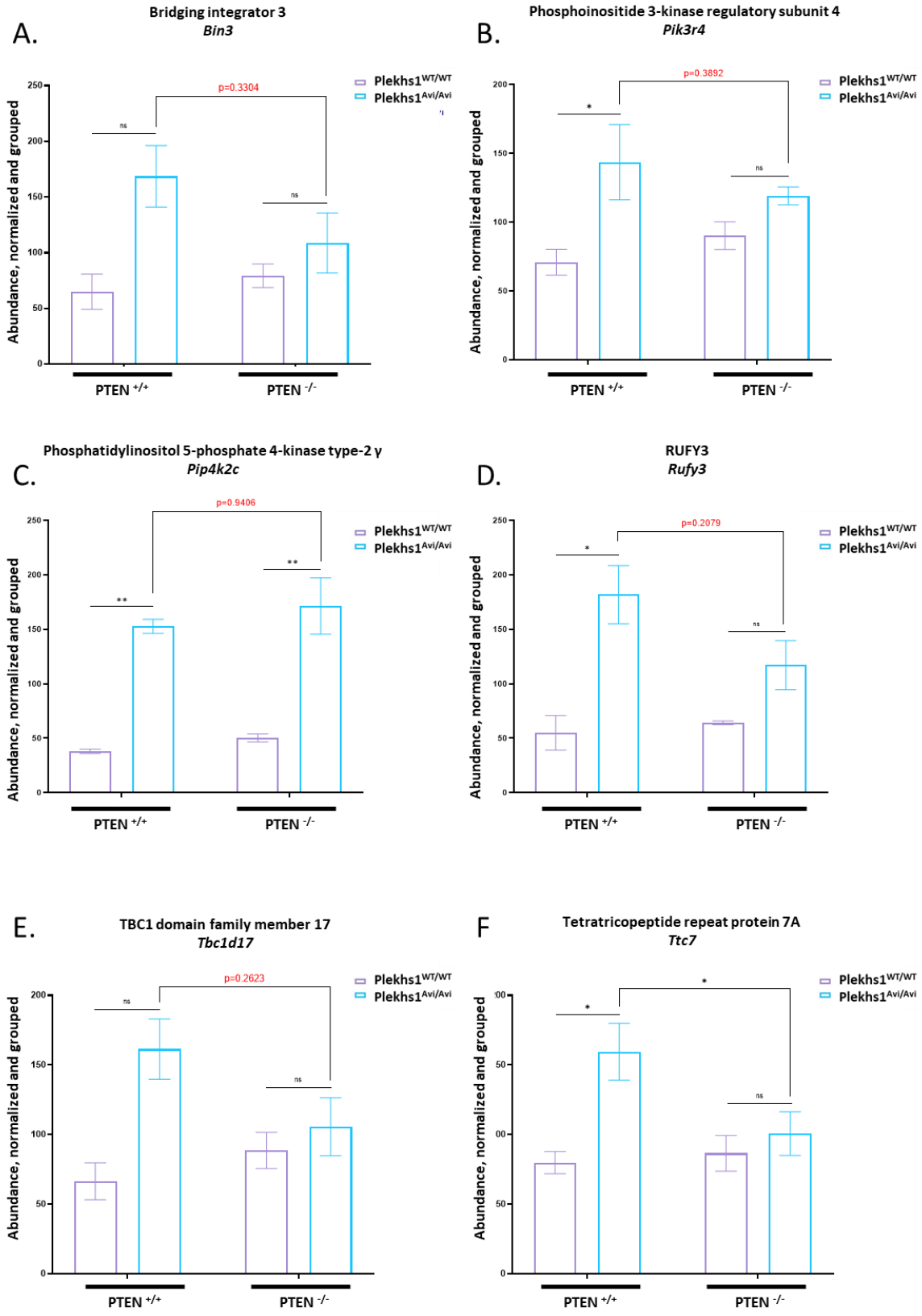
A.
Bridging integrator 3
Bin3
B.
Phosphoinositide 3-kinase regulatory subunit 4
Pik3r4
C.
Phosphatidylinositol 5-phosphate 4-kinase type-2 γ
Pip4k2c
D.
RUFY3
Rufy3
E.
TBC1 domain family member 17
Tbc1d17
F
Tetratricopeptide repeat protein 7A
Ttc7
Abundance, normalized and grouped
Plekhs1WT/WT
Plekhs1Avi/Avi
PTEN +/+
PTEN -/-
p=0.3304
p=0.3892
p=0.9406
p=0.2079
p=0.2623
ns

**Figure 5.17 The relative abundance of proteins associated with general cell signalling in Avi-pulldowns from mouse prostate**

*Refer to the legend of Figure 5.4 for an explanation of this figure.*
*Some proteins are presented in more than one of the classes of protein types presented in the following figures.*

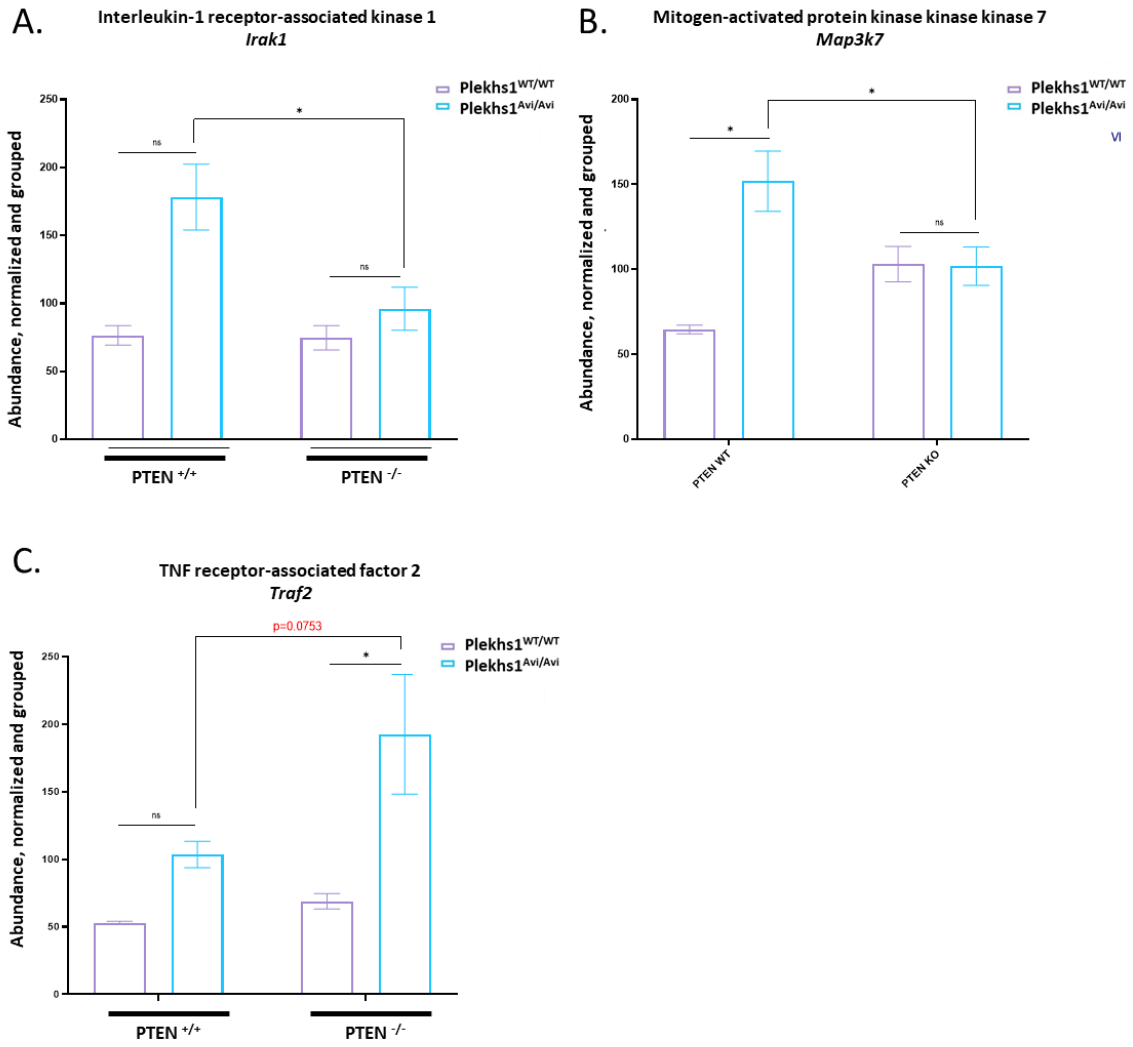


**Figure 5.18 The relative abundance of proteins associated with NF-κB signalling in Avi-pulldowns from mouse prostate**

*Refer to the legend of Figure 5.4 for an explanation of this figure.*

*Some proteins are presented in more than one of the classes of protein types presented in the following figures.*

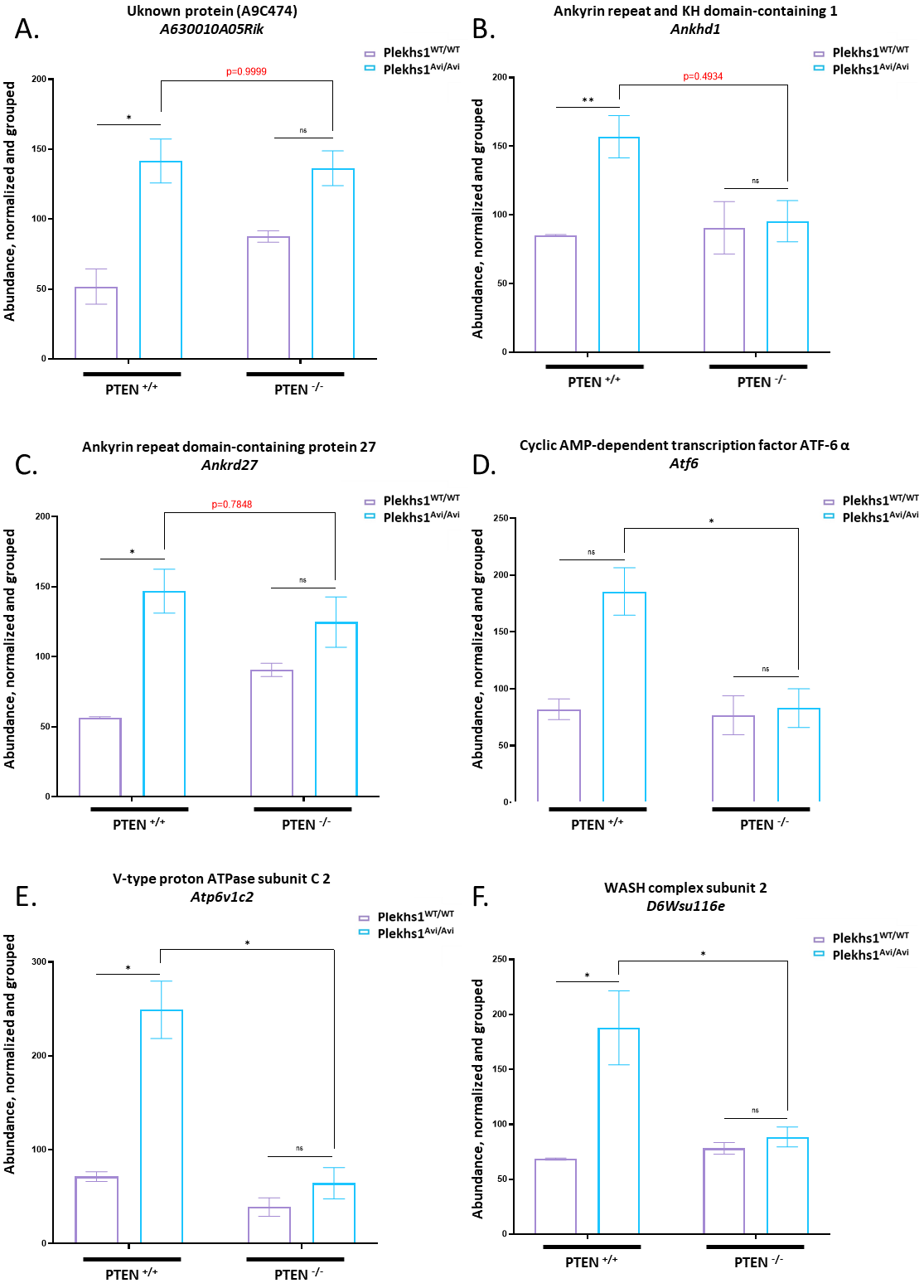
A.
Uknown protein (A9C474)
A630010A05Rik
B.
Ankyrin repeat and KH domain-containing 1
Ankhd1
C.
Ankyrin repeat domain-containing protein 27
Ankrd27
D.
Cyclic AMP-dependent transcription factor ATF-6 α
Atf6
E.
V-type proton ATPase subunit C 2
Atp6v1c2
F.
WASH complex subunit 2
D6Wsu116e
Plekhs1WT/WT
Plekhs1Avi/Avi
Abundance, normalized and grouped
p=0.9999
p=0.4934
p=0.7848
ns
PTEN +/+
PTEN -/-

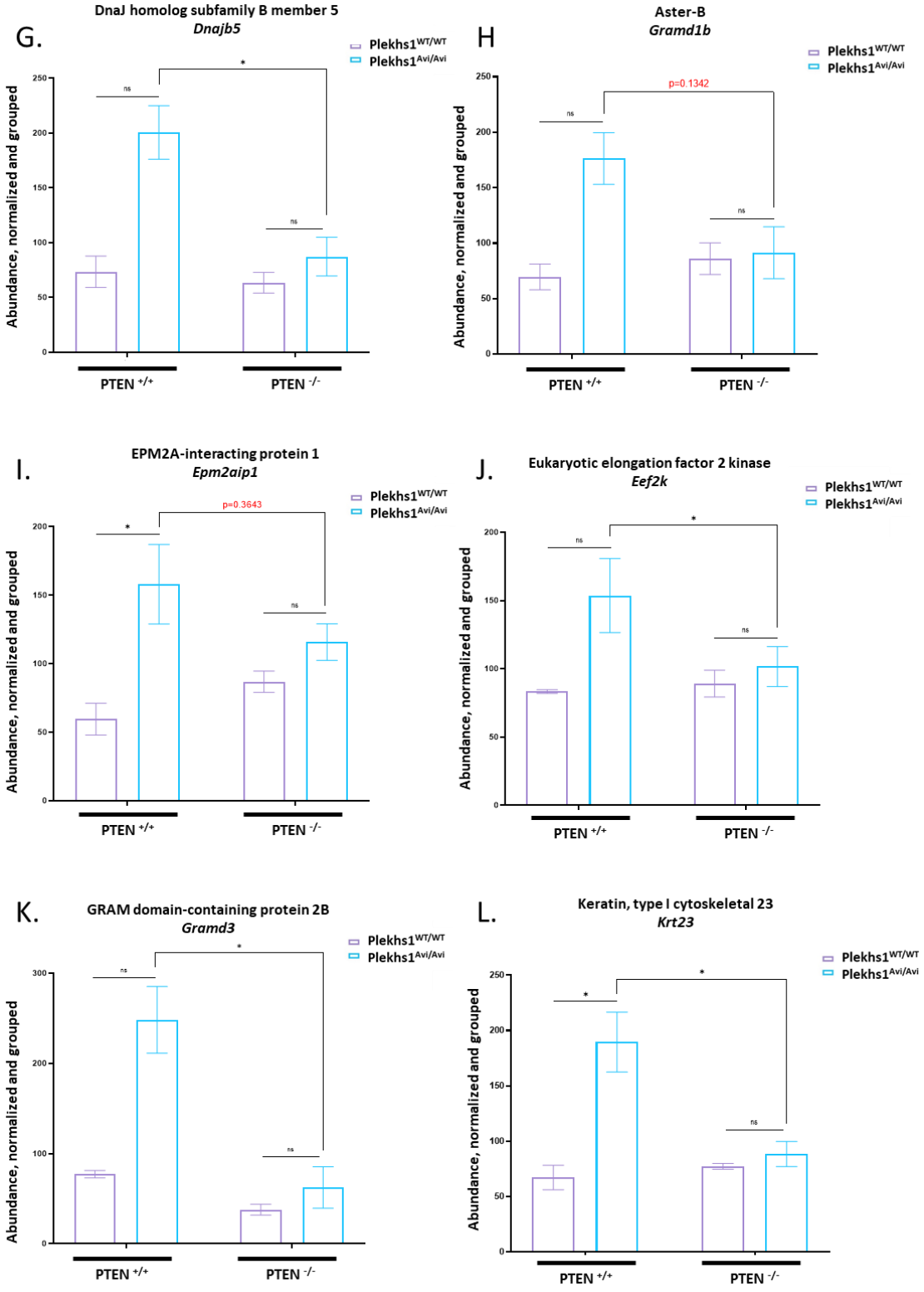
G.
DnaJ homolog subfamily B member 5
Dnajb5
Plekhs1WT/WT
Plekhs1Avi/Avi
Abundance, normalized and grouped
ns
*
ns
PTEN +/+
PTEN -/-
H
Aster-B
Gramd1b
p=0.1342
I.
EPM2A-interacting protein 1
Epm2aip1
p=0.3643
J.
Eukaryotic elongation factor 2 kinase
Eef2k
K.
GRAM domain-containing protein 2B
Gramd3
L.
Keratin, type I cytoskeletal 23
Krt23

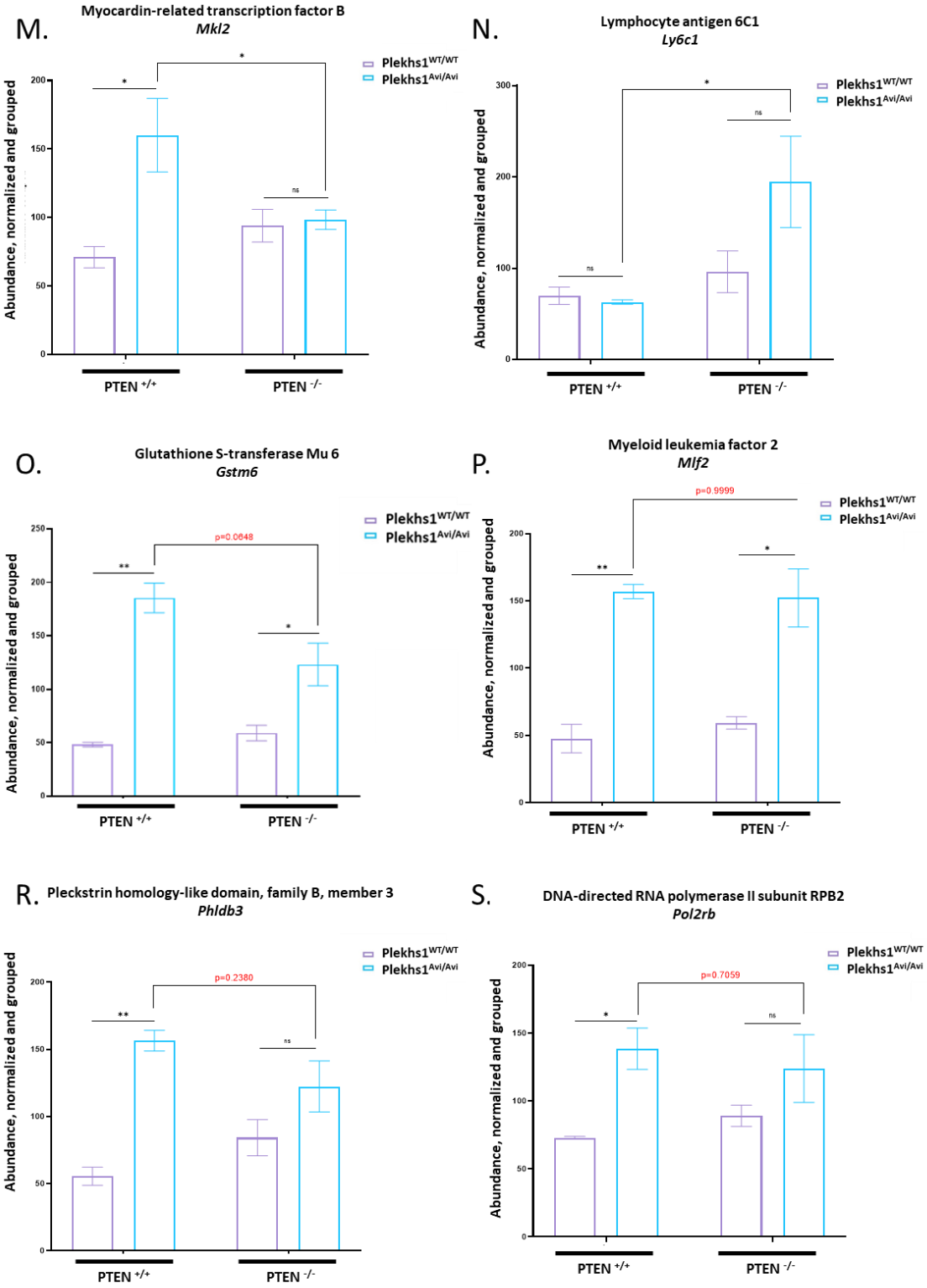
M.
Myocardin-related transcription factor B
Mkl2
Plekhs1WT/WT
Plekhs1Avi/Avi
Abundance, normalized and grouped
PTEN +/+
PTEN -/-
N.
Lymphocyte antigen 6C1
Ly6c1
O.
Glutathione S-transferase Mu 6
Gstm6
p=0.0648
P.
Myeloid leukemia factor 2
Mlf2
p=0.9999
R.
Pleckstrin homology-like domain, family B, member 3
Phldb3
p=0.2380
S.
DNA-directed RNA polymerase II subunit RPB2
Pol2rb
p=0.7059

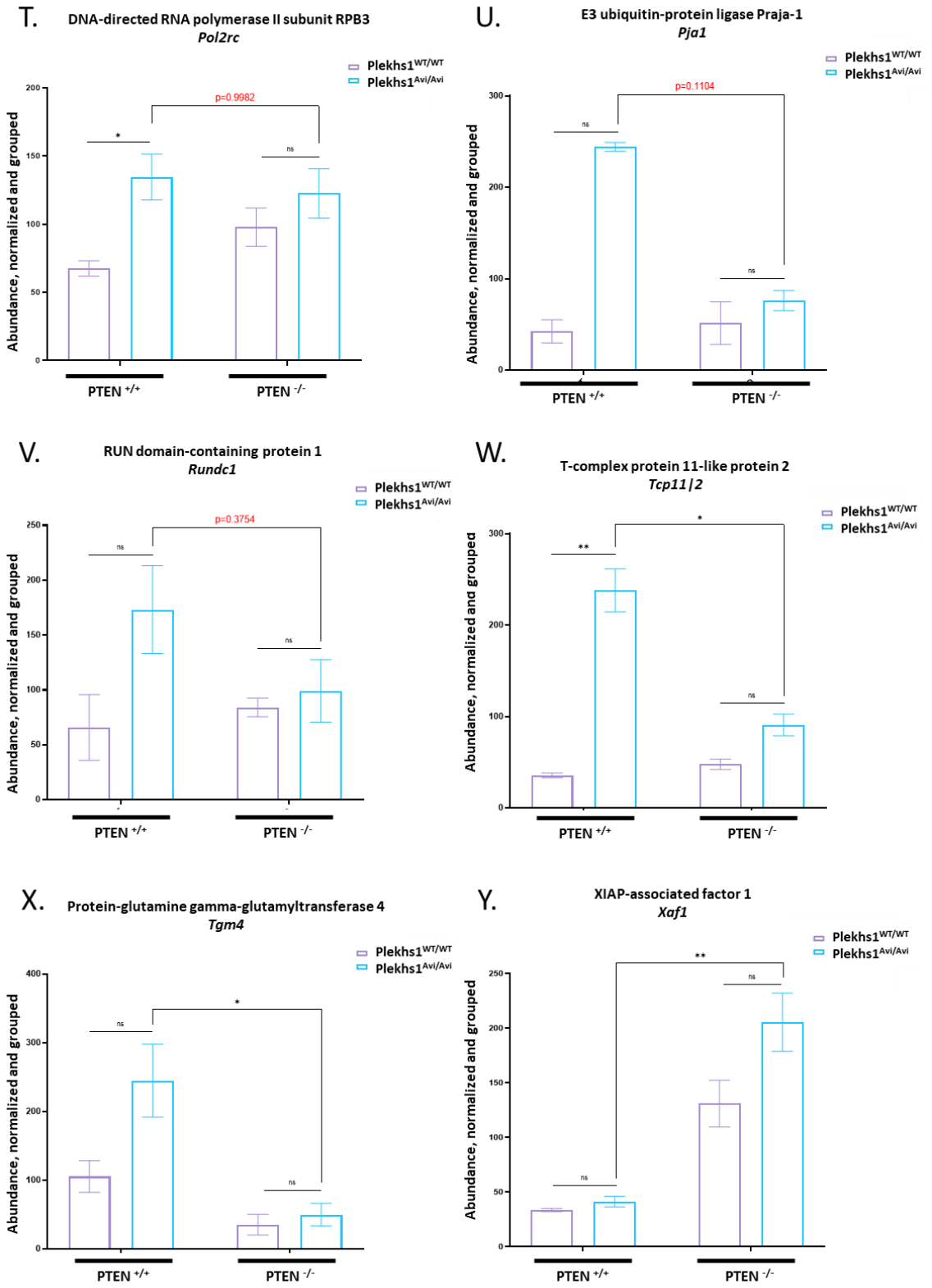
T.
DNA-directed RNA polymerase II subunit RPB3
Pol2rc
Plekhs1WT/WT
Plekhs1Avi/Avi
Abundance, normalized and grouped
p=0.9982
*
ns
PTEN +/+
PTEN -/-
U.
E3 ubiquitin-protein ligase Praja-1
Pja1
p=0.1104
V.
RUN domain-containing protein 1
Rundc1
p=0.3754
W.
T-complex protein 11-like protein 2
Tcp11|2
**
X.
Protein-glutamine gamma-glutamyltransferase 4
Tgm4
Y.
XIAP-associated factor 1
Xaf1

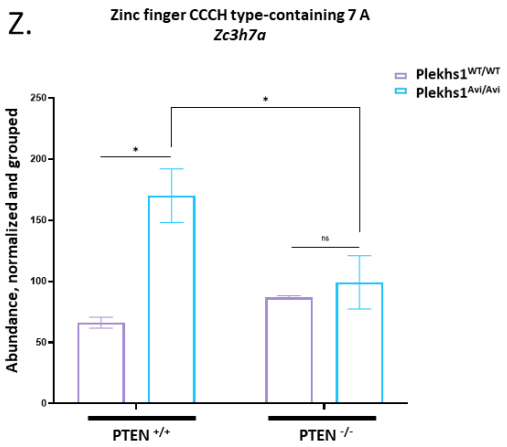


**Figure 5.19 The relative abundance of 'other' proteins in Avi-pulldowns from mouse prostate**

*Refer to the legend of Figure 5.4 for an explanation of this figure.*

*Some proteins are presented in more than one of the classes of protein types presented in the figures.*

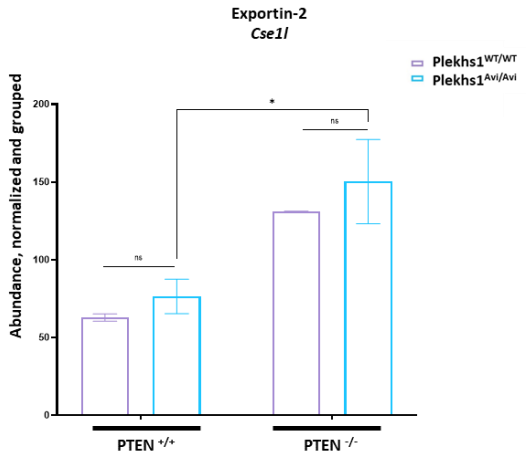


**Figure 5.20 The relative abundance of Exportin-2 (Cse1l) proteins in Avi-pulldowns from mouse prostate**

*Refer to the legend of Figure 5.4 for an explanation of this figure.*

*Some proteins are presented in more than one of the classes of protein types presented in the figures.*

## 5.6 Phosphoproteomics

Phospho-proteomic techniques were applied to analysis of the same PLEKHS1-pulldowns from mouse prostate that were presented above (this was performed by Dr David Oxley in the Proteomics Facility at the Babraham Institute). Out of 33 potential phosphorylation sites in PLEKHS1, we detected 26 unique phospho-peptides (Figure 5.21). The data were presented as ratios of the specific phosphorylation of a site or peptide in *Pten* $^{-/-}$/ *Pten* $^{+/+}$ samples (the specific phosphorylation was measured as the ratio of the abundance of a phosphorylated peptide / the abundance of its non-phosphorylated counterpart in the Avitagged- PLEKHS1 samples; which is a measure of the stoichiometry of phosphorylation of that site and hence the *Pten* $^{-/-}$/ *Pten* $^{+/+}$ ratio represents the relative change in the stoichiometry of phosphorylation of a phospho-site or phospho-peptide between *Pten* $^{-/-}$ and *Pten* $^{+/+}$ prostate). It is important to note that peptides phosphorylated on tyrosine residues are more difficult to detect than otherwise equivalent serine or threonine residues.

In this dataset we were able to detect and measure phosphorylation of a single YXXM-consensus motif (Y258). The stoichiometry of phosphorylation of Y258 was greater in *Pten* $^{-/-}$ than *Pten* $^{+/+}$ prostate but not by a significant amount. Other results presented in this thesis indicate that phosphorylation of Y258 is significantly increased in *Pten* $^{-/-}$ prostate (both total tyrosine phosphorylation and specific phosphorylation (YP-PLEKHS1/total PLEKHS1), see Figure 4.5), however, given the relatively large error in quantitating protein phosphorylation using phospho-proteomic techniques compared to that obtained through use of immuno-blotting with phospho-specific antibodies, it is entirely appropriate to rely on the immuno-blotting data to establish whether a change in phosphorylation is significant. Only one further phosphorylated tyrosine residue was detected (Y217) at relatively low levels.

As noted above, there are four potential phospho-sites in PLEKHS1 that could represent binding sites for 14-3-3 proteins, the three highest confidence sites (S157, S256, S180, in order of decreasing confidence) were all found to be phosphorylated and the stoichiometry of that phosphorylation was increased in *Pten* $^{-/-}$ prostate (Figure 5.21).

None of these changes reached statistical significance in these experiments and it is clear that to statistically validate these changes further experiments will be required. Clearly, these data suggest that it is possible that one or more of these sites underlay the interactions between PLEKHS1 and 14-3-3 proteins in the *Pten* $^{-/-}$ prostate samples. However, it remains unproven until further experiments, in which point-mutated versions of PLEKHS1 in which these phosphor-sites are individually switched to non-phosphorylatable residues, are conducted.

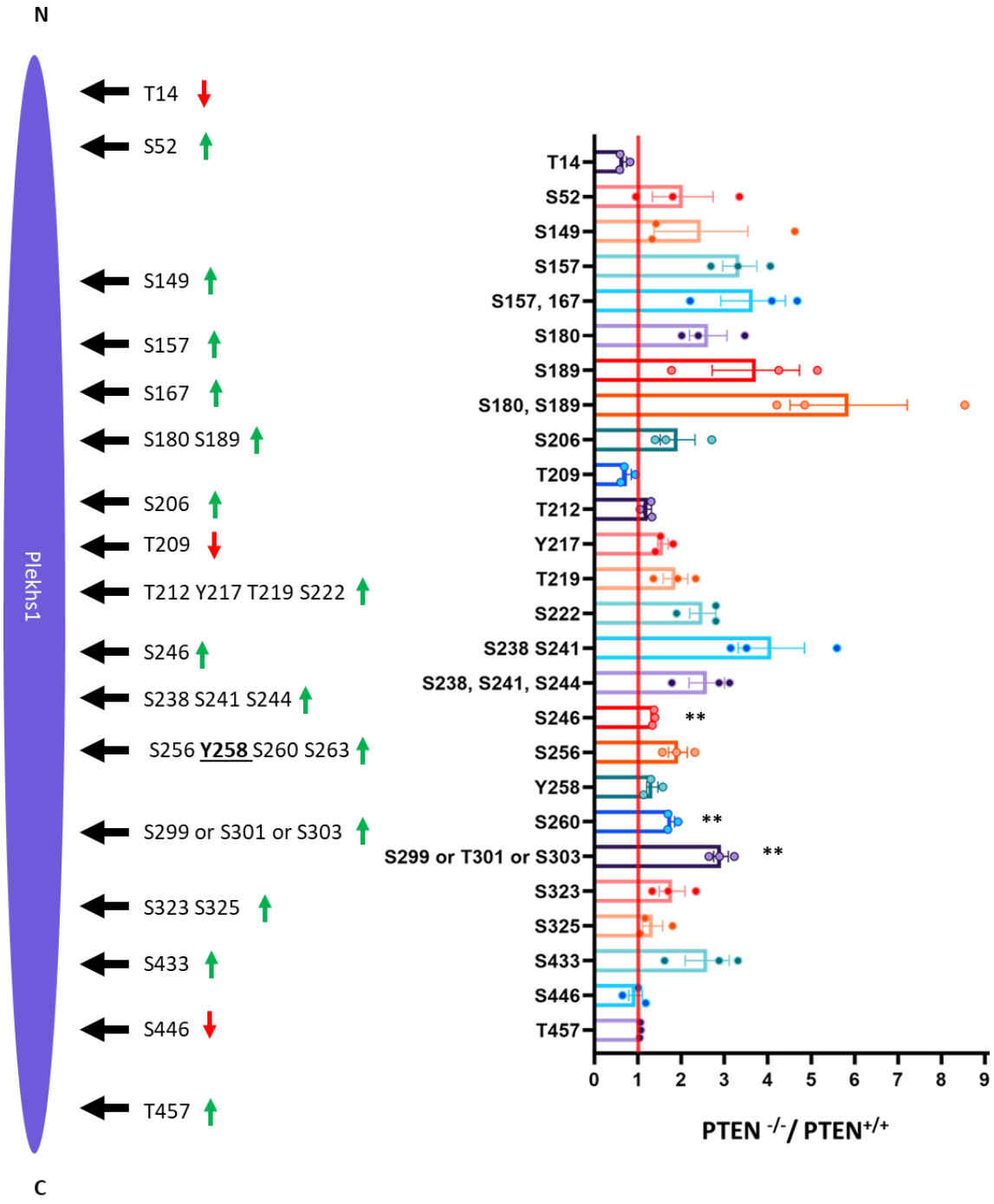
N
Plekhs1
T14
S52
S149
S157
S167
S180 S189
S206
T209
T212 Y217 T219 S222
S246
S238 S241 S244
S256 Y258 S260 S263
S299 or S301 or S303
S323 S325
S433
S446
T457
C
T14
S52
S149
S157
S157, 167
S180
S189
S180, S189
S206
T209
T212
Y217
T219
S222
S238 S241
S238, S241, S244
S246
S256
Y258
S260
S299 or T301 or S303
S323
S325
S433
S446
T457
**
**
**
0 1 2 3 4 5 6 7 8 9
PTEN -/-/ PTEN+/+

**Figure 5.21 Phospho-serine, phospho-threonine and phospho-tyrosine peptides identified in Plekhs1 from $PTEN^{+/+}$ and $PTEN^{-/-}$ mouse prostate**

*Plekhs1 recovered in Avi-pulldowns from $Plekhs1^{Avi/Avi}$ –expressing, $PTEN^{+/+}$ or $PTEN^{-/-}$ prostate tissue was analyzed using phosphoproteomic techniques (see the Materials and Methods section). 26 unique phospho-peptides were identified in the context of 33 potential phosphorylation sites. The stoichiometry of phosphorylation at individual potential phosphosites was estimated by calculating the abundance ratios of the phosphorylated/unphosphorylated versions of given peptides.*

*The graph and schematic show the location and relative stoichiometry of phosphorylation of individual phosphosites detected in $PTEN^{-/-}$ and $PTEN^{+/+}$ tissue. The data is presented as the ratio of phosphorylation ("stoichiometry") of sites in Plekhs1 in $PTEN^{-/-}$/$PTEN^{+/+}$ prostate.*

*Left: the green and red arrows indicate ratio >1 and ratio <1, respectively. Right: the red line marks the position where there is no change between $PTEN^{-/-}$ and $PTEN^{+/+}$ tissue (ratio=1). To estimate whether there were significant differences in the data a multicomparison T-test was applied. Data represent means ± SD of 3 biological replicates.*

# 6 GENERAL DISCUSSION

## 6.1 Summary and overview of other related studies

Proteins are key structural and functional elements of the cells and tissues. They act as signalling messengers and molecular machines across all biological processes[194]. Protein-protein interactions (PPI) play a critical role in the vast majority of signalling pathways as well as in the regulation of transcriptional processes [195]. In the process of protein-focused research, understanding of PPI has deepened in parallel with the advancement of various technologies[196]. Different techniques focus on detecting direct physical interactions between molecules or identifying predicted interactions based on computational analysis of known functional and structural linkages. Classic yeast two-hybrid systems along with protein sequence and structure based computational methods have been the work horse approaches to discover new protein interactions[197]. Recent developments in proteomics techniques, such as TMT and SILAC labelling, combined with increased sensitivity of the mass spectrometers and high throughput genomic techniques enabling large numbers of proteins to be systemically genetically tagged and used as baits in pulldown experiments have led to the definition of data-rich large-scale proteomes and interactomes from a variety of cell types or tissues. The analysis of data from these experiments has also required the evolution of new bioinformatics tools to aid their presentation and intepretation[198] [199] [200]. This large volume of data has made a significant impact but is limited by the fact the majority of major studies have focused on a narrow set of cell lines (e.g. HEK293) where many proteins are either not expressed or expressed but in the absence of their physiological interactors.

Dr Tamara Chessa (based in my host lab at BI) Avitagged endogenous Class IA PI3K subunits in order to define their interactors *in vivo.* The Avitag system allows very specific attachment of biotin to the 17aa (15aa tag + 2aa linker) Avitag peptide that is catalysed by BirA[201] [202] and hence subsequent application of streptavidin-based pulldown techniques. Combining this very powerful approach along with TMT labelling and cutting-edge proteomic analysis allowed the definition of a large network of Class

IA PI3K-interacting proteins in mouse prostate. TMT-labelling has become accepted to be a reliable technology to apply to quantitative proteomics analysis[138]. What is important, each of the TMT tags within one 'plex' (in for example an 11-plex library of regents) has the same mass and it contains the following three elements: 1) an amine-reactive NHS-ester group 2) a spacer and 3) an MS/MS reporter. Each of the samples has a divergent reporter mass that makes it possible to calculate the relative abundance of a peptide in different multiplexed samples [203] [204].

Stewart et al. applied TMT labelling in proteomics analysis of squamous cell lung cancer (SCC). This study integrated DNA copy number, somatic mutations, RNAseq data and proteomics to samples isolated from 108 patients. Based on protein clusters, three proteomic subtypes of SCC (redox, mixed and inflamed) were distinguished. Even though proteomic subgroups were not associated with patients survival, this research enriched our knowledge of SCC biology and could be an therapy indicator based on redox metabolism or immune cells response[205].

TMT technology also found an application in analysis of salivary proteins in order to develop a potential biomarker to help in the diagnosis of gastric cancer. 500 proteins were identified, with 48 showing a significantly different expression between tissue from a healthy donor and a patient suffering from gastric cancer. The top three proteins were validated and could help differentiate healthy from gastric cancer patients with high accuracy[206].

A TMT labelling strategy was also applied in neuroscience[207]. Tank et al. reported using TMT 10-plex to study genome-wide RNA instability in fibroblast-derived IPSC cells from patients suffering from amyotrophic lateral sclerosis (ALS) and frontotemporal dementia (FTD). This study also revealed, that RNA transcripts, previously tagged with bromo-uridine were destabilised in ribosomes and mitochondria[208].

A major study aiming to identify p85-interacting proteins has recently been published. Breitkop et el. performed very detailed analysis of p85 interactomes, comparing human and drosophila cell lines. Their approach was based on immunoprecipitation (IP) followed by shotgun mass spec and BLAST alignment. These data revealed direct interaction of the non-receptor protein tyrosine phosphatase type II (SHP2) with p85 regulatory subunits that was mirrored in drosophila orthologues of these proteins:

corkscrew and p60, respectively. It is worth noting, that the interaction did not occur with the p110 catalytic subunit directly (PI3K92e in drosophila)[104].

Importantly, PLEKHS1 has not been identified as a potential interactor in any of these studies. That could be a result of the cell-line based approach of these experiments and/or the restricted expression of PLEKHS1. To our knowledge, our group is the first to perform detailed analyses of p85 interactomes in prostate tissue. There are some proteomic studies, which do focus on identifying PI3K interactors in prostate cancer cell lines. Mass Spec analysis of p85 interactors in serum-starved LNCap cells revealed that p85 preferentially binds to p110βand p110δ and too a much smaller extent, p110α. ErbB3 was shown to be an interactor, although the interaction was P-tyrosine independent and does not affect PI3K signalling activation[209]. Global proteomics studies performed on the androgen resistant LNCap cell line (LNCap-95) in comparison with WT LNCap cells, revealed that 15 proteins were upregulated in PI3K signalling pathway. Among the upregulated proteins were AMPK, ITGB, GRB2, HSP90 and 14-3-3 proteins[210]. The two last proteins were also upregulated in our M/S analysis of PTEN deficient mouse prostate (discussed further in this section). Similarly, in studies on human cell lines, PLEKHS1 was not detected as a PI3K interactor nor was it upregulated in an androgen-independent cell line model of prostate cancer. This could indicate a big difference between PI3K interactors between *in vivo* and *in vitro* contexts. Alternatively, it could indicate a difference between the mouse and human Class IA interactomes in *Pten* -null -driven prostate tumorigenesis.

The PbCre$^{+/-}$ x *Pten* $^{LoxP/LoxP}$ prostate model, used to pursue our project, where Cre recombinase-driven recombination specifically in the prostate results in a homozygous ablation of *Pten* in prostate epithelial cells is well established and widely used by many different groups studying prostate tumorigenesis. It has been shown to be an excellent model to examine the importance of key players in prostate cancer such as: KRAS, BRAF, P53, SOX2, TERT, SMAD4 and SPOP[211 212 213]. Recently a Sleeping Beauty (SB) strategy to conditionally inactivate *Pten* was described[214]. The SB-based system was used to generate *Pten* -deficient mouse (*Pten* $^{SBm2/+}$) prostate which showed a dramatic increase in size compared to the control[214] that correlated with the data generated in our laboratory.

## 6.2 A general discussion and future directions of the work presented in thesis

As described in Chapter 3 we did not detect PLEKHS1 expression in a panel of tissues, except for prostate, isolated from male mice. However, we detected high PLEKHS1 expression in uterus (what agrees with published RNAseq data) and oviducts (which were not shown in the BioGPS nor EMBL databases). Interestingly, ovaries, which were described as a tissue with one of the highest levels of PLEKHS1 transcript do not express the protein. It remains possible that the ovaries prepared in these studies were contaminated with oviducts. Tumour formation driven by PTEN loss has already been reported in the context of hormone-dependent epithelial cells, such as prostate epithelium, thyroid and endometrium[215]. Eddie et al. hypothesised that High-Grade Serous Carcinoma (HGSC) can originate from oviducts, something that has been previously suggested by other groups studying mouse models with a deletion of *Pten*, BRCA1/2 and mutation, or deletion, of p53[216] [217]. It has been reported that *PTEN* loss appears in 80% in endometrioid tumours[218]. Mutations in PIK3CA gene were found in 25% endometrial tumours based on COSMIC database[219], in 51% based on TCGA-UCEC database and 53% based on TCGA database[220] [221]. In studies performed by An *et. al.* treating endometrial cancer cell line by p110β-specific siRNA resulted in increased apoptosis and inhibited proliferation of cancer cells[222]. Furthermore, p110β has been shown to be overexpressed in 7 different endometrial cancer cell lines. In analysed panel of 234 patients samples PIK3CB mRNA is significantly elevated in the early phase of tumorigenesis, what can be a potential indicator of poor prognosis for the patient [223].

In Chapter 4 we described *in transfecto* experiments, where we investigated the potential of PLEKHS1 to bind to class IA p85 regulatory subunits. We proved that upon activation of Src (and potentially other kinases) PLEKHS1 can bind to p85s and could therefore activate Class IA PI3Ks. The experiment confirmed previously published work of Grossman *et. al.* (section 1.5 of the Introduction) and unpublished work of Dr Tamara Chessa, BI (Figure 4.7). In this chapter, we also measured phosphorylation of Akt and other kinases involved in PI3K and/or other parallel signalling pathways. We noticed elevated level of that phosphorylation of Akt was increased in *Pten* $^{-/-}$ prostate, as previously described in the literature and confirming the role of PTEN as an direct

antagonist of class I PI3K activity [162]. What was unexpected, was that we observed a significant decrease in Akt phosphorylation in *Pten* $^{-/-}$ x *Plekhs1*$^{-/-}$ prostate; which suggests that PLEKHS1 plays a non-redundant role in prostate hyperplasia and tumour progression *in vivo*. Other proteins that were analysed were not significantly changed in *Pten* $^{-/-}$ *PLEKHS1*$^{-/-}$ compared to *Pten* $^{-/-}$ prostate. As a second method of measuring class I PI3K activity we decided to measure $PIP_3$, which is a direct product of Class I PI3K-mediated phosphorylation of $PIP_2$. We observed a strong elevation in $PIP_3$ levels in *Pten* $^{-/-}$compared to *Pten* $^{+/+}$ prostate. The most prominent increase was in C34:1-$PIP_3$, the most abundant species, as well as in C36:1-, C36:2- and C38:4-$PIP_3$. Strikingly, the increases in the levels of several $PIP_3$ species and total $PIP_3$ in *Pten* $^{-/-}$ prostate were significantly decreased by combined loss of PLEKHS1. These results support the results of measuring Akt phosphorylation and prostate growth in PLEKHS1 and/or *Pten* -null prostate described above. It is noteworthy, that the pattern of reduction in PTEN-driven accumulation of $PIP_3$ species elicited by loss of PLEKHS1, did not perfectly match the pattern of increase in $PIP_3$ species elicited by loss of PTEN. The underlying explanation for why there is a preferential accumulation of C34:1-$PIP_3$ or for the different patterns of change in the molecular species of $PIP_3$ between different genotypes remains unclear but similar interesting differences in the accumulation of different molecular species of $PIP_2$ and $PIP_3$ have been observed in other studies [224] [142]. Some of these phenomena could be a result of the prostate epithelial cells that express PbCre being constitutively enriched in C34:1-$PIP_2$ and $PIP_3$ species and their expansion in the absence of PTEN leads to the increase in their relative abundance and/or it could be an intrinsic feature of PTEN-substrate selectivity such that when deleted its preferred substrates preferentially accumulate. This will only be resolved by further studies that are going-on in the lab.

Measurement of $PIP_3$ levels in *Pten* $^{-/-}$ has been already studied and analysed by our group[143]. Malek *et. al.* showed there was an increase in $PIP_3$ and $PI(3,4)P_2$ in *Pten* $^{-/-}$ compared to *Pten* $^{+/+}$ prostate.

We sought to obtain novel insights into the molecular mechanisms of PLEKHS1-regulated signalling pathways underlying the observed functional significance of PLEKHS1 in PI3K signalling and prostate growth in *Pten* $^{-/-}$ prostates at the HG-PIN stage of tumorigenesis (as described in Chapters 3 and 4). The results we obtained, indicating that prostate hyperplasia induced by loss of PLEKHS1 was dependent on PLEKHS1

expression, were very clear but it would be very interesting to undertake a more detailed histological of the prostate tissue, both at 12w and at later stages of progression, to understand whether specific cell types had been preferentially impacted. For example, there were indications that the PLEKHS1 and *Pten* -null prostate was significantly less vascularised than prostate that was only *Pten* -null. These studies are currently being taken forward in collaborations with expert histologists. To understand the molecular basis of the interesting phenotype of PLEKHS1 and *Pten* -null prostate we aimed to identify, and subsequently investigate, the proteins specifically interacting with PLEKHS1, with focus being placed on those that might change between *Pten* $^{+/+}$ and *Pten* $^{-/-}$ prostate tissue.

In Chapter 5, we employed a combination of techniques that were previously validated in our laboratory, allowing highly specific and efficient streptavidin-mediated pulldown of endogenously Avitagged/biotinylated PLEKHS1 protein from lysates derived from *Pten* $^{+/+}$ and *Pten* $^{-/-}$ prostates, followed by TMT-LC-MS/MS. Isobaric tagging-based quantification (TMT) allowed multiplex analysis of biological samples (we used an 11-plex library, which was the maximum available at the time, but now 16-plex libraries are commercially available[181]). Relative quantification of identified peptides was executed through a direct comparison of the intensity of reporter ions in the MS/MS spectra.

In order to identify specific, high-confidence PLEKHS1 interactors, we included control samples to account for 'background' biotinylation (prostate lysates from mice lacking Avitagged PLEKHS1, but expressing biotin ligase BirA, in the context of *Pten* $^{+/+}$ and *Pten* $^{-/-}$ prostate tissue). Rigorous selection and analysis of proteins specifically enriched in Avi-pulldowns from prostates expressing Avi- PLEKHS1 and BirA, versus non-labelled PLEKHS1 and BirA, allowed a stringent approach to identify and eliminate from further analysis non-specifically interacting proteins. This methodology, even though very sensitive and powerful does have some limitations and disadvantages. Generating very broad dataset with potential number of false positive hits. Using 'No Avi' control and setting up a high statistical threshold significantly reduced the number of candidates, although there is a chance that some of the proteins interact solely with the streptavidin beads, are a result of contamination during the experimental procedure or interact with Plekhs1 in an indirect way (binds to Plekhs1 interactors). It is necessary to further

validate key interacting proteins. This process of protein verification is usually achieved using antibody based methods, such as immunoprecipitation or in our case streptavidin-based pulldown and immunoblotting or gene targeting- like designing Crispr/Cas9 screen panel.

Using these approaches, we identified a number of interactors/signalling pathways linked to PLEKHS1 in both *Pten* $^{+/+}$ and *Pten* $^{-/-}$ backgrounds. We also took into careful consideration any potential changes in the levels of protein expression between *Pten* $^{+/+}$ and *Pten* $^{-/-}$ samples through RNAseq analysis of publicly available datasets, to understand the possible reasons why the association of a protein with PLEKHS1 might have changed between *Pten* $^{-/-}$ and *Pten* $^{+/+}$ prostate [183].

In the context of *Pten* $^{+/+}$ prostate tissue, we have identified a number of PLEKHS1-interacting proteins that are involved in protein quality control and degradation (autophagy-related proteins, chaperones and ubiquitin ligases), which are largely reduced in *Pten* $^{-/-}$ prostate. It is possible these are proteins that are involved in the physiological turnover of PLEKHS1 and the reduction in their association with PLEKHS1 in the absence of PTEN represents an important aspect of the phenotype of that hyperplasic tissue.

Intriguingly, the most abundant interactors that are enhanced in *Pten* $^{-/-}$ prostate compared to *Pten* $^{+/+}$ prostate are members of the 14-3-3 family. In line with these findings, phospho-proteomic analysis of PLEKHS1 peptides identified in the PLEKHS1-Avi pulldowns from *Pten* $^{-/-}$ compared to *Pten* $^{+/+}$ prostate demonstrated increased stoichiometries of phosphorylation of three serine residues in the *Pten* $^{-/-}$ prostate, that are consensus 14-3-3 interaction sites. These results indicate that increased association may be driven by increased PLEKHS1 phosphorylation on these sites. 14-3-3 proteins have been implicated in a vast range of protein-protein interactions and cellular functions, including cancer, where both tumour-suppressive or tumour-promoting roles have been attributed to 14-3-3 family members, depending on the isoform and the cellular context[188]. The functional relevance of the increased association between PLEKHS1 and 14-3-3 protein family members to the *Pten* $^{-/-}$ phenotype remains to be elucidated and will only be meaningfully addressed by a combination of genetic studies in which non-phosphorylatable residues are knocked-in to the potential 14-3-3 binding sites in PLEKHS1 and/or prostate-specific knock-out of individual 14-3-3 proteins.

In addition, we observed increased association between PLEKHS1 and the Class 1A PI3K regulatory subunits, p85α and p85β, as well as the catalytic subunit p110β, in *Pten* $^{-/-}$ compared to *Pten* $^{+/+}$ prostate (there were increases in p110α and p55γ association but they were not statistically significant). These observations directly and independently confirm the unpublished findings of Dr Tamara Chessa in our lab who found increased recovery of PLEKHS1 in p85-pulldowns from *Pten* -null, compared to *Pten* -wild-type, prostate. These results could be a partial effect on higher expression of Plekhs1 in *Pten*-null prostate and phosphorylation-based activation of this protein. As it has been shown, PLEKHS1 is significantly higher phosphorylated in *Pten*-null prostate what results in increased p85-PLEKHS1 interaction and activation of PI3K signalling pathway. Kinase(s) and phosphatases of PLEKHS1 in this context are yet to be discovered.

Following on from our previous observations in Chapter 3, where loss of PLEKHS1 in *Pten* $^{-/-}$ prostate led to decreased prostate size, as well as decreased levels of $PIP_3$ and phosphorylation of Akt, these findings provide insight into the functional role for selective PLEKHS1-PI3K regulatory subunit and -PI3K catalytic subunit interactions in prostate growth/tumorigenesis and PI3K signalling.

Other proteins that display increased association with PLEKHS1 in the *Pten* $^{-/-}$ prostate and that are likely candidates to promote the *Pten* $^{-/-}$ phenotype are PhldB2, Stat3, Memo1, Ly6C1 and Gpx2.

The PLEKHS1 protein interactions that are identified as significant in *Pten* $^{+/+}$ (Figure 6.1 A) and *Pten* $^{-/-}$ (Figure 6.1 B) prostate are summarised in STRING diagrams below, and grouped according to protein family or molecular function.

A.

PLEKHS1 interactions enriched in the *Pten* $^{+/+}$ prostate:

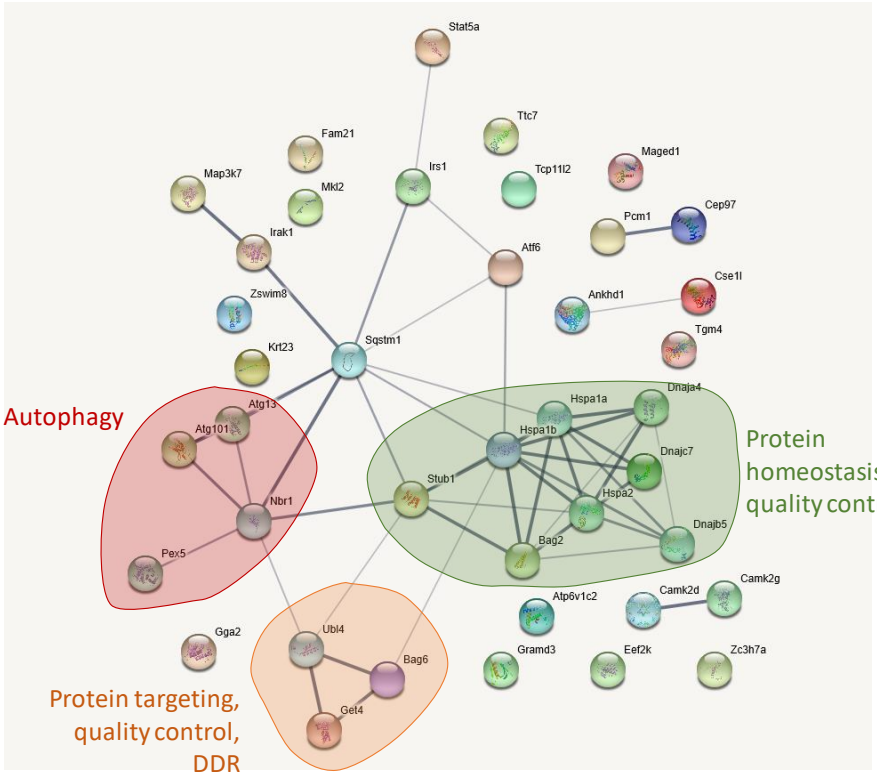


B.

PLEKHS1 interactions enriched in the *Pten* $^{-/-}$ prostate:

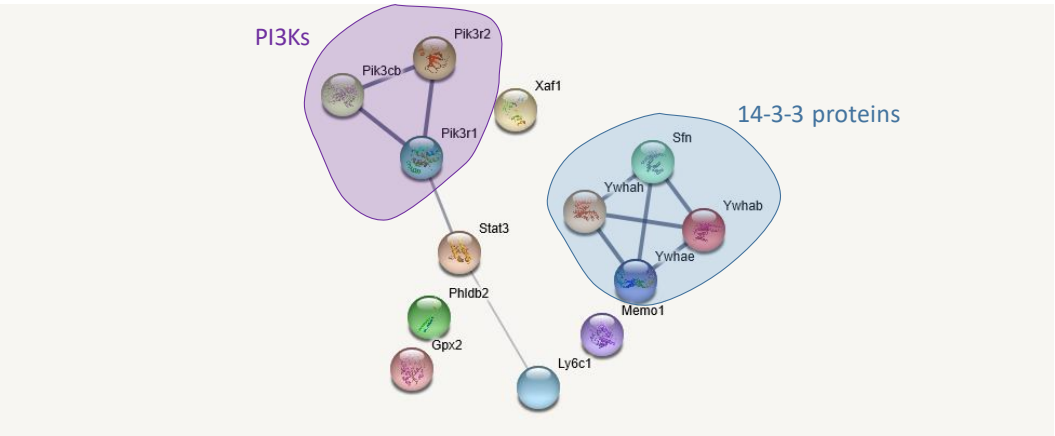

**Figure 6.1 STRING analysis of Plekhs1 interactors in PTEN$^{+/+}$ and PTEN$^{-/-}$ prostates**

*A-B. Analysis of Plekhs1 interactors. Lines represent protein-protein associations (which includes, but is not limited to, physical binding of proteins). The width of the lines correlates with the confidence of indicated association. Nodes represent proteins, each of which represents all of the proteins encoded by a single gene. Filled nodes indicate that there is 3D structural data available for the indicated protein.*
*The analysis was performed by Dr T. Chessa (BI) using STRING web-based software (www.string-db.org).*

Future studies will focus on validation of these results by independent approaches, as well as to determine to what extent the observed changes in interactions between the *Pten* $^{+/+}$ and *Pten* $^{-/-}$ prostate are driven by alterations in protein expression. In some cases, it will be possible to directly quantify changes in a selected proteins abundance in different prostate samples by immuno-blotting with relevant antibodies. In addition, as discussed in Chapter 5, it is possible that certain chaperones identified in our studies may not interact with PLEKHS1 or associated proteins *in vivo*, but rather recognise these proteins as misfolded during the experimental protocol. Further experiments should be performed, to determine whether these protein complexes form post-lysis of prostate tissue, or whether they play a functional role in the folding and refolding of PLEKHS1 in an *in vivo* cellular context. It is likely that a subset of the proteins identified to interact with PLEKHS1 in prostate are indeed a physiological determinant of PLEKHS1 and/or its interactors' degradation and turnover *in vivo*.
Broadly, loss of *Pten* expression in the mouse prostate leads to a downregulation in PLEKHS1 interaction with proteins that are involved in protein folding and turnover, and an upregulation in PLEKHS1 interaction with 14-3-3 family members and Class IA PI3Ks. Although it is clear that PLEKHS1 plays an important non-redundant role in the growth and $PIP_3$ signalling pathway of *Pten* -null mouse prostate, understanding of the molecular causalities involved, and whether any therapeutic opportunities arise from that, requires further work.
A major focus for further work is to understand how many of the observations made in this thesis are relevant to human prostate and prostate tumour progression. A

substantial problem confronting progress towards this is the fact that the commercial anti- PLEKHS1 antibodies we have tested (including the antibodies we have routinely used and validated to be capable of detecting mouse PLEKHS1) do not appear to detect human PLEKHS1. Solving this problem is a major priority for future work and is being addressed in experiments in which human PLEKHS1 is being targeted with CRISPR/Cas9 technology in human prostate cell lines. These experiments have the potential to directly validate both potential anti-human PLEKHS1 antibodies and the targeting strategies being applied and are currently on going. Important to the broader aims of these studies are collaborations that are being built with Cambridge clinicians who are experts in prostate cancer.

## 6.3 Summary

Our work provided an insight into the ability of PLEKHS1 to interact with Class IA PI3Ks and the functions of PLEKHS1 in the process of prostate tumorigenesis. Our results show that PLEKHS1 is a key regulator of the Class IA PI3K network in mouse prostate *in vivo.* We hypothesize that PLEKHS1, can activate Class IA PI3K in two ways; 1) *via* its YXXM motif (by binding to p85) and 2) *via* its PH domain (by binding to $PIP_3$) and effect $PIP_3$-dependent cellular processes. PLEKHS1, once activated by SRC other cellular kinases with a mediatory role of 14-3-3 can specifically bind to regulatory subunit of PI3K. PI3K then phosphorylates $PI(4,5)P_2$ and generates $PIP_3$. In a feed-forward loop, PLEKHS1 binds to newly generated $PIP_3$, what resulted in another stimulation of PI3K signalling pathway and increased of tumorigenesis in mouse prostate.

A schematic illustration of the hypothesis is shown in Figure 6.2.

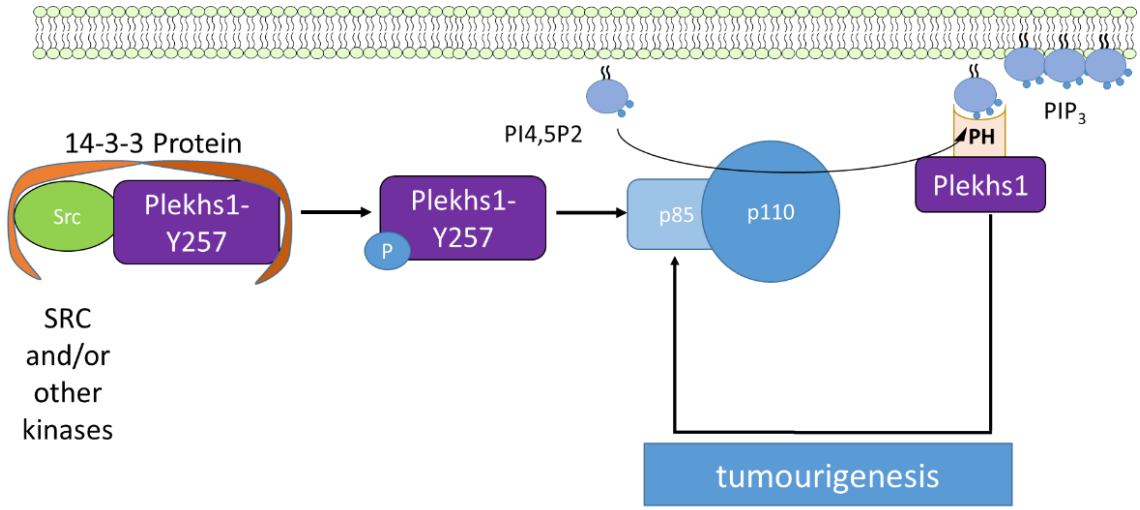


**Figure 6.2 Schematic to illustrate the potential role of Plekhs1 in the process of prostate tumorigenesis**

*14-3-3 proteins mediate phosphorylation of Plekhs1 in YXXM motif by Src (and/or possibly other kinases). This leads to binding of the SH2 domains of p85s and activation of Class IA PI3K. Once activated, PI3K generates $PIP_3$, which can then bind to Plekhs1 via its PH domain. We propose that $PIP_3$-bound Plekhs1 is more efficiently phosphorylated on its YXXM-motif, and hence via a positive-feedback loop, further augments $PIP_3$ accumulation.*

# 7 REFERENCES


1. Katso, R. *et al.* Cellular Function of Phosphoinositide 3-Kinases: Implications for Development, Immunity, Homeostasis, and Cancer. *Annu. Rev. Cell Dev* **17**, 615–75 (2001).
2. Vanhaesebroeck, B., Stephens, L. & Hawkins, P. PI3K signalling: The path to discovery and understanding. *Nature Reviews Molecular Cell Biology* vol. 13 195–203 (2012).
3. Campa, C. C., Ciraolo, E., Ghigo, A., Germena, G. & Hirsch, E. Crossroads of PI3K and Rac pathways. *Small GTPases* **6**, 71–80 (2015).
4. Rathinaswamy, M. K. & Burke, J. E. Class I phosphoinositide 3-kinase (PI3K) regulatory subunits and their roles in signaling and disease. *Advances in Biological Regulation* (2019) doi:10.1016/j.jbior.2019.100657.
5. Bilanges, B., Posor, Y. & Vanhaesebroeck, B. PI3K isoforms in cell signalling and vesicle trafficking. *Nat. Rev. Mol. Cell Biol.* doi:10.1038/s41580-019-0129-z.
6. Chen, C. Y., Chen, J., He, L. & Stiles, B. L. PTEN: Tumor suppressor and metabolic regulator. *Frontiers in Endocrinology* vol. 9 (2018).
7. Fresno Vara, J. Á. *et al.* P13K/Akt signalling pathway and cancer. *Cancer Treatment Reviews* vol. 30 193–204 (2004).
8. Fruman, D. A., Meyers, R. E. & Cantley, L. C. PHOSPHOINOSITIDE KINASES. *Annu. Rev. Biochem.* **67**, 481–507 (1998).
9. Testa, J. R. & Bellacosa, A. AKT plays a central role in tumorigenesis. *Proceedings of the National Academy of Sciences of the United States of America* vol. 98 10983–10985 (2001).
10. Pawson, T. & Nash, P. Protein-protein interactions define specificity in signal transduction. *Genes and Development* vol. 14 1027–1047 (2000).
11. Chen, X. *et al.* Constitutively active Akt is an important regulator of TRAIL sensitivity in prostate cancer. *Oncogene* **20**, 6073–6083 (2001).
12. Hussain, A. R. *et al.* Cross-talk between NFkB and the PI3-kinase/AKT pathway can be targeted in primary effusion lymphoma (PEL) cell lines for efficient apoptosis.

*PLoS One* **7**, (2012).

13. Liang, J. & Slingerland, J. M. Multiple roles of the PI3K/PKB (Akt) pathway in cell cycle progression. *Cell cycle (Georgetown, Tex.)* vol. 2 336–342 (2003).
14. Lloyd, R. V. *et al.* p27(kip1): A multifunctional cyclin-dependent kinase inhibitor with prognostic significance in human cancers. *American Journal of Pathology* vol. 154 313–323 (1999).
15. Pridham, K. J., Varghese, R. T. & Sheng, Z. The role of class IA phosphatidylinositol-4,5-bisphosphate 3-kinase catalytic subunits in glioblastoma. *Frontiers in Oncology* vol. 7 (2017).
16. Okkenhaug, K. & Vanhaesebroeck, B. New responsibilities for the PI3K regulatory subunit p85 alpha. *Science's STKE : signal transduction knowledge environment* vol. 2001 pe1–pe1 (2001).
17. Huang, C. H. *et al.* The structure of a human p110α/p85α complex elucidates the effects of oncogenic PI3Kα mutations. *Science (80-. ).* **318**, 1744–1748 (2007).
18. Amzel, L. M. *et al.* Structural comparisons of class I phosphoinositide 3-kinases. *Nature Reviews Cancer* vol. 8 665–669 (2008).
19. Tsolakos, N. *et al.* Quantitation of class IA PI3Ks in mice reveals p110-free-p85s and isoform-selective subunit associations and recruitment to receptors. *Proc. Natl. Acad. Sci. U. S. A.* **115**, 12176–12181 (2018).
20. Cheung, L. W. T. *et al.* Regulation of the PI3K pathway through a p85α monomer–homodimer equilibrium. *Elife* **4**, 1–28 (2015).
21. Sacks, D. *et al.* Multisociety Consensus Quality Improvement Revised Consensus Statement for Endovascular Therapy of Acute Ischemic Stroke. *Int. J. Stroke* **13**, 612–632 (2018).
22. Guillermet-Guibert, J. *et al.* The p110β isoform of phosphoinositide 3-kinase signals downstream of G protein-coupled receptors and is functionally redundant with p110γ. *Proc. Natl. Acad. Sci. U. S. A.* **105**, 8292–8297 (2008).
23. Houslay, D. M. *et al.* Coincident signals from GPCRs and receptor tyrosine kinases are uniquely transduced by PI3Kβ in myeloid cells. *Sci. Signal.* **9**, 1–13 (2016).
24. Kulkarni, S. *et al.* PI3Kβ plays a critical role in neutrophil activation by immune complexes. *Sci. Signal.* **4**, 1–12 (2011).

25. Madsen, R. R. & Vanhaesebroeck, B. *Cracking the context-specific PI3K signaling code*. *Sci. Signal* vol. 13 http://stke.sciencemag.org/ (2020).
26. Dituri, F. *et al.* PI3K class IB controls the cell cycle checkpoint promoting cell proliferation in hepatocellular carcinoma. *Int. J. Cancer* **130**, 2505–2513 (2012).
27. Stephens, L. R. *et al.* The Gβγ/sensitivity of a PI3K is dependent upon a tightly associated adaptor, p101. *Cell* **89**, 105–114 (1997).
28. Leopoldt, D. *et al.* Gβγ stimulates phosphoinositide 3-kinase-γ by direct interaction with two domains of the catalytic p110 subunit. *J. Biol. Chem.* **273**, 7024–7029 (1998).
29. Vadas, O. *et al.* Molecular determinants of PI3Kγ-mediated activation downstream of G-protein-coupled receptors (GPCRs). *Proc. Natl. Acad. Sci. U. S. A.* **110**, 18862–18867 (2013).
30. Suire, S. *et al.* Gβγs and the Ras binding domain of p110γ are both important regulators of PI3Kγ signalling in neutrophils. *Nat. Cell Biol.* **8**, 1303–1309 (2006).
31. Suire, S., Hawkins, P. & Stephens, L. Activation of phosphoinositide 3-kinase γ by Ras. *Curr. Biol.* **12**, 1068–1075 (2002).
32. Pacold, M. E. *et al.* Crystal structure and functional analysis of Ras binding to its effector phosphoinositide 3-kinase γ. *Cell* **103**, 931–944 (2000).
33. Suire, S. *et al.* GPCR activation of Ras and PI3Kγ in neutrophils depends on PLCβ2/β3 and the RasGEF RasGRP4. *EMBO J.* **31**, 3118–3129 (2012).
34. Nürnberg, B. & Beer-Hammer, S. Function, regulation and biological roles of PI3Kγ variants. *Biomolecules* vol. 9 (2019).
35. Braccini, L. *et al.* PI3K-C2γ 3 is a Rab5 effector selectively controlling endosomal Akt2 activation downstream of insulin signalling. *Nat. Commun.* **6**, (2015).
36. Posor, Y. *et al.* Spatiotemporal control of endocytosis by phosphatidylinositol-3,4-bisphosphate. *Nature* **499**, 233–237 (2013).
37. Franco, I. *et al.* PI3K class II α controls spatially restricted endosomal PtdIns3P and Rab11 activation to promote primary cilium function. *Dev. Cell* **28**, 647–658 (2014).
38. O'farrell, F. *et al.* Class III phosphatidylinositol-3-OH kinase controls epithelial integrity through endosomal LKB1 regulation. *Nat. Cell Biol.* **19**, (2017).
39. Jaber, N. *et al.* Class III PI3K Vps34 plays an essential role in autophagy and in

heart and liver function. doi:10.1073/pnas.1112848109.

40. Song, M. S., Salmena, L. & Pandolfi, P. P. The functions and regulation of the PTEN tumour suppressor. *Nature Reviews Molecular Cell Biology* vol. 13 283–296 (2012).
41. Yamamoto, H. *et al.* PIK3CA mutations and copy number gains in human lung cancers. *Cancer Res.* **68**, 6913–6921 (2008).
42. Engelman, J. A. Targeting PI3K signalling in cancer: Opportunities, challenges and limitations. *Nature Reviews Cancer* vol. 9 550–562 (2009).
43. Vadas, O., Burke, J. E., Zhang, X., Berndt, A. & Williams, R. L. Structural biology structural basis for activation and inhibition of class I phosphoinositide 3-kinases. *Science Signaling* vol. 4 (2011).
44. Berndt, A. *et al.* The p110δ structure: Mechanisms for selectivity and potency of new PI(3)K inhibitors. *Nat. Chem. Biol.* **6**, 117–124 (2010).
45. Garcia-Echeverria, C. & Sellers, W. R. Drug discovery approaches targeting the PI3K/Akt pathway in cancer. *Oncogene* vol. 27 5511–5526 (2008).
46. Workman, P., Clarke, P. A., Raynaud, F. I. & Van Montfort, R. L. M. Drugging the PI3 kinome: From chemical tools to drugs in the clinic. *Cancer Research* vol. 70 2146–2157 (2010).
47. Wander, S. A., Hennessy, B. T. & Slingerland, J. M. Next-generation mTOR inhibitors in clinical oncology: How pathway complexity informs therapeutic strategy. *Journal of Clinical Investigation* vol. 121 1231–1241 (2011).
48. Engelman, J. A. *et al.* Effective use of PI3K and MEK inhibitors to treat mutant Kras G12D and PIK3CA H1047R murine lung cancers. *Nat. Med.* **14**, 1351–1356 (2008).
49. Klempner, S. J., Myers, A. P. & Cantley, L. C. What a tangled web we weave: Emerging resistance mechanisms to inhibition of the phosphoinositide 3-kinase pathway. *Cancer Discovery* vol. 3 1345–1354 (2013).
50. Rodon, J., Dienstmann, R., Serra, V. & Tabernero, J. Development of PI3K inhibitors: Lessons learned from early clinical trials. *Nature Reviews Clinical Oncology* vol. 10 143–153 (2013).
51. Liu, P. *et al.* Oncogenic PIK3CA-driven mammary tumors frequently recur via PI3K pathway-dependent and PI3K pathway-independent mechanisms. *Nat. Med.* **17**,

1116–1121 (2011).

52. Ilic, N., Utermark, T., Widlund, H. R. & Roberts, T. M. PI3K-targeted therapy can be evaded by gene amplification along the MYC-eukaryotic translation initiation factor 4E (eIF4E) axis. *Proc. Natl. Acad. Sci. U. S. A.* **108**, (2011).
53. Tikoo, A. *et al.* Physiological levels of Pik3caH1047R mutation in the mouse mammary gland results in ductal hyperplasia and formation of ERα-positive tumors. *PLoS One* **7**, (2012).
54. Kinross, K. M. *et al.* An activating Pik3ca mutation coupled with Pten loss is sufficient to initiate ovarian tumorigenesis in mice. *J. Clin. Invest.* **122**, 553–557 (2012).
55. Porta, C., Paglino, C. & Mosca, A. Targeting PI3K/Akt/mTOR signaling in cancer. *Frontiers in Oncology* vol. 4 APR (2014).
56. Francis, J. C. & Swain, A. Prostate Organogenesis. (2017) doi:10.1101/cshperspect.a030353.
57. Abate-Shen, C. & Shen, M. M. Molecular genetics of prostate cancer. *Genes and Development* vol. 14 2410–2434 (2000).
58. Montano, M. & Bushman, W. Morphoregulatory pathways in prostate ductal development. *Dev. Dyn.* **246**, 89–99 (2017).
59. Hayward, S. W. *et al.* Epithelial development in the rat ventral prostate, anterior prostate and seminal vesicle. *Cells Tissues Organs* **155**, 81–93 (1996).
60. Hayward, S. W. *et al.* Stromal development in the ventral prostate, anterior prostate and seminal vesicle of the rat. *Cells Tissues Organs* **155**, 94–103 (1996).
61. American Cancer Society- website. https://cancerstatisticscenter.cancer.org/?_ga=2.160725621.931526280.1582122955-774200741.1582122955#!/.
62. Packer, J. R. & Maitland, N. J. The molecular and cellular origin of human prostate cancer. *Biochim. Biophys. Acta - Mol. Cell Res.* **1863**, 1238–1260 (2016).
63. Sathianathen, N. J., Konety, B. R., Crook, J., Saad, F. & Lawrentschuk, N. Landmarks in prostate cancer. *Nature Reviews Urology* vol. 15 627–642 (2018).
64. Kessler, B. & Albertsen, P. The natural history of prostate cancer. *Urologic Clinics of North America* vol. 30 219–226 (2003).
65. Shankar, E. *et al.* Complex Systems Biology Approach in Connecting PI3K-Akt and

NF-κB Pathways in Prostate Cancer. *Cells* **8**, 201 (2019).

66. Taylor, L. G., Canfield, S. E. & Du, X. L. Review of major adverse effects of androgen-deprivation therapy in men with prostate cancer. *Cancer* vol. 115 2388–2399 (2009).
67. Liu, X. *et al.* Systematic dissection of phenotypic, functional, and tumorigenic heterogeneity of human prostate cancer cells. *Oncotarget* **6**, 23959–23986 (2015).
68. Zhang, D., Zhao, S., Li, X., Kirk, J. S. & Tang, D. G. Prostate Luminal Progenitor Cells in Development and Cancer HHS Public Access. *Trends Cancer* **4**, 769–783 (2018).
69. Leon, C. G. *et al.* Alterations in cholesterol regulation contribute to the production of intratumoral androgens during progression to castration-resistant prostate cancer in a mouse xenograft model. *Prostate* **70**, 390–400 (2010).
70. Yue, S. *et al.* Cholesteryl ester accumulation induced by PTEN loss and PI3K/AKT activation underlies human prostate cancer aggressiveness. *Cell Metab.* **19**, 393–406 (2014).
71. Allott, E. H. *et al.* Serum lipid profile and risk of prostate cancer recurrence: Results from the SEARCH database. *Cancer Epidemiol. Biomarkers Prev.* **23**, 2349–2356 (2014).
72. Wang, S. *et al.* Prostate-specific deletion of the murine Pten tumor suppressor gene leads to metastatic prostate cancer. *Cancer Cell* **4**, 209–221 (2003).
73. Ferraldeschi, R. *et al.* PTEN protein loss and clinical outcome from castration-resistant prostate cancer treated with abiraterone acetate. *Eur. Urol.* **67**, 795–802 (2015).
74. Taylor, B. S. *et al.* Integrative Genomic Profiling of Human Prostate Cancer. *Cancer Cell* **18**, 11–22 (2010).
75. Jemal, A. *et al.* Global cancer statistics. *CA. Cancer J. Clin.* **61**, 69–90 (2011).
76. Yoshida, K. & Miki, Y. Role of BRCA1 and BRCA2 as regulators of DNA repair, transcription, and cell cycle in response to DNA damage. *Cancer Science* vol. 95 866–871 (2004).
77. Boormans, J. L. & Schröder, F. H. Re: Prostate Cancer Progression and Survival in BRCA2 Mutation Carriers. *Eur. Urol.* **52**, 1529 (2007).

78. Kote-Jarai, Z. *et al.* BRCA2 is a moderate penetrance gene contributing to young-onset prostate cancer: Implications for genetic testing in prostate cancer patients. *Br. J. Cancer* **105**, 1230–1234 (2011).
79. Cox, V. L. *et al.* Lynch syndrome: Genomics update and imaging review. *Radiographics* vol. 38 483–499 (2018).
80. Das, S. *et al.* Bringing Prostate Cancer Germline Genetics into Clinical Practice. *J. Urol.* **202**, 223–230 (2019).
81. Ewing, C. M. *et al.* Germline mutations in HOXB13 and prostate-cancer risk. *N. Engl. J. Med.* **366**, 141–149 (2012).
82. Huang, H. & Cai, B. G84E mutation in HOXB13 is firmly associated with prostate cancer risk: A meta-analysis. *Tumor Biol.* **35**, 1177–1182 (2014).
83. Hale, V., M., W. & JY., P. CHEK2 (∗) 1100delC Mutation and Risk of Prostate Cancer. *Prostate Cancer* **2014**, 1–9 (2014).
84. Grasso, C. S. *et al.* The mutational landscape of lethal castration-resistant prostate cancer. *Nature* **487**, 239–243 (2012).
85. Graça, I. *et al.* Epigenetic modulators as therapeutic targets in prostate cancer. *Clinical Epigenetics* vol. 8 (2016).
86. Lim, M. *et al.* RNAs as Candidate Diagnostic and Prognostic Markers of Prostate Cancer—From Cell Line Models to Liquid Biopsies. *Diagnostics* **8**, 60 (2018).
87. LoRusso, P. M. Inhibition of the PI3K/AKT/mTOR pathway in solid tumors. *J. Clin. Oncol.* **34**, 3803–3815 (2016).
88. Gyori, D., Chessa, T., Hawkins, P. & Stephens, L. Class (I) Phosphoinositide 3-Kinases in the Tumor Microenvironment. *Cancers (Basel).* **9**, 24 (2017).
89. Okkenhaug, K., Graupera, M. & Vanhaesebroeck, B. Targeting PI3K in cancer: Impact on tumor cells, their protective stroma, angiogenesis, and immunotherapy. *Cancer Discovery* vol. 6 1090–1105 (2016).
90. Robinson, D. *et al.* Integrative clinical genomics of advanced prostate cancer. *Cell* **161**, 1215–1228 (2015).
91. Pearson, H. B. *et al.* Identifi cation of pik3ca mutation as a genetic driver of prostate cancer that cooperates with pten loss to accelerate progression and castration-resistant growth. *Cancer Discov.* **8**, 764–779 (2018).
92. Jia, S. *et al.* Opposing effects of androgen deprivation and targeted therapy on

prostate cancer prevention. *Cancer Discov.* **3**, 44–51 (2013).

93. Wee, S. *et al.* PTEN-deficient cancers depend on PIK3CB. *Proc. Natl. Acad. Sci. U. S. A.* **105**, 13057–13062 (2008).
94. Jia, S. *et al.* Essential roles of PI(3)K-p110β in cell growth, metabolism and tumorigenesis. *Nature* **454**, 776–779 (2008).
95. Fruman, D. A. & Rommel, C. PI3K and cancer: Lessons, challenges and opportunities. *Nat. Rev. Drug Discov.* **13**, 140–156 (2014).
96. Podsypanina, K. *et al.* Mutation of Pten/Mmac1 in mice causes neoplasia in multiple organ systems. *Proc. Natl. Acad. Sci. U. S. A.* **96**, 1563–1568 (1999).
97. Stambolic, V. *et al.* High incidence of breast and endometrial neoplasia resembling human Cowden syndrome in pten(+/-) mice. *Cancer Res.* **60**, 3605–3611 (2000).
98. Di Cristofano, A., De Acetis, M., Koff, A., Cordon-Cardo, C. & P Pandolfi, P. Pten and p27KIP1 cooperate in prostate cancer tumor suppression in the mouse. *Nat. Genet.* **27**, 222–224 (2001).
99. Kim, M. J. *et al.* Nkx3.1 mutant mice recapitulate early stages of prostate carcinogenesis. *Cancer Res.* **62**, 2999–3004 (2002).
100. You, M. J. *et al.* Genetic analysis of Pten and Ink4a/Arf interactions in the suppression of tumorigenesis in mice. *Proc. Natl. Acad. Sci. U. S. A.* **99**, 1455–1460 (2002).
101. Kwabi-Addo, B. *et al.* Haploinsufficiency of the Pten tumor suppressor gene promotes prostate cancer progression. *Proc. Natl. Acad. Sci. U. S. A.* **98**, 11563–11568 (2001).
102. Majumder, P. K. *et al.* Prostate intraepithelial neoplasia induced by prostate restricted Akt activation: The MPAKT model. *Proc. Natl. Acad. Sci. U. S. A.* **100**, 7841–7846 (2003).
103. Birbach, A. Use of PB-Cre4 Mice for Mosaic Gene Deletion. *PLoS One* **8**, (2013).
104. Breitkopf, S. B. *et al.* A Cross-Species Study of PI3K Protein-Protein Interactions Reveals the Direct Interaction of P85 and SHP2. *Sci. Rep.* **6**, (2016).
105. Huttlin, E. L. *et al.* Architecture of the human interactome defines protein communities and disease networks. *Nature* **545**, 505–509 (2017).

106. Chiu, Y. H., Lee, J. Y. & Cantley, L. C. BRD7, a Tumor Suppressor, Interacts with p85α and Regulates PI3K Activity. *Mol. Cell* **54**, 193–202 (2014).

107. Pilot-Storck, F. *et al.* Interactome mapping of the phosphatidylinositol 3-kinase-mammalian target of rapamycin pathway identifies deformed epidermal autoregulatory factor-1 as a new glycogen synthase kinase-3 interactor. *Mol. Cell. Proteomics* **9**, 1578–1593 (2010).

108. Uniport Database- website. Plekhs1 - Pleckstrin homology domain-containing family S member 1. https://www.uniprot.org/uniprot/Q8BW88.

109. Grossmann, A. *et al.* Phospho-tyrosine dependent protein – protein interaction network. 1–15 (2015).

110. Wang, W., Xu, S., Yin, M. & Jin, Z. G. Essential roles of Gab1 tyrosine phosphorylation in growth factor-mediated signaling and angiogenesis. *International Journal of Cardiology* vol. 181 180–184 (2015).

111. Mattoon, D. R., Lamothe, B., Lax, I. & Schlessinger, J. The docking protein Gab1 is the primary mediator of EGF-stimulated activation of the PI-3K/Akt cell survival pathway. *BMC Biol.* **2**, (2004).

112. Kiyatkin, A. *et al.* Scaffolding protein Grb2-associated binder 1 sustains epidermal growth factor-induced mitogenic and survival signaling by multiple positive feedback loops. *J. Biol. Chem.* **281**, 19925–19938 (2006).

113. Human Protein Atlas-website. Plekhs1. https://www.proteinatlas.org/ENSG00000148735-PLEKHS1/cell.

114. EMBL-EBI Expression Atlas-website. Plekhs1. https://www.ebi.ac.uk/gxa/genes/ensmusg00000035818?bs=%7B%22mus musculus%22%3A%5B%22ORGANISM_PART%22%2C%22CELL_TYPE%22%5D%7D&ds=%7B%22kingdom%22%3A%5B%22animals%22%5D%7D#baseline.

115. Weinhold, N., Jacobsen, A., Schultz, N., Sander, C. & Lee, W. Genome-wide analysis of noncoding regulatory mutations in cancer. *Nat. Genet.* **46**, 1160–1165 (2014).

116. Pignot, G. *et al.* PleKHS1: A new molecular marker predicting risk of progression of non-muscle-invasive bladder cancer. *Oncol. Lett.* **18**, 3471–3480 (2019).

117. Wu, S. *et al.* Whole-genome sequencing identifies ADGRG6 enhancer mutations and FRS2 duplications as angiogenesis-related drivers in bladder cancer. *Nat.*

*Commun.* **10**, (2019).

118. Melton, C., Reuter, J. A., Spacek, D. V. & Snyder, M. Recurrent somatic mutations in regulatory regions of human cancer genomes. *Nat. Genet.* **47**, 710–716 (2015).
119. Dudley, J. C. *et al.* Detection and surveillance of bladder cancer using urine tumor DNA. *Cancer Discov.* **9**, 500–509 (2019).
120. Deng, Z. *et al.* Mining TCGA Database for Tumor Microenvironment-Related Genes of Prognostic Value in Hepatocellular Carcinoma. (2019) doi:10.1155/2019/2408348.
121. Liu, X. *et al.* Identification of potential key genes associated with the pathogenesis and prognosis of gastric cancer based on integrated bioinformatics analysis. *Front. Genet.* **9**, 1–14 (2018).
122. Kotoh, J., Sasaki, D., Matsumoto, K. & Maeda, A. Plekhs1 and Prdx3 are candidate genes responsible for mild hyperglycemia associated with obesity in a new animal model of F344-fa-nidd6 rat. *J. Vet. Med. Sci* **78**, 1683–1691 (2016).
123. Kawano, K. *et al.* Spontaneous long-term hyperglycemic rat with diabetic complications: Otsuka Long-Evans Tokushima Fatty (OLETF) strain. *Diabetes* **41**, 1422–1428 (1992).
124. Tang, Z. *et al.* GEPIA: a web server for cancer and normal gene expression profiling and interactive analyses. *Web Serv. issue Publ. online* **45**, (2017).
125. Weber, P. C., Ohlendorf, D. H., Wendoloski, J. J. & Salemme, F. R. Structural origins of high-affinity biotin binding to streptavidin. *Science (80-. ).* **243**, 85–88 (1989).
126. Schatz, P. J. *Use of Peptide Libraries to Map the Substrate Specificity of a Peptide-Modifying Enzyme: A 13 Residue Consensus Peptide Specifies Biotinylation in Escherichia coli*. http://www.nature.com/naturebiotechnology (1993).
127. Huang, C. & Jacobson, K. Detection of protein-protein interactions using nonimmune igg and bira-mediated biotinylation. *Biotechniques* **49**, 881–886 (2010).
128. Fairhead, M. & Howarth, M. Site-specific biotinylation of purified proteins using BirA. *Methods Mol. Biol.* **1266**, 171–184 (2015).
129. Li, Y. & Sousa, R. Expression and purification of E. coli BirA biotin ligase for in vitro biotinylation. *Protein Expr. Purif.* **82**, 162–167 (2012).

130. Diamandis, E. P. & Christopoulos, T. K. The biotin-(strept)avidin system: Principles and applications in biotechnology. *Clinical Chemistry* vol. 37 625–636 (1991).

131. Cull, M. G. & Schatz, P. J. Biotinylation of proteins in vivo and in vitro using small peptide tags. *Appl. Chimeric Genes Hybrid Proteins Part A Gene Expr. Protein Purif.* **Volume 326**, 430–440 (2000).

132. Chapman-Smith, A. & Cronan, J. E. In vivo enzymatic protein biotinylation. *Biomol. Eng.* **16**, 119–125 (1999).

133. Marttila, A. T. *et al.* Recombinant NeutraLite Avidin: A non-glycosylated, acidic mutant of chicken avidin that exhibits high affinity for biotin and low non-specific binding properties. *FEBS Lett.* **467**, 31–36 (2000).

134. Lim, K. H., Huang, H., Pralle, A. & Park, S. Stable, high-affinity streptavidin monomer for protein labeling and monovalent biotin detection. *Biotechnol. Bioeng.* **110**, 57–67 (2013).

135. Bantscheff, M., Lemeer, S., Savitski, M. M. & Kuster, B. Quantitative mass spectrometry in proteomics: Critical review update from 2007 to the present. *Analytical and Bioanalytical Chemistry* vol. 404 939–965 (2012).

136. Thermo Fisher Scientific- website. Tandem Mass Tag Systems. https://www.thermofisher.com/uk/en/home/life-science/protein-biology/protein-mass-spectrometry-analysis/protein-quantitation-mass-spectrometry/tandem-mass-tag-systems.html.

137. Tsai, C. F. *et al.* Tandem Mass Tag Labeling Facilitates Reversed-Phase Liquid Chromatography-Mass Spectrometry Analysis of Hydrophilic Phosphopeptides. *Anal. Chem.* **91**, 11606–11613 (2019).

138. Werner, T. *et al.* Ion Coalescence of Neutron Encoded TMT 10-Plex Reporter Ions. *Anal. Chem* **86**, (2014).

139. Thompson, A. *et al.* Tandem Mass Tags: A Novel Quantification Strategy for Comparative Analysis of Complex Protein Mixtures by MS/MS. (2003) doi:10.1021/ac0262560.

140. Barneda, D., Cosulich, S., Stephens, L. & Hawkins, P. How is the acyl chain composition of phosphoinositides created and does it matter? *Biochem. Soc. Trans.* **47**, 1291–1305 (2019).

141. Clark, J. *et al.* Quantification of PtdInsP3 molecular species in cells and tissues by

mass spectrometry. *Nat. Methods* **8**, 267–272 (2011).

142. Mujalli, A. *et al.* Profiling of phosphoinositide molecular species in human and mouse platelets identifies new species increasing following stimulation. *Biochim. Biophys. Acta - Mol. Cell Biol. Lipids* **1863**, 1121–1131 (2018).
143. Malek, M. *et al.* PTEN Regulates PI(3,4)P2 Signaling Downstream of Class I PI3K. *Mol. Cell* **68**, 566-580.e10 (2017).
144. Trotman, L. C. *et al.* Pten Dose Dictates Cancer Progression in the Prostate. doi:10.1371/journal.pbio.0000059.
145. Wakelam, M. J. O. & Clark, J. Methods for analyzing phosphoinositides using mass spectrometry. *Biochimica et Biophysica Acta - Molecular and Cell Biology of Lipids* vol. 1811 758–762 (2011).
146. Stephens, L. R., Anderson, K. E. & Hawkins, P. T. Src Family Kinases Mediate Receptor-stimulated, Phosphoinositide 3-Kinase-dependent, Tyrosine Phosphorylation of Dual Adaptor for Phosphotyrosine and 3-Phosphoinositides-1 in Endothelial and B Cell Lines. *J. Biol. Chem.* **276**, 42767–42773 (2001).
147. Trotman, L. C. *et al.* Pten dose dictates cancer progression in the prostate. *PLoS Biol.* **1**, (2003).
148. Raveux, A., Vandormael-Pournin, S. & Cohen-Tannoudji, M. Optimization of the production of knock-in alleles by CRISPR/Cas9 microinjection into the mouse zygote OPEN. (2017) doi:10.1038/srep42661.
149. Sentmanat, M. F., Peters, S. T., Florian, C. P., Connelly, J. P. & Pruett-Miller, S. M. A Survey of Validation Strategies for CRISPR-Cas9 Editing OPEN. *Sci. RePoRTS* | **8**, 888 (2018).
150. Scott, M. A. & Hu, Y.-C. Generation of CRISPR-Edited Rodents Using a Piezo-Driven Zygote Injection Technique. doi:10.1007/978-1-4939-8831-0_9.
151. Ran, F. A. *et al.* Genome engineering using the CRISPR-Cas9 system. *Nat. Protoc.* **8**, 2281–2308 (2013).
152. Lanza, D. G. *et al.* Comparative analysis of single-stranded DNA donors to generate conditional null mouse alleles. *BMC Biol.* **16**, 69 (2018).
153. Yang, H. *et al.* XOne-step generation of mice carrying reporter and conditional alleles by CRISPR/cas-mediated genome engineering. *Cell* **154**, 1370 (2013).

154. Ayabe, S., Nakashima, K. & Yoshiki, A. Opinions and Hypotheses Off-and on-target effects of genome editing in mouse embryos. *J. Reprod. Dev.* **65**, (2019).
155. *Generating Mouse Models with CRISPR/Cas9*.
156. Wang, C. *et al.* PTEN deletion drives aberrations of DNA methylome and transcriptome in different stages of prostate cancer. *FASEB J.* **34**, 1304–1318 (2020).
157. Boniface, E. J., Lu, J., Victoroff, T., Zhu, M. & Chen, W. FlEx-based transgenic reporter lines for visualization of Cre and Flp activity in live zebrafish. *Genesis* **47**, 484–491 (2009).
158. Mitchell, K. J. *et al.* Functional analysis of secreted and transmembrane proteins critical to mouse development. *Nat. Genet.* **28**, 241–249 (2001).
159. Skarnes, W. C. *et al.* A conditional knockout resource for the genome-wide study of mouse gene function. (2011) doi:10.1038/nature10163.
160. De Velasco, M. A. *et al.* Efficacy of targeted AKT inhibition in genetically engineered mouse models of PTEN-deficient prostate cancer. *Oncotarget* **7**, 15959–15976 (2016).
161. Ittmann, M. *et al.* Animal models of human prostate cancer: The Consensus Report of the New York Meeting of the Mouse Models of Human Cancers Consortium Prostate Pathology Committee NIH Public Access. *Cancer Res* **73**, 2718–2736 (2013).
162. De Velasco, M. A. *et al.* Efficacy of targeted AKT inhibition in genetically engineered mouse models of PTEN-deficient prostate cancer. *Oncotarget* **7**, 15959–15976 (2016).
163. Chanhee, H. *et al.* Novel targeted therapies in ovarian and uterine carcinosarcomas. *Discov Med .* **25**, 309–319 (2018).
164. Boggon, T. J. & Eck, M. J. Structure and regulation of Src family kinases. *Oncogene* **23**, 7918–7927 (2004).
165. Hellyer, N. J., Cheng, K. & Koland, J. G. ErbB3 (HER3) interaction with the p85 regulatory subunit of phosphoinositide 3-kinase. *Biochem. J.* **333**, 757–763 (1998).
166. Irtegun, S., Wood, R. J., Ormsby, A. R., Mulhern, T. D. & Hatters, D. M. Tyrosine 416 Is Phosphorylated in the Closed, Repressed Conformation of c-Src. *PLoS One*

**8**, (2013).

167. Stambolic, V. *et al.* Negative regulation of PKB/Akt-dependent cell survival by the tumor suppressor PTEN. *Cell* **95**, 29–39 (1998).
168. Di Cristofano, A., Pesce, B., Cordon-Cardo, C. & Pandolfi, P. P. Pten is essential for embryonic development and tumour suppression. *Nat. Genet.* **19**, 348–355 (1998).
169. Maehama, T. & Dixon, J. E. The tumor suppressor, PTEN/MMAC1, dephosphorylates the lipid second messenger, phosphatidylinositol 3,4,5-trisphosphate. *J. Biol. Chem.* **273**, 13375–13378 (1998).
170. Feng, J., Park, J., Cron, P., Hess, D. & Hemmings, B. A. Identification of a PKB/Akt hydrophobic motif Ser-473 kinase as DNA-dependent protein kinase. *J. Biol. Chem.* **279**, 41189–41196 (2004).
171. Stephens, L. *et al.* Protein kinase B kinases that mediate phosphatidylinositol 3,4,5- trisphosphate-dependent activation of protein kinase B. *Science (80-. ).* **279**, 710–714 (1998).
172. Bowman, A. P. *et al.* Evaluation of lipid coverage and high spatial resolution MALDI-imaging capabilities of oversampling combined with laser post-ionisation. *Anal. Bioanal. Chem.* **412**, (2019).
173. Bose, U., Wijffels, G., Howitt, C. A. & Colgrave, M. L. Proteomics: Tools of the Trade. in *Advances in Experimental Medicine and Biology* vol. 1073 1–22 (Springer New York LLC, 2019).
174. Aslam, B., Basit, M., Nisar, M. A., Khurshid, M. & Rasool, M. H. Proteomics: Technologies and their applications. *Journal of Chromatographic Science* vol. 55 182–196 (2017).
175. Marouga, R., David, S. & Hawkins, E. The development of the DIGE system: 2D fluorescence difference gel analysis technology. *Analytical and Bioanalytical Chemistry* vol. 382 669–678 (2005).
176. Gel Electrophoresis of Proteins - Google Książki. https://books.google.co.uk/books?hl=pl&lr=&id=wIKQBQAAQBAJ&oi=fnd&pg=PP1&ots=brUYyv_uno&sig=GGuOlxCIPtBnq_-4n9mA_u9ezIQ&redir_esc=y#v=onepage&q&f=false.

177. Issaq, H. J. & Veenstra, T. D. Two-dimensional polyacrylamide gel electrophoresis (2D-PAGE): Advances and perspectives. *BioTechniques* vol. 44 697–700 (2008).
178. Shiio, Y. & Aebersold, R. Quantitative proteome analysis using isotope-coded affinity tags and mass spectrometry. *Nat. Protoc.* **1**, 139–145 (2006).
179. Wiese, S., Reidegeld, K. A., Meyer, H. E. & Warscheid, B. Protein labeling by iTRAQ: A new tool for quantitative mass spectrometry in proteome research. *Proteomics* **7**, 340–350 (2007).
180. Smyth, M. S. & Martin, J. H. J. x Ray crystallography. *Journal of Clinical Pathology - Molecular Pathology* vol. 53 8–14 (2000).
181. TMT 16plex-website. https://www.thermofisher.com/order/catalog/product/A44520#/A44520.
182. Aggarwal, S. & Yadav, A. K. Dissecting the iTRAQ data analysis. in *Methods in Molecular Biology* vol. 1362 277–291 (Humana Press Inc., 2016).
183. Jurmeister, S. *et al.* Identification of potential therapeutic targets in prostate cancer through a cross-species approach. *EMBO Mol. Med.* **10**, (2018).
184. Tsai, F. T. F., Jeng, W., Lee, S., Sung, N. & Lee, J. Molecular chaperones: Guardians of the proteome in normal and disease states. *F1000Research* vol. 4 (2015).
185. STRING: functional protein association networks- website. https://version11.string-db.org/.
186. Zhang, J. *et al.* Proteomic and transcriptomic profiling of Pten gene-knockout mouse model of prostate cancer. *Prostate* **80**, 588–605 (2020).
187. CRAPome-website. http://www.crapome.org/.
188. Pennington, K., Chan, T., Torres, M. & Andersen, J. The dynamic and stress-adaptive signaling hub of 14-3-3: emerging mechanisms of regulation and context-dependent protein–protein interactions. *Oncogene* vol. 37 5587–5604 (2018).
189. Paranavitane, V., John Coadwell, W., Eguinoa, A., Hawkins, P. T. & Stephens, L. LL5β is a phosphatidylinositol (3,4,5)-trisphosphate sensor that can bind the cytoskeletal adaptor, γ-filamin. *J. Biol. Chem.* **278**, 1328–1335 (2003).
190. Takabayashi, T. *et al.* LL5βdirects the translocation of Filamin A and SHIP2 to sites of phosphatidylinositol 3,4,5-triphosphate (PtdIns(3,4,5)P3) accumulation, and PtdIns(3,4,5)P3 localization is mutually modified by co-recruited SHIP2. *J. Biol.*

*Chem.* **285**, 16155–16165 (2010).

191. Marone, R. *et al.* Memo mediates ErbB2-driven cell motility. *Nat. Cell Biol.* **6**, 515–522 (2004).
192. Zaoui, K., Honoré, S., Isnardon, D., Braguer, D. & Badache, A. Memo - RhoA - mDia1 signaling controls microtubules, the actin network, and adhesion site formation in migrating cells. *J. Cell Biol.* **183**, 401–408 (2008).
193. Qiu, C., Lienhard, S., Hynes, N. E., Badache, A. & Leahy, D. J. Memo is homologous to nonheme iron dioxygenases and binds an ErbB2-derived phosphopeptide in its vestigial active site. *J. Biol. Chem.* **283**, 2734–2740 (2008).
194. Eisenberg, D., Marcotte, E. M., Xenarios, I. & Yeates, T. O. Protein function the post-genomic era. *Nature* vol. 405 823–826 (2000).
195. De Las Rivas, J. & Fontanillo, C. Protein–Protein Interactions Essentials: Key Concepts to Building and Analyzing Interactome Networks. *PLoS Comput. Biol.* **6**, e1000807 (2010).
196. Raman, K. Construction and analysis of protein-protein interaction networks. *Automated Experimentation* vol. 2 (2010).
197. Vinayagam, A. *et al.* Integrating protein-protein interaction networks with phenotypes reveals signs of interactions. *Nat. Methods* **11**, 94–99 (2014).
198. Rual, J. F. *et al.* Towards a proteome-scale map of the human protein-protein interaction network. *Nature* **437**, 1173–1178 (2005).
199. Gavin, A. C. *et al.* Functional organization of the yeast proteome by systematic analysis of protein complexes. *Nature* **415**, 141–147 (2002).
200. Valencia, A. & Pazos, F. Computational methods for the prediction of protein interactions. *Current Opinion in Structural Biology* vol. 12 368–373 (2002).
201. Tirat, A., Freuler, F., Stettler, T., Mayr, L. M. & Leder, L. Evaluation of two novel tag-based labelling technologies for site-specific modification of proteins. *Int. J. Biol. Macromol.* **39**, 66–76 (2006).
202. Leder, L. Site-specific protein labeling in the pharmaceutical industry: Experiences from novartis drug discovery. *Methods Mol. Biol.* **1266**, 7–27 (2015).
203. Dayon, L. *et al.* Relative quantification of proteins in human cerebrospinal fluids by MS/MS using 6-plex isobaric tags. *Anal. Chem.* **80**, 2921–2931 (2008).

204. Savitski, M. M. *et al.* Measuring and managing ratio compression for accurate iTRAQ/TMT quantification. *J. Proteome Res.* **12**, 3586–3598 (2013).

205. Stewart, P. A. *et al.* Proteogenomic landscape of squamous cell lung cancer. doi:10.1038/s41467-019-11452-x.

206. Xiao, H. *et al.* Differential Proteomic Analysis of Human Saliva using Tandem Mass Tags Quantification for Gastric Cancer Detection OPEN. *Nat. Publ. Gr.* (2016) doi:10.1038/srep22165.

207. Hedl, T. J. *et al.* Proteomics approaches for biomarker and drug target discovery in als and ftd. *Frontiers in Neuroscience* vol. 13 548 (2019).

208. Tank, E. M. *et al.* Abnormal RNA stability in amyotrophic lateral sclerosis. *Nat. Commun.* **9**, (2018).

209. Jiang, X., Chen, S., Asara, J. M. & Balk, S. P. Phosphoinositide 3-kinase pathway activation in phosphate and tensin homolog (PTEN)-deficient prostate cancer cells is independent of receptor tyrosine kinases and mediated by the p110β and p110δ catalytic subunits. *J. Biol. Chem.* **285**, 14980–14989 (2010).

210. Höti, N., Shah, P., Hu, Y., Yang, S. & Zhang, H. Proteomics analyses of prostate cancer cells reveal cellular pathways associated with androgen resistance. *Proteomics* **17**, 1600228 (2017).

211. Blattner, M. *et al.* SPOP Mutation Drives Prostate Tumorigenesis In Vivo through Coordinate Regulation of PI3K/mTOR and AR Signaling. *Cancer Cell* **31**, 436–451 (2017).

212. Valkenburg, K. C. & Pienta, K. J. Drug discovery in prostate cancer mouse models. *Expert Opinion on Drug Discovery* vol. 10 1011–1024 (2015).

213. Triscott, J. & Rubin, M. A. VIeWs Prostate Power Play : Does Pik3ca Accelerate Pten-Defi cient Cancer Progression? (2018) doi:10.1158/2159-8290.CD-18-0369.

214. de la Rosa, J. *et al.* A single-copy Sleeping Beauty transposon mutagenesis screen identifies new PTEN-cooperating tumor suppressor genes. *Nat. Publ. Gr.* (2017) doi:10.1038/ng.3817.

215. Mirantes, C. *et al.* An inducible knockout mouse to model the cell-autonomous role of PTEN in initiating endometrial, prostate and thyroid neoplasias. *DMM Dis. Model. Mech.* **6**, 710–720 (2013).

216. Perets, R. *et al.* Transformation of the Fallopian Tube Secretory Epithelium Leads

to High-Grade Serous Ovarian Cancer in Brca;Tp53;Pten Models. *Cancer Cell* **24**, 751–765 (2013).

217. Eddie, S. L. *et al.* Tumorigenesis and peritoneal colonization from fallopian tube epithelium. *Oncotarget* **6**, 20500–20512 (2015).
218. Gavgani, F. M. *et al.* Class I phosphoinositide 3-kinase PIK3CA/p110α and PIK3CB/p110β isoforms in endometrial cancer. *International Journal of Molecular Sciences* vol. 19 (2018).
219. Forbes, S. A. *et al.* COSMIC: mining complete cancer genomes in the Catalogue of Somatic Mutations in Cancer. doi:10.1093/nar/gkq929.
220. Getz, G. *et al.* Integrated genomic characterization of endometrial carcinoma. *Nature* **497**, 67–73 (2013).
221. Gao, J. *et al.* Integrative analysis of complex cancer genomics and clinical profiles using the cBioPortal. *Sci. Signal.* **6**, (2013).
222. An, H. J. *et al.* Targeted RNA interference of phosphatidylinositol 3-kinase p110-β induces apoptosis and proliferation arrest in endometrial carcinoma cells. *J. Pathol.* **212**, 161–169 (2007).
223. Karlsson, T. *et al.* Endometrial cancer cells exhibit high expression of p 110β and its selective inhibition induces variable responses on PI3K signaling, cell survival and proliferation. *Oncotarget* **8**, 3881–3894 (2017).
224. Milne, S. B., Ivanova, P. T., DeCamp, D., Hsueh, R. C. & Brown, H. A. A targeted mass spectrometric analysis of phosphatidylinositol phosphate species. *J. Lipid Res.* **46**, 1796–1802 (2005).